UNIVERSITÉ DE STRASBOURG

ÉCOLE DOCTORALE DES SCIENCES CHIMIQUES

UMR 7515

THÈSE présentée par :

Adela NANO

soutenue le: **25 mars 2015**

pour obtenir le grade de : **Docteur de l'Université de Strasbourg**

Discipline: Chimie

Towards optical memories: switchable optical systems for electron and energy transfer processes

JURY :

1- M. ZIESSEL Raymond	Directeur de thèse, Directeur de recherche, Université de Strasbourg

Rapporteur :

2- M. NAKATANI Keitaro	Professeur, ENS Cachan
3- M. McCLENAGHAN Nathan D.	Directeur de recherche, Université de Bordeaux

Examinateur :

4- M. NIERENGARTEN Jean-François	Directeur de recherche, Université de Strasbourg

---

INVITÉ :

- M. DENNLER Gilles	Docteur, IMRA EUROPE S. A. S., France

To my sisters

Ilda and Denada

To my parents

Tefta and Vasili

ACKNOWLEDGEMENTS (in french)

Cette thèse a été réalisée au sein du Laboratoire de Chimie Organique et Spectroscopie Avancée sous la direction du Dr. Raymond Ziessel. Ces trois années et demie passé au laboratoire, malgré les hauts et les bas rencontrés, m'ont permis de grandir et évoluer tant du point de vue professionnel que personnel. Pour cela je tiens à remercier Raymond de m'avoir donné l'occasion de vivre ce passage de ma vie dans son laboratoire en sa direction.

Je remercie la Société IMRA située en France, pour avoir financé cette thèse ainsi que le Dr. Stéphane Jacob et plus particulièrement le Dr. Gilles Dennler de la Société IMRA pour avoir également suivi et encadré ces travaux. Je les remercie pour nos nombreuses discussions téléphoniques ou autour d'un repas à Nice ou Strasbourg. Merci Gilles pour le soutien que tu m'as accordé notamment pour la recherche de mon Post-doc en Californie!

J'en profite ici pour témoigner ma gratitude aussi au Dr. Stéphane Bellemin-Laponnaz que j'ai eu la chance d'avoir rencontré lors de mon premier stage en chimie et qui a encadré également mes stages de fin d'étude de Master. Je te remercie Stéphane d'avoir été toujours prêt à m'aider et me soutenir même durant la thèse!

Je suis très honorée et je remercie le Prof. Keitaro Nakatani, le Dr. Nathan McClenaghan et le Dr. Jean-François Nierengarten pour avoir accepté de juger le travail réalisé au cours de cette thèse. Je m'excuse très sincèrement de leur avoir laissé si peu de temps pour lire mon manuscrit!

Je remercie le Dr. Pascal Retailleau (ICSN) pour la résolution et l'étude des structures cristallographiques obtenues au cours de cette thèse et le Dr. Michel Schmitt du service commun de la RMN de l'ECPM.

Et puis un merci très chaleureux à Véro, tes bonbons et ta gentillesse vont me manquer mais aussi à tout le personnel de l'ICPEES! Merci!

Un profond remerciement va à tous ceux que j'ai pu rencontrer dans le laboratoire notamment le Dr. Gilles Ulrich et le Dr. Antoinette De Nicola, les habitants du labo 3, Antoine (ou Alexendre!), Quentin et son petit grain de 'folie' qui a animé le labo, et plus particulièrement merci à Alex, ma voisinne de paillasse! Comment je pourrai oublier Julien, Elsa, Elodie, Arnaud, Seb, Karima, Soumya, Wenzis, Mus, Vincent, Kevin et encore les amis des autres labos, Irene, Marissa, Haifa, Antonella, Lucie, Mathieu…

Je remercie les amis du club de la natation « Leo Lagrange », Nadège, Danièle, Briec, Hubert, Marie, Said, Sandrine (the coach) etc. avec qui j'ai partagé bien plus qu'une ligne d'eau. Je ne pouvais pas avoir de meilleur remède pour les moments difficiles… Mes ami(e)s Virginie, Laurine, Michael, Rezi qui malgré loin de Strasbourg ont su me rester proches. Et puis Fanny, Cynthia et plus particulièrement ma meilleur amie Redona pour l'encouragement lors de ces presque deux mois et demi de rédaction assez intense!

Enfin je ne pourrais pas trouver les mots pour exprimer la reconnaissance et l'amour que je porte pour mes sœurs, Ilda et Denada et me parents, Vasili et Tefta. C'est la confience qu'ils m'ont accordé depuis mon plus jeune âge, leur support inconditionnel et leurs sacrifices qui m'ont permis de réaliser mes souhaits et mes projets. Mami, babi, faleminderit qe jeni prinder kaq te veçante! C'est grâce à vous que je continue d'avancer! Faleminderit!

SYMBOLS & ABBREVIATIONS

h	Plank's constant
J	Chemical constant coupling given in Hz
δ	Chemical shift given in parts per million (ppm)
$\Delta\omega$	Stokes's shift
ε	Extinction coefficient
λ_{Abs}	Absorption wavelength
λ_{em}	Emission wavelength
λ_{exc}	Excitation wavelength
μ_{GS}	Ground state dipole moment given in Debye (D)
ν	Frequency given in cm^{-1}
σ^*, π^*	Antibonding molecular orbitals
σ, π	Bonding molecular orbitals
τ	Luminescence lifetime
φ_F	Fluorescence quantum yield
φ_P	Phosphorescence quantum yield

A	Acceptor
AcOH	Acetic acid
bhqH	Benzo[*h*]quinoline
BODIPY	BoronDIPYrromethene
bpy	2,2-bipyridine
CH_3CN	Acetonitrile
CS	Charge-Separated
D	Donor
DCM	2-(2-*tert*-butyl-6-mehtyl-4*H*-pyran-4-ylidene)malonitrile
DCVJ	9-(Dicyanovinyl)-julolidine
DFT	Density Functional Theory

DIPA	*N*,*N*-Diisopropylamine
DIPEA	*N*,*N*-diisopropylethylamine
DMF	Dimethylformamide
dppf	1,1'-Bis(diphenylphosphino)ferrocene ligand
DSSC	Dye-Sensitized Solar Cell
E	Enol form
EET	Electronic Energy Transfer
EI-MS	Electron Ionization Mass Spectrometry
ESIPT	Excited State Intramolecular Proton Transfer
ES-MS	Electrospray mass spectrometry
EtOH	Ethanol
EX	Exciplex state
Fl	Fluorescence
FRET	Fluorescence Resonance Energy Transfer
HOMO	Highest Occupied Molecular Orbital
IC	Internal Conversation
ICT	Intramolecular Charge Transfer
ISC	Intersystem Crossing
K	Keto form
LC	Ligand-Centered transition
LH	Light Harvesting
LLCT	Ligand-to-Ligand Charge Transfer transition
LUMO	Lowest Occupied Molecular Orbital
MC	Metal-Centered, transition involved into a metal complex
MeOH	Methanol
MLCT	Metal-to-Ligand Charge Transfer, transition
MO	Molecular Orbital
MTHF	Methyltetrahydrofuran
NIR	Near-Infra Red

NLO	NonLinear Optic
NMe_4OH	tetramethylammonium hydroxide
NMR	Nuclear Magnetic Resonance spectroscopy
OLED	Organic Light Emitting Diode
PEG	Polyethylene glycol
PeT	Photoinduced electron Transfer
Ph	Phosphorescence
PPh_3	Triphenyl phosphine ligand
ppyH	2-phenylpyridine
S	Singlet state
SCE	Saturated Calomel Electrode, the reference electrode
SO	Spiroxazine
SP	Spiropyran
T	Triplet state
TAT	Triazatruxene
TBAPF	tetra-N-butylammonium hexafluorophosphate
TFA	Trifluoroacetic acid
THF	Tetrahydrofuran
TICT	Twisted Intramolecular Charge Transfer
TMJ	1,1,7,7-tetramethyljulolidine
TMS	Trimethylsylyl
Tol	Toluene
TPA	Two Photon Absorbing materials
UV	Ultra Violet
VR	Vibrational Relaxation

THESIS OUTLINE

The work of this doctoral thesis consists on the design, synthesis and characterization of optical molecular frameworks which allow us to trigger important optical phenomena, such as Photoinduced electron Transfer (PeT) or Electronic Energy Transfer (EET) processes.

Chapter I is a general overview on important concepts in photochemistry and photophysics. Chapter II deals with the design, synthesis and characterization of organic push-pull systems based on an electron-donor and an electron-acceptor moiety bridged with a Boron DIPYrromethene (BODIPY) dye. The electron-donor is a julolidine or a triazatruxene moiety, selected because of their strong electron-donor property, and the electron-acceptor is a dicyanovinyl unit.

Furthermore, in this chapter we have reported the synthesis of a hybrid distyryl BODIPY dye bearing a julolidine and a N,N-dimethylaniline arm which act as a fluorescent pH sensor. The absorption and emission spectral titration confirm the disparate character of the amino-derivative sites regarding protonation in acidic media. It was found that the first protonation step occurs on the julolidine site rendering the protonation of the second amino-site very difficult.

In Chapter III we have exploited the unusual reactivity of julolidine by such a series of novel ligands and their complexation with boron and transition metals as iridium (III) and platinium (II). The free ligands display an *Excited State Intramolecular Proton Transfer* (ESIPT) character from the oxygen to the nitrogen atom. Interestingly according to the photophysical measurements it was found that the ligands exhibit a *panchromatic* photoluminescence. On the other hand the photophysical behavior of the boron complexes and transition metal complexes were also evaluated and investigated. The coordination of the julolidine derivative ligand to platinium (II) and iridium (III) highly affects their photophysical properties.

Finally, in Chapter IV we have described the design and synthesis of innovative switches based on a [1,3]oxazine scaffold. The control of the fluorescence emission (output) in a dyad or triad is possible by controlling the transformation of the *photochromic* core (input) under chemical and/or optical external stimuli. We have synthetized and fully characterized a series of photochromic molecules by using a Knoevenagel condensation of a given dihalogenated spiroxazine and various aldehydes.

Among several photochromes synthesized, one was selected for the elaboration of the final switchable system. The photochrome was covalently attached to an energy-donor and an energy-acceptor fluorophore specifically selected for the purpose. In principle, by optical or chemical opening/closing of the photochromic core, we can control the direction of the electronic energy transfer from the donor to the acceptor. The synthetic strategy employed for providing the target triad as well as the preliminary optical behavior under illumination is treated in more detail in Chapter IV.

CONTENTS

« *Il faut faire de la vie un rêve et faire d'un rêve une réalité* »

Pierre Curie

Extrait du livre « La radioactivité artificielle et son histoire »

« *You need to do of life a dream and make the dream a reality* »

Pierre Curie

Extract from the book « La radioactivité artificielle et son histoire »

Chapter I

Chapter 1- General Background

Light and photochemistry[1]

If we are able to see objects and colors around us, it is because we have a perception of light. It is the principal way by which we have perception of the world and obviously read these lines at the moment. Light interacts with the *rhodopsin*, a pigment which is found in the eye's retina, causing a *photochemical* change which provokes the nervous system to tell the brain that light has been received. Professor George Wald of the Harvard University earned the Nobel Prize in medicine in 1967 for his work on chemical visual processes in the eye.[2] Another important *photochemical* process is *photosynthesis* which occurs in plants, some bacteria and algae (*e.g. Kingdom Protista*). In the presence of light, the carbon dioxide is reduced into sugar and simultaneously the energy harvested *via* from the light is stored by production of adenosine triphosphate (ATP).

Photochemistry is of crucial interest in the development of life on earth but so does for its protection from harmful electromagnetic irradiation coming from the sun. The ozone which is found in the upper atmosphere protects the surface of our planet by absorbing wavelength below 320 nm. It dissociates by photolysis into oxygen which in turn is reconverted *photochemically* into ozone again. Nature has plenty of examples of chemical systems which demand light as an external stimulus source for their achievement and which show the important role of photochemistry in everyday life.

In this chapter we will give a general introduction in photophysics and photochemistry dealing with important concepts, the purpose being to introduce the reader to essential topics in order to better understand the choices made and the results described in the following chapters. Herein we will discuss molecule-light interactions with an overview on the ground and excited states of the molecule and the various processes leading to the formation and the relaxation pathways of excited states. A section is dedicated to the description of *photochromism*, a fascinating photochemical phenomenon which will be treated in the last chapter. Further we will introduce

[1] Borrell, P. *Photochemistry - A Primer*, eds. Edward Arnold, 1973. ebook: https://archive.org.

[2] The Nobel Prize was shared with Professor Ragnar Granit (University of Stockholm) and Professor Haldan Keffer Hartline (University of Rockefeller) for their works in physiological processes in the eye.

the julolidine fragment, a compound that we have thoroughly investigated throughout this doctoral thesis.

1. Electronic excitation - Light absorption[3,4]

The absorption of electromagnetic radiation by a molecule M causes the formation of an electronically excited molecule M*. It results because the absorption of a given photon energizes an electron which "jumps" from the *Highest Occupied Molecular Orbital* (HOMO) to the *Lowest Unoccupied Molecular Orbital* (LUMO) as depicted in Figure 1.1a.

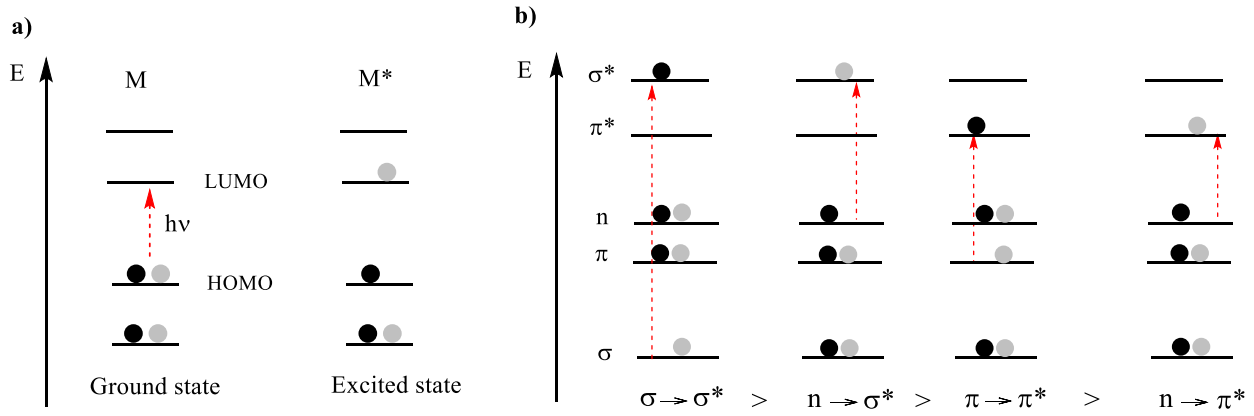

Figure 1.1. a) Absorption transition between HOMO and LUMO levels. b) Energy levels diagram showing the different types of electronic transitions within organic molecules from the more energetic $\sigma \rightarrow \sigma^*$ to the less energetic $n \rightarrow \pi^*$.

The energy required for the absorption transition from the HOMO level into the LUMO level is given by the following expression:

$$\Delta E = E_{LUMO} - E_{HOMO} \qquad \text{Eq. 1.1}$$

This energy can be supplied by a photon of appropriate frequency given by the Planck relationship:

$$E = h\nu = hc/\lambda \qquad \text{Eq. 1.2}$$

Where h is the Planck's constant, ν is the frequency of the wave, c the speed of light, λ the wavelength.

[3] Turro, N.J. *Modern molecular photochemistry*, Eds. The Benjamin/Cummings Publishing Company, Inc. California, 1978.

[4] Gilbert, A. and Baggott, J. foreward by Wagner, P. J. *Essentials of Molecular Photochemistry*, 1991, ISBN 0-8493-7727-7.

In organic chemistry we generally refer to HOMO and LUMO orbital, but it is necessary to remember that the molecular orbitals found in organic molecules derive from the overlap of the atomic s and p orbitals thus forming three main classes: σ and π bonding; σ* and π* antibonding and n nonbonding orbitals. HOMOs are bonding or nonbonding orbitals (*i.e.* σ, π or n) and LUMOs are antibonding orbitals (*i.e.* σ^*, π^*). Figure 1.1b shows the general energy levels of the different orbitals and the electronic transitions that may be involved. The situation is not the same when considering organometallic compounds (*vide infra*). The part or region of the molecule which is involved in the electronic transition hence responsible for its photophysical and photochemical activity (*i.e.* the color) is termed *chromophore*.

- *Transition metals complexes*

The nature of molecular orbitals (MO) and electronic transitions involved in metallic complexes differ from the organic molecules; they derive from the combination of atomic orbitals of the metal center (usually *d* orbitals for transition metals) with those of ligands. Contrary to organic molecule MOs, within a metal complex the MOs are not distributed evenly, they are polarized hence localized onto the metal or the ligand. Depending on the type of ligand, a covalent bond can be established with the metal centre thus enhancing the hybridization and mixing between orbitals. When light absorption occurs, subsequently an electronic transition occurs between molecular orbitals. The main electronic transitions involved into a transition metal complex are:

a. *metal-centered* (MC), the electron of a *d* orbital of the metal is promted into a higher *d**-orbital;
b. *metal-to-ligand charge-transfer* (MLCT), involves a transition from a *d*-orbital of the metal to a low energy σ* or π*-orbital of the ligand. These types of processes mostly involve metals having an electronic configuration d^6, d^8, d^9 and ligands such as 2,2-bipyridine or 1,10-phenanthroline;
c. *ligand-to-ligand charge-transfer* (LLCT) is observed when a ligand with strong reductive character and a ligand with a strong oxidative character are introduced on the same complex. The electron is usually transferred from a π-orbital to a π*- orbital of another ligand;
d. *ligand-centered transitions* (LC) may involve a transition from the σ-orbital formed between the ligand and the metal into the π* of the same ligand. Another possibility would be a π→π* transition and concern ligands with a π-extended chemical structure.

Each electron in a molecule carries a spin quantum number $s = +1/2$ or $-1/2$ also known as "spin-up" or "spin-down". In the presence of a magnetic field, its magnetic moment may be aligned in the direction of force of the applied magnetic field or opposed to it. As described in Figure 1.2, two excited electronic states can derive by the interaction with light. In one state, upon excitation the electron remains in the same spin state resulting in an antiparallel configuration or paired (spin allowed by the *rule's selections*)[5] and in the other state the spin flips resulting in a parallel configuration (spin forbidden by the *rule's selections*).[5]

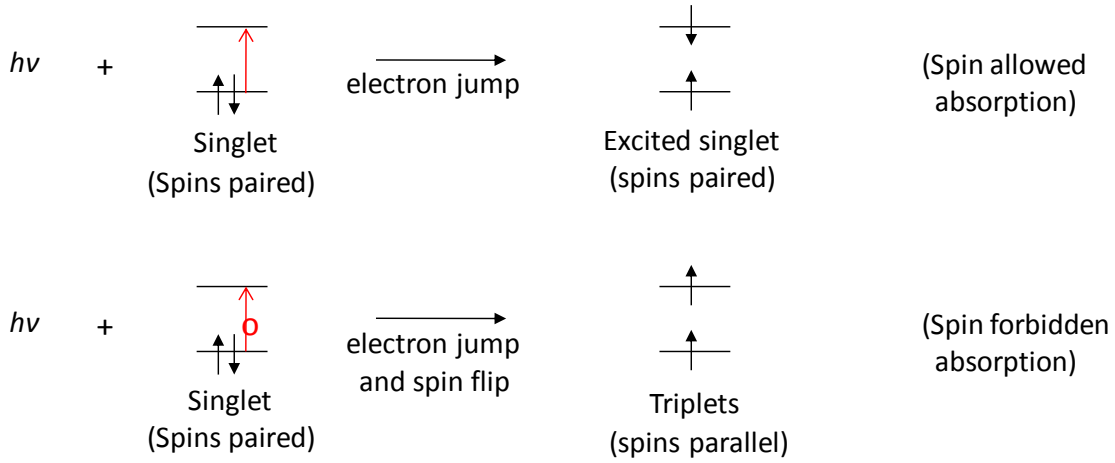

Figure 1.2. Orbital energy level description of absorption transition. Figure adapted from ref. [3], pp 3.

In the paired configuration state the total spin number $S = \sum S_i$ where $S_i = +1/2, -1/2$, is zero. Its multiplicity $M = 2S + 1$ being one the state is termed a *singlet state* S. It has no resultant magnetic moment, thus in the presence of an external magnetic field it remains a single state. The unpaired configuration (parallel spins) has a total spin number $|S| = 1$ and a multiplicity number three and is termed a *triplet state* T. It reacts with an external magnetic field and splits into three degenerate quantized states with the resulting projection of spin angular momentum onto *z*-axis being M_s = -1, 0, +1 (Figure 1.3). *It appears that the energy of a triplet state is lower than the energy of a singlet state despite the fact they derive from the same fundamental electron orbital configuration.*

[5] The selection rules which govern the electronic transitions are the *spin rule* and the *orbital rule*. The former says that allowed transitions involve the promotion of an electron without change of its spin. The latter states that in a centrosymmetric environment, transitions between same atomic orbitals (*e.g.* s-s, d-d etc.) are forbidden.

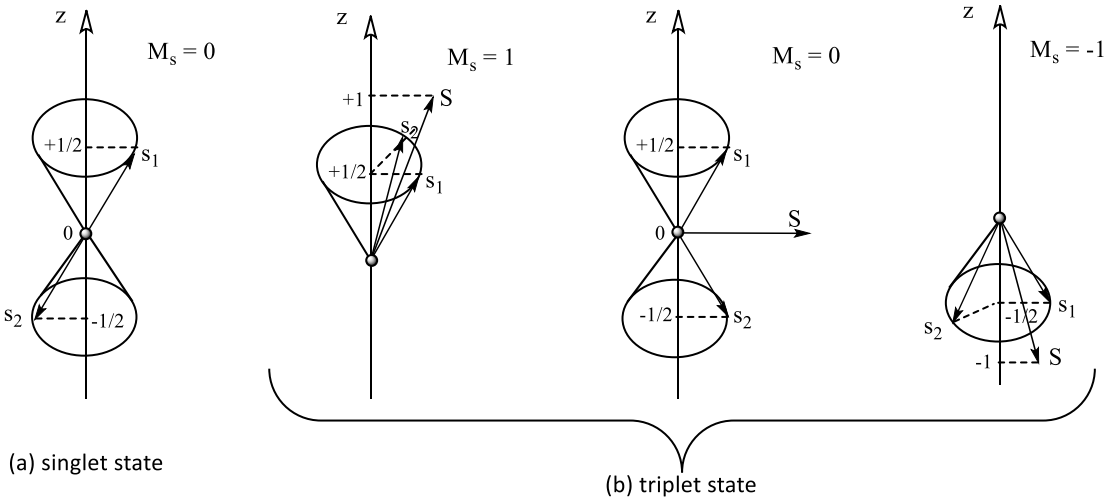

Figure 1.3. Vector addition, **S**, of individual electron spin angular momentum. The projection onto the *z*-axis of the vector sum may give no net result (a) or three different components (b). Figure adapted from ref. [3], pp 31.

According to the Pauli's principle[6] two electrons with paired spin have a non-zero probability to be found in a same location. For electrons with unpaired spin this probability is near zero. Because there is a better correlation of electron motions in space in the triplet state the Coulomb repulsion is lower, thus lowering its energy compared to singlet state.

The promotion of a given molecule to its excited state is accompanied with changes to its electronic distribution, while the nuclei remains at the same configuration. Indeed, electrons have much smaller masses then nuclei, as such their motions are so fast that the nuclei motions (*i.e.* vibrational and rotational motions) are neglected during the timescale of the electronic absorption ($\approx 10^{-15}$ s). As a result, the structure of the molecule (*i.e.* bond lengths and angles) in the excited state is identical to that in the ground state. This is known as the *Born-Oppenheimer approximation*[7] and the consequence is that nuclear motions and electronic motions hence can be treated separately in a potential energy diagram.

Each diagram well representing the ground and electronic excited state is characterized by a discrete number of vibrational levels (*i.e.* v" or v' = 0, 1, 2, 3…n), each of them may be considered as a vibrational nuclear wavefunction (Figure 1.4). According to the *Franck-Condon principle*, because the electronic transition is much faster than vibrational motion of nuclei, the most probable transition take place *vertically* (represented by vertical arrows) between states

[6] The Pauli's principle states that it is impossible for two electrons of a poly-electron atom to have the same values of the four quantum numbers (n, ℓ, m_ℓ and m_s). For two electrons residing in the same orbital, n, ℓ, and m_ℓ are the same, so m_s must be different and the electrons have opposite spins.

[7] Born, M.; Oppenheimer, R. *Ann. Phys*. **1927**, *84*, 457.

with the same nuclear coordinates and where the wavefunctions have a maximum overlap integral (Figure 1.4). At room temperature most of the transitions take place from the zero vibrational (ν' = 0) level of the ground state through zero or higher (ν" = 0, 1, 2, 3…n) vibrational levels of the excited state.

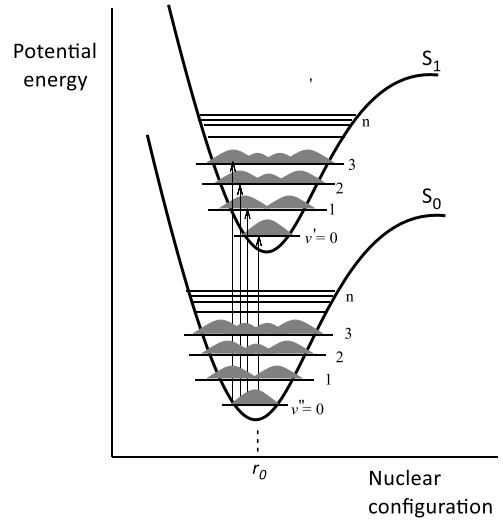

Figure 1.4. Diagram wells of ground and singlet excited states where the vibrational levels are represented as wavefunctions and absorption electronic transitions are represented by vertical arrows following the Franck-Condon principle.

The absorption of light from a molecule is characterized by a parameter known as the *extinction coefficient* (ε). It gives the probability for a photon of a particular energy to be absorbed by the sample. According to Beer-Lambert low:

$$A = \varepsilon . l . c \qquad \text{Eq. 1.3}$$

The absorbance A is proportional to the concentration of the solute given in molarity (*c*), the optical path length (*l*) given in cm and the molar extinction coefficient (ε) expressed in $M^{-1}.cm^{-1}$.

2. De-excitation processes of electronically excited molecules[3]

It was described in the previous section that when a molecule absorbs a photon, it transforms electromagnetic energy into electronic excitation energy. The resulting electronically excited molecule is energetically unstable, thus it will rapidly find a way to dissipate its excess energy and return to the ground state. It can lose its excitation energy *photochemically*, by involving changes in the chemical nature of the molecule, *i.e.* rearrangement or fragmentation or isomerization. *Photophysical* processes may be defined as transitions which interconvert excited

states with each other or excited states with the ground state. Here we will describe three possible photophysical de-excitation pathways:

a. *Radiative processes*, are accompanied by emission of light when an excited molecule returns to the ground state,
b. *Radiationless processes*, in which the passing from an excited state to others is not accompanied with light emission and,
c. *Quenching mechanism*, involve an energy or electron transfer process from the initially excited molecule to others molecules in collision with it. They are in general bi- or trimolecular de-excitation processes, but they can also be performed within a unimolecular system. Note that quenching could also occur intramolecularly by linking two or more molecules in the same skeleton.

2.1. Radiative processes

By means of absorption and emission spectroscopy we can get much information about the fate of excited molecules, about its structure and energetics. When the de-excitation proceeds by emission of light, then the process is named *luminescence*. Depending on the type of excited state, the *luminescence* is divided into two categories known as *fluorescence* and *phosphorescence*. The former is the emission of a photon from an excited state of the same spin multiplicity as the ground state (*i.e.* $S_1 \rightarrow S_0$). Since there is no change on spin multiplicity, the transition is spin-allowed and occurs rapidly. It is characterized by a radiative rate constant k_F typically 10^8 s^{-1} and a life time (τ) of the fluorescence which lies in the nanosecond (10^{-9} s) to microsecond (10^{-6} s) range.

If the radiation proceeds from an excited state with different spin multiplicity with respect to that of the lower state (*i.e.* $T_1 \rightarrow S_0$), the emission is called *phosphorescence*. In fact the triplet-singlet transition is spin-forbidden according to the *selection rules*, meaning that phosphorescence cannot be observed. However the transition becomes weakly allowed because of the spin-orbit coupling which permits the mixing of singlet and triplet states. As a consequence the phosphorescence does occur relatively slowly, with a typical timescale ranging from millisecond (10^{-3} s) to second. It is thus characterized by a radiative rate constant of phosphorescence k_p ranging from 10^3 to 10^0 s^{-1}.

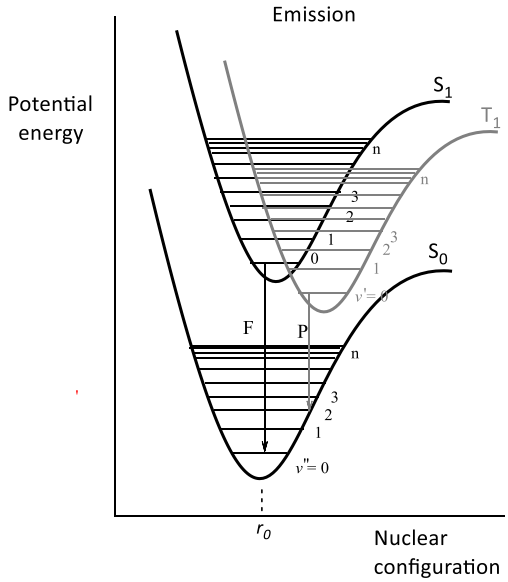

Figure 1.5. Diagram of potential wells of ground, singlet and triplet excited states showing electronic transitions corresponding to emission (F = Fluorescence, P = Phosorescence) represented by vertical arrows following the Franck-Condon principle.

According to the Franck-Condon principle (as previously mentioned for absorption transition), both radiative transitions (fluorescence and phosphorescence) are so fast that they are produced before changes in nuclear configuration. Minor changes in the bond lengths and angles are occurring. If we refer to a potential energy curve the most probable emissions will be those which occur "*vertically*" between states with different electronic configuration (Figure 1.5). The "vertical" transition refers to the arrow that should be drawn to represent the transition on potential energy curve *vs.* nuclear configuration as represented.

The rate of the vibrational and electronic–energy relaxation in excited states is very rapid (10^{-12} s to 10^{-10} s) compared to the rate of emission, thus the emission proceeds from the lowest vibrational level of the excited state $S_{1(v'=0)}$ to one of the S_0 state vibrational levels. Even when absorption occurs into higher excited state S_n, in most cases it relaxes to the S_1 state. These observations are known as the *Kasha's rule*. However in some special cases (*e.g.* azobenzenes)[8] Kasha's rule may not be respected. The Franck-Condon principle applied to absorption and emission in relation with Kasha's rule gives rise to the *mirror symmetry* (*i.e.* the emission spectra profile is the mirror image of the absorption spectra profile) which is found for many compounds (Figure 1.6b). The difference between the maxima of the lowest energy absorption and highest energy fluorescence bands is termed *Stokes shift* (named by the Irish physicist George G. Stokes), a parameter related to the reorganization energy of the molecule (see Figure 1.6b).

[8] Hoffman, D. P.; Mathies, R. A. *Phys. Chem. Chem. Phys.* **2012**, *14*, 6298.

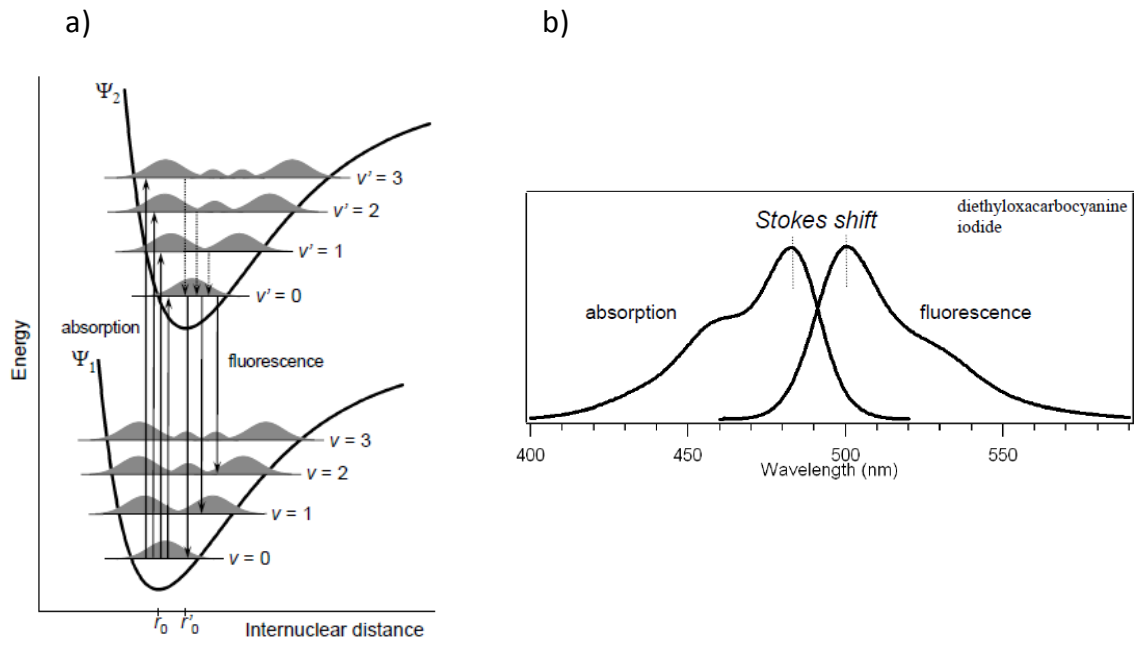

Figure 1.6. (a) Diagram wells representing the Franck-Condon principle and Kasha's rule for the absorption and fluorescence emission processes. (b) Example of an organic compound showing the mirror image of absorption and emission spectra and the Stokes shift.

2.2. Radiationless Transitions

Radiationless transitions are de-excitation pathways which do not result in the emission of photons. All the various photophysical processes that may occur after light absorption can be summarized in a Jablonski-Perrin diagram (Figure 1.7). The absorption of a photon, promotes the molecule to a singlet excited state S_n. It may return to a lower singlet excited state (*i.e.* S_1) without emitting a photon, thus converting the excitation energy into vibrational thermal energy. The transition is named *internal conversion* (IC) and involves the transfer of population (electron density) between electronic states with the same spin multiplicity. The nonradiative transitions are characterized as *"horizontal"* which means that they occur between quantum states with the same energy (isoenergetic levels).

The *intersystem crossing* (ISC) is another nonradiative process which proceeds between two isoenergetic vibrational levels of excited states with different spin multiplicity (*e.g.* $S_1 \rightarrow T_1$). We have to note that these transitions occur via spin-orbit coupling which is enhanced in molecules possessing "heavy atoms" (*e.g.* Br, I or transition metals). As a consequence the ISC rate constant of compounds containing heavy atoms is considerably higher ($k_{ISC} \approx 10^{10}$ to $10^{11} s^{-1}$) than for aromatic hydrocarbons ($k_{ICS} \approx 10^{6}\ s^{-1}$).

Since when T_1 state is populated by an intersystem crossing from S_1 state, it gains an excess of vibrational energy which is rapidly dissipated by collisions with the solvent molecules. According to the operation of Franck-Condon principle, all electronically excited states are produced with an excess of vibrational energy. In a solution phase, the excited molecule is relaxed to the lowest vibrational levels by *vibrational relaxation* (VR) after collision with the solvent molecules. In the case of vapor-phase compounds, where the collisions are not happening frequently, relaxation could be accomplished by emission of a photon.

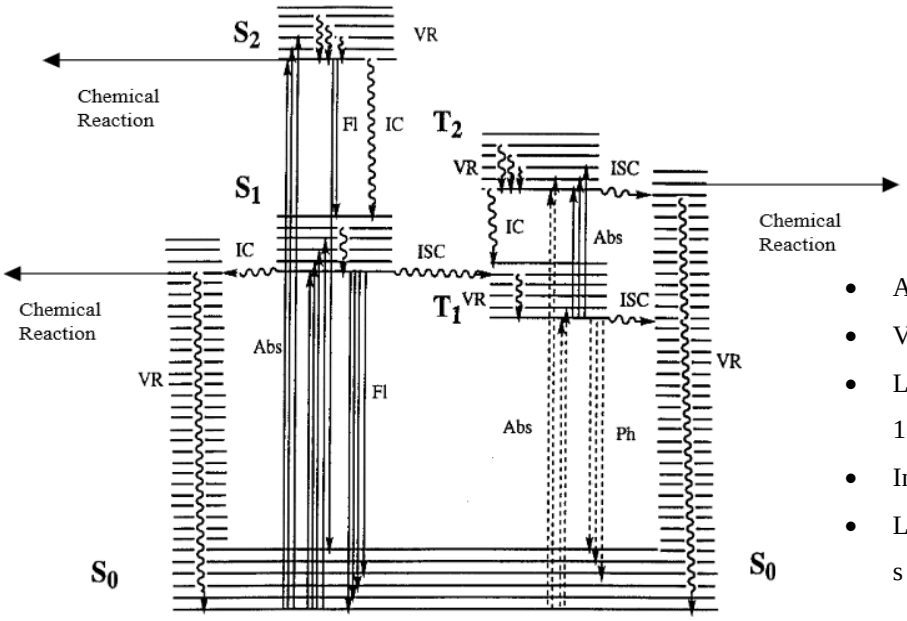

- Absorption: 10^{-15} s
- Vibrational relaxation: 10^{-10}-10^{-8} s
- Lifetime of excited state S_1: 10^{-10}-10^{-7} s (fluorescence)
- Internal conversion: 10^{-11}-10^{-9} s
- Lifetime of excited state T_1: 10^{-6}-1 s (phosphorescence)

Figure 1.7. Jablonski-Perrin diagram illustrating the various photophysical processes.

- *Parameters of emission radiation*

The principle parameters of the emission radiation are the quantum yield (φ) and the lifetime (τ) of the luminescent excited state. The emission efficiency is given by the quantum yield which is expressed by the ratio of number of photons emitted per time form the molecules (*n)* and the number of photons absorbed by a molecule per time (n_A):

$$\varphi_F = n_F/n_A \text{ (if emission is fluorescence)} \qquad \text{Eq. 1.4}$$

$$\varphi_P = n_P/n_A \text{ (if emission is phosphorescence)} \qquad \text{Eq. 1.5}$$

The lifetime of the fluorescence (τ_F) and phosphorescence (τ_P) emission is given as the inverse of the rate constant *k*:

$$\tau_F = {}^{1}/_{k_F} \qquad \text{Eq. 1.6}$$

$$\tau_P = {}^{1}/_{k_P} \qquad \text{Eq. 1.7}$$

Where k_F and k_p are the rates of fluorescence and phosphorescence respectively.

2.3. Quenching mechanisms

In fluid solution, when the lifetime of the excited state is sufficiently long (*i.e.* > 10 ns), the excited molecule can encounter another molecule and proceeds to dissipation of the excited energy through electron or energy transfer processes or triplet sensitization. Such processes may *quench* the luminescence of the excited molecule.

2.3.1. Energy Transfer Process

If a molecule is in proximity (or even covalently attached) to a suitable energy acceptor molecule, it is possible to transfer the excitation energy of the donor (D*) within the acceptor or quencher (A) as written above:

$$D^* + A \rightarrow D + A^*$$

In order for this mechanism to occur, the energy transfer must be faster than the lifetime of D* and the energy level of D* must be higher than that of A*. However, the acceptor can be in its ground or excited electronic state. The electronic energy transfer process may be radiative or non radiative.

- ***Radiative energy transfer***

Radiative energy transfer is a two step mechanism, involving first the emission of a photon by an excited donor molecule D* followed by the re-absorption of the emitted photon by the acceptor A.

$$\text{Step 1: } D^* \rightarrow D + h\nu$$

$$\text{Step 2: } h\nu + A \rightarrow A^*$$

The efficiency of radiative energy transfer is determined by four important factors: the quantum yield (φ_D) of D*, the concentration of A, the extinction coefficient (ε) of A and the overlap between the emission spectrum of D* and absorption spectrum of A as schematically depicted in Figure 1.8. This mechanism is favored when all these important factors are maximized. Thus, in optically dilute solutions the probability of radiative electronic energy transfer is negligible (*i.e.* A and D are very distant to each other).

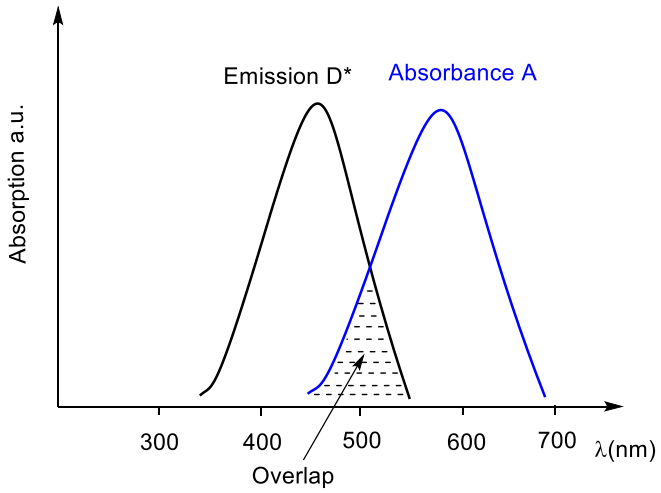

Figure 1.8 Schematic representation of the spectral overlap between the emission of D* and absorption of A.

- ***Nonradiative energy transfer***

In the case of a nonradiative energy transfer there is no fluorescence emission, nevertheless the spectral overlap of donor emission and acceptor absorption molecules is effective. This type of process involves specific interactions which may occur via collisions such as the electron clouds of donors and acceptors overlap significantly in space (electron-exchange process) or by dipole-dipole interactions (Coulomb interactions). The former is referred to as *Dexter mechanism* and the latter as *Förster mechanism*.

➢ *Dexter energy transfer mechanism*[9]

The Dexter excitation energy transfer involves an electron transfer mechanism between donor and acceptor moieties (Figure 1.9), which means that an important overlap between the wavefunction of the energy donor and energy acceptor is required. As a consequence the two molecular systems need to be in very short distance from each other (6-20 Å).

[9] Dexter, D. L. *J. Chem. Phys.* **1953**, *21*, 836.

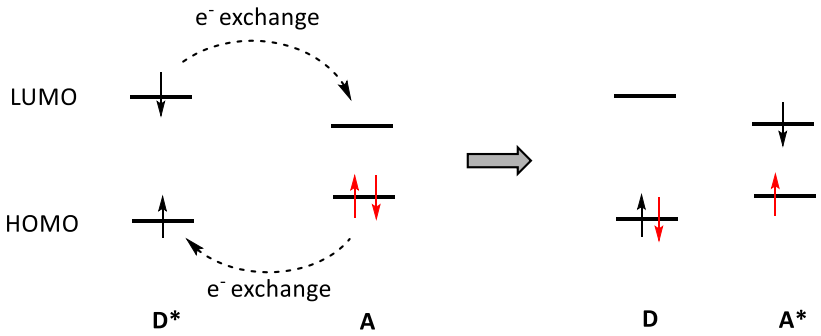

Figure 1.9. Concerted electron-exchange mechanism in Dexter energy transfer.

Once the donor energy is promoted to its excited state, there are different possibilities for the electron exchange to occur:

- *Concerted* manner, the excited electron of molecule D* jumps into the lowest unoccupied molecular orbital (LUMO) of A with simultaneous transfer of an electron from the highest occupied molecular orbital (HOMO) of A into the corresponding orbital on D.
- *Charge transfer* exchange, the process occurs in two steps via a radical ion pair.
- *Chemical or covalent bonding exchange of electrons, i.e.* the donor and acceptor exchange electrons because of the formation of a chemical bond via production of a diradical or zwitterions.

The rate of electron-exchange energy transfer determined by D. L. Dexter is given by:

$$k_{ET} = KJ\ exp\left(\frac{-2R_{DA}}{L}\right) \qquad \text{Eq. 1.8}$$

Where K is a collection of constants related to orbital interactions, J is the spectral overlap integral, R_{DA} is the donor acceptor distance and L is the sum of the Van der Waals radii of the donor and acceptor molecules.

- *Förster energy transfer*[10]

Fluorescence Resonance Energy Transfer (FRET) or Förster mechanism is another radiationless energy transfer process. The latter term is also usually used in the literature but it may somewhat induce some erroneous interpretation since fluorescence is not involved during the energy transfer. Unlike the Dexter mechanism, the Förster mechanism does not require close contact (wavefunctions overlap) of the interacting species for transfer of the excitation energy. The energy is transferred through "space" by dipole-dipole interactions and is also known as the

[10] Förster, T. *Ann. Phys.* **1948**, *2*, 55.

Coulombic mechanism. After absorption of light by D, the resulting excited D* and A interact together by Coulombic forces. The excited electron in the HOMO orbital of D*, represented as an oscillating dipole, perturbs the orbital motions (oscillations) of the electron into the HOMO of the acceptor. If resonance occurs then electrons of A oscillates more strongly leading to its jump into the LUMO of A (A→A*) while the excited electron of D* is relaxed into its ground state (D*→D) as schematically depicted in Figure 1.10. No double exchange of electrons occurs contrary to the Dexter-type mechanism.

Two conditions are necessary for A* to be produced, the resonance condition where $\Delta E(D^* \rightarrow D) = \Delta E(A \rightarrow A^*)$ and coupling of electron oscillating of D* and electrons of A.

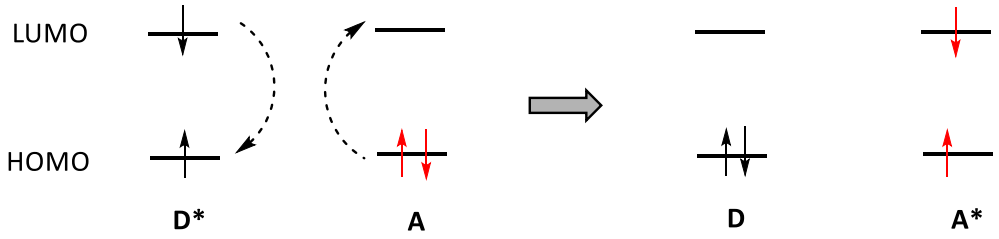

Figure 1.10 Schematic representation of Förster mechanism for electronic energy transfer.

As for the Dexter mechanism, the fluorescence is not involved in the dipole-dipole energy transfer, but the spectral overlap J of the D* emission with A absorption is a major requirement for the rate of energy transfer as shown by the equation:

$$k_{ET}(\text{Coulombic}) = k\frac{K^2 k_{\text{D}}^{\circ}}{R_{\text{DA}}^6} J(\varepsilon_{\text{A}}) \qquad \text{Eq. 1.9}$$

$$J = \int_0^{\infty} \left[\frac{f_D'(\sigma)\varepsilon_A(\sigma)}{\sigma^4}\right] d\sigma \qquad \text{Eq. 1.10}$$

k is a constant determined by experimental conditions (*i.e.* concentration, solvent refractive index), K^2 is a term that takes into account the orientation of the dipoles in space, $J(\varepsilon_{\text{A}})$ is the spectral overlap integral where the extinction coefficient of the A is included in the integration, k_{D}° is the pure radiative lifetime of donor and R_{DA} is the disctance of D* and A.

Where $f_D^{'}$ is the normalized emission of the donor :

$$f_D' = \frac{f_D(\sigma)}{\int_0^{\infty} f_D(\sigma) d\sigma} \qquad \text{Eq. 1.11}$$

2.4. The photo-induced electron transfer process

The Photoinduced Electron Transfer (PeT) is a second highly important emission quenching process. This phenomenon related to unimolecular systems is part of the work of this thesis. However, we shall discuss in this section first the photoinduced electron transfer in a general bimolecular system, where the molecules encounter by diffusion in solution. In polar solvents capable of solvating charged species (*e.g.* water, acetonitrile), the quenching of emission of species D^* by another species A, may involve an electron transfer process. The excited molecule (D^*) can transfer the excited electron to a vacant orbital of a molecule (A). The process is known as *oxidative quenching* (Figure 1.11a). The second possible process called *reductive quenching* corresponds to the transfer of an electron from species A into the vacancy created after electron excitation within the species D (Figure 1.11b).

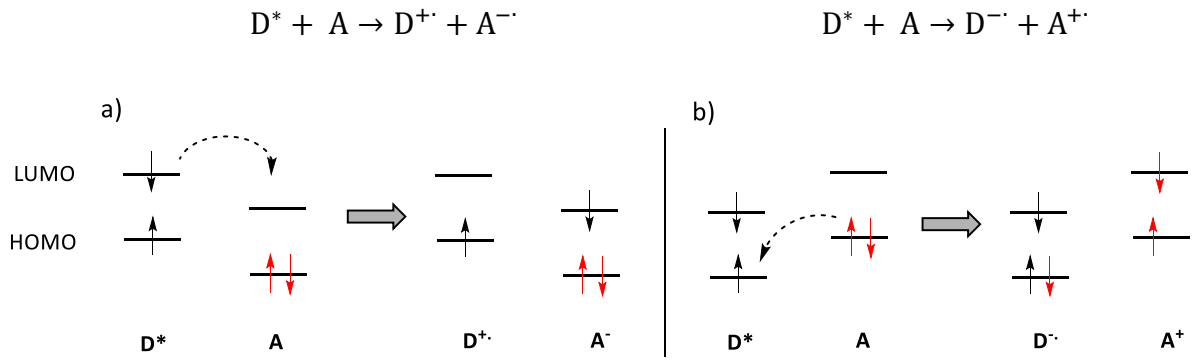

Figure 1.11. Schematic representation of the oxidative and reductive quenching mechanism.

We have to note that an excited state is both a stronger reductant and a stronger oxidant than the ground state because of the high level energy. However, the exact nature of the electron transfer process (oxidative or reductive) will depend on the redox properties of D^* and A. The driving force is determined by the positions of their frontier orbitals.

The photoinduced electron transfer process is most often interpreted by the classical electron transfer theory of Marcus.[11] Here, the chemical reactions are described by parabolic potential energy wells *vs.* reaction coordinates. The Product (P) may be obtained by shifting the parabola of the Reactant (R) in energy and reaction coordinates as depicted in Figure 1.12. The reaction will likely take place at the cross-point *i* corresponding to the transition state (the point where the reactant and product have the same configuration of nuclear coordinates).

[11] (a) Marcus, R. A. *Rev. Mod. Phys.* **1993**, *65*, 599. (b) Suppan, P. in *Topics in Current Chemistry*, **1992**, *163*, 95.

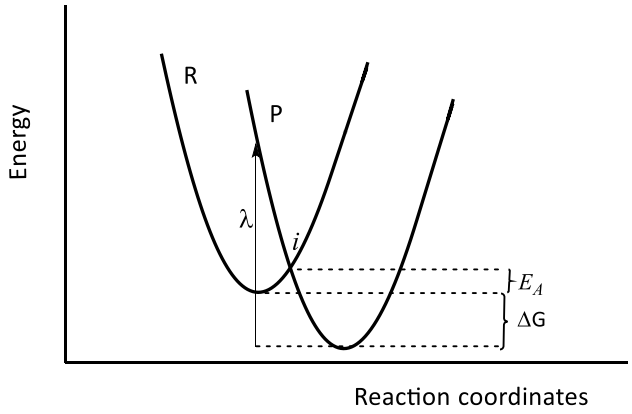

Figure 1.12. Potential wells of reactant and product in a PeT process.

In order for the eT to take place, an activation energy E_A depending on free energy (ΔG) and reorganization energy (λ) is necessary.

$$E_A = \frac{(\Delta G+\lambda)^2}{4\lambda} \qquad \text{Eq. 1.12}$$

The reaction free energies can be calculated from the Rhem-Weller equation[12] which is based on electrochemical and spectroscopic data. The equation relates the oxidation potential of the donor $E_{ox}(D)$, the reductive potential of the acceptor $E_{red}(A)$ and the energy of the excited state E^* and the Coulombic term *C* which describes the electrostatic interactions of the products.

$$\Delta G = E_{ox}(D) - E_{red}(A) - E^* + C \qquad \text{Eq. 1.13}$$

The rate constant of the PeT process is given by:

$$k_{eT} = K_{el}\nu_n exp\left[-\frac{(\Delta G+\lambda)^2}{4\lambda k_B T}\right] \qquad \text{Eq. 1.14}$$

Where K_{el} is the electronic transmission coefficient (describing the probability that the reaction occurs at the transition state and is assumed as unity in the classical theory), ν_n is the frequency of passage through the transition state, k_B is the Boltzman constant, *T* is the temperature.

2.4.1. Intramolecular photoinduced electron transfer

In order for a PeT to be efficient, the donor and acceptor moieties have to diffuse to each other to a short distance, meaning that a high concentration of the quencher and long lifetime of the excited species is required.

[12] Rhem, D.; Weller, A. *Israel J. Chem.* **1970**, *8*, 259.

In covalently linked systems or supramolecular assemblies based on coordinative interactions or hydrogen bonding these conditions are not required. We can more or less control easily the PeT efficiency by controlling the structural parameters (*i.e.* distance, mutual orientation and nature of the spacer) and thermodynamic parameters (*i.e.* excitation energy, redox potentials) of the D-A system.[13]

Photoinduced electron transfer is a highly important process found in nature for the accomplishment of the photosynthesis in plants and obviously has become one of the most studied subjects in contemporary science. Innumerable studies have investigated the factors that influence and govern this mechanism in rigid linked D-A dyads. Such molecular systems have played an important role in understanding the mechanism of the photoinduced electron transfer.[14,15,16,17] Designing bridged D-A systems for understanding the PeT phenomenon is the principal goal of the second chapter of this thesis.

The photoexcitation of a molecule can cause the transfer of an electron from the donor to the acceptor leading to a Charge Separated (CS) state. It appears from the numerous studies that the formation of intramolecular *exciplexes* is an important step for achieving a CS state. The *exciplex* is a complex of the D/A species which exists only in the excited state (D/A)*. It is a common excited state where the electron is delocalized within all the system. It can show a strong emission and it can decrease the overall activation energy of the electron transfer reaction and increase the electron transfer rate constant k_{eT} as depicted in Figure 1.13c.

[13] Marcus, R. A. *J. Chem. Phys.* **1956**, *24*, 966.
[14] Wasielewski, M. *Chem. Rev.* **1992**, *92*, 435.
[15] Gust, D.; Moore, T. A.; Moore, A. L. *Acc. Chem. Res.* **1993**, *26*, 198.
[16] Williams, R. M. *Photochem. Photobiol. Sci.* **2010**, *9*, 1018.
[17]Lemmetyinen, H.; Tkachenko, N. V.; Efimov, A.; Niemi, M. Phys. *Chem. Chem. Phys*. **2011**, *13*, 397.

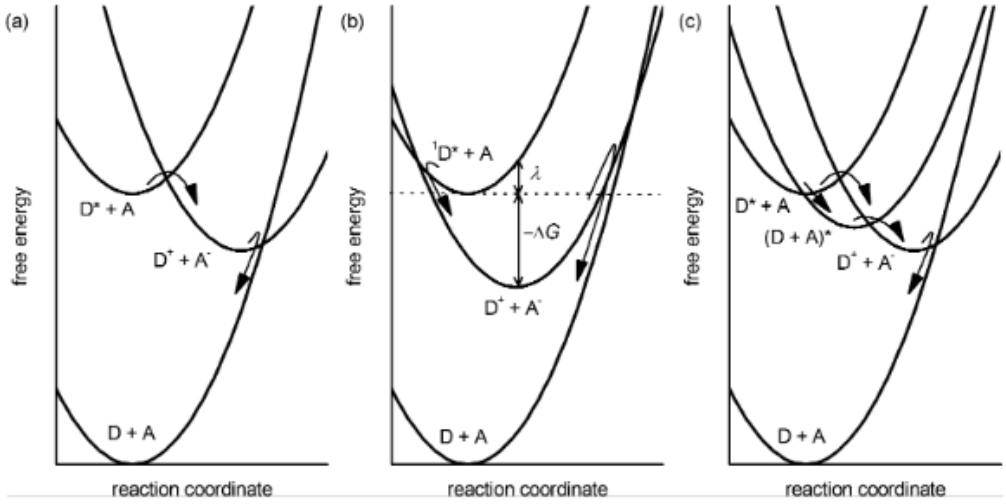

Figure 1.13. Gibbs free energy surface of eT and back eT processes. (a) eT in normal region and BeT in inverted region. (b) eT and BeT for decreasing the reorganization energy λ. (c) eT through formation of an exciplex intermediate. Figure reprinted from ref. [17].

2.5. Photochemical Reactions

For an excited molecule, the de-excitation pathway may occur with emission of luminescence (*i.e.* fluorescence or phosphorescence), or by a photochemical reaction. The latter may give rise to chemical transformations such as a change in conformation (*e.g. cis-trans* isomerization of stilbenes or azo-derivatives, *vide infra*) or bond making/cleaving (*e.g.* dithienylethenes or spiroxazines, *vide infra*).[3] This type of compound which is also known as *molecular switches*[18] will be seen in detail in § 3.4 dedicated to the different families of photochromic compounds.

3. Photochromism - A photochemical phenomenon

We shall present in this section the photochemical phenomenon of photochromism. The project around the phenomenon of photochromism was introduced very recently in LCOSA group. Hence, a discussion on why photochromic compounds are so attracting as well as a brief history of the field would be of interest. The different families of the photochromic compounds and finally some examples of photochromic switches will be described.

3.1. Introduction

During the past few decades a growing interest has been shown regarding molecules and assemblies which exist in two forms interconverting under external stimuli. The interesting point

[18] (a) Irie, M. *Chem. Rev.* **2000**, *100*, 1685. (b) Feringa, B. L. *J. Org. Chem.* **2007**, *72*, 6635.

is the fact that these types of compounds may represent two-bit logic elements (0 and 1) of nanoscopic size. Hence they can find potential applications in computing, molecular electronic and photonics.[19,20] Nevertheless, we have to note that nature has been using such systems for the accomplishment of important processes, *i.e.* photosynthesis and visual perception. One of the most convenient methods for inducing interconvertible rearrangements is by mean of light absorption that comes directly from sunlight or artificial sources (*e.g.* lasers).[21]

The transformation of a chemical species A into species B under electromagnetic irradiation at a given wavelength in a reversible manner and accompanied with changes in absorption spectra and physical properties is known under the name of *photochromism*. When the changes are induced thermally then the phenomenon is assigned as *thermochromism*. However the switching between two chemical species with different colors may be produced electrochemically by generation of species with different redox states (*electrochromism*) or by acidic treatment of a solution for a given molecule (*acidochromism*). In this thesis work we are concerned mainly with the phenomenon of photochromism which will be described in more detail later.

Currently all electronic digital devices such as computers, telephones and so forth use binary logic gate for information transmission, processing and storage. Logic gates function as switches whose output 0 or 1 depends on input conditions. Actually the structures of all electronic digital devices are based on silicon-circuitry which is attaining its physical limits of miniaturization and monetary restrictions.[22] Also the present data-recording techniques such as Compact Disks (CD) and Magnetoptical Disks (MO) etc. are attaining their limit of memory density capacity. To overcome some of the limits imposed by the silicon technology and those for increasing the memory density of optical devices, the design and investigation of new molecular switches systems has attracted much attention.[21,23] The design and synthesis of molecular switches which are sensible to light stimulus was very stimulating and attracting to us as well as numerous other research groups.

[19] Szacilowski, K. *Chem. Rev.* **2008**, *108*, 3481.
[20] Andréasson, J.; Pischel, U. *Chem. Soc. Rev.* **2010**, *39*, 174.
[21] Laser is the english acronym for Light Amplification by Stimulated Emission of Radiation.
[22] Tour, J. M. *Acc. Chem. Res.* **2000**, *33*, 791.
[23] (a)Tamai,N.; Miyasaka, H. *Chem. Rev*. **2000**, *100*, 1875. (b) Kawata, S.; Kawata, Y. *Chem. Rev.* **2000**, 100, 1777.

3.2. Brief history of photochromism[24]

For certain organic compounds in solution, others in the solid state, the reversible change in color under light irradiation dates back to over a century ago. The phenomenon was first reported by J. Fritsche in 1867; he observed the bleaching of an orange-colored solution of tetracene exposed to air in daylight and regeneration of the color of the solution after heating (Scheme 1.1).[25]

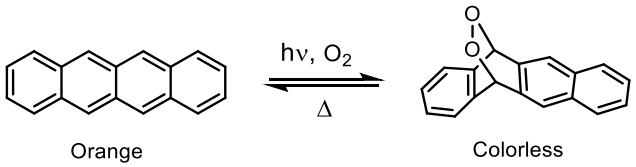

Scheme 1.1. Tetracene photobleaching and regeneration of color after heating.[25]

Further in 1899 W. Markwald reported the reversible change in color of 2,3,4,4-tetrachloronaphtalen-1(4H)-one (β-TCDHN) and the benzo-1-naphthpyridine in the solid state.

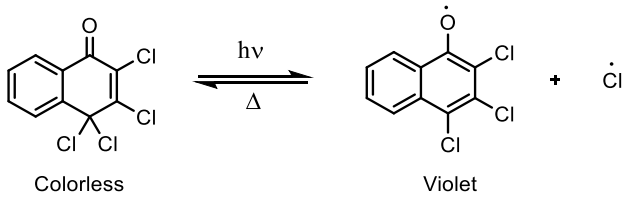

Scheme 1.2. Photochromism of β-TCDHN.[26]

After these investigations he named the phenomenon "*phototropy*".[26] Nowadays the term *phototropy* denotes biological phenomena.[27] It was used until Y. Hirshberg replaced it by "*photochromism*", a word deriving from Greek (*phos:* light and *chroma*: color), after his work on bianthrone derivatives in 1950 (Scheme 1.3).[28]

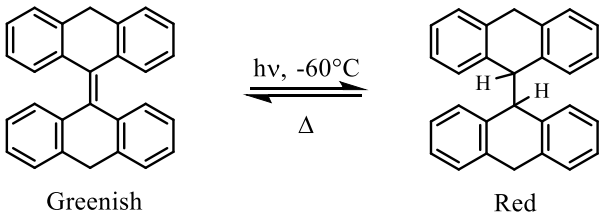

Scheme 1.3. Photochromism of bianthrone discovered by Hirshberg.[28]

[24] Bouas-Laurent, H.; Dürr, H. *Pure. Appl. Chem.* **2001**, *74*, 639.
[25] Fritsche, J. *Comp. Rend. Acad. Sci.* **1867**, *69*, 1035.
[26] Markwald, W. *Phys. Chem.* **1899**, *30*, 140.
[27] Phototropy relates to "*phototropism"* which defines the growth of plants in response to light.
[28] Hirshberg, Y. *Compt. Rend. Acad. Sci.*, **1950**, *231*, 903.

Until the year 1921 many other articles reporting photochromic compounds have appeared but they were restricted to synthesis and description of the phenomenon. From the year 1940 numerous investigations were carried out in order to get much more information about the mechanism of the photochromic reaction, about the intermediate species and the structure of the products and the photodegradation resistance. During the sixties, with the development of more sophisticated synthetic skills and characterization techniques (flash-photolysis, NMR, IR, X-ray) the photochromism enter a new area.

At this time, Corning Incorporated[29] manufactured the first photochromic sunglasses based on the redox properties of zinc or silver halides. When developing the organic photochromic *spiropyrans* (*vide infra*), Hirshberg suggested their use in data storage in 1956[30] and it is finally at the end of 1980 that Peter M. Rentzepis and co-workers[31] showed that photochromism could lead to 3D optical data storage. In the following years researchers and industrials have worked on the development of 3D data storage and new technologies. The photodegradation of organic photochromes (*i.e. spiropyrans*) used at that period limited the various applications. In 1980s the problem was highlighted with the synthesis of fatigue-resistant photochromes (*i.e. spiroxazines* and *2H-chromene, vide infra*). This allowed the commercial application of photochromic ophthalmic lenses. Since then, the interest in the design and synthesis of new photochromic systems, and obviously the number of publications increases exponentially.

3.3. Definition of photochromism

"Photochromism is a reversible transformation of a chemical species induced in one or both directions by absorption of electromagnetic radiation between two forms A and B, with different absorption spectra". [24]

[29] Corning Incorporated is an American manufacturer of glass, ceramic and related materials for industrial and scientific applications, known under the name of Corning Glass Work until 1989.
[30] Hirshberg, Y. *J. Am. Chem. Soc*. **1956,** *78*, 2304.
[31] Parthenopoulos, D. A.; Rentzepis, P. M. *Science*, **1989**, *24*, 843.

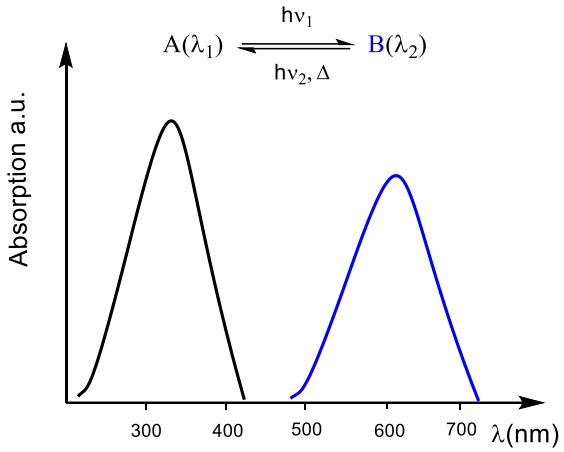

Figure 1.14. General representation of the absorption spectra of a photoinduced transformation of a species A into B.

Generally these transformations involve the coloration of colorless or pale yellow compounds under light irradiation. In this case the absorption spectrum of species B is shifted into the visible region (400-700 nm) while the absorption spectrum of A is in the near UV region. This is a coloration process and is referred to as *positive photochromism*. Though less common, transition from a colored to a colorless state $[i.e. \lambda_{max}(A) > \lambda_{max}(B)]$ is also possible and the photochromism is defined as *negative*. Rather than a transition between two species with dramatically different absorption spectra, the photochromism may involve the interconversion between two colored forms.

Reversibility is a parameter of crucial interest for photochromic transformations. The thermodynamically stable isomer A interconverts into isomer B which is less stable. Depending on the manner that B reverts back, we distinguish two types of photochromism:

- *Photochromism of T-type*, when the back return may be thermally and/or photochemically. This type of photochromism is thermally driven, but it can also be induced by light absorption.
- *Photochromism of P-type*, when it occurs exclusively photochemically. This means that the species B is thermally stable and the interconvertion into A take place by light (UV or visible) irradiation.

Photochromic transformations are *unimolecular* or *bimolecular* reactions. Unimolecular processes involve the interconvertion between two isomers. A bimolecular process which occurs less commonly, involves a photoinduced cycloaddition reactions and generally shows a negative photochromism *e.g.* the bleaching of the tetracene solution in daylight (*vide supra* § 3.2, Scheme 1.1).

3.4. Different families of organic photochromes

Several thousand organic photochromic systems have been elaborated since the early stage of the field. Despite the high number of such compounds, only several chemical reactions are known to be responsible for their photochemical behavior: *cis-trans* isomerization, pericyclic reactions, intramolecular hydrogen or group transfer, electron transfer and dissociation processes. Herein we shall describe some of the most studied photochromic molecules divided in families according to the reaction process they involve.

3.4.1. Cis-trans isomerization – azo compounds and stilbenes

The *cis-trans* photoisomerization of the N=N bond of *azobenzene* derivatives or C=C bond of *stilbens* gives rise to photochromic properties. This process is common also in azines, thioindigo derivatives as well as some natural molecules which will be discussed latter. Azobenzenes are highly investigated for applications such as high density data storage and nonlinear optics.[32]

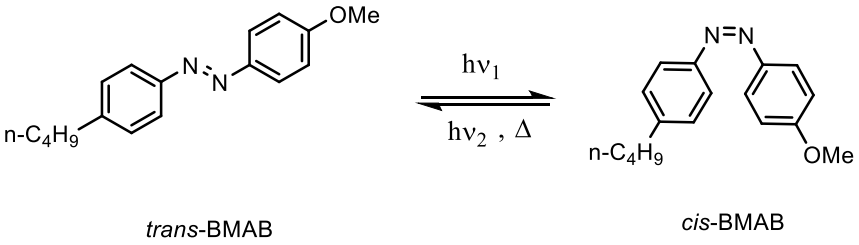

Scheme 1.4. Photoisomerization of *trans*-(4-butyl-4'-methoxyazobenzene), *trans*-BMAB.

Under UV irradiation their *trans*-form goes through the *cis*-form which is not thermally stable and reverts back in the dark. The *cis*-isomer of stilbenes is however, more stable than their azobenzenes counterpart. In addition, for both *trans*-isomers, the photochromic quantum yield is temperature dependent.

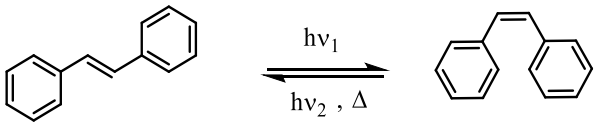

Scheme 1.5. Example of stilbene photoisomerization.

[32] (a) Ikeda, T.; Tsutsumi, O. *Science* **1995**, *268*, 1837. (b) Liu, Z. F.; Fujishima, A.; Hashimoto, K. *Nature* **1990**, *347*, 658. (c) Blanchard, P. M.; Mitchell, G. R. *Appl. Phys. Lett.* **1993**, *63*, 2038. (d)Spiridon, M. C.; Iliopoulos, K.; Jerca, F.A.; Jerca, V. V.; Vuluga, D. M. ; Vasilescu, D. S., Gindre, D. ; Sahraoui, B. *Dyes and Pigments*, **2015**, *114*, 24.

3.4.2. Intramolecular hydrogen transfer – Anils

Intramolecular hydrogen transfer is found in many photochromic compounds *e.g.* benzylpyridine, salycilate, triazole, oxazole etc. but herein only the class of *anil* [33] compounds is described. Anils are a class of Schiff bases[34] family obtained from the condensation of a primary amine (*i.e.* aniline derivative) with an aldehyde. Since the primary amine is an aniline derivative, the name of the final product is "*anil*". Upon photo-irradiation, anils undergo an *excited state intramolecular proton transfer* (ESIPT) from the *ortho*-hydroxy group to the nitrogen atom of imine fragment, inducing a tautomerization from the *enol* to the k*eto* form (Scheme 1.6). The *cis*-keto species which are formed subsequently after irradiation undergoes a photoisomerization to the *trans*-keto form. The *enol* is generally yellow and the *keto* tautomer goes generally from deep yellow to red due to the additional n-π*electronic transition involved in the *trans*-keto form.[34]

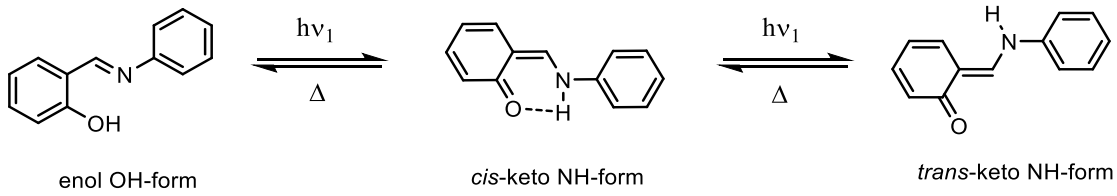

Scheme 1.6. Examples of photochromism of anil compounds.

3.4.3 Heterolytic bond cleavage – Spiropyrans, Spiroxazine and 2H-Chromens

The discovery of photochromism of *spiropyrans*[35,36] and recognition of the possibility for their uses in data storage by Hirshberg[37] stimulated an intensive interest around this phenomenon. Since then, *spiropyrans* are by far the most intensively studied family of organic photochromic compounds. However, more recently attention is turned to their congener *spiroxazines* and *diarylethenes* (*vide infra*). Spiropyrans (SP) and spiro[1,4]oxazine (SO) named spiroheterocyclic compounds, are the combination of two orthogonal π-moieties; indoline and pyran or oxazine for SP or SO respectively, connected through a tetrahedral carbon center (C2-position, Figure 1.15) termed spiro carbon (C_{spiro}).

[33] Hadjoudis, E. *Mol. Eng.* **1995**, *5*, 301.
[34] Schiff bases are secondary imines named after the German chemist Hugo Schiff, where the nitrogen atom of the C=N double bond is connected to an aryl or alkyl group, not to a hydrogen atom.
[35] Chaudé, O.; Rumpf, P. *C.R. Acad. Sci*. **1953**, *236*, 697.
[36] (a) Fischer, E.; Hirshberg, Y. *J. Chem. Soc.* **1952**, 4522. (b) Heilgman-Rim, R.; Hirshberg, Y.; Fischer, E. *J. Phys. Chem*. **1962**, *66*, 2470.
[37] (a) Hirshberg, Y. *J. Am. Chem. Soc*. **1956**, *78*, 2304. (b) Hirshberg, Y. *New Scientist* **1960**, *7*, 1243.

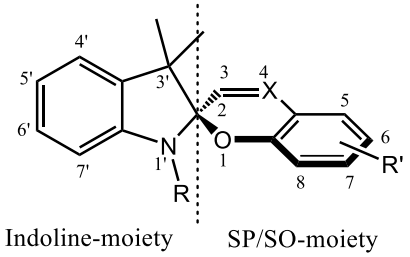

Figure 1.15. General chemical structure of a spiroheterocyclic compound.

Their capacity for being photochromic results from the cleavage of C_{spiro}-O bond upon irradiation, thus generating structural changes to form merocyanine (MC). This latter is characterized by a deep color due to the increased conjugation path in the open form. The deep colored merocyanine is an equilibrium mixture of geometrical conformations and mesomeric structures between a zwitterionic and a non charged *ortho*-quinoidal form as described in the scheme below:

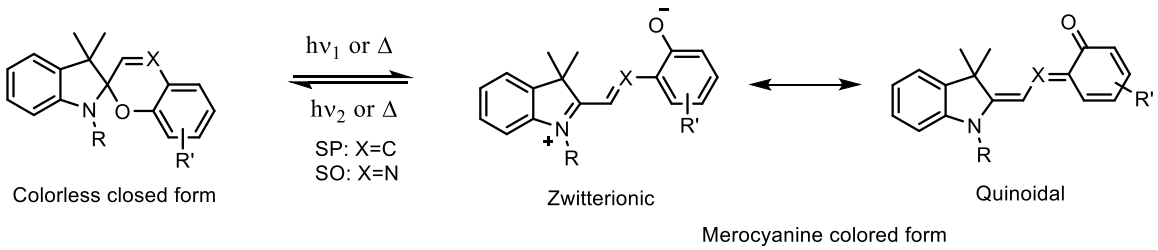

Scheme 1.7. Photochromism of spiroheterocyclic compounds.

2H-Chromens are photochromic molecules (Scheme 1.8), less known than spiropyrans and spiroxazine, consisting on a pyran connected to two substituents through the carbon spiro. The irradiation induces the rupture of C_{spiro}-O bond yielding a colored open form.

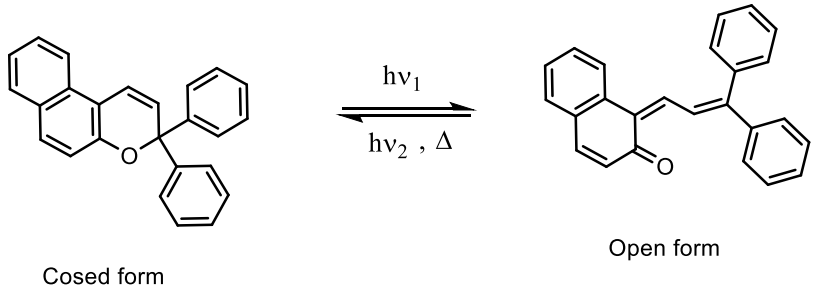

Scheme 1.8. Photochromism of 2*H*-chromen compounds.

The presence of a spiro center into the skeleton of the spiroheterocyclic compounds gives them a particular structure which allows a specific orbital interaction resulting (Figure 1.16a) in the partial donation of an electron lone pair of the nitrogen atom, to a vacant antibonding σ* orbital

of the C_{spiro}-O bond ($n_N \rightarrow \sigma^*_{CO}$). This interaction manifests itself in lengthening the C_{spiro}-O bond in spiropyrans and spiroxazines and is partially compensated by the donation of lone pair of oxygen to antibonding σ* orbital of C_{spiro}-N bond ($n_O \rightarrow \sigma^*_{CN}$) as shown in Figure 1.16b. The structural studies of a large variety of spiroheterocyclic molecules by X-ray crystallography have shown that the C_{spiro}-O bond lengths are considerably longer than normal Csp^3-O bond (1.41-1.43 Å).[38] They range in 1.45(2)-1.50(1) Å for spiropyrans and 1.45 -1.47 Å for spiroxazines according to X-ray studies reported.[39]

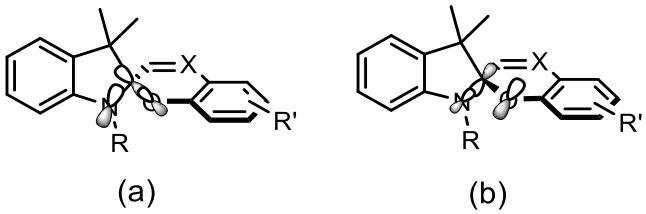

Figure 1.16.

It results from experimental observations that spiropyrans with C_{spiro}-O bonds which are longer than 1.42 Å, undergo thermal and photochemical isomerizations. Spiropyrans with shorter bond length, usually do not exhibit photochromic or thermochromic properties (example Figure 1.17).[39]

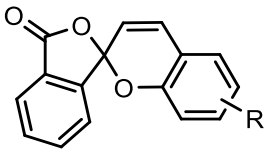

Figure 1.17. Example of spiropyrans that do not undergo thermochromic or photochromic properties where the C-O bond is in the range 1.39(9)-1.41(8) Å.

Spiroheterocyclic compounds are also known for being thermochromes, which means that structural rearrangements, accompanied by reversible color changes are induced thermally. The absorption spectra of the colored species are similar with the ones produced photochemically.

---

[38] (a) Aldoshin, S. M. In *Organic Photochromic and Thermochromic Compounds*, Crano, J. C., Guglielmetti, R. J., Eds.; Plenum Press: New York, 1999; Vol. 2, pp 297-392. (b) Aldoshin, S. M. *Ups. Khim*. **1990**, *59*, 1144 (English version in *Russ. Chem. Rev.* **1990**, *59*, 663). (c) Anisimov, V. M.; Aldoshin, S. M. *J. Mol. Struc.* (THEOCHEM). **1997**, *419*, 37. (d) Millini, R.; Del Piero, G.; Allegrini, P.; Crisci, L.; Malatesta, V. *Acta Crystallogr,. Sect. C : Cryst. Struct. Commun.* **1991**, *47*, 2567. (e) Gao, Y.; Zou, W.; Zhang, W.; Li, J;. Meng, J. Acta *Crystallogr., Sect. E (Struct. Rep. Online)* **2003**, *59*, 135.

[39] Karaev, S.; Furmanova, N. G.; Belov, N. V. *Dokl. Akad. Nauk SSSR*, **1982**, *262*, 609 (Russian version) found in: Minkin, V. I. *Chem. Rev.* **2004**, *104*, 2751.

- *Thermal equilibrum*

For most of spiropyrans and spiroxazines the photochromism is dependent on the polarity of the solvent. In particular in non polar solvents they exist in the closed form and in polar solvent they can go through the merocyanine open form thermally. The thermal equilibrium between the ring-closed and ring-open species depends on solvent polarity mainly, nature of the substituents and concentration of the solution. The cleavage of the C-O bond begins with the formation of a sterically strained chiral isomer which is followed by a series of *cis-trans* transformations leading to a final merocyanine with an interconverted chirality (*R* to *S*). The entire cycle (opening/closing) implies eight conformational isomers termed *cisoïds* and *transoïds*. The existence of the various merocyanine isomers is explained by the presence of the double bonds and the low stability of the conformers. However, the four *cis* (C) conformations are much less stable than their *trans* (T) counterpart.

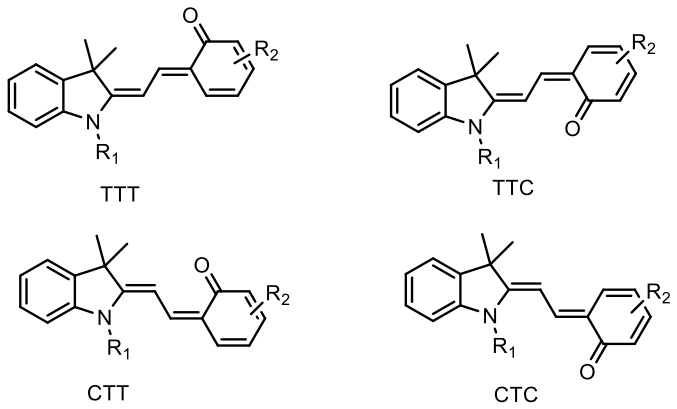

Figure 1.18. Some of the intermediates of SP and MC interconversion.

The structure dependence on the stability of the different isomers in the open or closed form has been studied in much detail for spiropyrans. It results that the half left part of the molecules does not greatly affect the equilibrium in non polar solvent, but so does the right part containing the pyran moiety. Electron-withdrawing substitutents in right part favor the stabilization of the open forms. The effect is maximal when strong electron-accepting groups are placed in *ortho* or *para*-position relative to the phenylate oxygen of the merocyanine.

Spiropyrans and spiroxazine are also *acidochromes*, they can be open under acidic treatment of the closed form, generating stable open forms (Scheme 1.9). The acidochromism of spiropyrans was introduced by Raymo and co-workers in 2008.[40] The back return may be achieved by light irradiation or basic treatment.

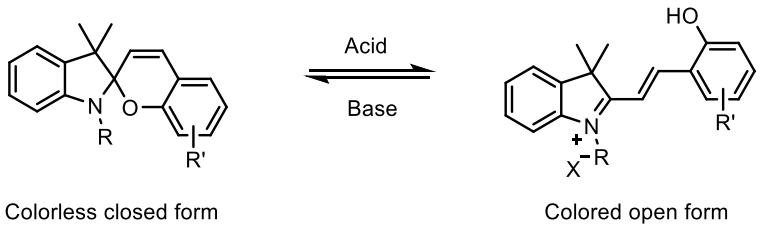

Scheme 1.9. Acidochromism of spiropyrans developed by Francisco Raymo.[40]

3.4.4. Ring closing photochromes – Fulgides and diarylethenes[41]

The photochromic properties of *fulgides* and *diaryethenes* arise from a photoinduced [1,6] electrocyclization reaction. Thus, the colorless open form undergoes ring cyclization upon UV irradiation generating a colored closed form with a higher conjugated pathway. They are both thermally stable and the interconversion within the initial state is exclusively photochemically under visible light irradiation.

Fulgides were discovered by Stobbe[42] over 100 years ago. They derive from bismethylene succinic anhydride where at least one of the substituent is an aromatic group as depicted in Figure 1.19.

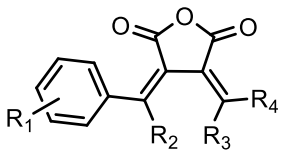

Figure 1.19. General chemical structure of fulgide compounds.

The 2-[1-(2,5)-dimethyl-3-furyl) ethylidene]-3-isopropylidenesuccinic anhydride (**F1,** Scheme 1.10) was the first example of a thermally irreversible fulgide and the first thermally irreversible

[40] Raymo, F.; Giordani, S. *J. Am. Chem. Soc.* **2001**, *123*, 4651.
[41] Tamai, N.; Miyasaka, H. *Chem. Rev***. 2000**, *100*, 1875.
[42] Stobbe, H. *Ber.* **1907**, *40*, 3370.

photochromic molecule ever reported, introduced by Heller and co-workers.[43] Because the aromatic group of this fulgide is a furan, it is termed furylfulgide.

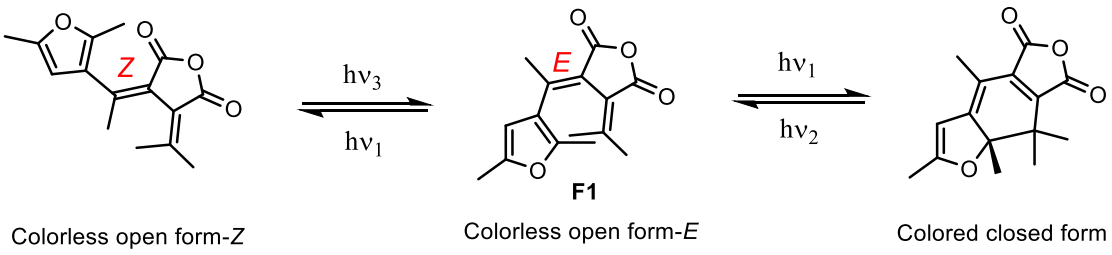

Scheme 1.10. Electrocyclic reaction of 2[1-(2,5-dimethyl-3-furyl) ethylidene]-3-isopropylidenesuccinic anhydride (**F1**).[22]

However, the cyclization process into these compounds enters in competition with the *cis-trans* isomerization of the aromatic substituted double bond, thus lowering the quantum yield of the photoreaction. Kurita and co-workers realized that the introduction of isopropyl group prevents the *E-Z* isomerization (Scheme 1.11), thus the electrocyclization take place from the *E* species.[44] Since the first synthesis of thermally irreversible fulgides, an important number of such derivatives has been synthesized and applied to optical devices and switches.[45]

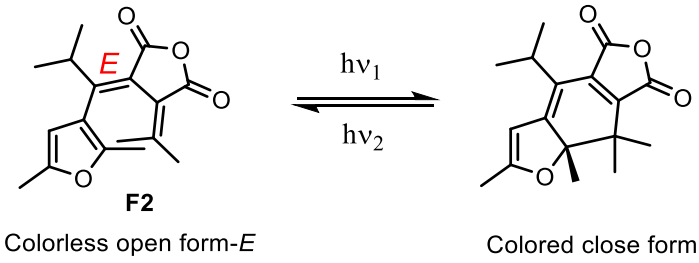

Scheme 1.11. Photocyclization process of 2[1-(2,5-dimethyl-3-furyl)-2-methylpropylidene]-3-isopropylidenesuccinic anhydride (**F2**).[22]

Diarylethenes consist in general in two aryl groups connected through a C=C bond in the *cis*-form. They derive from *cis*-stilbene which undergoes [1,6]electrocyclisation by irradiation.[46] In the presence of air the colored dihydrophenanthrene transforms irreversably through H_2 elimination, thus yielding the phenanthrene (Scheme 1.12).

[43] Heller, H. G.; Langen, J. R. *J. Chem. Soc., Perkin Trans. 2,* **1981**, 341.
[44] Kurita, S.; Kashiwagi, A.; Kurita, Y.; Miyasaka, H.; Mataga, N. *Chem. Phys. Lett*. **1990**, *171*, 553.
[45] Yokoyama, Y. *Chem. Rev.* **2000**, *100*, 1717.
[46] (a)Waldek, D. H. *Chem. Rev*. **1991**, 415. (b) Saltiel, J.; Sun, Y.-P. In *Photchromism: Molecules and System*; Durr, H., Bouas-Laurent, H., Eds., Elsevier: Amsterdam, 1990; p 64. (c) Mallory, F. B.; Mallory, C. W. *Org. React*. **1984**, *30*, 1.

The substitution of hydrogens on 2- and 6-positions with methyl groups, avoids the hydrogen-elimination step rendering the cyclization reaction reversible even in the presence of oxygen.

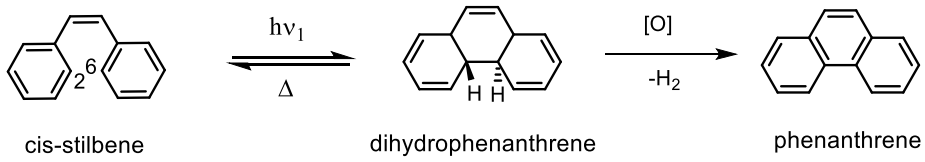

Scheme 1.12. Electrocylisation of *cis*-stilben followed by H_2 elimination step.

The pioneering work of Irie and co-workers[47] in the domain are noteworthy, because they developed the first photochromic diarylethenes thermally irreversible and fatigue-resistant, properties which are essential to applications in optoelectronic devices. They showed (Scheme 1.13) that diarylethenes with heteroaryl groups of low aromatic stabilization energy such as furan or thiophene have both isomers highly stable thermally and return to the initial open state only by irradiation, contrary to those containing phenyl or indol group.[48]

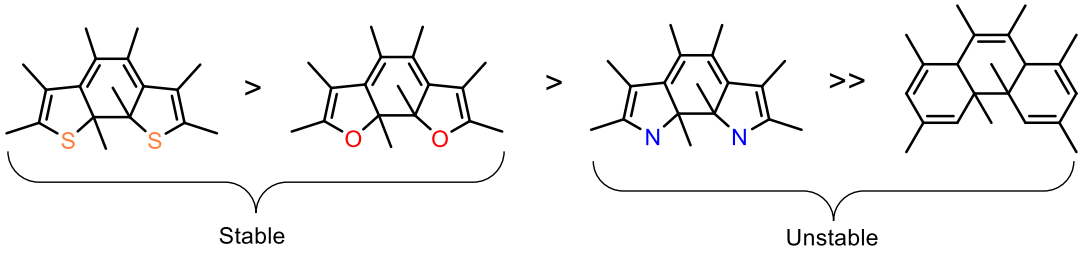

Scheme 1.13. Stability of diarylethenes containing heteroaryl groups.

In order to avoid the competition between *cis-trans* isomerization of the C=C bond and 6π-electrocyclization process, a cyclopentene (*i.e.* perfluorocyclopentene **D1**, maleic anhydride **D2** or cyclopentene **D3**) is introduced in the double bond (Scheme 1.14). It has been shown that some diarylethenes undergo ring-closing and ring-opening process even in the crystalline phase, while this phenomenon is unusual in the solid state.[49,50]

[47] Irie, M. *Jpn. J. Appl. Phys*. **1989**, *28*, 215.
[48] Irie, M. *Chem. Rev.* **2000**, *100*, 1685.
[49] Irie, M. *Pure. Appl. Chem*. **1996**, *68*, 1367.
[50] Irie, M.; Uchida, K.; Eriguchi, T.; Tsuzuki, H. *Chem. Lett*. **1995**, 899.

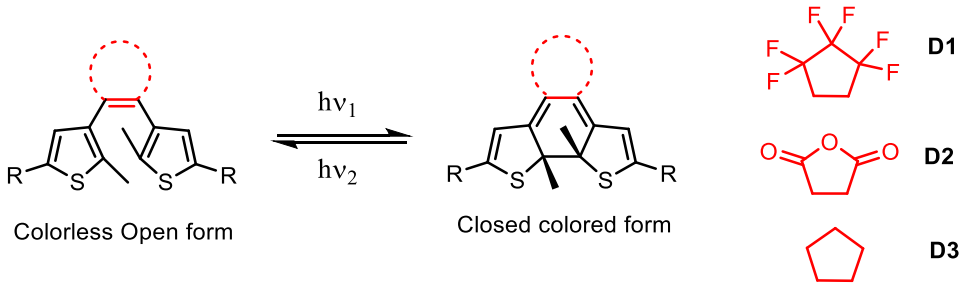

Scheme 1.14. Photocyclization of dithienylethenes **D1**, **D2**, **D3**.

3.4.5. Natural organic photochromes

The phenomenon of the reversible change in color is also found in nature as for example the rhodopsine (the pigment of vision), bacteriorhodopsine and the phytochrome in plants. Rhodopsine and other natural organic photochromes are very difficult to be extracted with organic solvent and make possible their characterization; however the bacteriorhodopsine protein is nowadays well known.

- *Rhodopsin*[51]

The rhodopsin is a photosensitive pigment found in the rods of retina, first discovered by Boll (1877) in frog retina. This pigment is a complex of a chromophore *i.e.* 11-*cis*-retinyl and *opsin* protein attached together in a Schiff base linkage through an amino group of lysine (Scheme 1.15). It has a deep reddish-purple color in the dark and yellow after exposure to visible light. The change in color is due to photo-isomerization of 11-*cis*-retinyl (λ_{abs} = 498 nm) to all-*trans*-retinal (λ_{abs} = 387 nm) occuring *via* four steps, defined by Professor G. Wald.[52] Herein, the process is simplified showing only the final all-*trans*-retinal chromophore.

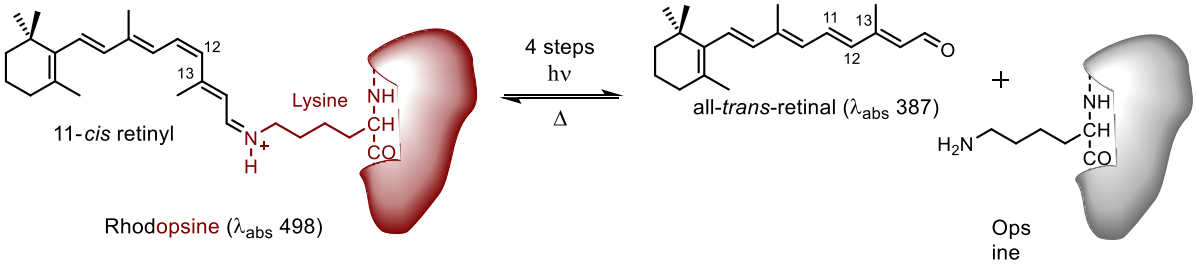

Scheme 1.15. Photochromic cycle of the rhodopsin.

[51] Seliger, H. H. and McElroy, W. D. *Light: Physical and Biological Action*, Academic press, New York and London, I[st] ed., **1965**.
[52] Wald, G. *Science*, **1968**, *16*, 231.

- *Bacteriorhodopsine*[53]

Bacteriorhodopsine, a rhodopsine-like protein isolated from the purple membrane of *Halobacterium halobium* bacteria,[54] is one of the key proteins known for their photosynthetic capabilities. It is actually one of the most studied natural photochromic molecules and has found applications in optical logic and information storage devices.[55,56]

- *Phytochrome (P)*[57]

The phytochromes are photosensory proteins which control the photomorphogenesis (*i.e.* intensity, duration and color of environmental light) in plants. For sensing red light, the plants use phytochromes (P) possessing a covalenty linked tetrapyrrole (bilin) chromophore (phytochromobilin) which is bound to the protein through a cystein as shown in Figure 1.20a. As depicted in Figure 1.20b, the physiologically inactive form P_r absorbs red light (660 nm) and interconverts into the active form P_{fr}. The later absorbs in the far-red region (730 nm) and reverts back to the initial inactive form thermally or under irradiation with far-red light.

It is well established now that inactive chromophore form (P_r) adopts the C5-*Z,syn*/C10-*Z,syn*/C15-*Z,anti* conformation shown in Figure 1.20a. Supported by recent theoretical studies, the photoconversion is accepted to involve an isomerization from *Z* to *E*-configuration around the C15-C16 double bond. However, this is not definitely elucidated. Certainly, the illumination under red or far-red light induces important changes in the conformation and subsequently the activity of the protein into which is bound the phytochrome.

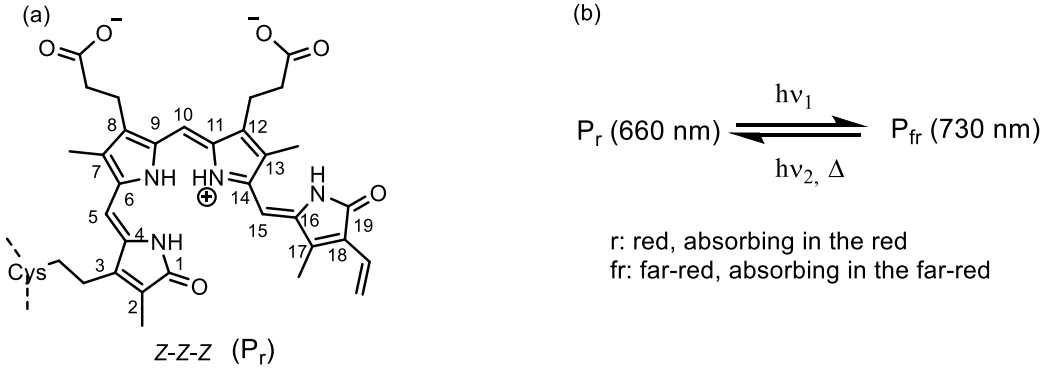

Figure 1.20. (a) Structure of the Phytochrome P_r absorbing at 660 nm. (b) The photochromic reaction of P.

[53] Hampp, N. *Chem. Rev*. **2000**, *100*, 1755.
[54] Oesterhelt, D.; Stoeckenius, W. *Nature New Biology*. **1971**, *233*, 149.
[55] Szacilowski, K. *Chem Rev*. **2008**, *108*, 3481.
[56] Hampp, N. *Chem. Rev.* **2000**, *100*, 1755.
[57] Rockwell, N. C.; Lagarias, J. C. *Plant Cell*, **2006**, *18*, 4.

3.4.6. Inorganic and organometallic photochromes

Inorganic salts such as silver halides (*e.g.* AgCl) and zinc halides (*e.g.* ZnCl) also show photochromic properties and are largely used in manufacturing of photochromic lenses. They are embedded in a borosilicate or aluminophosphate glass matrix and are susceptible to oxidation and reduction by light illumination as depicted below for AgCl:

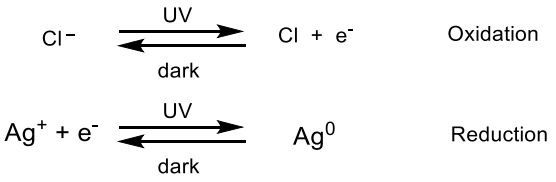

Scheme 1.16. Redox process of AgCl embedded in glass matrix.

Under light irradiation, the silver cations are reduced in the presence of chloride anions which can transfer an electron. As a consequence the atomic silver forms aggregates and darken the glass. The process is reversible in absence of light. Organometallic photochromes are rarer compared to organic photochromes; nevertheless some examples of ruthenium sulfoxide complexes are reported in the literature.[58]

3.5. Parameters of photochromism

Herein we shall describe some important parameters which characterize the phenomenon of photochromism.

- *Colorability*

Describes the ability of a colorless solution or a slightly colored solution to coloration. In diluted solution, after photolysis the absorbance (A_0) is proportional to the quantum yield of coloration (Φ_{col}), molar absorption coefficient (ε_B) and concentration of the colorless species (C_A) at a given wavelength of irradiation.

$$A_0(\lambda) = k\Phi_{col}\varepsilon_B C_A \qquad \text{Eq. 1.15}$$

- *Fatigue resistance*

[58] McClure, B. A.; Rack, J. J. *Eur. J. Inorg. Chem.* **2010**, 3895.

Over time, the photochromic systems may decompose (usually they undergo oxidation) and loose performance. The term used for this is "*fatigue*", and the class of diarylethene family displays high resistance.

- *Number of cycles*

In a *cycle*, considering the different conditions (solution, concentration and temperature) the species A undergo photochemical transformation in species B and revert back thermally or photochemically in A form. Ideally, the two reactions should be quantitative, but byproducts are formed from side reactions. If *X* is the degree of degradation in a cycle, the nondegradated fraction after *n* cycles is given by:

$$Y = (1 - X)^n \qquad \text{Eq. 1.16}$$

If *X* is very small and *n* very large, the equation can be approximated to Eq. 1.17.

$$Y = 1 - nX \qquad \text{Eq. 1.17}$$

- *Cyclability* (Z_{50})

Z_{50} is the number of cycles required to reduce the initial absorbance by 50 % at a given wavelength.

- *Half-time* $\left(T_{1/2}\right)$

$T_{1/2}$ is the time necessary for thermal bleaching to half of the absorbance of the colored form at a specific wavelength during one cycle.

- *Readout number/Non destructive readout capacity*

This parameter is the number of readings under continuous irradiation and is very important for ROM (read only memory) devices. It means that the information can be erased when necessary but is not destroyed by the readout.

3.6. The use of photochromic units for molecular photo-switches

The first applications of the photochromic compounds were focused on exploring their capacity of reversible change of color. Taking due account of this property they were and continue to be largely used in ophthalmic lenses or eye glasses, in cosmetics, toys etc. Nevertheless, since Rentzepis reported their capacities for uses in 3D optical storage, the interest in such molecules

has taken another dimension, being oriented toward the enhancement of new technologies. Modern investigations in conjunction with innovative synthetic chemistry are involved in understanding of the physical-chemical properties (*i.e.* emission, refractive index, dipolar moment and conductivity) associated with the photoinduced structural changes of the photochromic molecule.[59] Herein we shall focus only on the ability of emission switching.

3.6.1. Fluorescent switching

The photoirradiation of a photochromic compound induces structural and electronic modifications which can alter the intrinsic ability of one of the isomers to emit light. One of the species has significant quantum yield of florescence, while the other one does not emit. The scheme below indicates an example of a dithienylethene compound which is highly fluorescent in the open state ($\varphi_F = 0.46$) and non fluorescent in the closed state ($\varphi_F = 0.015$).

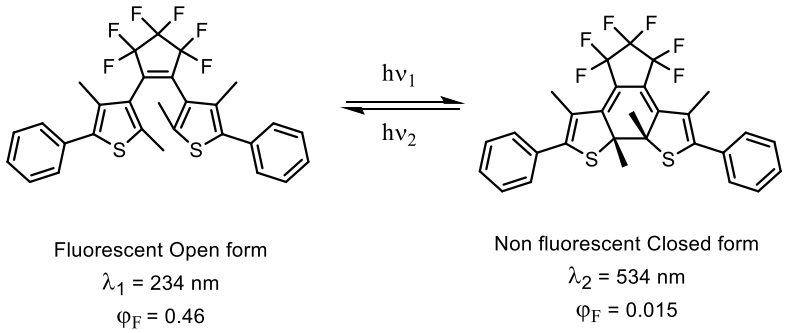

Scheme 1.17. Example of a dithienylethene showing a switching of emission in its closed form after irradiation in 1,2-dichloroethane solution.

This is an example of an intrinsically fluorescent photochromic molecule, but they can also be covalently connected to another fluorophore unit and control the emission intensity of the latter by optical stimulations. Effenberger is indeed the first who combined the photochromism to the fluorescence in order to use them for a direct control of the electronic energy transfer process.[60] In the system they synthesized, two fluorophore moieties (9-anthracene unit and coumarin unit) are covalently attached to a central fulgide (Scheme 1.18).[61] The energy is transferred from the donor anthracene moiety to the push-pull coumarin acceptor fluorophore only when the fulgide is in its open form, as described in the scheme below.

---

[59] Barachevsky, V. A. *Int. J. Photoenergy*, **1999**, *1*, 1.

[60] Walz, J.; Ulrich, K.; Port, H.; Wolf, H. C.; Wonner, J.; Effenberger, F. *Chem. Phys. Lett*. **1993**, *213*, 321 found in : De Silva, A. P.; Nimal Gunarante, H. Q.; Gunnlaugsson, T.; Huxley, A. J. M.; McCoy, C. P.; Rademacher, J. T.; Rice, T. E. *Chem. Rev.* **1997**, *97*, 1515.

[61] Krayushkin, M. M.; Barachevsky, V. A. ; Irie, M. *Heteroatom chem.* **2007**, *18*, 557.

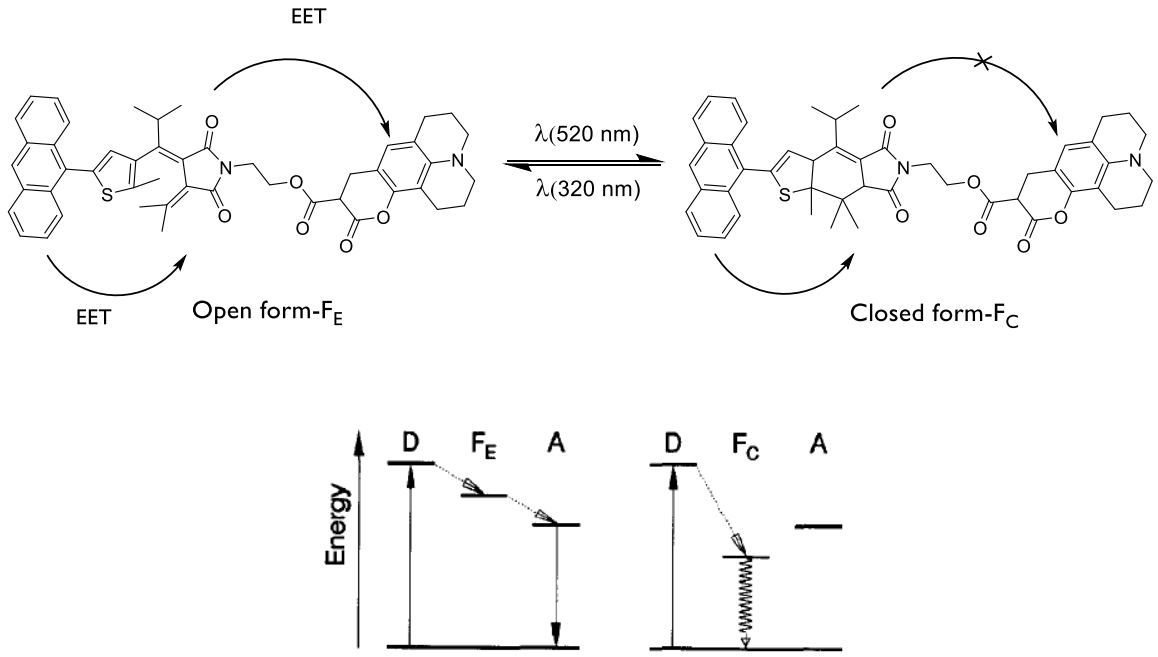

Scheme 1.18. The photo-switch triad reported by Effenberger et *al.*.[60] The anthacene (donor energy) is attached to the coumarin (energy acceptor) through a central fulgide. In the F_E form the acceptor display the lower energy level while in the F_C form the closed fulgide has the deepest energy level. Figure adapted from ref. [60].

More recently Feringa et *al.*[62] have published the synthesis of a donor-acceptor system that allows the modulation of the energy transfer by introducing a switchable molecule thereby allowing the emission output. The donor is a coumarin moiety and the acceptor a perylene bisimide moiety attached to a central dithienylcyclopentene photochrome (Scheme 1.19).

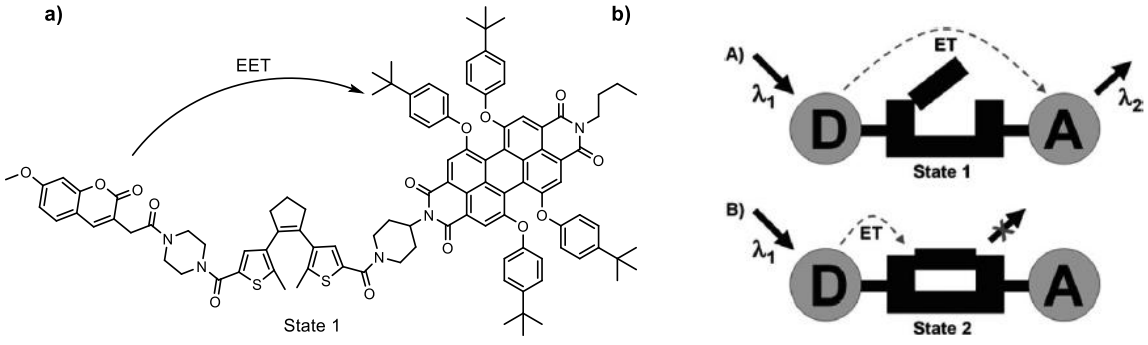

Scheme 1.19. (a) The donor-dithienylcyclopentene-acceptor triad synthesized by Feringa et *al.*.[62] (b) Schematic representation of the triad in two different states: (A) open state of the photochrome allowing for EET transfer and (B) closed photochrome prevention of emission from the acceptor by quenching from the central unit. Figure partially printed from ref. [62].

[62] Hurenkamp, J. H.; de Jong, J. J. D.; van Esch, J. H.; Feringa, B. L. *Org. Biomol. Chem.* **2008**, *6*, 1268.

3.6.2. Luminescence of metal complexes anchoring photochromic units

Considering the large variety of properties of metallic complexes (optical, electric, magnetic or redox), their combination with organic photochromes in view to photoswitch the properties of the metal centers or to merely study their impact in the photochromic behavior is attracting much interest. Prof. J.-M. Lehn was among the first who have associated the photochromism to organometallic complexes. Fifteen years ago A. Fernández-Acebes and J.-M. Lehn reported some novel dithienylethene-tungsten, rhenium and ruthenium complexes (Figure 1.21).[63] Their compounds were found to display fluorescence discrimination between the two photochromic states (open and closed form) when excited with wavelengths that almost did not affect the state of the photochromic system.

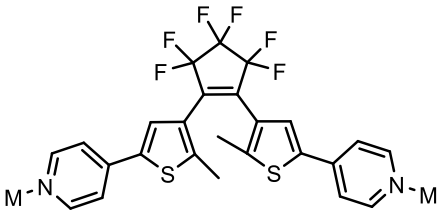

a) M = $Re(bpy)(CO)_3(CF_3SO)_3$
b) M = $W(CO)_5$
c) M = $Ru(NH_3)_5(PF_6)_2$

Figure 1.21. Photochromic diarylethene bearing metallic units reported by F.-Acebes and Lehn.[63]

They utilized the emission from the metal center which is coordinated to a pyridyl dithienylethene moiety. The problem with these systems is that the excitation of the fluorophore cannot be addressed independently by a specific wavelength of light. Utilizing the same pyridyl-derivatized photochromic core used by J.- M. Lehn, Norsten and Branda reported two years latter an optical switch based on the phosphorescence of a ruthenium porphyrine complex axially coordinated to pyridyl dithienylethene ligands as demonstrated in Scheme 1.20.[64] The open form reverts to the closed form when irradiated with 365 nm light with a conversion rate of 95 % while the closed isomer reverts back to the open one when irradiated with visible light (470-685 nm).

[63] Fernández-Acebes, A.; Lehn, J.-M. *Chem. Eur. J*. **1999**, *5*, 3285.
[64] Norsten, T. B.; Branda, N. R. *Adv. Mater*. **2001**, *13*, 347.

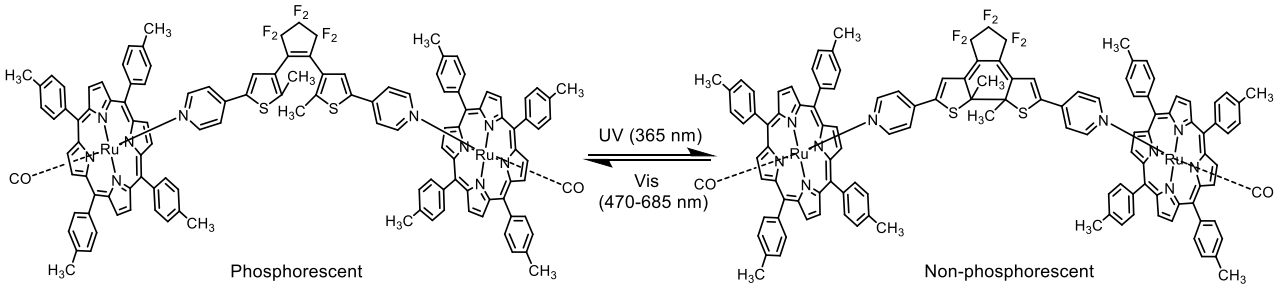

Scheme 1.20. The phosphorescent optical switch presented by Branda and Norsten.[64]

The open ring phosphoresced at 730 nm when excited with 400-480 nm; the closed ring did not. For this system, it is interesting to note that excitation with 400-480 nm light did not affect the photochromic reaction. As a result it can be promising for optical storage devices because it provides a non-destructive readout capability.

Taking inspiration from the work of Professors Branda and Norsten, De Cola *et al.*[65] reported in 2004 on the synthesis and optical properties of photochromic diarylethene containing covalently attached ruthenium(II) or osmium(II) complexes with polypyridine ligands. The interesting point noted in their work is the photocyclization of diarylethene core from a triplet state contrary to the singlet state photocyclization observed usually.

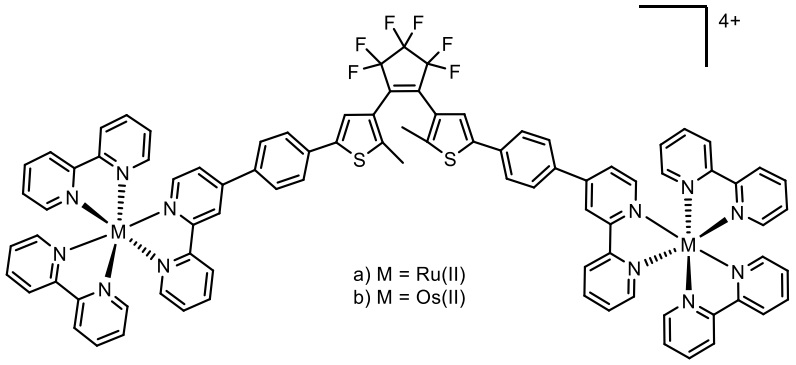

Figure 1.22. Photochromic diarylethene bearing Ru^{II}/Os^{II} complexes reported by De Cola *et al.*.[67]

The metallation of a photochromic compound may also be used to directly tune the properties of the compound. Frank *et al.* have synthetised a hybrid organic photochromic metal complex and have investigated the effect of the metal on the photochromic behavior of the spiroxazine (Scheme 1.21).[66]

[65] Jukes, R. T. L.; Adamo, V.; Hartl, F.; Belser, P.; De Cola. L. *Inorg. Chem.* **2004**, *43*, 2779.
[66] Paquette, M. M.; Patrick, O. B.; Frank, N. L. *J. Am. Chem. Soc.* **2011**, 133, 10081.

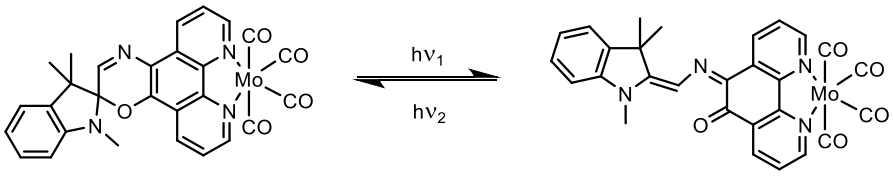

Scheme 1.21. Photoresponse of the hybride spiroxazine-Molybdenum complex reported by Frank et *al.*

4. The Julolidine - A key structural skeleton

In this section we shall present the julolidine, molecule which we have been exploring throughout this doctoral thesis as the key component of the final compounds. A brief historical view and various synthesis paths of julolidine-derivatives will be described as well as some important applications.

4.1. Historical background[67]

The *julolidine* (2,3,6,7-tetrahydro-1*H*,5*H*-benzo[*ij*]quinolizidine) as well as *lilolidine* (1,2,5,6-tetrahydro-4*H*-pyrrolo[3,2,1-*ij*]quinoline) are synthetic alkaloids[68] deriving from *quinolizidine*, a key fragment present in numerous natural alkaloids skeleton[69] and in many pharmacological applications such as thrombin inhibitors[70] and anticoagulants agents[71] (Figure 1.21). Their basic skeleton is constructed around three fused cycles containing a locked nitrogen atom. Julolidine was first synthesized in 1892 by Pinkus when he reacted 3-chloro-1-bromopropane with 1,2,3,4-tetrahydroquinoline.[72] Therefore the name "julolidine" which does not originate from plants as it is the case for many alkaloids was given by Reissert in 1893.[73]

---

[67] "*The synthesis of potential anti-parasitic compounds*", Dr. Rakesh Bhupatrai Bhatt, PhD thesis dissertation, 2001.

[68] Alkaloids are secondary metabolites produced by living systems based on cyclic nitrogen-containing compounds.

[69] Shen, L.; Ye, Y.-H.; Wang, X.-T.; Zhu, H.-L.; Xu, C.; Song, Y.-C.; Li, H.; Tan, R.-X. *Chem. Eur. J.* **2006**, *12*, 4393.

[70] Brundish, D.; Bull, A.; Donovan, V.; Fullerton, J. D.; Garman, S. M.; Hayler, J. F.; Janus, D.; Kane, P. D.; McDonnell, M.; Smith, G. P.; Wakeford, R.; Walker, C. V.; Howarth, G.; Hoyle, W.; Allen, M. C.; Ambler, J.; Butler, K.; Talbot, M. D. *J. Med. Chem.* **1999**, *42*, 4584.

[71] Heissböck, R.; Wolf, C.; Richter, E.; Hitzler, M.; Chiba, P.; Kratzel, M.; Ecker, G. *J. Med. Chem.* **1999**, *42*, 1921.

[72] Pinkus, G. *Ber*. **1892**, *25*, 2798.

[73] (a) Reissert, R. *Ber*. **1893**, *26*, 1291. (b) Mann, F. G.; Smith, B. B. *J. Chem. Soc.* **1951**, 1898.

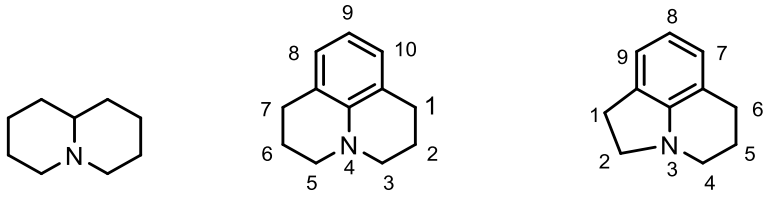

Figure 1.23

In the recent years the reputation of diverse alkaloids concerning their pharmacological properties has increased. As such, it has attracted an interest in designing new modern drug molecules with structural similarities to alkaloids or their synthetic analogues. The julolidine skeleton appears in many natural products (*i.e.* annotinine and lycopodine shown in Figure 1.23) which belong to the *Lycopodium* alkaloids family. They were isolated and characterized first by Manske and Marion.[74] Note that members of this family are known to have cardiovascular and neuromuscular benefits. Hence, compounds containing julolidine ring skeleton, seem to be interesting for exploring their pharmacological and toxicological activities.

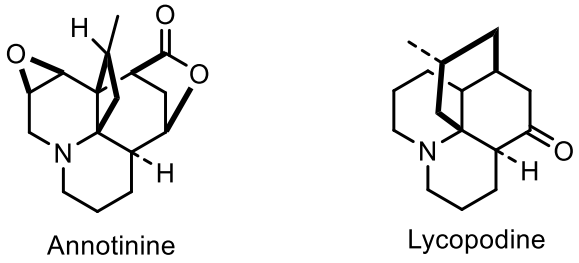

Figure 1.24

The Julolidine ring has a similar chemical structure with N,N-alkylated aniline. In the former two N-alkyl chains undergo bis-annulation back to the aromatic ring locking the nitrogen lone pair into conjugation with the aromatic cycle, thus leading to unusual properties. Mainly due to this efficient π-conjugation, molecular systems constructed around julolidines derivatives are also useful as dyes which may exhibit interesting biological activities or used for applications in optoelectronic devices.[75] It appears from the work of Castelino and co-workers that the conjugation of nitrogen lone pair with the benzene ring in lilolidine analogues (see Figure 1.23 for lilolidine chemical structure) is less efficient compared to julolidines because in the former,

[74] Manske, R. H. F.; Marion, L. *Can. J. Res*. **1943**, *21B*, 92.
[75] Balaganesan, B.; Wen, S.-W.; Chen, C. H. *Tet. Lett.* **2003**, *44*, 145.

the nitrogen is twisted from the optimum position of conjugation.[76] As a result, the julolidine compounds are more attractive for the elaboration of advanced dyes.

4.2. Synthesis of julolidine

The first synthesis was reported by Pinkus, but later by Glass and Weissberger[77] which improved the yield of the same reaction by refluxing the reactants during 20 hours.

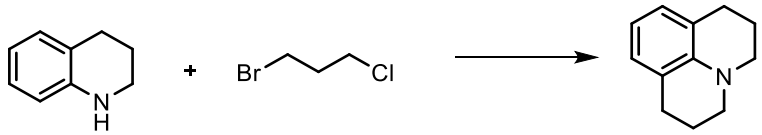

Scheme 1.22. The first synthetic procedure used by Pinkus and improved by Glass and Weissberger for the synthesis of julolidine.

The classical methods for the synthesis of julolidines involve the N-alkylation of tetrahydroquinoline or aniline derivatives followed by an intramolecular electrophilic cyclisation.[78] However, other synthetic ways have been exploited and continue to be reported, especially synthesis allowing the substitution at different positions of julolidine core. In 1982 Kashimura and co-workers reported a synthetic method of julolidines which involve the anodic oxidation of amines or their derivatives in methanol to generate iminium ions which in turn react with nucleophiles (*i.e.* alkene, styrene, enol ether, silyl enol ether, enamine and enol ester).[79] However this electro-organic chemistry method is fastidious and long. More recently Kartritzky *et al.*[80] presented a novel synthesis of julolidine based on benzotriazole intermediates (Scheme 1.23). This method allows the preparation of symmetrically and asymmetrically 1,7-disubstituted julolidines as well as the introduction of one, two or three substituents at C-1, C-2 and C-3 position.

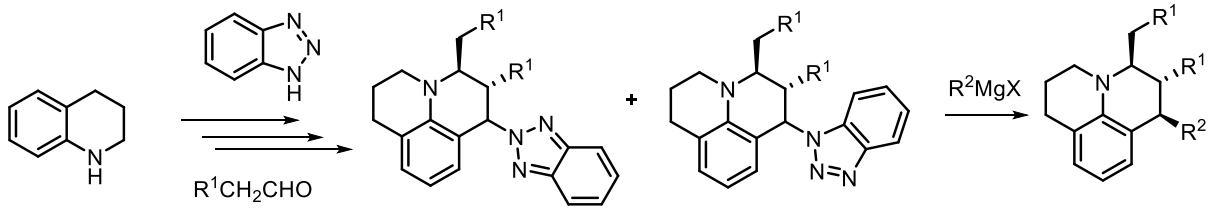

Scheme 1.23. Three substituted julolidines according to synthetic method by Katritzky *et al.*.[80]

[76] Castelino, R. W.; Hallas, G.; Taylor, D. C.; *J. Soc. Dyers Colour*. **1972**, *88*, 25.
[77] Glass, D. B.; Weissberger, A. *Org. Synth*, Wiley: New York, 1955 Collect. Vol. III, p 504.
[78] Katayama, H.; Abe, E.; Kaneko, K. *J. Heterocycl. Chem*. **1982**, *19*, 925.
[79] Shono, T.; Matsumura, Y.; Inoue, K. ; Ohmizu, H.; Kashimura, S. *J. Am. Chem. Soc*. **1982**, *104*, 5753.
[80] Kartritzky, A. R.; Rachwald, B.; Rashwald, S.; Abboud, K. A. *J. Org. Chem*. **1996**, *61*, 3117.

A useful path for julolidine synthesis involves a three-component reaction following an aza-Diels-Alder reaction or also called Povarov reaction presented by Legros *et al.*.[81] According to this method, aldehydes, anilines and enol ether react in trifluoroethanol (TFE) to afford substituted tetrahydroquinolines. In the presence of formaldehyde and an excess of dienophile the product undergoes a second Povarov reaction yielding new julolidines derivatives (Scheme 1.24).

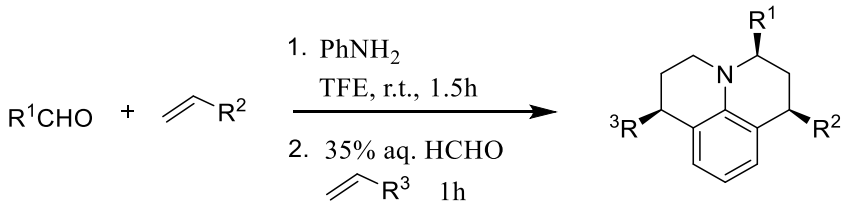

Scheme 1.24. The synthetic path followed by Legros et *al.* for julolidine synthesis.[81]

Chen *et al.* synthesized a symmetric 1,1,7,7-tetramethyljulolidine (TMJ) using an aniline as starting material (Scheme 1.25).[82] The N,N-alkylation of the amine group is followed by intramolecular electrophilic cyclization in acidic media. The authors tested several acidic conditions but the reaction yields were not satisfactory. In fact, the TMJ was our first choice as intermediate for the design and synthesis of our compounds, however regarding the difficulties of the synthesis and the low reaction yield, we abandoned it and focused on its hydroxylated analog 8-hydroxy-1,1,7,7-tetramethyljulolidine (TMJ-OH). It will be presented in more detail in the next chapter.

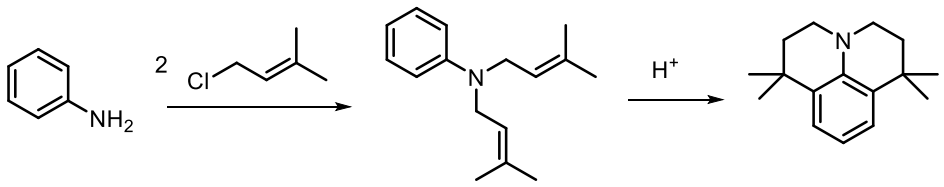

Scheme 1.25. Method used by Chen *et al*. for the synthesis of 1,1,7,7-tetramethyljulolidine.[82]

Intramolecular Friedel-Craft cycloalkylations promoted both by Bronsted and Lewis acid catalysts is a promising method for the preparation of substituted julolidines.[83] However, despite the numerous advances in synthetic organic chemistry and the synthetic methods developed, the synthesis of julolidine derivatives still remain challenging.

[81] Legros, J.; Crousse, B.; Ourévitch, M.; Bonnet-Delpon, D. *Synlett*. **2006**, 12, 1899.
[82] Balaganesan,B.; Wen, S.-W.; Chen, C. H. *Tetrahedron Lett.* **2003**, *44*, 145.
[83] Abd El-Aal, H. A. K.; Khalaf, A. A.; El-Khawaga, A. M. A. *J. Heterocycl. Chem.* **2014**, *51*, 262.

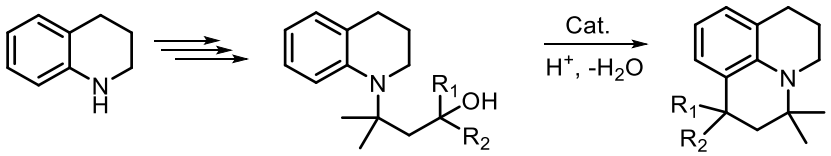

Scheme 1.26. Intramolecular Friedel-Craft cyclialkylation method applied by Abd El-Aal.[83]

4.3. Applications

The julolidine fragment is part of the skeleton of a large number of compounds having found many applications. In this section we will focus in particular on their promises in biology (*e.g.* the fluorescent viscosity sensors) and photonic devices (*e.g.* Organic Light-Emitting Diodes, OLEDs).

- *Fluorescent molecular rotors*[84,85]

The *molecular rotors* are fluorescent molecules which can perform an intramolecular rotation (*i.e.* the subunits are placed perpendicularly to each other) upon photoexcitation. Also known as *Twisted Intramolecular Charge transfer* (TICT) complexes they are characterized by dual de-excitation pathways. If the photoinduced charge transfer does not occur with a subsequent rotation in the singlet excited state, then de-excitation proceeds by fluorescence emission. Generally, their photophysical properties depend on the characteristics of the environment they are introduced in (*i.e.* polarity and particularly viscosity). In this group of molecules, julolidine containing materials are among the most prominent showing encouraging results as florescent viscosity sensors. Indeed, many physiological functions are related to the viscosity of the environment. It appears that several diseases such as artherosclerosis, hypercholesterolemia and diabetes are accompanied by viscosity alteration of the cell membrane. Various other diseases are related to the viscosity changes in the blood plasma or lymphatic fluid.
9-(Dicyanovinyl)-julolidine (DCVJ) depicted in Figure 1.25 is one of the earliest and most studied molecular rotors for biological applications.[86] As indicated from its absorption and emission spectra (Figure 1.25), the quantum yield of florescence increases with increasing the solvent viscosity η.

[84] Haidekker, M. A.; Brady, T. P.; Lichlyter, D.; Theodorakis, E. A. *Bioinorg. Chem.* **2005**, *33*, 415.
[85] Haidekker, M. A.; Theodorakis, E. A. *Org. Biomol. Chem.* **2007**, *5*, 1669.
[86] Kung, C. E.; Reed, J. K. *Biochem.* **1986**, **25**, 6114.

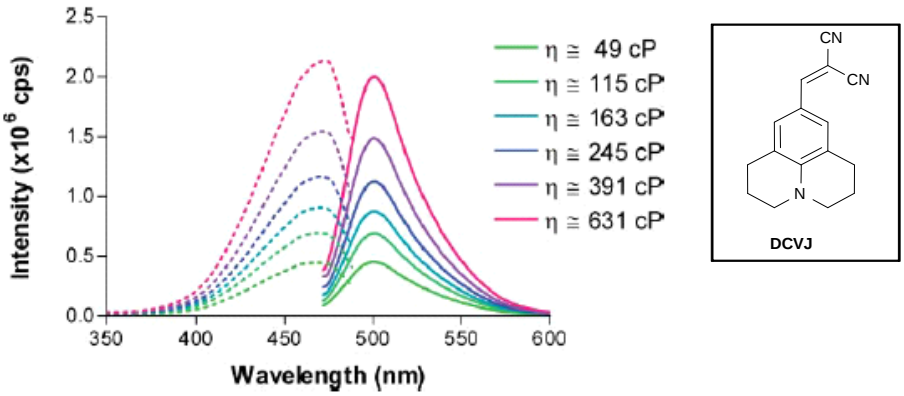

Figure 1.25. Absorption (dashed line) and emission (solid line) spectra of DCVJ rotor in a mixture of ethylene glycol and glycerol. The viscosity increases as the concentration of glycerol in the mixture increases. In the box is represented the chemical structure of DCVJ rotor. Figure printed from ref. [86].

Interestingly, chemical modifications which do not perturb their photophysical properties are possible. These modifications may allow the linkage of various motifs (hydrophilic or hydrophobic) serving as targeting or recognition elements. We can mention the work of Theodorakis's group from the University of California centered on chemistry and photophysics of molecular rotors.[84,85] They have published a series of molecules based on julolidine moiety with specific chains (*e.g.* hydrophobic chain, phospholipid chains) that integrate very specifically into the membrane and show high viscosity sensing.[85] Two examples are shown in the Figure below:

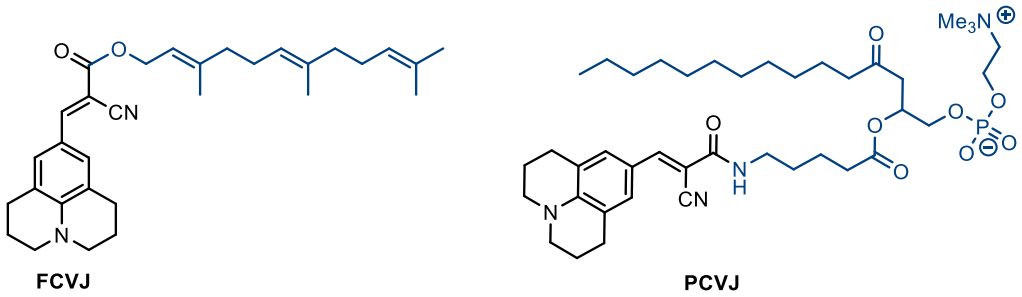

Figure 1.25. Membrane-compatible rotor probes containing a farnesyl ester chain (composed of three isoprenyl groups) FCVJ and a phospholipide PCVJ covalently linked to the rotor.[85]

- *Photonic devices – OLEDs*[87,88]

Julolidine containing materials also appear to be very attractive as red-emitting dopant for OLED applications. This provides from the fact that its tricyclic rigid structure, which locks the nitrogen atom, prevents the energy dissipation which would be caused by the rotation and vibration of the uncyclized amino groups. Furthermore, the presence of tetramethyl groups on the julolidine scaffold avoids molecular aggregation in the solid state, thus increasing the efficiency of luminescence of OLEDs.

4-(Dicyanomethylene)-2-*t*-butyl-6-(1,1,7,7-tetramethyl-julolidyl-9-enyl)-4*H*-pyran (DCJTB) shown in Figure 1.26 is one of the best dyes used as red emitter. In 2010, Lee *et al.* reported the synthesis of Red 2 (Figure 1.26), a modified DCJTB dye containing more bulky groups.[89] The OLED device doped with this dye showed improved luminous efficiency compared to is analogue DCJTB. Another article published by Huang *et al.* reported the prominent efficiency of a cyanocoumarin containing red emitter based on julolidine scaffold, 9-cyano-10-(2-benzothiazolyl)-1,1,7,7-tetramethyl-2,3,6,7-tetrahydro-1*H*,5*H*,11*H*-benzo [*l*] pyrano[6,7,8-*ij*]quinolizin-11-one (RC545T), Figure 1.26 .[85] Contrary to the two previous molecules, RC545T lacks the vinyl moiety connecting the two parts of the compound. The structural constraines that are imposed to this molecule give rise to high fluorescence and a narrower *Full Width at Half Maximum* (FWHM) parameter (*ca.* 48 nm for RC545T, *ca.* 73 nm for DCJTB). Hence, the RC545T is an excellent candidate for OLEDs.

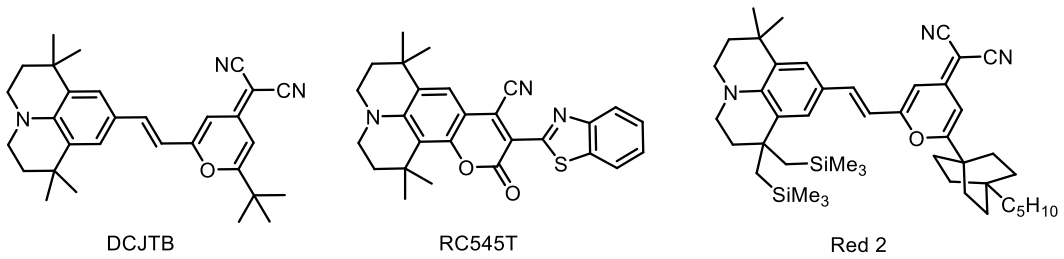

Figure 1.26. The chemical structures of RC545T, DCJTB and Red 2 dye; high efficient red emitters for uses in OLED devices.

[87] Chang, M.-Y.; Han, Y.-K.; Wang, C.-C.; Lin, S.-C.; Tsai, Y.-J.; Huang, W.-Y. *J. Electrochem. Soc.* **2008**, *155*, J365.
[88] Hong, Y.; Yu, J.-G.; Huang, K.-L.; Xiao, J.-Y. *X-ray Structure Analysis Online*, **2009**, *25*, 115.
[89] Lee, K. H.; Park, M. H.; Kim, S. M.; Kim, Y. K.; Yoon, S. S. *Jpn. J. Appl. Phys.* **2010**, *49*, 08JG02.

5. Summary

The scheme below summarizes all the various processes which may be produced by the interaction of light-molecule beginning with the absorption process and followed by the electronic excitation and the series of processes that may be produced thereafter. An excited molecule is no long stable; as a result it can be rapidly involved in a physical de-excitation process or in a chemical reaction. The photochemical process of photochromism has retained our attention for the design and synthesis of elaborating molecular systems in order to control an electronic energy transfer process.

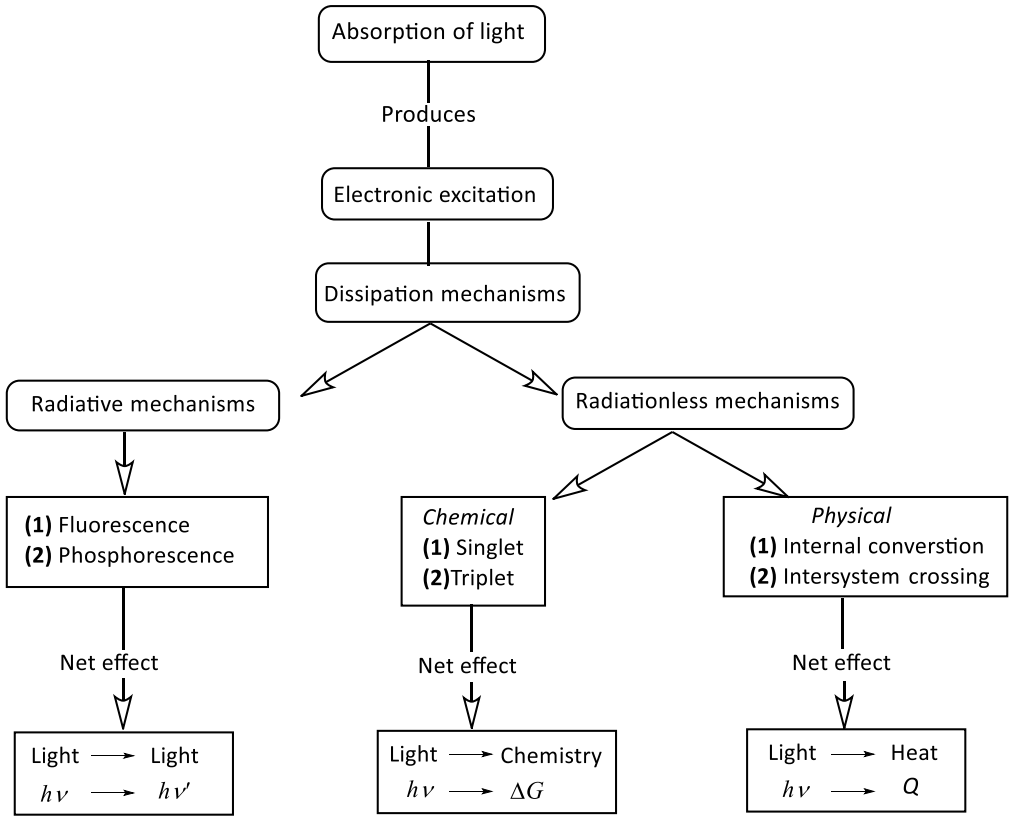

Figure 1.27. Schematic representations of the many processes deriving from the light-molecule interaction. Figure adapted from ref. [3], pp 15.

Chapter II

Chapter II - Design, synthesis, photophysical and electrochemical studies of push-pull amino-styryl BODIPY dyes

I. The push-pull chromophores

1.1. Introduction

Push-pull π-conjugated chromophores are molecular systems constructed around an electron-donor (D) and an electron-withdrawing (A) group connected through a π-conjugated spacer (D-π-A). They are characterized by a high dipolar moment (μ) in the ground and excited states and exhibit an *Intramolecular Charge Transfer* (ICT) process from the D to the A. Currently due to their physico-chemical properties they are attracting an important interest for various applications in optoelectronics,[90] organic electronics[91] and information-storage devices.[92] A large variety of D-π-A systems were synthesized so far by combining different donor/acceptor modules with known π-spacer units.

Many of the original series of D-π-A compounds were based on a 4-nitrophenyl moiety as the electron acceptor with an *N*,*N*-dimethylanilino group as the electron donor. More recently, attention has turned to the use of stronger organic donor and acceptor functions, including julolidine[9] derivatives, pyran-containing compounds such as 2-(2-*tert*-butyl-6-methyl-4*H*-pyran-4-ylidene)malonitrile (DCM),[10] 4,5-dicyanoimidazole derivatives[11] and the so-called "super-acceptor" 7,7,8,8-tetracyanoquino-dimethene (TCNQ).[12] It has been demonstrated that the nature of the donor/acceptor terminals affects the optical and electronic properties of the resultant materials, but so does the composition and length of the π-conjugated backbone. It might be mentioned here that various conjugated spacers, such as polyenes,[93] stilbene,[94] thiophene,[95]

---

[90] Ruiz Delgado, M. C.; Casado, J.; Hernández, V.; López Navarrete, J. T.; Orduna, J.; Villacampa, B.; Alicante, R.; Raimundo, J.-M.; Blanchard, Ph.; Roncali, J. *J. Phys. Chem. C* **2008**, *112*, 3109.

[91] Li, J.; Liu, D.; Hong, Z., Tong, Sh.; Wang, P.; Ma, Ch.; Lengyel, O.; Lee, C.-S.; Kwong, H.-L.; Lee, Sh. *Chem. Mater*. **2003**, *15*, 1486.

[92] Reinhardt, B. A.; Brott, L. L.; Clarson, S. J.; Dillard, A. G.; Bhatt, J. C.; Kannan, R.; Yuan, L.; He, G. S.; Prasad, P. N. *Chem. Mater*. **1998**, *10*, 1863.

[93] Blanchard-Desce, M.; Alain, V.; Bedworth, P. V.; Marder, S. R.; Fort, A.; Runser, C.; Barzoukas, M.; Lebus, S.; Wortmann, R. *Chem. Eur. J*. **1997**, *3*, 1091.

[94] Rijkenberg, R. A.; Benelaar, D.; Buma, W. J.; Hofstraat, J. W. *J. Phys. Chem. A* **2002**, *106*, 2446.

[95] Ortí, E.; Viruela, P. M.; Viruela, R.; Effenberger, F.; Hernández, V.; López Navarrete, J. T. *J. Phys. Chem A* **2005**, *109*, 8724.

porphyrins[96] etc., have been incorporated into push-pull electronic systems (some examples are shown in Figure 2.1). It appears clear from the literature that push-pull chromophores are the major class of organic compounds highly investigated in particular for their *NonLinear Optical* (NLO) properties.[93,97,98] In addition they are useful model systems for studying the mechanism of photoinduced electron transfer process. Furthermore, it is recognized that photoinduced electron transfer remains one of the most intensively studied subjects in contemporary science considering the importance of both natural and artificial photosynthesis for *Light Harvesting* (LH) molecular systems.[99]

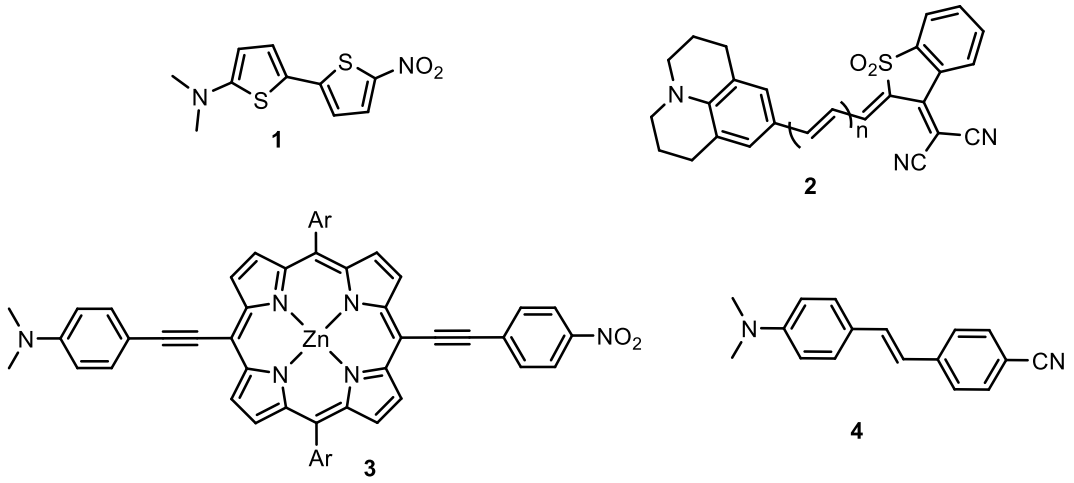

Figure 2.1. Examples of published push-pull chromophores.

The rate of electron transfer between a donor and an acceptor depends not only on the parameters of the former (*i.e.* the driving force $\Delta G°$ and the reorganization energy λ) but also on parameters which are governed by the bridging unit (*i.e.* the electronic coupling and the donor-bridge energy gap).[100] Many variables including thermodynamic properties (excitation energy and redox

[96] (a) Zhang, T. G.; Zhao, Y.; Asselberghs, I.; Persoons, A.; Clays, K.; Therien, M. J. *J. Am. Chem. Soc.* **2005**, *127*, 9710. (b) Jiang, N.; Zuber, G.; Keinan, Sh.; Nayak, A.; Yang, W.; Therien, M. J.; Beratan, D. N. *J. Phys. Chem. C* **2012**, *116*, 9724.

[97] Kanis, D. R.; Ratner, M. A.; Marks, T. J. *Chem. Rev.* **1994**, *94*, 195.

[98](a) Tancini, F.; Wu, Y.-L.; Schweizer, B.; Gisselbrecht, J.-P.; Boudon, C.; Jarowski, P. D.; Beels, M. T.; Biaggo, I.; Diederich, F. *Eur. J. Org. Chem.* **2012**, 2756. (b) Kivala, M., Diedrich, F. *Acc. Chem. Res.* **2009**, *42*, 235.

[99] (a) Lewis, N. S.; Nocera, D. G. *Proc. Natl. Acad. Sci. U.S.A* **2006**, *103*, 15729. (b) Armaroli, N.; Balzani, V. *Angew. Chem. Int. Ed.* **2007**, *46*, 52.

[100] (a) Winters, M. U.; Dahlstedt, E.; Blades, H. E.; Wilson, C. J.; Frampton, M. J.; Andresson, H. L.; Albinsson, B. *J. Am. Chem. Soc.* **2007**, *129*, 4291. (b) Eng, M. P.; Albinsson, B. *Angew. Chem. Int. Ed.* **2006**, *45*, 5626.

potentials) and structural elements (separation distance, mutual orientation and nature of the bridge) intervene in the achievement of a PeT process.

Surprisingly, BODIPY derivatives have not been widely exploited as photoactive bridges in D-π-A chromophores. Also photoinduced electron transfer involving BODIPY dyes is not so common. The most popular reactants for such materials are bio-inspired (*e.g.* porphyrins and carotenes). However, it might be mentioned that there have been few reports in incorporating BODIPY dyes into push-pull molecules.[101,102] Notably S. Niu *et* co-workers from this laboratory (LCOSA) have previously reported D-π-A chromophores built from a BODIPY-based core with electron-donor and electron-acceptor units attached at the 2 (or 3) and 6 positions as demonstrated by compound **10** and **11** in the Figure 2.2.[102]

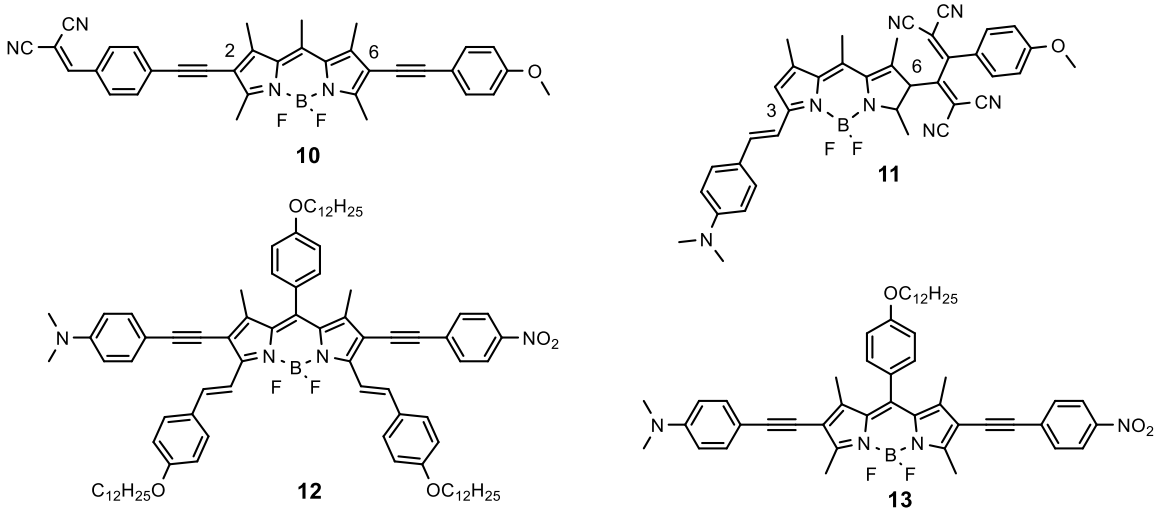

Figure 2.2. Examples of push-pull chromophores containing a BODIPY bridge **10**, **11**[102] and **12**, **13**.[101]

Such compounds enable facile tuning of the optoelctronic properties but they do not promote light-induced charge separation. However, the push-pull **11** represented in Figure 2.2 shows interesting NLO response.[102b]

- ***Objectives of the work***

The present work focuses on the design and synthesis of D-bridge-A systems with a push-pull effect based on a BODIPY dye bridge. The prior goal being the photoinduced charge-separated excited state (Figure 2.3). Among the donor units we have selected the julolidine and the triazatruxene entities because of their strong-electron donor property, anchored on the bridging

[101] Shi, W.-J. ; Lo, P.-C. ; Singh, A. ; Ledoux-Rak, I.; K. P. Ng, D. *Tetrahedron* **2012**, *68*, 8712.
[102] (a) Niu, S.; Ullrich, G.; Retailleau, P.; Ziessel, R. *Org. Lett*. **2011**, *13*, 4996. (b) Ullrich, G.; Barsella, A.; Boeglin, A.; Niu, S.; Ziessel, R. *Chem. Phys. Chem.* **2014**, *15*, 2693.

unit (BODIPY) at 3-position through a vinyl fragment. The electron-acceptor is a dicyanovinyl attached onto the phenyl ring at the *meso*-position of the BODIPY core as depicted in Figure 2.3. A series of model compounds lacking the donor or acceptor or bridging subunit were also synthesized. Their optical and electronic properties were studied by means of advanced absorption and emission spectroscopy and cyclic voltammetry. DFT calculations were realized as support to the experimental analysis.

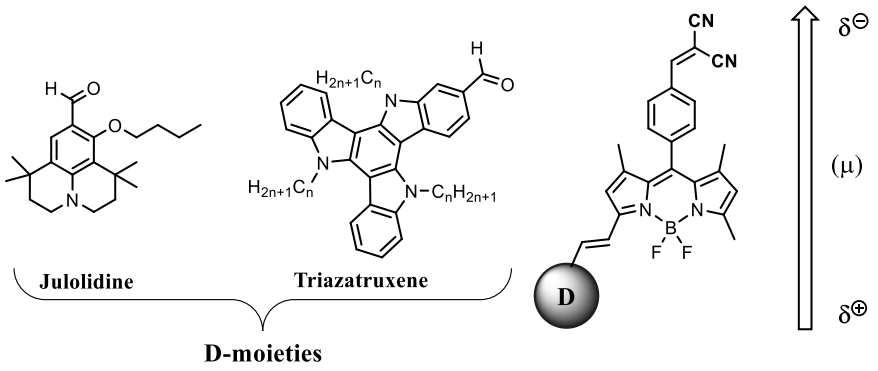

Figure 2.3. General representation of the dipolar push-pull systems synthesized.

2.1. BODIPY dyes

The molecular structure of BODIPYs is based on a 4,4-difluoro-4-bora-3a,4a-diaza-*s*-indacene scaffold represented in Figure 2.4. It should be mentioned that since their discovery by Treibs and Kreuzer,[103] the borondipyromethene derivatives have known an impressive success notably due to their excellent properties: high extinction coefficient ($\varepsilon > 50\,000$ M^{-1} cm^{-1}); high fluorescence quantum yield ($\varphi > 70$ %); sharp fluorescence peaks and they are chemically and spectroscopically stable. Furthermore, their optical and electrochemical properties may be easily tuned by functionalization at the pyrrole, *meso* and N-*ortho* positions as well as by boron substitution of the BODIPY core.[104] Some examples of various functionalizations giving rise to BODIPY derivatives with different optical properties are sketched in Figure 2.4.

[103] Treibs, A.; Kreuzer, F. H. *Justus Liebigs Ann. Chem.* **1986**, *718*, 208.
[104] (a) Ziessel, R.; Ullrich, G.; Harriman, A. *New. J. Chem.* **2007**, *31*, 496. (b) Loudet, A.; Burgess, K. *Chem. Rev.* **2007**, *107*, 4891. (c) Ullrich,G.; Ziessel, R.; Harriman, A. *Angew. Chem. Int. Ed.* **2008**, *47*, 1184.

Because of these remarkable points, BODIPY dyes have been used successfully in photovoltaic devices,[105] as ion sensors[106] and as fluorescent probes in biological analyses.[107]

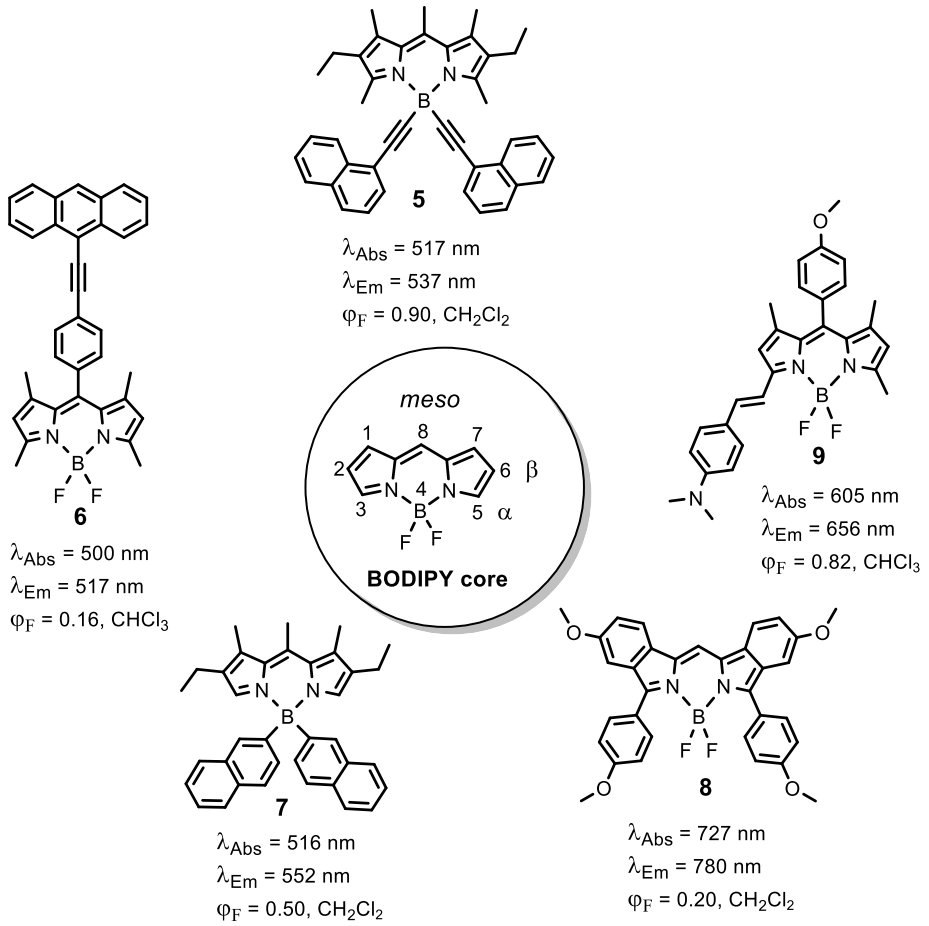

Figure 2.4. The BODIPY core and various examples of BODIPY derivatives.

2.1.1. Synthesis of the BODIPY core 15

Meso-substiuted BODIPY dyes are generally prepared *via* condensation of acyl chlorides with pyrroles.[104b] The iodophenyl-tetramethyl BODIPY **15** was chosen as the starting material for the design and synthesis of D-π-A systems and is obviously needed as the photo-active bridge. It consists on the condensation of 4-iodobenzoyl chloride with 2,4-dimethylpyrrole (also known as *Knorr pyrrole*) in freshly distillated dichloromethane at room temperature during one week,

[105] (a) Kolemen, S.; Cakmak, Y.; Erten-Ela, S.; Altay, Y.; Brendel, J.; Thelakkat, M.; Akkaya, E. U. *Org. Lett.* **2010**, *12*, 3812. (b) Rousseau, T.; Cravino, A.; Roncali, J.; Bura, T.; Ullrich, G.; Ziessel, R. *J. Mater. Chem.* **2009**, *19*, 2298.

[106](a) Ullrich, G.; Goze, C.; Charbonnière, L.; Ziessel, R. *Chem. Eur. J.* **2003**, *9*, 3748. (b) Atligan, S.; Ozdemir, T.; Akkaya, E. U. *Org. Lett.* **2010**, *12*, 4792.

[107] (a) Niu, S. L.; Massif, C.; Ullrich, G.; Ziessel, R. Renard, P.-Y.; Romieu, A. *Org. Biomol. Chem.* **2010**, *8*, 66. (b) Ono, M.; Watanabe, H.; Kimura, H.; Saji, H. *ACS, Chem. Neurosci.* **2012**, *3*, 319.

forming first the intermediate iodophenyl dipyrromethene (or *dipyrrin*) **14**. The latter, indeed not isolated, in the presence of triethylamine and boron trifluoride etherate under stirring overnight, afforded the boron difluoride complex **15**.

The maximum yield for this reaction, under these reaction conditions does not exceed 50 % in general, which is very good compared to other methods providing *ca.* 15 % yield. The presence of iodo group allows easy post-functionalization using metal-catalyzed cross-coupling reactions and is a tool for anchoring the electron-acceptor subunit.

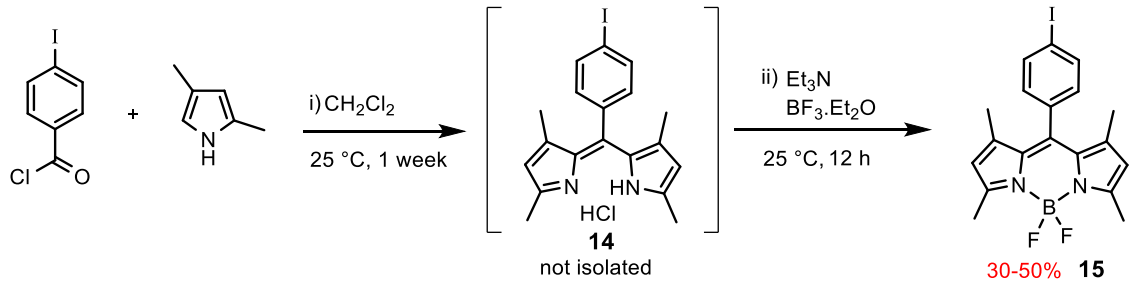

Scheme 2.1. Description of the synthetic method used for the preparation of BODIPY **15**.

2.2. Julolidine moiety as electron-donor group

The julolidine fragment, introduced in more detail in Chapter I-§ 4, is a strong electron-donor scaffold which can influence the strength and overlap of the nitrogen lone pair with a conjugated system. Initially, we selected the 1,1,7,7-tetramethyljulolidine TMJ[108] (Figure 2.5a) as electron-donor group for the design of the push-pull systems. Taking into account its synthetic complications and the low reaction yield (*ca.* 5%) we obtained following literature procedures (ref. [82], Chapter I), an alternative solution was of clear evidence. Indeed, the synthesis of its analogue TMJ-OH (Figure 2.5b) is well reported and allows accessible reaction yields.[109] Furthermore, the presence of hydroxyl group onto the julolidine scaffold opens various possibilities for tuning its chemical structure thus providing interesting derivatives (*e.g. anils* and *boranils*) which will be seen in more details in Chapter III.

[108] Balaganesan, B.; Wen, S.-W.; Chen, C. H. *Tetrahedron Lett.* **2003**, *44*, 145.
[109] Lee C.-C.; Hu, A. T. *Dyes Pigm.* **2003**, *59*, 63.

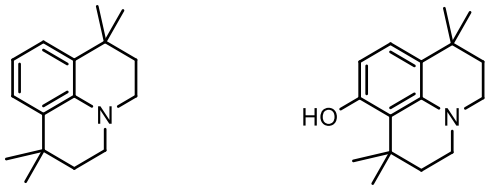

(a) (b)

Figure 2.5. Chemical structure of (a) TMJ and (b) TMJ-OH.

2.2.1 Synthesis of TMJ-OH 16

TMJ-OH (1,1,7,7-Tetramethyl-2,3,6,7-tetrahydro-1H,5H-pyrido[3,2,1-ij]quinolizidine) **16** was prepared according to the method reported by Lee and Hu and depicted in Scheme 2.2.[109] The reaction involves first the N,N-alkylation of 3-aminophenol with 1-chloro-3-methyl-2-butene in DMF and subsequently precipitation of the product as ammonium salts with addition of concentrated HCl. Afterwards, the bis-alkylated ammonium salts were heated at 95 °C in methanesulfonic acid during two hours. The bis-cyclized julolidine **16** was afforded by precipitation of the reaction media with dropwise addition of a solution of ammonium hydroxide. ^{1}H NMR spectroscopy confirmed the structure of the expected molecule.

The electron-rich aromatic ring of the julolidine core is activated to electrophilic attack. Hence, a Vilsmeier-Haack formylation[110] allows the introduction of an aldehyde group selectively in the *para*-position of the aromatic ring of **16** using $POCl_3$ in anhydrous DMF solution at room temperature over-night. The functional formyl group is indeed necessary for attaching the molecule onto the final push-pull systems following a Knoevenagel condensation.[111] In order to avoid the problems due to the reactivity of the hydroxyl group of **17** in the next steps, it was preferentially O-alkylated with a butyl or hexyl or dodecyl chain in DMF using NaH as base. The products were confirmed from ^{1}H NMR spectroscopy.

[110] Vilsmeier, A.; Haack, A. *Ber. Dtsch. Chem. Ges*. **1927**, *60*, 119.
[111] Knoevenagel, E. *Ber. Dtsch. Chem. Ges*. **1898**, *31*, 2596.

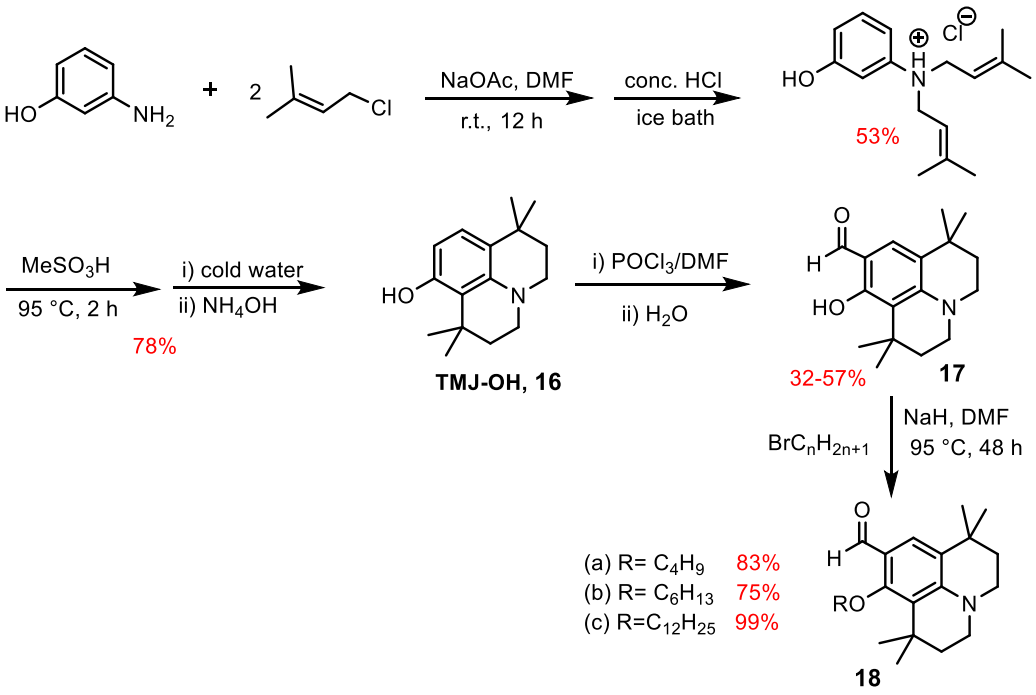

Scheme 2.2. The method followed for the synthesis of the julolidine derivative of choice.

2.3. Triazatruxene moiety as electron-donor group

The second electron donor subunit selected for the design of the donor-bridge-acceptor compounds is the *triazatruxene* (TAT); a scaffold composed by three indole moieties connected through a central benzene ring (Figure 2.6a). It originates from *truxene*, a heptacyclic polyarene (Figure 2.6b) where the carbons at 5, 10, 15-position are replaced by nitrogen atoms. As a consequence the TAT results on a *discotic* π-extended and electron-rich aromatic core. Given its excellent electron-donor properties and therefore its capacity for achieving a photoinduced intramolecular charge transfer, it was used in OLEDs, Two Photon Absorbing (TPA) materials and more recently in Dye-Sensitized Solar Cells (DSSC).[112]

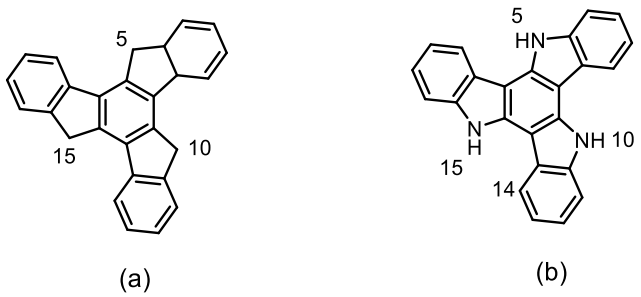

Figure 2.6. The chemical structure of (a) truxene and (b) triazatruxene molecules.

[112] Qiani, X.; Zhu, Y.-Z.; Song, J.; Gao, X.-P.; Zheng, J.-Y. *Org. Lett.* **2013**, *15*, 6034.

2.3.1. Synthesis of the triazatruxene derivative moiety

The target TAT-aldehyde **22** was prepared in four steps (described in Scheme 2.3) using the oxo-indole as the starting material according to a procedure developed in the LCOSA laboratory.[113] The triazatruxene core **19** was obtained by the condensation of three oxo-indoles in $POCl_3$ heating at 100 °C. The product was obtained as a white solid in 11 % yield after precipitation. Compound **19** has low solubility in the usual organic solvents. In order to solve this problem, long alkyl (hexyl or dodecyl) chains were introduced by N-alkylation of **19** with a bromoalkyl in the presence of NaH in THF solution. The reaction gave rise to **20** in high yield. In the next step, a bromide is introduced selectively in 2-position of the phenyl group of **20** using N-bromosuccinimide in anhydrous chloroform solution during 1.5 hours. The product was purified over a silica column chromatography and was obtained in good yield as colourless oil which solidifies at room temperature. Finally, the bromide of **21** was converted into the corresponding formyl derivative **22** by using a carbo-formylation reaction Pd(II)-catalyzed in anhydrous DMF solution. The aldehyde was collected as yellow oil solidifying at room temperature after purification in 58 % yield for **22a** and 95 % yield for **22b**. The difference on the reaction yield observed between **22a** and **22b** comes probably as a result of the steric hindrance caused by the long alkyl chains of **21a**, thus rendering difficult the insertion of the catalyser to the aryl-Br bond during the formylation reaction.

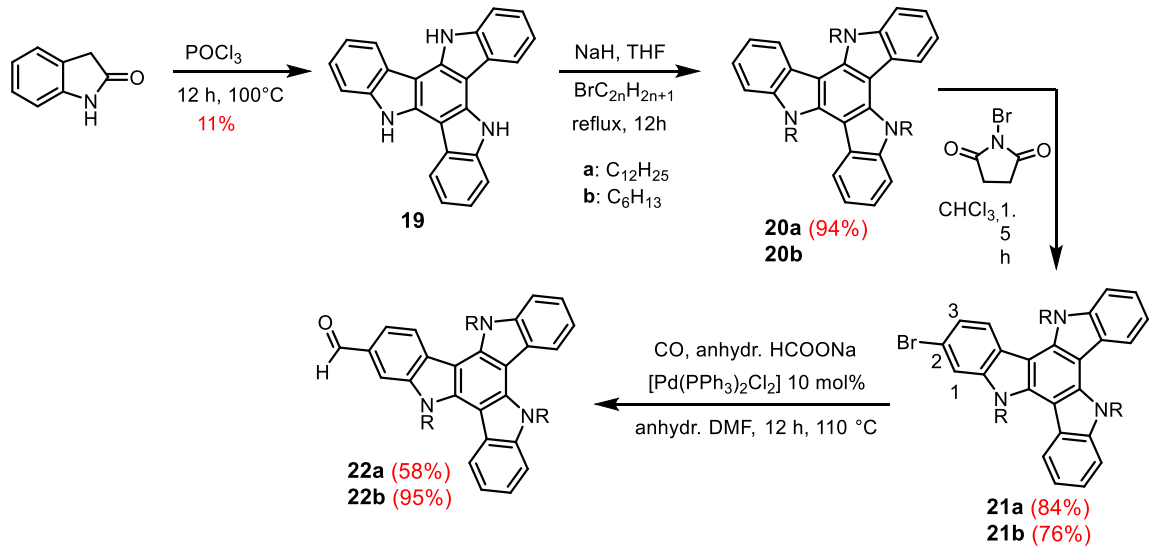

Scheme 2.3. Synthesis pathway employed for the TAT derivative **22**.[113]

[113] (a) Bura, T.; Leclerc, N.; Fall, S.; Lévêque, P.; Heiser, T.; Ziessel, R. *Org. Lett.* **2011**, *13*, 6030. (b) Ruiz, C.; López Navarrete, J. T.; Ruiz Delgado, M. C.; Lor-Gómez Berta, *Org. Lett.* **2015**, DOI: 10.1021/acs.orglett.5b00900.

2.4. Dicyano-derivatives as electron-acceptor group

As electron acceptors modules the malonitrile and 4-(dicyanomethylene)-2-(*t-butyl*)-6-methyl-4*H*-pyran (DCM) were chosen for investigation. Such electron acceptor moieties are largely utilized in the design of organic push-pull chromophores. The synthesis of DCM is not well reported in the literature; however we could obtain the molecule following a two-step protocol inspired by the work of Chow *et al.* [114] The pyran derivative **23** was obtained from the condensation of acetylacetone with methyl trimethylacetate in DMF solution in 11 % yield as sketched in Scheme 2.4. Finally, the reaction of **23** with malonitrile in refluxing anhydride acetic during 12 hours gave the DCM **24** as a brownish solid in excellent yield. The chemical structure was confirmed by ^{1}H NMR spectroscopy.

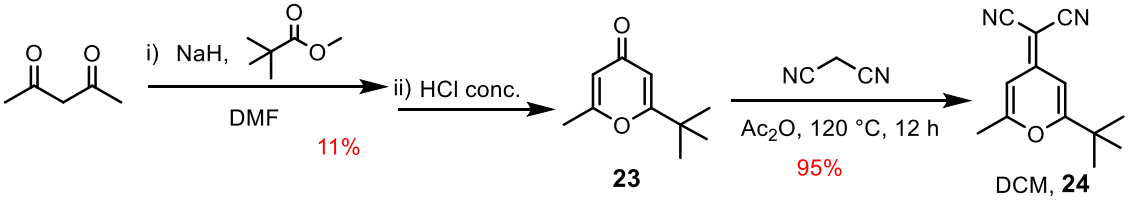

Scheme 2.4. Description of the synthetic pathway used for the preparation of DCM **24**.

3.1. Synthesis of julolidine-BODIPY-dicyanovinyl push-pull 27

The push-pull chromophore **27** was prepared in three steps from iodophenyl tetramethyl BODIPY **15** as depicted in Scheme 2.5. Condensation of **15** with 9-formyl-10-butoxy-1,1,7,7-tetramethyl-2,3,6,7-tetrahydro-1H, 5H-pyrido-[3,2,1-ij]quinolizidine **18** provides a mono-styryl derivative **25** despite the presence of excess aldehyde. The monostyryl was obtained as a dark blue solid in 58 % yield after purification over column chromatography and recrystallization in a dichloromethane/ethanol mixture. The mono-substitution was unambiguously characterized from the proton NMR spectroscopy and supported by electron ionization (EI) mass spectroscopy analysis where the most intense peak with *m/z* value 761.1 corresponds to the expected cationic molecular peak. Moreover, single crystals of **25** could be obtained confirming its structure from X-ray crystallography analysis (*vide infra*). Other cases restricted to one condensation of 3,5-methyl-BODIPY with aldehydes are reported in the literature. The mono-substitution of the precursor dye **15** might be explained in terms of steric hindrance caused by the julolidine moiety. However, it might not be attributed to a deactivation of the second methyl group after addition of the julolidine unit (*vide infra*).

[114] Jag Chang, Y.; Chow, T. J. *J. Mater. Chem.* **2011**, *11*, 3091.

Transformation of **25** into aldehyde derivative **26** was realized using a carbo-formylation reaction catalyzed by a Pd(II) and sodium formate as the source of protons under a flow of CO at atmospheric pressure. The reaction was heated at 100 °C in anhydrous DMF solution during 3 hours. The aldehyde **26** was obtained as a dark blue solid in 71 % yield following purification. Electron ionization mass spectrometry confirms the molecule by the presence of the *m/z* (663.2) peak at 100 % intensity corresponding to the expected radical cationic molecule and an *m/z* value at 35 % intensity being attributed to the molecule having loss the butoxy chain [M-OC_4H_5]. Also, the IR spectra shows an intense band appearing at ν = 1700 cm^{-1} assigned to the vibration of C=O bond of the formyl functional group. Moreover the compound was characterized using ^{1}H, ^{13}C, ^{11}B NMR (*vide infra*) spectroscopy and elemental analysis.

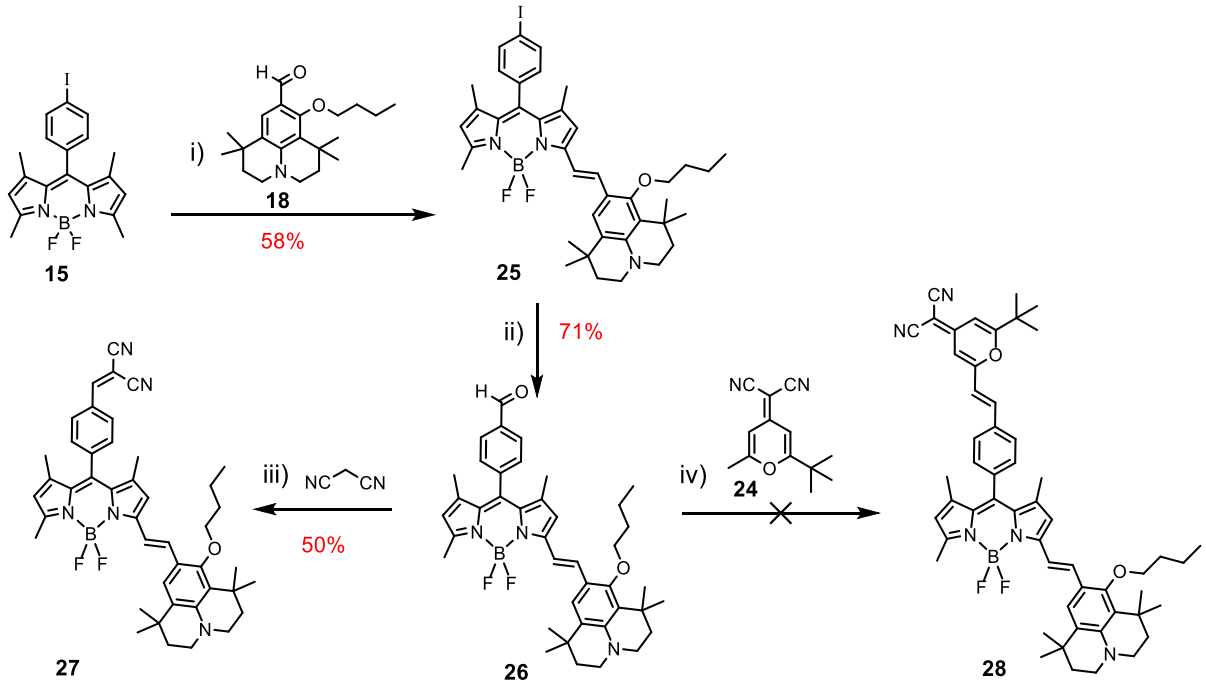

Scheme 2.5. Synthesis of compound **27** and its precursors: i) p-TsOH cat., piperidine, toluene, 140 °C; ii) [$Pd(PPh_3)_2Cl_2$] (10 mol%), HCOONa, DMF under a flow of CO, 100 °C, 3 h; iii) AcOH/piperidine, methanol, 85 °C, 1h; iv) p-TsOH cat., piperidine, toluene, 140 °C.

The procedure of condensation of the formyl group of **26** with the malonitrile, using a Knoevenagel-type reaction was inspired by a reported method.[115] The reaction was catalyzed by small amounts of acetic acid and piperidine in anhydrous methanol solution at 85 °C during 1 hour. It appeared that controlling the reaction time is very important, since a longer time reaction leads to the degradation or the formation of non-desired products.

[115] Lee, C.-H.; Yoon, H.-J.; Shim, J.-S.; Jang, W.-D. *Chem. Eur. J.* **2012**, *18*, 4513.

Also, it was noted that purification over a silica column chromatography degrades the push-pull molecule. The product precipitates in methanol solution, thus it was recuperated as dark blue powder in 50 % yield by centrifugation and washing several times with methanol. ^{1}H NMR spectroscopy confirms the structure of the expected molecule and the infrared spectrum exhibits a band at ν = 2228 cm^{-1} associated to the vibration of the nitriles triple bonds. EI mass spectrometry displays *m/z* peak (711.2) associated with the radical cation molecular peak and a fragmentation *m/z* peak (692.2) at 30 % intensity assigned to the molecule missing a fluorine.

One of the first molecules we designed was the push-pull system **28** depicted in Scheme 2.5 where the selected electron-acceptor module was the DCM **24** entity. However, the Knoevenagel condensation of **26** with **24** in toluene in the presence of piperidine and a catalytic amount of p-TsOH did not afford the target compound **28**. Non-successful attempts have been carried out in other solvents such as ethanol and acetonitrile with piperidine as the catalyst applying various temperatures. The result might be explained in terms of methyl group of **24** not being activated enough allowing reaction with the formyl function of **26**.

3.1.1. ^{1}H NMR characterization of 26 and 27

The proton NMR spectra of the aldehyde precursor **26** and the push-pull system **27** were measured in deuterated chloroform at room temperature (Figure 2.7). As indicated from the spectra shown in the figure below, no displacement on the resonance signals of **27** was observed after addition of the electron-acceptor dicyano vinyl moiety. However, the signal assigned to the proton of C*H*O group at δ = 10.12 ppm in **26** (lower spectrum, Figure 2.7), is absent in the proton spectrum of **27** (upper figure) where a peak appearing at δ = 7.85 ppm was unambiguously assigned to the proton "10" of the dicyanovinyl fragment. In both molecules, the coupling $^{3}J_{H,H}$ between the vicinal protons "4" and "5" is 16.0 Hz, typical value for the double bond being in *trans*-configuration. The styryl keeps the (*E*)-configuration as is well established for styryl-based BODIPY dyes in general, where the $^{3}J_{H,H}$ is in 14.0-16.0 Hz range.[116] Also similar typical values are found for *trans*-stilbene derivatives, while the *cis*-stilbene derivatives show vicinal interaction constant $^{3}J_{H,H}$ *ca.* 12 Hz.[117]

[116] Ziessel, R.; Retailleau, P.; Elliott, K. J.; Harriman, A. *Chem. Eur. J.* **2009**, *15*, 10369.
[117] Almonasy, N.; Bureš, F.; Kulahánek, J.; Machalicky, O. *J. Mater. Sci. Eng. A.* **2011**, *1*, 146.

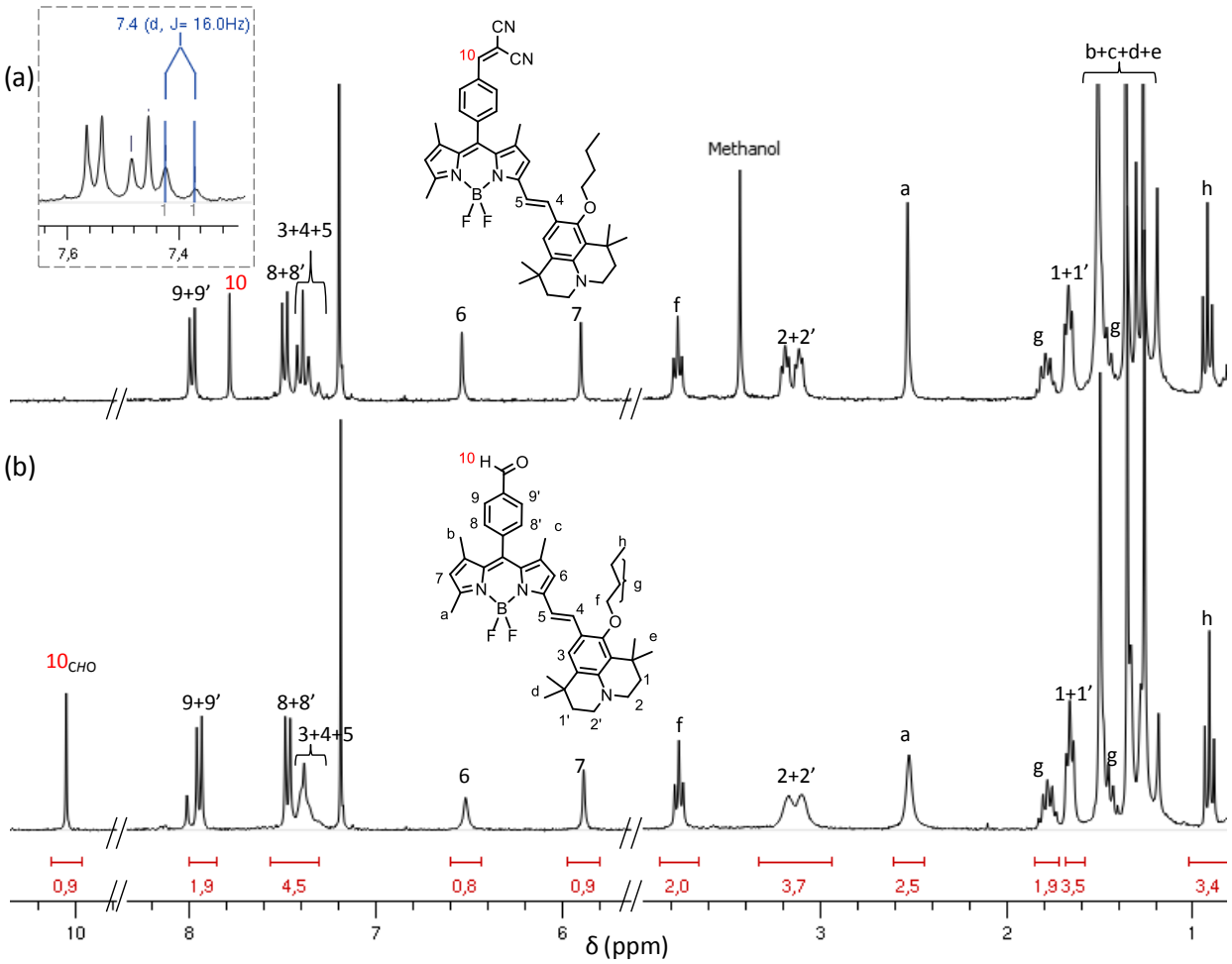

Figure 2.7. ^{1}H NMR spectra of (a) compound **27** and (b) compound **26** in deuterated chloroform at room temperature.

3.1.2. X-ray structure of mono-styryl 25

The molecular structure of compound **25** represented in Figure 2.8 was resolved by X-ray diffraction technique by Dr. Pascal Retailleau (ICSN, Gif-sur-Yvette) in Paris, confirming the formation of the mono-condensed product. Suitable crystals for X-ray analysis were obtained by slow evaporation of a concentrated solution of **25** in an ethanol/dichloromethane mixture. The molecular structure shows a rough planarity for the overall molecule. We can however note that the iodophenyl group placed at the *meso*-position of the indacene scaffold is orthogonal with respect to the dipyrrin core, hence forming a dihedral angel of 86.4°. The ethylene bridge between the BODIPY core and the julolidine moiety adopts an (*E*)-configuration as supported from the proton NMR analysis. The angles N-B-N and F-B-F are 107.2° (6) and 107.7° (6) respectively confirming the tetrahedral geometry of the boron centre.

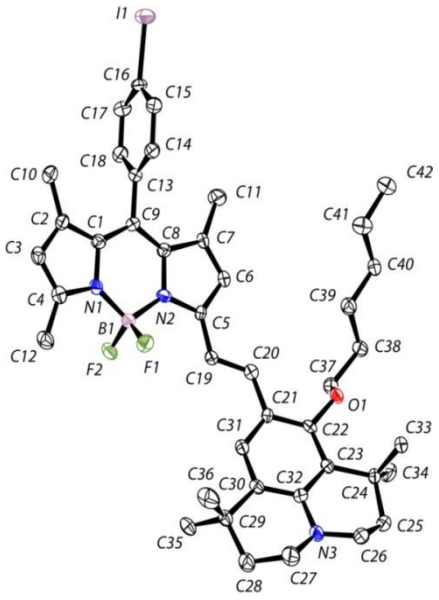

Figure 2.8. ORTEP view of compound **25** with displacement ellipsoids plotted at the 30 % probability level. H atoms are omitted for clarity.

3.2. Synthesis of triazatruxene-BODIPY-dicyanovinyl push-pull 31

The push-pull system **31** was prepared by way of analogy with the julolidine-based system, as described in Scheme 2.6. The condensation of TAT-aldehyde **22** with the BODIPY derivative **15** in toluene gives exclusively the mono-styryl **29** despite the excess of aldehyde precursor. No di-substituted derivative was formed as previously reported in literature from LCOSA laboratory for this mono-styryl.[113] The dye was collected as dark blue solids after purification over a silica column chromatography in 41 % yield and the structure confirmed by NMR spectroscopy.

Afterwards, the iodo group of compound **29** was converted into the corresponding formyl derivative **30** using a carbo-formylation reaction Pd(II) catalysed in anhydrous DMF solution. The reaction was carried out at 100 °C during 2-3 hours. The aldehyde obtained was engaged in the next step after purification and characterization with the usual ^{1}H, ^{13}C and ^{11}B NMR spectroscopy. Infra-red spectrum indicates an intense band at $\nu = 1705$ cm^{-1} which is assigned to the vibration of C=O bond of the formyl functional group.

Finally, condensation of compound **30** with malonitrile catalyzed with small addition of acetic acid and piperidine in THF during 20 to 30 minutes at 95 °C provided the push-pull **31**. It was observed that stirring the reaction media longer than 30 minutes leads to degradation of the product. The push-pull **31** was obtained as dark blue solids in 50 % yield following a rapid

purification over a silica column chromatography and precipitation in a mixture of THF and methanol solution.

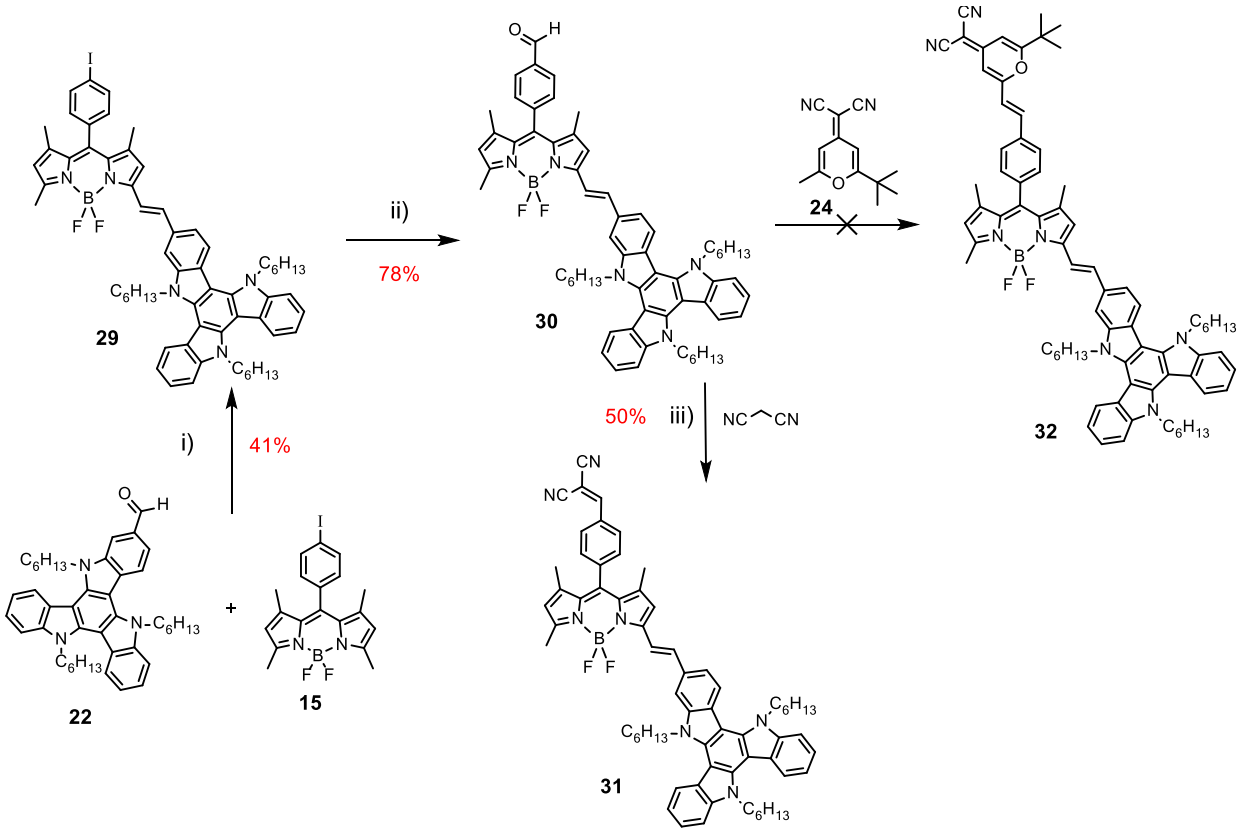

Scheme 2.6. Key. i) Toluene, piperidine, p-TsOH, 140 °C ii) [$Pd(PPh_3)_2Cl_2$] (10 mol%), HCOONa, DMF under a flow of CO, 100 °C; iii) AcOH/piperidine, THF, 95 °C, 20-30 min.

EI mass spectrometry confirms the structure of **31** since the highest intense *m/z* peak with a value 1007.5 corresponds to the final radical cationic molecule. A fragmentation peak at *m/z* = 988.3 with 20 % intensity was assigned to the molecule having lost a fluoride and IR spectrum shows a band at $\nu = 2229$ cm^{-1} resulting from the vibration of the nitrile bonds ν(CN).

As previously announced for compound **26**, the condensation of **30** with DCM **24** did not afford the designed push-pull molecule **32** depicted in Scheme 2.6. Once again, these results may be explained as: i) the activity of the methyl group of **24** is not sufficiently strong compared to the malonitrile methylene, ii) the formyl group of the BODIPY dye is probably not enough electron deficient δ^+. Further we will see that **24** can however undergo condensation with another formyl group.

3.2.1. ^{1}H NMR characterization of 30 and 31

The proton NMR spectra of dye **30** and **31** were measured in deuterated chloroform at room temperature and shown in Figure 2.9. Appending the dicyanovinyl moiety onto **30** is accompanied with the disappearance of the aldehyde group proton at δ = 10.13 ppm (Figure 2.9b) and appearance of a signal at δ = 7.85 ppm assigned to dicyanovinyl proton "10" (Figure 2.9a). The latter has the same chemical shift as the vinylic proton of push-pull **27**. Herein as well as in the previous push-pull **27**, the addition of the acceptor fragment does not influence the chemical shifts of the different resonance signals of the molecule, which remain unaffected.

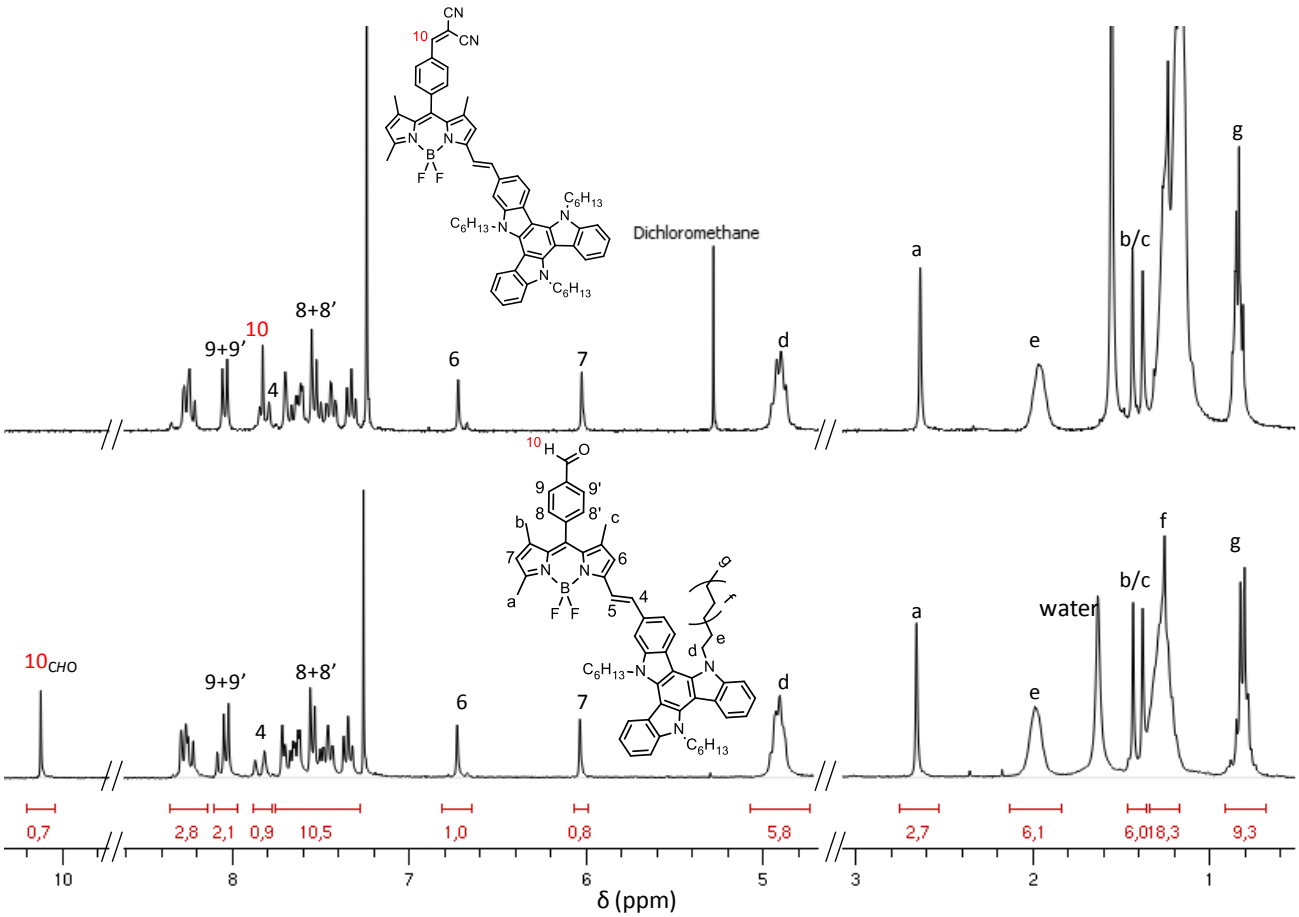

Figure 2.9. ^{1}H NMR spectra of (a) compound **30** and (b) compound **31** in deuterated chloroform at room temperature.

3.3 Models compounds

3.3.1. Synthesis of directly linked donor-acceptor models 33, 34

The photophysical properties of the final target push-pull systems become much clearer if model compounds are regularly investigated. As such, we synthesized compound **33** and **34** where the donor and the acceptor moieties are directly linked together (*i.e.* the BODIPY bridge is missing). As indicated in Scheme 2.7 the malonitrile was reacted with the aldehyde group of **22** in a methanol solution using acetic acid and piperidine as catalytic system at 95 °C during 10-15 minutes. The dye was isolated as red powder in 80% yield following purification over column and precipitation in pentane at low temperature. The condensation of **24** with TAT-aldehyde **22** in toluene with catalytic amount of p-TsOH at high temperature yielded the linked donor-acceptor **33** system in much lower yield. The product was isolated as red powder after purification over column and precipitation in pentane at low temperature. Note that despite the low yield reaction, the latter compound could be afforded contrary to the designed push-pull **28** and **32**. This result is probably due to the low reactivity of 6-methyl group of DCM **24** and the lower electrophilicity of aldehyde **26** and **30** compared to **18** and **22**.

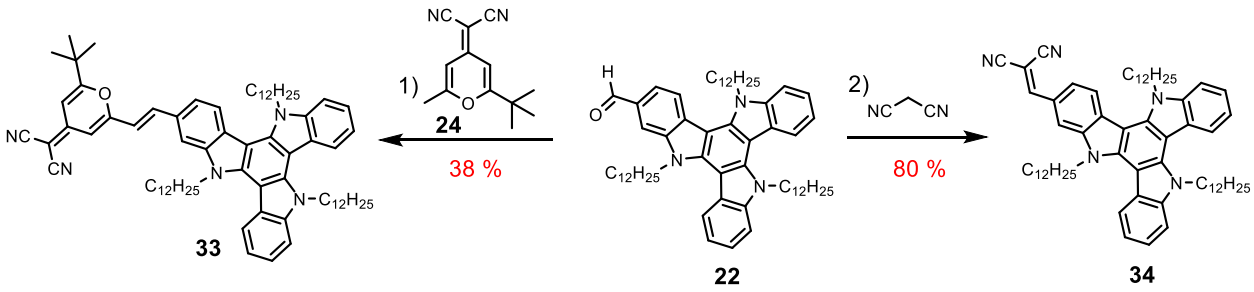

Scheme 2.7. Key. 1) p-TsOH cat., piperidine, toluene, 140 °C; 2) AcOH/piperidine, methanol, 95 °C, 10-15 min.

The proton NMR spectra of dyad **33** and **34** analysed in deuterated chloroform confirm their structures and are shown in Figure 2.10. In both spectra the disappearance of the resonance signal of the aldehyde proton C*H*O is accompanied with the appearance of new signals. For compound **34** (Figure 2.10b) the peak with a chemical shift δ = 7.79 ppm is assigned unambiguously to the proton of dicyanovinyl unit (noted "a" in the Figure 2.10b). Compared to the push-pull systems bearing a BODIPY core *i.e.* **27** and **31** (where δ = 7.85 ppm) this signal is slightly upfield.

For compound **33** the protons of DCM core are identified as doublet at δ = 6.60 ppm and 6.77 ppm with a proton-proton coupling $^{4}J_{H,H}$ = 2.0 Hz. The condensation of the formyl group with the methyl-DCM results in the formation of an ethylene bridge which adopts an (*E*)-configuration as confirmed by the typical value of vicinal protons constant $^{3}J_{H,H}$ = 15.7 Hz. The doublet of proton "3" (Figure 2.10a) is well indicated at δ = 6.87 ppm, whereas the second is downfield and overlapped with other signals.

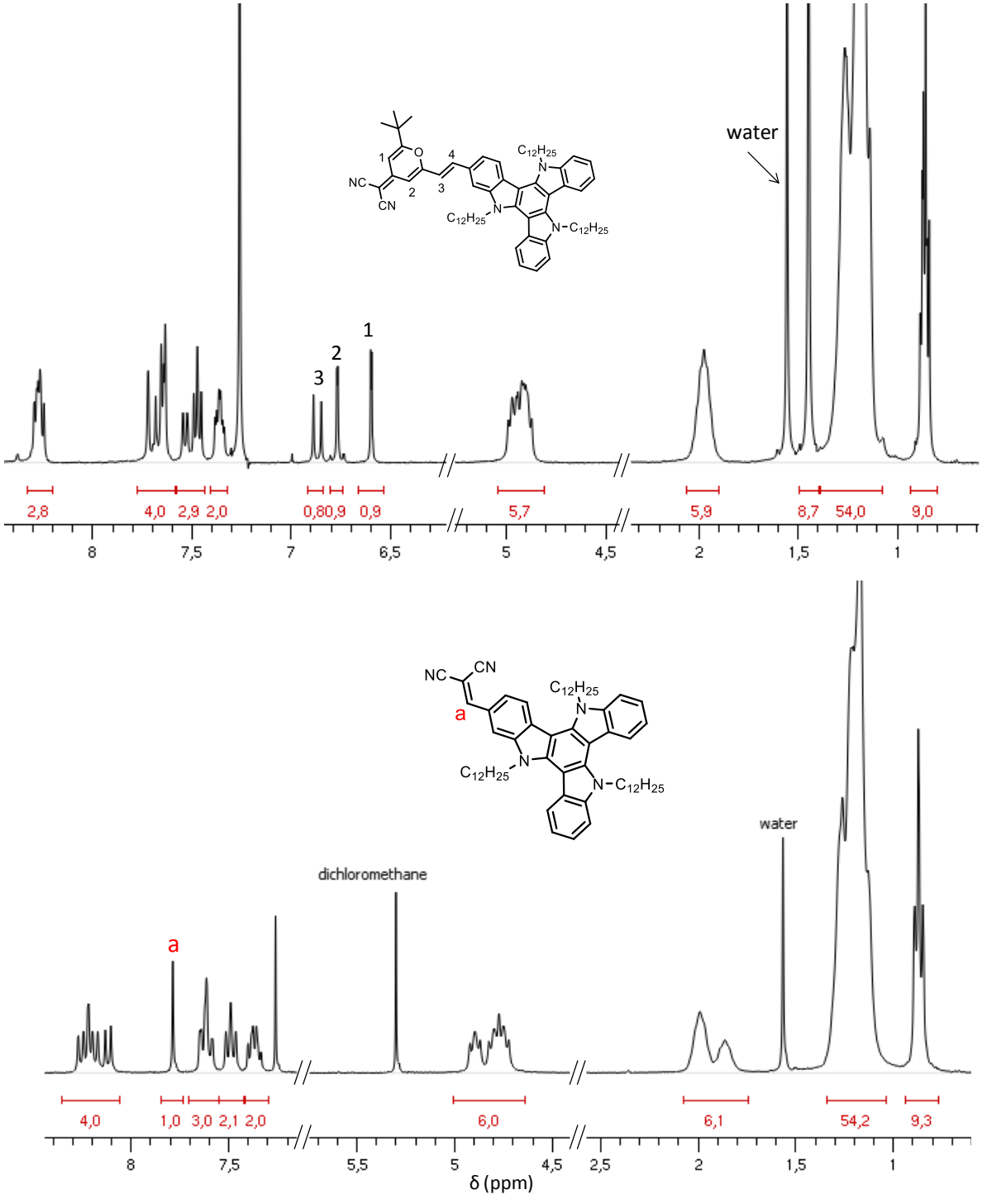

Figure 2.10. ^{1}H NMR spectra of dye **33** (upper) and dye **34** (lower) in deuterated chloroform.

3.3.2. Synthesis of the BODIPY-acceptor model 36

BODIPY-dicyanovinyl **36** lacks the electron-donor subunit *i.e.* julolidine or triazatruxene moiety and serves as a convenient model for the photophysical studies of the final push-pull chromophores. The synthesis of the target molecule was already reported in the literature by Jang and co-workers[115] however herein it is prepared according a different route in two steps from BODIPY **15** (Scheme 2.8). The carbo-formylation reaction of **15** catalyzed by palladium(II) in anhydrous DMF solution under a flow of CO at atmospheric pressure, gave **35** in good yield. The condensation of **35** with malonitrile in THF solution yielded the final dye **36** bearing a dicyanovinyl unit in 86% yield.

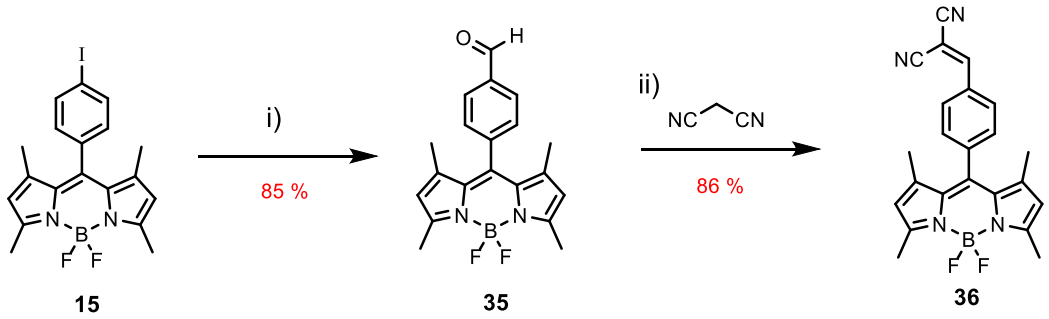

Scheme 2.8. Key. i) $[Pd(PPh_3)_2Cl_2]$ (10 mol%), HCOONa, DMF under a flow of CO at atmospheric pressure, 100 °C; ii) malonitrile, AcOH/piperidine, THF, 95 °C, 20-30 min.

4.1. Electrochemical measurements

The redox properties of the different compounds were measured by cyclic voltammetry in deoxygenated CH_2Cl_2 solution containing 0.1 M tetra-N-butylammonium hexafluorophosphate ($TBAPF_6$) as supporting electrolyte. Compound **25** which containe a julolidine arm as electron donor, displays two reversible oxidative waves at positive potentials as shown from the red cyclic voltammogram in Figure 2.11. They are fully reversible and correspond to a single electron process. These oxidations (having a half-wave potential of +0.38 V and +0.79 V *vs.* SCE) occur more easily comparing to the initial fragments **18** (julolidine-CHO, +0.86 V *vs.* SCE) and **15** (tetramethyl BODIPY +1.15 V *vs.* SCE). *This observation is a clear consequence of the increased overall conjugation in dye **25** due to coupling between the BODIPY core and the vinyl julolidine subunits.*

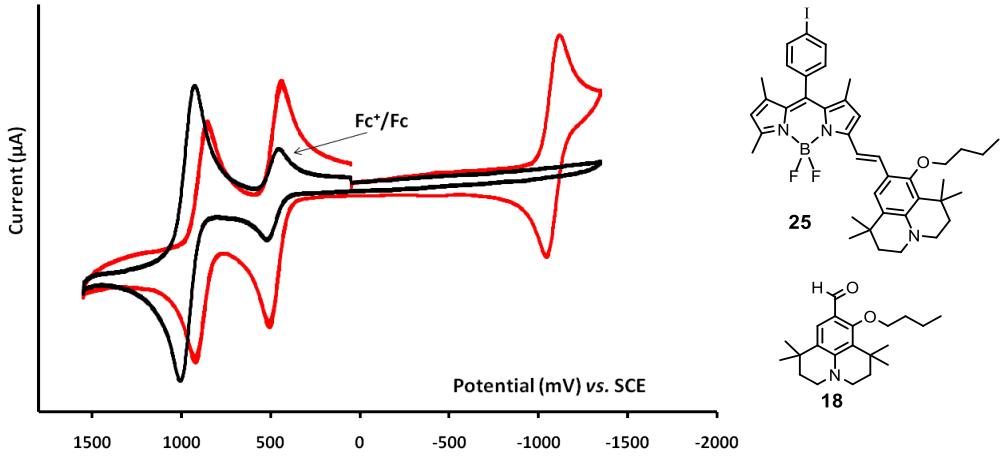

Figure 2.11. Cyclic voltammograms of compound **25** (in red) and **18** (in black). Concentration of dyes are 1.5 mM in CH_2Cl_2 (0.1 M $TBAF_6$), Fc^+/Fc refers to the ferrocenium/ferrocene couple used as internal reference $E_{1/2}$ (Fc^+/Fc) = +0.38 V (ΔEp = 60 mV).

The redox properties of triazatruxene **22** and mono-styryl **29** have already been reported and discussed in previous studies by T. Bura *et al.*.[113] The triazatruxene fragment **22** shows two reversible oxidative waves corresponding to one-electron transfer with half-wave potentials of +0.86 V and +1.45 V *vs.* SCE (*cf.* Table 2.1). The third oxidative wave is not seen within the anodic window.

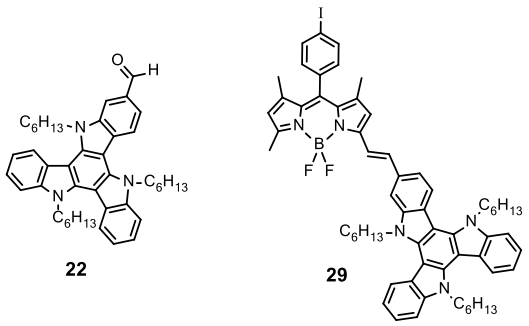

When the triazatruxene **22** is attached to the BODIPY core through the vinylic bridge thus forming **29**, the first oxidation step occurring with a half-wave potential of +0.67 V *vs.* SCE is easier by *ca.* 100 mV relative to the isolated triazatruxene **22** moiety. *As previously observed for **25**, the lower half-wave potentials are due to the increased conjugation in the final molecule*. Although the julolidine **18** and triazatruxene **22** have similar half-wave potential when isolated (*cf.* Table 2.1), the first oxidation of dye **29** bearing the TAT unit (+0.67 V *vs.* SCE) is however more difficult by *ca.* 300 mV relative to the first oxidation of dye **25** bearing the julolidine unit (+0.38 V *vs.* SCE). *This observation illustrates the differing degree to which the donor couples to the BODIPY moiety*. More evidence about that comes from the energy-minimized structures

indicating that julolidine-based nitrogen atom in **25** is out of alignment with the styryl unit only *ca.* 2.5° whereas the proximal N atom on the triazatruxene core **29** is twisted out of alignment by *ca.* 10°. The π-conjugation path of the molecular system being more efficient with the julolidine donor, the oxidation steps of the resulting dye occur easily comparing with dye **29** bearing the TAT. The consequence of this slight structural change between the dyes will be manifested also in their optical properties (*vide infra*).

Table 2.1. Electrochemical data of the key compounds.

Compound	$E°_{ox}$ [V] (ΔE [mV])	$E°_{red}$ [V] (ΔE [mV])
15	+1.15 (70)	-1.24 (60)
18	+0.86 (60)	-
25	+0.38 (70), +0.79 (60)	-1.17 (70)
27	+0.38 (70), +0.80 (60)	-1.04 (irr.), -1.24 (70)
29	+0.67 (70), +0.90 (70)	-1.09 (70)
31	+0.72 (60), +0.97 (60)	-0.98 (irr.), -1.10 (60)
22	+0.86 (70), +1.45 (70)	-

Potentials measured by cyclic voltammetry in deoxygenated CH_2Cl_2/0.1 M $TBAPF_6$ [electrochemical window from +1.6 to -2.2 V], solute concentration approximately 1.5 mM, at rt. Potentials were standardized *vs.* ferrocene (Fc) an internal reference and converted to the SCE scale assuming that $E_{1/2}(Fc/Fc^+)$ = 0.38 V *vs.* SCE. The error in half-wave potential is ± 10 mV.

At first sight, we may think that the first oxidation of both dyes **25** and **29** is assigned to the electron-donor subunit, but investigations at the DFT level (B3LYP6-31G) performed by Professor Anthony Harriman from the University of Newcastle,[118] (Figure 2.12) indicate that HOMO orbitals of **25** and **29** are not localized into the amino electron-donor subunits. They are spread over the molecule, taking contributions from the BODIPY and the amino-based cores (*i.e.* julolidine and triazatruxene). Taking account of the DFT results, we cannot assign the first oxidation step to the electron donor moiety. The LUMO level is distributed over the styryl-BODIPY fragment without contribution from the amino scaffold. The reduction of tetramethyl BODIPY **15** occurs with a half-wave potential of -1.24 V *vs.* SCE and is *quasi*-reversible when isolated but this process is easier by *ca.* 70 mV in **25** and *ca.* 150 mV in **29**. The electrochemical data are gathered in Table 2.1.

[118] Molecular Photonics Laboratory, School of Chemistry, Bedson Building, Newcastle University, Newcastle upon Tyne, NEI 7RU, UK.

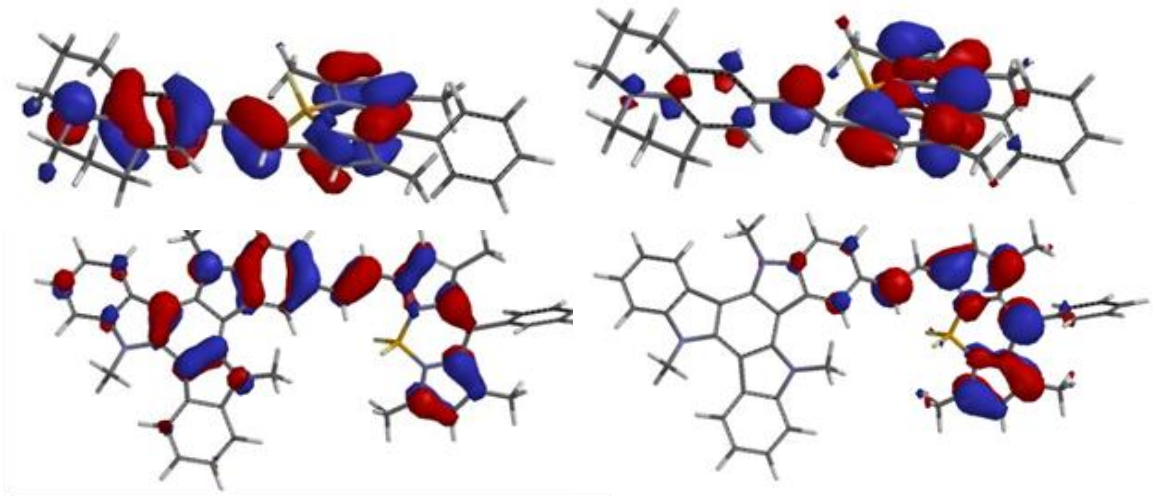

Figure 2.12. DFT calculations for compound **25** upper side: HOMO (left side) and LUMO (right side) and compound **29** lower side: HOMO (left side) and LUMO (right side).

When a dicyanovinyl fragment is appended to the mono-styryl **25** and **29** thus forming **27** and **31**, an irreversible wave appears at negative potentials *i.e.* -1.04 V and -0.98 V *vs.* SCE respectively as depicted in Figure 2.13. This is unambiguously assigned to one-electron reduction of the dicyanovinyl unit as supported by DFT calculations (*vide infra*). The *quasi*-reversible reduction at -1.24 V for **27** and -1.10 V for **31** corresponds to the radical anion of the BODIPY core. Interestingly, the addition of dicyano group on **29** does not perturb the reduction potential of BODIPY core but it induces an anodic shift by *ca.* 70 mV on oxidation processes, while addition of dicyano group on **25** thus providing **27** induces a cathodic *ca.* 70 mV for the reduction of BODIPY core but it does not perturb the oxidation processes (*cf.* redox values in Table 2.1).

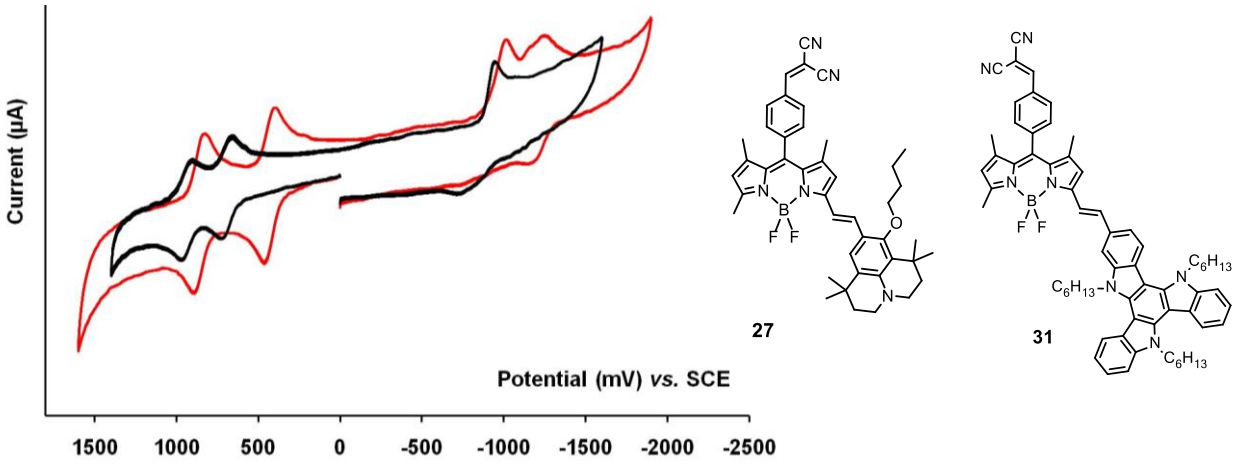

Figure 2.13. Cyclic voltammograms of **27** (red) and **31** (black). Concentrations of dyes are 1.5 mM in CH_2Cl_2 (0.1 M $TBAPF_6$).

Two reversible oxidative waves appear in positive scans for both molecular systems corresponding to one-electron oxidation of the amino and BODIPY subunits. The values are reported in Table 2.1. As previously announced for the mono-stryryl **25** lacking the acceptor group, investigations from DFT calculations for **27** localize the HOMO orbital over both julolidine and BODIPY core (Figure 2.14). As a consequence we cannot assign the first oxidation step appearing on the cyclic voltammogram (Figure 2.13, red) to the julolidine electron-donor module. The same is true for **31**; the HOMO is spread over the triazatruxene taking contribution also from the BODIPY moiety. The LUMO level in contrary is distributed only over the electron-attractor group (*i.e.* dicyanovinyl fragment), thus the irreversible reduction is unambiguously attributed to the dicyanovinyl fragment for both molecules. These results confirm the push-pull character of our final amino-BODIPY-dicyanovinyl molecular systems.

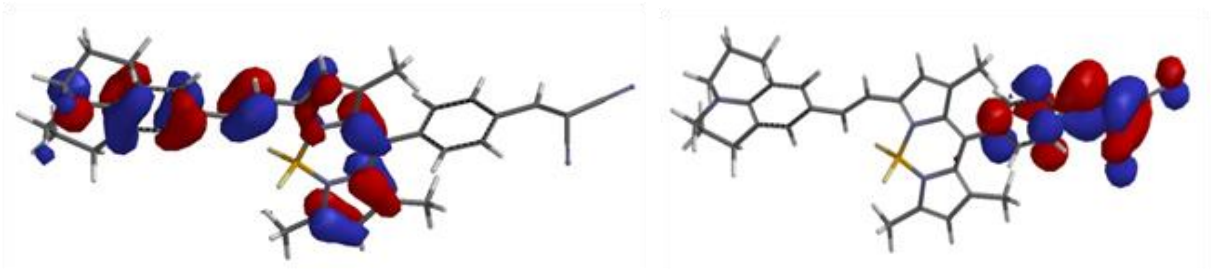

Figure 2.14. Representation of the HOMO (left) and LUMO (right) distribution of **27**.

The redox properties of the model compounds **33**, **34** and **36** were also measured; the data are gathered in the Table 2.2 and cyclic voltammograms depicted in Figure 2.15. The directly linked systems **33** and **34** show the two expected oxidations of the triazatruxene and the irreversible reduction of the dicyano fragment at -1.36 V *vs.* SCE for **33** and -1.30 V *vs.* SCE for **34**. The latter reduction is shifted by *ca.* 320 mV at higher negative potential comparing to **31** which includes the BODIPY bridge in its skeleton due to the absence of the phenyl ring in these systems. The oxidation occurs at the same potential as observed for the TAT **22** (*cf.* Table 2.1).
The cyclic voltammogram of **36** in Figure 2.15 displays an oxidative half-wave potential +1.19 V *vs.* SCE which corresponds to the radical cation of BODIPY unit. At negative potentials we note an irreversible reduction (-1.03 V *vs.* SCE) assigned to one electron transfer on the dicyanovinyl unit and a reversible one-electron reduction of BODIPY core at -1.32 V *vs.* SCE. In a general manner, the reduction of the dicyano group occurs at lower half wave potentials for **27**, **31** and **36** *i.e.* $\approx$ 1.0 V, relative to the models **33** and **34** lacking it.

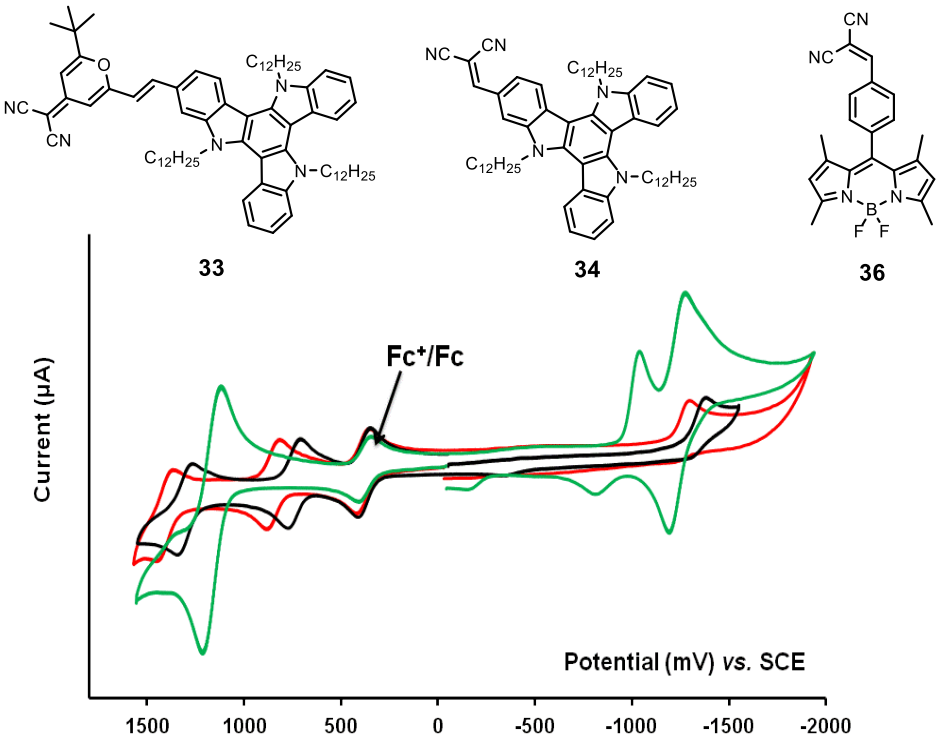

Figure 2.15. Cyclic voltammograms of dye **33** (black curve), **34** (red curve) and **36** (green curve) measured in deoxygenated CH_2Cl_2 using $TBAPF_6$ as supporting electrolyte.

Table 2.2. Electrochemical data of the target compounds.

Compound	$E°_{ox}$ [V] (ΔE [mV])	$E°_{red}$ [V] (ΔE [mV])
33	+0.75 (70), +1.31 (90)	-1.36 (irr.)
34	+0.92 (70), +1.49 (70)	-1.30 (irr.)
36	+1.19 (70)	-1.03 (irr.), -1.32 (70)

Potentials measured by cyclic voltammetry in deoxygenated CH_2Cl_2/0.1 M $TBAPF_6$ [electrochemical window from +1.6 to -2.2 V], solute concentration approximately 1.5 mM, at rt. Potentials were standardized *vs.* ferrocene (Fc) an internal reference and converted to the SCE scale assuming that $E_{1/2}(Fc/Fc^+)$ = 0.38 V *vs.* SCE. The error in half-wave potential is ± 10 mV.

5.1. Optical properties

The preliminary photophysical measurements of the compounds synthesized in the context of this work were realised in our laboratory while advanced photophysical measurements and analysis were conducted in collaboration with Professor Anthony Harriman and his co-workers from the University of Newcastle.[119]

[119] Prof. Anthony Harriman, Patrycja Stachelek, Mohammed A. H. Alamiry, "*Molecular Photonics Laboratory*", School of Chemistry, Bedson Bldg, Newcastle University.

5.1.1. Photophysical studies of mono-styryl dyes 25 and 29.

Absorption and emission spectra of **25** and **29** lacking the dicyanovinyl fragment were measured in various solvents at room temperature. The data of the optical properties are gathered in the Table 2.3 and 2.4. Considering the mono-styryl **29** the absorption spectrum displays three weak high energy bands and a broad low energy intense band centred at 607 nm (ε = 89 630 $M^{-1}cm^{-1}$) in MTHF solution. This band corresponds to $S_0 \rightarrow S_1$ transition of the BODIPY core but having a pronounced *charge-transfer character* as supported by the large increase of the transition dipole moment spread over the molecule. The computed (DFT-UHF-B3LYP/6-31G)[119] dipole moment is estimated to be 3.0 D in the ground state and 15.7 D in the excited state.

The absorbance maximum of the low energy band is slightly red-shifted in apolar solvents *i.e.* from 559 nm in CH_3CN to 616 nm in hexane. The fluorescence emission in MTHF has a maximum at 670 nm and a quantum yield φ_F = 0.56 and the excited singlet state lifetime is τ_s = 3.5 ns. The Stokes' shift ($\Delta\omega$ = 1550 cm^{-1}) is unusually large indicating that an important structural change takes place in the excited state. Indeed the fluorescence is strongly dependent on the solvent polarity; it is pronounced in nonpolar media (e.g. hexane, φ_F = 0.91 but strongly diminished in polar solvents (*e.g.* CH_3CN, φ_F = 0.13). For more value see Table 2.3

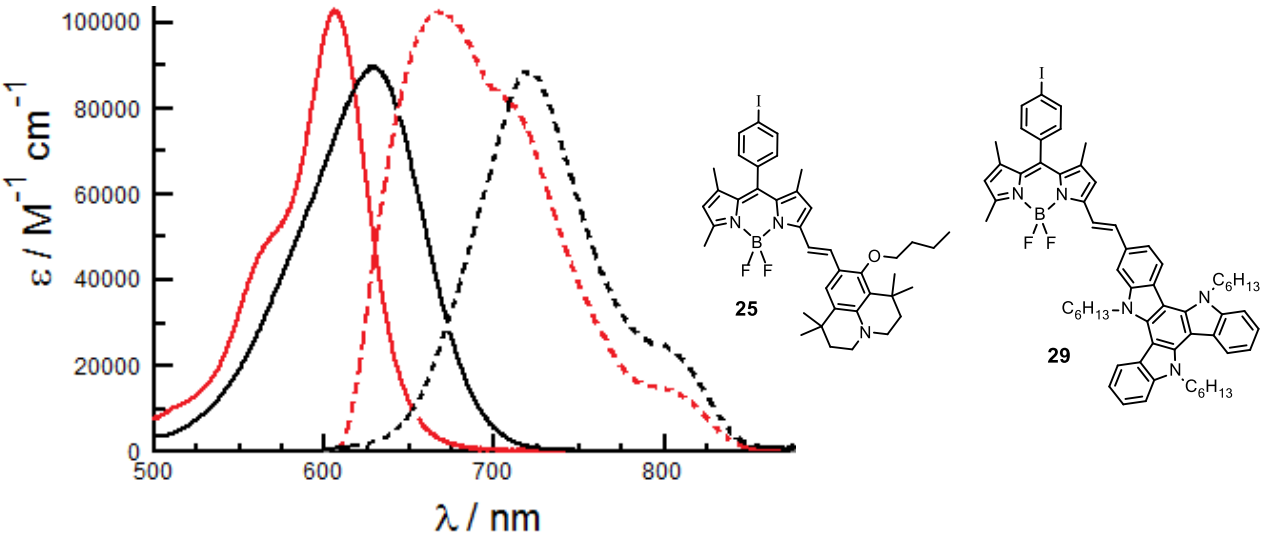

Figure 2.16. Absorption (full curves) and emission (dashed curves) spectra of **25** (black curves) and **29** (red curves) in MTHF at room temperature.

Table 2.3. Photophysical properties collected for **29** in various solvents at room temperature.

Solvent	λ_{abs} / nm	λ_{em}/ nm	φ_F	τ_S / ns	k_{rad}[a] / $10^8 s^{-1}$	k_{nr}[b] /$10^8 s^{-1}$
CH_3CN	599	709	0.135	1.30	1.04	6.70
Et_2O	606	653	0.710	4.00	1.78	0.72
EtOAc	605	668	0.560	3.50	1.60	1.26
Bu_2O	607	642	0.785	4.05	1.94	0.53
MTHF	608	668	0.540	3.45	1.56	1.33
CH_2Cl_2	610	700	0.208	1.70	1.20	4.60
C_6H_{12}	616	632	0.907	4.25	2.14	0.22

[a] k_{Rad} was calculated following the equation $k_{rad} = \varphi_F/\tau_F$. [b] $k_{nr} = (1-\varphi_F)/\tau_F$

The same behaviour is observed for the mono-styryl **25**. The absorption spectrum in MTHF solution sketched in Figure 2.16 is red shifted compared to **29** by *ca*. 24 nm consistently with the electrochemical studies (*vide supra*). It presents a broad intense band centred at 631 nm (ε_{max} = 103 055 $M^{-1}cm^{-1}$) which has *a significant charge-transfer character*. The molecule does not appear to be polar in the ground state as calculated theoretically (d_{GS} = 2.7 D), but the transition dipolar moment in the excited state estimated from Lippert-Mataga relationship[119] is enhanced at 17 D. Also the Stokes' shift is unusually large ($\Delta\omega$ = 1960 cm^{-1}) relative to general observations on BODIPY dyes. These results support the charge-transfer character of **25** in the excited state. The emission spectrum of **25** has a maximum at λ =720 nm, a quantum yield φ_F = 0.30 and the excited singlet state lifetime is τ = 2.8 ns. Measurements in various solvents indicate strong solvent-dependence for the emission. The latter is red-shifted from apolar solvents (hexane, λ_{em} = 661, φ_F = 0.92) to polar solvents with a quenching of the fluorescence (acetonitrile, λ_{em} = 775, φ_F = 0.023).

Table 2.4. Photophysical properties collected for **25** in various solvents at room temperature.

Solvent	λ_{abs} / nm	λ_{em}/ nm	φ_F	τ_S / ns	k_{rad} / $10^8 s^{-1}$	k_{nr} / $10^8 s^{-1}$
CH_3CN	644	775	0.023	0.88	0.26	11.0
EtOAc	637	725	0.450	3.15	1.43	1.75
Bu_2O	640	682	0.82	3.9	2.10	0.46
MTHF	631	720	0.30	2.8	10.7	0.10
CH_2Cl_2	642	766	0.003	1.1	0.25	9.2
C_6H_{12}	638	661	0.92	3.7	2.50	0.22

5.1.2. Photophysical studies of the linked push-pull systems 33 and 34

In order to better understand the role of the BODIPY bridge in the final push-pull systems **27** and **31**, the synthesis of the directly linked dicyanovinyl-amine-based molecules becomes helpful. These systems as well as the other models described before, show a broad absorption band. Their absorption maximum appears at *ca.* 480 nm in MTHF and 490 nm in CH_2Cl_2 and the band corresponding to an internal charge-transfer transition (Figure 2.17). As indicated in Table 2.5, **33** and **34** display a large dipole moment in the ground state and slightly higher transition dipole moment in the excited state. This information is consistent with the DFT calculations which localize the HOMO over the triazatruxene without contribution to the dicyanovinyl fragment and the LUMO over the latter. Both compounds show fluorescence emission in MTHF with low quantum yield. The Stokes's shifts are much larger ($\Delta\omega$ = 4787 cm^{-1} for **33** and 3575 cm^{-1} for **34**) compared to the mono-styryl BODIPYs **25** ($\Delta\omega$ = 1960 cm^{-1}) and **29** ($\Delta\omega$ = 1550 cm^{-1}) which clearly indicates that the excited state demands an important change in the geometry of the molecule. Although the BODIPY bridge is lacking in molecule **33** and **34**, they fulfil the requirements for being push-pull systems.

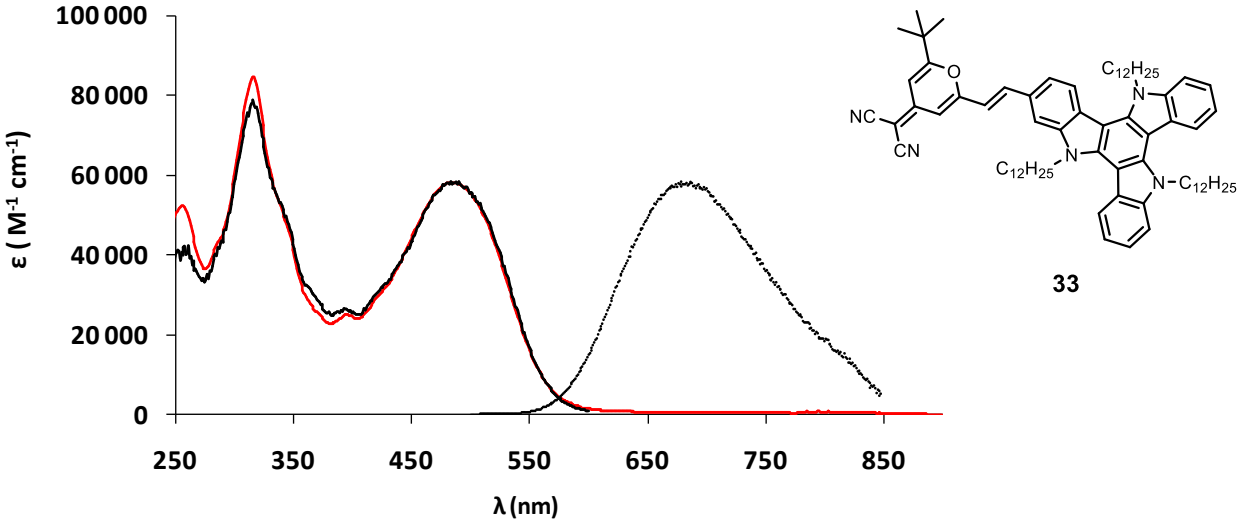

Figure 2.17. Absorption (black curve), emission (pointed black curve) and excitation (red curve) spectra of the push-pull system **33** in CH_2Cl_2 at rt. (c_1 = 2.08x10^{-6} M).

Table 2.5. Photophysical properties collected for **33** and **34** in MTHF at rt.

Cmp	λ_{Abs} (nm)	ε_{Max}/ ($M^{-1}cm^{-1}$)	d_{GS} (D)[a]	μ (D)[b]	λ_{Flu} (nm)	φ_F[c]	τ_F (ns)	k_{Rad} (10^7 s^{-1})[b]
33	484	85 500	9.1	10.8	626	0.033	3.3	1.0
33[d]	400	58 500	9.1	10.8	690	0.03	0.5	5.5
34	483	41 000	13.0	14.4	620	0.33	2.5	13.5
36	503	79 300	-	-	516	0.008	0.95	8.4

[a] Computed dipole moment for the ground state with DFT-UHF-B3LYP/6-31G[30]. [b]Transition dipole moment calculated from optical absorption spectra. [c]k_{Rad} was calculated following the equation $k_{Rad} = \varphi_F/\tau_F$.[d] Measured values for **33** in CH_2Cl_2 at rt.

5.1.3. Photophysical studies of BODIPY-dicyanovinyl compound, 36

The absorption spectrum of the BODIPY-dicyanovinyl **36** system in THF solution (Figure 2.18) at room temperature display a strong absorption band with λ_{max} = 502 nm and ε_{max} = 80 000 M^{-1} cm^{-1}. The same values are found in MTHF solution: λ_{max} = 502 nm and ε_{max} = 79 300 M^{-1} cm^{-1}. This absorption band corresponds to a $\pi \rightarrow \pi^*$ transition having also the character of a charge-transfer as previously observed for **27** and **29.** The result is supported by the DFT calculations which localize the HOMO onto the BODIPY unit and the LUMO onto the dicyanovinyl unit (Figure 2.20).

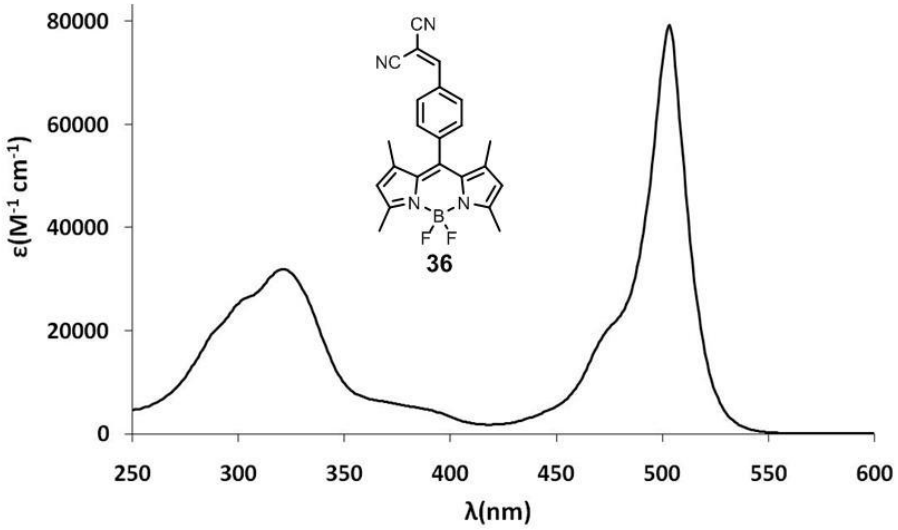

Figure 2.18. Absorption spectrum of compound **36** in THF solution at room temperature.

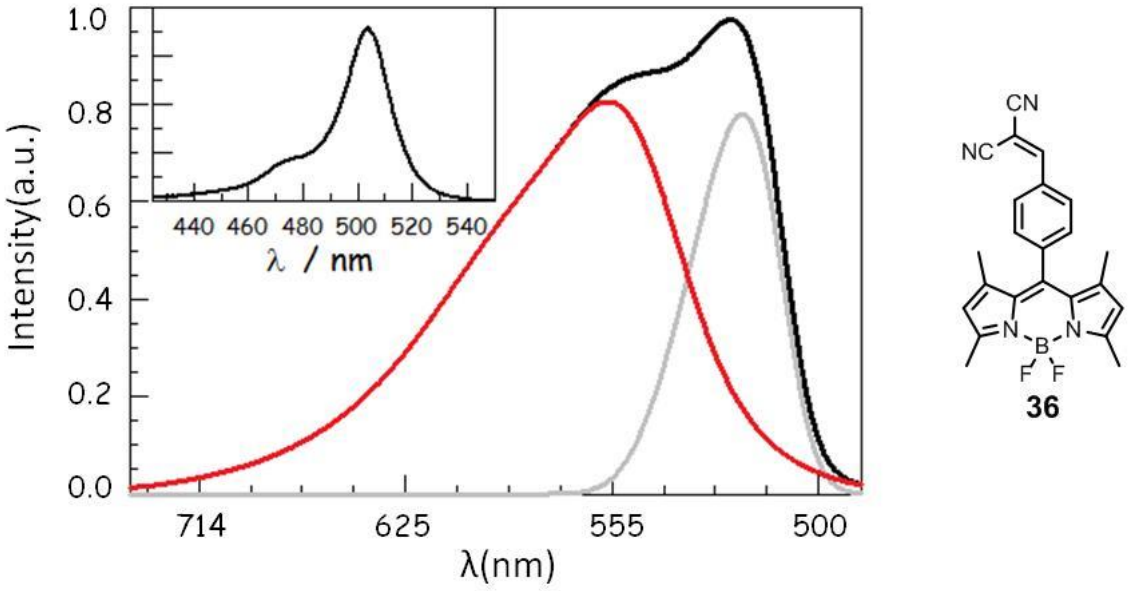

Figure 2.19. The solid black curve is the experimental fluorescence spectrum of **36** in MTHF at room temperature, the deconstructed red curve is the exciplex emission and the green curve is the local π,π* emission. In the insert is the lowest-energy absorption transition in MTHF at room temperature.

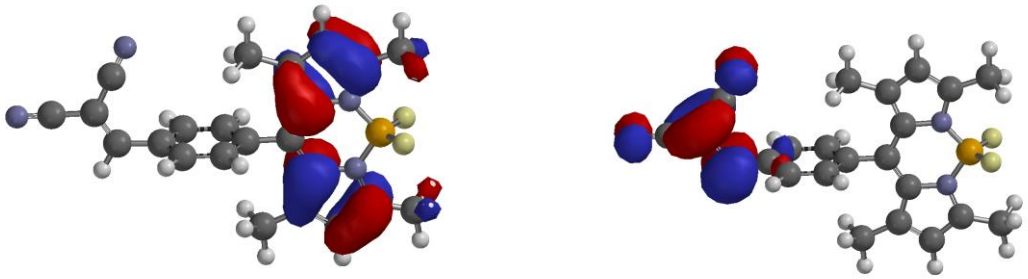

Figure 2.20. Representation of the HOMO (left-hand side) and LUMO (right-hand side) of compound **36** calculated by DFT.

The fluorescence emission is very weak (φ_F = 0.008) and the spectrum is broad displaying the appearance of two overlapping bands (λ_{max} = 516 nm and λ_{max} = 528 nm) as depicted in Figure 2.19. One corresponds to the contribution from the π,π* excited-singlet state and the second (red curve in Figure 2.19) corresponds to an *exciplex state* formed by partial charge transfer from the BODPIY to the dicyanovinyl unit. Both bands arise from direct excitation into the BODIPY absorption transition. Hence, excitation of compound **36** at room temperature induces the formation of a $\pi \rightarrow \pi^*$ excited singlet state S_1 which returns to the ground state S_0 *via* i) fluorescence, ii) or intersystem-crossing to T_1 state or iii) a partially charge-transfer to form an intramolecular *exciplex state* (EX) as depicted by the potential energy diagrams in the Figure 2.21.

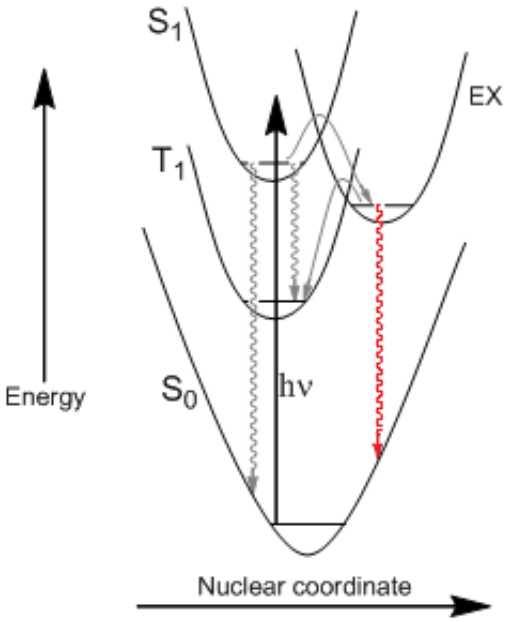

Figure 2.21. Potential energy diagrams of **36**.

The latter concept was introduced in Chapter 1 (§ 2.4.1) where was mentioned that the *exciplex transition* state favours the formation of a *charge-separated* (CS) state. On the basis of the electrochemistry, the broad fluorescence spectral profile obtained for **36** appears consistent with the formation of an emissive exciplex by way of partial charge transfer from the BODIPY excited state to the dicyanovinyl entity. Considering our system it is obvious that the exciplex state does not evolve into a CS state. Nevertheless, it is clear that a modest driving force for photoinduced charge-transfer (ΔG_{CT} = -0.17 eV) exists in MTHF at 20 °C**.** The value was determined from the Rhem-Weller equation based on the electrochemical data in conjunction with spectroscopic results.

$$\Delta G_{CT} = e[E_{ox} - E_{red}] - E^* - E_{ES} - E_{sol} \qquad \text{Eq. 1.18}$$

E^* is the energy of the excited state calculated from the intersection between normalized absorption and emission spectra (here E^* = 2.43 eV), E_{ES} is the energy resulting from the electrostatic attractive force pertinent to the charge-transfer state and E_{sol} correspond to the energy of the interaction with the solvent molecules.

- ***Effect of temperature and pressure on the exciplex emission***

In order to better understand the emission from the exciplex state, measurements on cooling the temperature of a THF solution of compound **36** have been performed. Thus on cooling the temperature of the solution, the emission from the locally π,π* excited-singlet state progressed becoming sharper while the emission from the exciplex state is extinguished (Figure 2.22). Additionally, the effect of the applied pressure on exciplexes behaviour has not been much reported in the literature. For this study, in order to measure the evolution of exciplex and the locally π,π* state as a function of pressure, deconstruction of the experimental spectrum as shown in Figure 2.19 is necessary.

Thus applying high pressure (P < 170 MPa) on a solution of **36** in MTHF solution extinguishes the exciplex emission because of the restricted rotation which subsequently enhances the emission essentially from the locally π,π* excited singlet state (Figure 2.23, left side). On the other hand at higher pressure 170 < P < 550 MPa (Figure 2.23, right side), **36** undergoes important structural changes because the molecule seeks to minimize its volume. The direct consequence of this is the completely extinguishing of exciplex emission and the fluorescence quenching of π,π* state through activating of other paths of nonradiative relaxation.

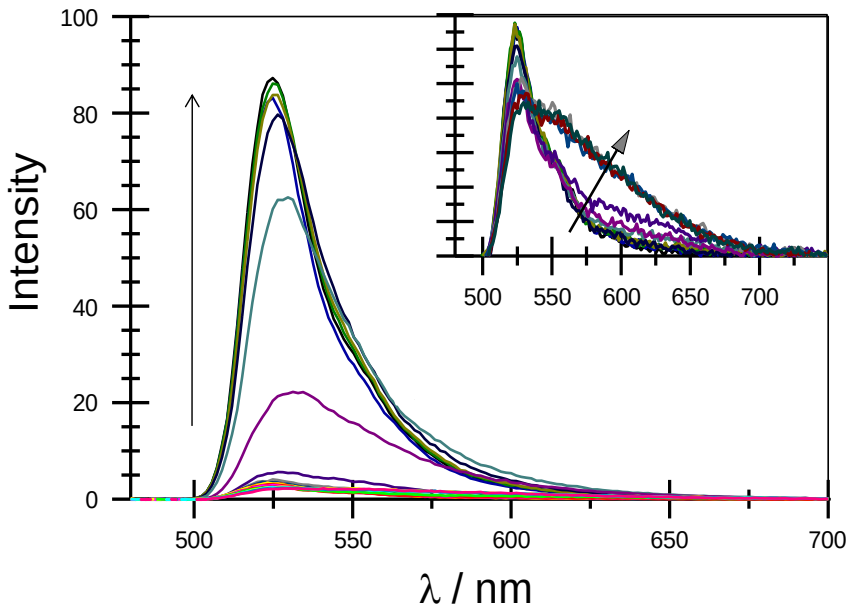

Figure 2.22. Effect of temperature on the emission of **36** in MTHF solution cooling the solution from 290K to 80K. The arrow indicates the progression of the emission through cooling the sample. The insert shows an expansion of spectral changes occurring from 180K to 290K.

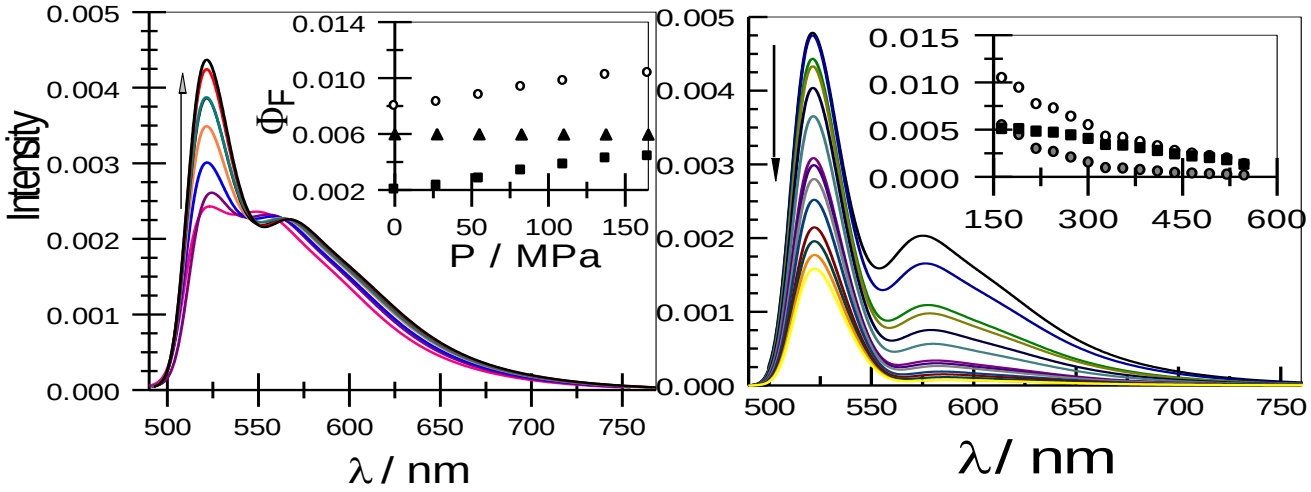

Figure 2.23. Effect of the applied pressure on the fluorescence emission of compound **36** in MTHF solution at room temperature. (Left side) Increasing of the pressure from atmospheric pressure to 165 MPa in regular increments. The insert indicates how the pressure affects the emission quantum yield for the total emission (O), for the π,π* excited state (■) and the exciplex emission (▲). (Right side) Effect of the applied pressure 170 < P < 550 MPa. The insert shows how pressure affects the fluorescence quantum yield for total emission (O), the π,π* excited state (■) and the exciplex (●).

5.1.4. Photophysical studies of the push-pull systems 27 and 31

The synthesized push-pull chromophores **27** and **31** contain a dicyanovinyl fragment as electron-attractor and an amino-derivative as electron-releasing moiety connected through the BODIPY bridge. Their normal absorption spectra are represented in Figure 2.24 and show similarities with those of parent dye **29** and **25** which lack the dicyanovinyl moiety. The formers are however red shifted by *ca.* 10 nm and slightly broadened. The absorption spectrum of **27** shows a large absorption band centred at 640 nm with an extinction coefficient ε = 88 900 $M^{-1}cm^{-1}$. Compound **31** as well presents a large band centred at 620 nm (ε = 114 720 M^{-1} cm^{-1}) represented in Figure 2.24.

In both cases, this absorption band accounts for the locally π → π* transition and a strong character of an electron density transfer from the electron-donor (aminostyryl-BODIPY residue) to the electron-acceptor dicyanovinyl fragment) since DFT predicts that the HOMO is spread over the aminostyryl-BODIPY residue and the LUMO on the dicyanovinyl fragment. The deconstruction of the low energy experimental band shown in Figure 2.25 and 2.26 clearly demonstrates the contribution from both transitions, *i.e.* CT and the local π,π*. Furthermore, the charge transfer character of this optical band is supported by the increased dipole moment of **27**

and **31** in the ground state compared to those of the parent **25** and **29** missing the dicyanovinyl (*cf.* Table 2.6). The calculated ground state dipole moment μ_{GS} of **31** is 8.0 D and for **27** is 9.3 D. The fluorescence of the push-pull dyes is quenched φ_F = 0.002 and radiative rate constant decrease relative the parent dyes **25** and **29**.

Table 2.6. Photophysical properties collected for **25**, **29**, **27** and **31** in MTHF at room temperature.

	λ_{Abs} (nm)	ε_{Max}/ ($M^{-1}cm^{-1}$)	d_{GS} (D)[a]	λ_{Flu} (nm)	φ_F	τ_F (ns)	k_{Rad} (10^7 s^{-1})[b]	λ_{CR} (eV)[c]
25	631	103 055	2.5	720	0.30	2.8	10.7	0.10
29	607	89 630	3.0	672	0.56	3.5	15.6	0.06
27	638	88 900	9.3	725	0.002	0.13	1.5	0.075
27[d]	637	88 980						
31	619	114 720	8.0	685	0.002	0.26	0.9	0.068
31[d]	619	114 900						

[a] Computed dipole moment for the ground state. [b] k_{Rad} was calculated following the equation $k_{Rad} = \varphi_F/\tau_F$. [c] Reorganisation energy accompanying charge-recombination emission extracted from spectral curve fitting. [d] Values found in THF solution of **27** and **31** at room temperature.

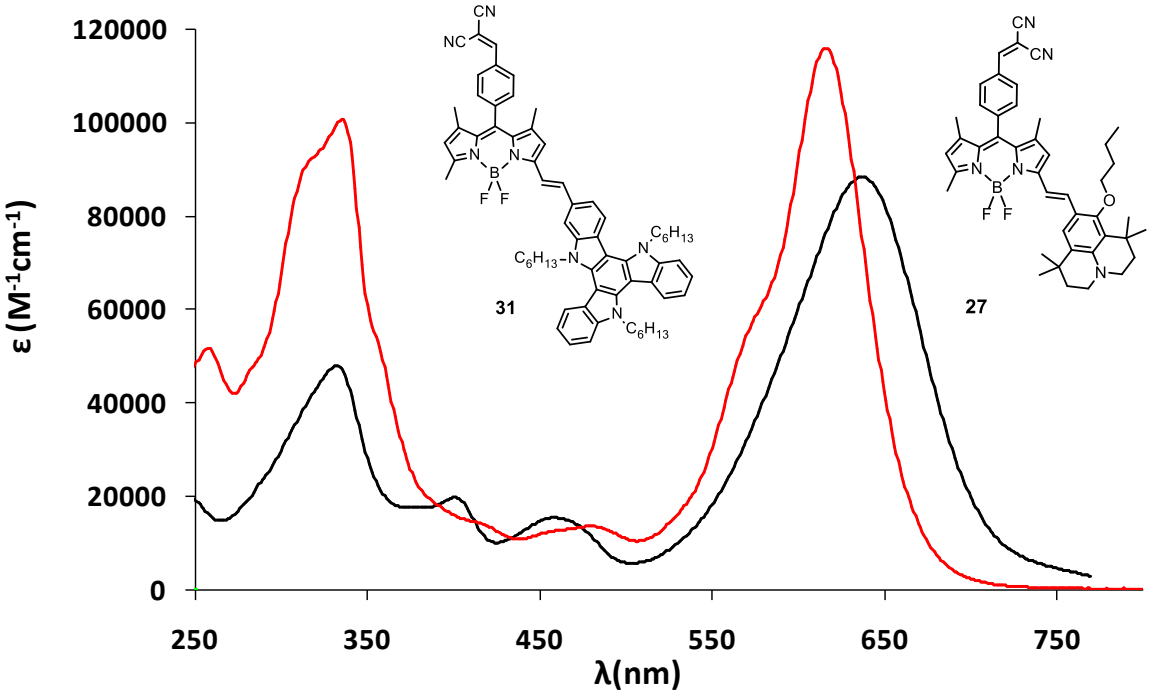

Figure 2.24. Absorption spectra of push-pull **27** (black curve) and **31** (red curve) in THF solution at room temperature.

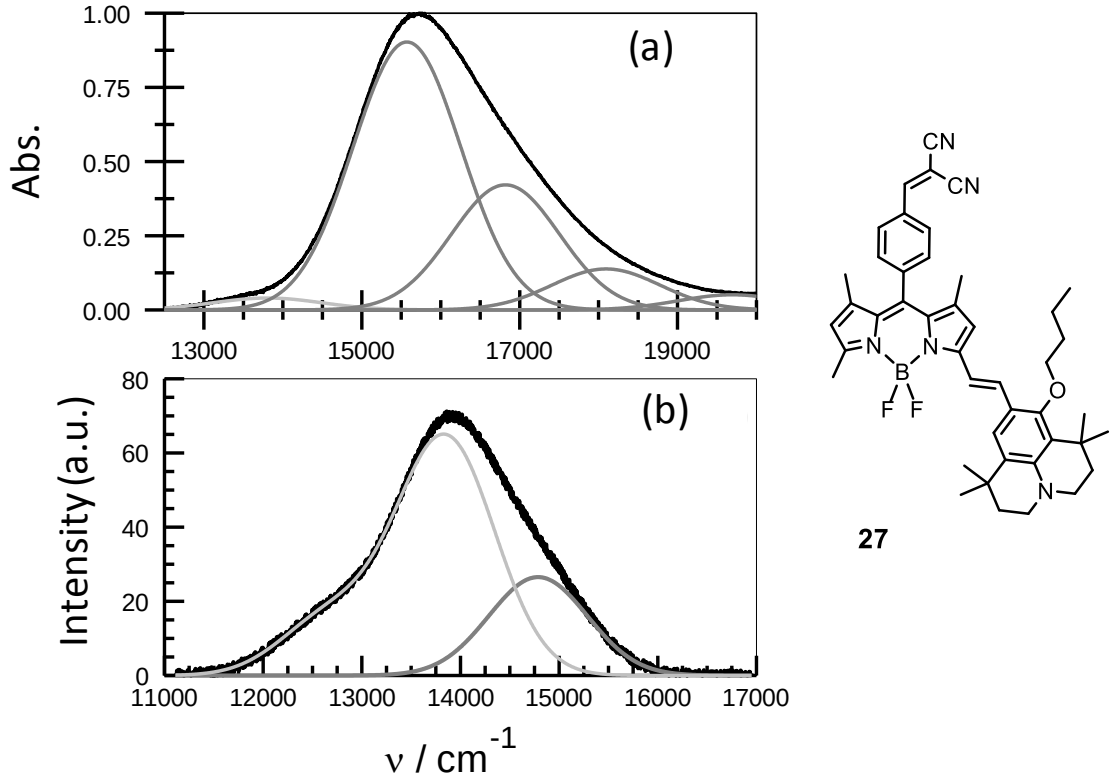

Figure 2.25. (a) Absorption and (b) fluorescence spectra recorded for **27** in MTHF at room temperature. In part (a), the solid black curve is the experimental spectrum, the light grey curve is the deconstructed charge-transfer transition and the dark grey curves are Gaussian components for the normal π,π* transition. In part (b), the solid black curve is the experimental spectrum; the light grey curve is the deconstructed spectrum for the emissive state.

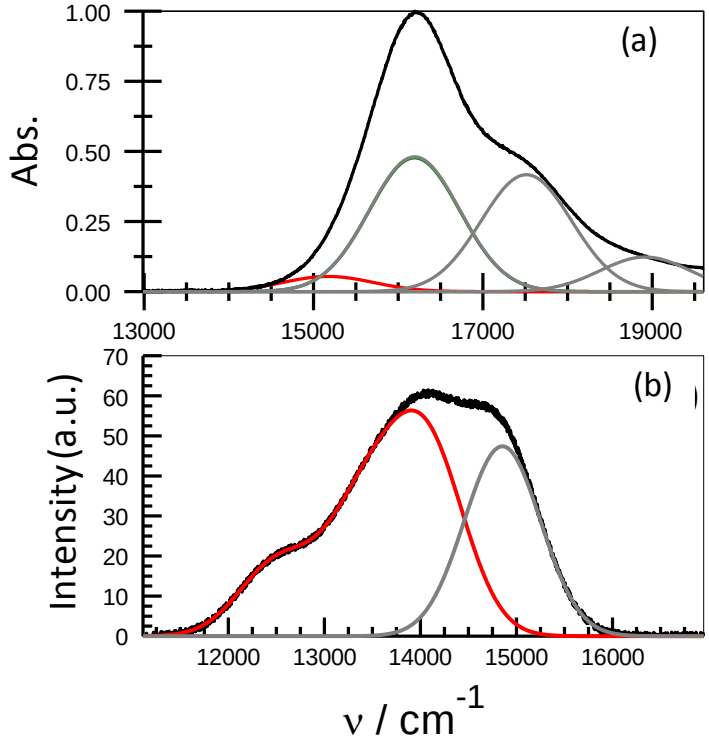

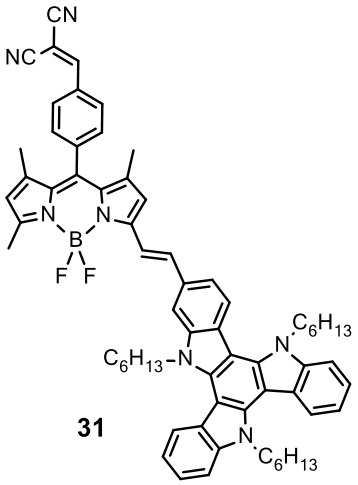

Figure 2.26. (a) Partial absorption and (b) fluorescence spectra recorded for **31** in MTHF at room temperature. In part (a), the solid black curve is the experimental spectrum, the red curve is the deconstructed charge-transfer transition and the grey curves are Gaussian components for the normal π,π* transition. In part (b), the solid black curve is the experimental spectrum; the red curve is the deconstructed spectrum for the emissive state.

6.1. Conclusion

The introduction of a dicyanovinyl unit onto the phenyl ring in the *meso*-position of the initial BODIPY dye **15** provides a route for quenching the fluorescence emission and increasing the dipole moment. The absorption transition displays a charge-transfer character and interestingly a modest thermodynamic driving force for a photoinduced electron transfer was calculated. Extension of the π-conjugation way by covalently linking strong electron-donor, thus forming **27** and **31,** results in systems with push-pull behaviour. This character is confirmed as the ground and excited state dipole moment are high and their radiative rate constants decrease relative to the parent dyes. Although the pronounced charge-transfer character, these push-pull systems do not promote a photoinduced charge-separation upon excitation. The mono-styryl **25** and **29** lacking the acceptor module show strong fluorescence with emission maximum depending on polarity of the solvent. Their rate constant of radiative decay k_{rad} are high and the computed dipole moments for the ground state are low compared to the push-pull systems **27** and **31**. The

dyes lacking the BODIPY bridging unit **33** and **34** indicate strong ICT character as supported by the DFT level calculation. These dyes are to be considered as push-pull systems since their ground state and excited state dipole moments are relatively high. However, under similar conditions, dye **34** bearing a dicyanovinyl shows significant emission quantum yield and high radiative rate constant relative to its analogue bearing a DCM unit.

II. Fluorescent probes

In this section we are concerned with the synthesis and the studies of a BODIPY dye which was obtained partially as a result of the work on the push-pull systems. This dye bearing two terminal aminostyryl-arms (*i.e.* the julolidine and the N,N-dimethylaniline) having a strong disparate character is much likely to be a promising fluorescent pH sensor. Before describing the synthesis and its electrochemical and optical properties, a general introduction on fluorescent pH probes would be of interest.

2.1. Introduction

The pH measurement constitutes an important parameter for widespread applications including medical diagnosis, water treatment and purification, food science, drug analysis and environmental monitoring. The most commonly used pH sensor is the pH glass electrode, which is however limited by its low performance at the extreme of pH scale.[120] Thus the development of novel pH sensor systems continues to be an attractive domain with increasing interest. During the past few years numerous efforts have been realized in the design and synthesis of optical sensors dealing almost with biotechnological and biomedical applications.[121] Intracellular pH (pH_i) is closely associated to the cell function and minor variation can cause different neurologic problem (*e.g.* Alzheimer's disease)[122] or cancer.[123] Thus, exact measurement of pH_i can be realized using fluorescent probes which switch "on" or "off" at specific pH values. The most widely used pH_i indicator is the 2',7'-bis-(2-carbooxyethyl)-5-(and-6-)carboxyfluorescein

[120] (a) Hecht, M.; Kraus, W.; Rurack, K. *Analyst*, **2013**, *138*, 325.(b) Belyustin, A. A. *J. Solide State Electrochem.* **2011**, *15*, 47.

[121] Urano, Y.; Asanuma, D.; Hama, Y.; Koyama, Y. Barrett, T.; Kamiya, M.; Watanaabe,T. Hasegawa, A.; Choyke, P. L. ; Kobayashi, H. *Nat. Med.* **2009**, *15*, 104.

[122]Davies, T. A.; Fine, R. E.; Johnson, R. J.; Levesque, C. A.; Rathbun, W. H.; Seetoo, K. F.; Smith, S. J.; Strohmeier, G.; Volicer, L.; Delva, L.; Simonis, E. R. *Biochem. Biophys. Res. Commun*. **1993**, *194*, 537.

[123]Izumi, H.; Torigoe, T.; Ishiguchi, H.; Yoshida, Y.; Tanabe, M.; Ise, T.; Murakami, T.; Yoshida, T.; Nomoto, M.; Kohno, K. *Cancer Treatment Rev*. **2003**, *29*, 541.

BCECF (Figure 2.27a), a fluorescein-based sensor introduced by Roger Tsien and co-workers in 1982.[124]

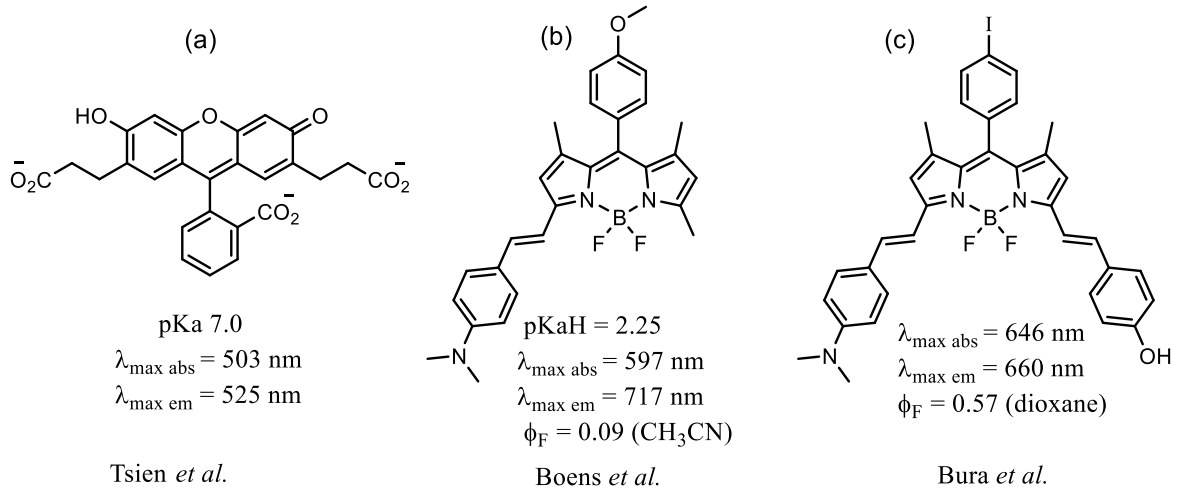

Figure 2.27

Diverse pH indicators for near-neutral pH values and acidic environment have been designed, synthesized and characterized, among them; the cyanine dyes which are one of the main class of the *Near-Infra Red* (NIR) fluorescent probes known for their biological applications.[125,126] Among the large library of dyes pointed as optimal choice for optical sensors, are notably those based on BODIPY scaffold. Generally, the pH-sensitivity into this type of pH-sensor probes is achieved by bearing a *p*-(*N*,*N*-dialkyl)aniline unit or by introducing a phenolic subunit at the *meso*-position of the BODIPY scaffold (*e. g.* the styryl BODIPY-dye in Figure 2.27b by Boens *et al.*).[127,128,129] The turning "on" and "off" of the fluorescence is controlled by protonation/deprotonation of the aniline nitrogen and hydroxyl group respectively. The fluorescence quenching mechanism of these dyes involves in most cases a photoinduced electron transfer process.

[124] Rink, T. J. ; Tsien, R. Y. T. Pozzan, *J. Cell. Biol.*, **1982**, *95*, 189.
[125] Patonay, G.; Salon, J.; Sowell, J.; Strekowski, L. *Molecules*, **2004**, *9*, 40.
[126] Tung, C.-H. *Biopolymers*, **2004**, *76*, 391.
[127] Kollmannsberger, M.; Gareis,T.; Heinl, S.; Breu, J. Daub, J. *Angew. Chem. Int. Ed. Engl*. **1997**, *36*, 1333.
[128] Gareis, T.; Huber, C.; Wolfbeis, O. S.; Daub, J. *Chem. Commun*. **1997**, 1717.
[129] (a) Coskun, A.; Deniz, E.; Akkaya, E. U. *Org. Lett.* **2005**, *7*, 5187. (b) Baruah, M.; Qin,W.; Flors, C.; Hofkens, J.; Vallée, R. A. L.; Beljonne, D.; der Auweraer, M. V.; De Borggraeve, W.; Boens, N. *J. Phys. Chem. A*. **2006**, 110, 5998. (c) Bura, T.; Retailleau, P.; Ulrich, G.; Ziessel, R. *J. Org. Chem*. **2011**, *76*, 1109.

The pH-sensitivity at the 3 and/or 5-position of BODIPY core for pH sensor system with a styryl bridge, has been studied more recently in a series of dyes prepared by T. Bura during his thesis work in this laboratory.[39c] Figure 2.27c represents one of the molecule bearing an amino and a phenolic subunit studied for this purpose. The principle point in the work presented herein focuses on BODIPY dye substituted with two different aromatic amines such as julolidine and N,N-dimethylamino benzaldehyde onto 3,5-positions. The synthesis, electrochemical and photophysical analysis as well as spectral titration studies determining the pKa values of the conjugated acid of both amino-sites will be discussed in this section

2.2. Synthesis of a mixed bis-styryl 38

In section 3.1 we already announced that the Knoevenagel reaction of BODIPY **15** with a large excess of julolidine **18** selectively gives the mono-condensed compound **25**. The bis-condensed product **37** was not observed. However, here we demonstrate that the condensation of the mono-styryl **25** with the 4-*N*,*N*-dimethylbenzaldehyde in toluene using piperidine as the base and catalytic amount of p-TsOH gave the hybrid bis-styryl **38** (Scheme 2.9). The product was isolated as a dark green solid in 75% yield following purification *via* a silica column chromatography and recrystallization. Also it was demonstrated that it could be afforded from the condensation of the known mono-styryl **39** with julolidine-aldehyde **18** following the same procedure (Scheme 2.9). The structure of the dye was confirmed by ^{1}H (*vide infra*), ^{13}C, ^{11}B NMR spectroscopy as well as IR, elemental analysis and EI mass spectrometry. The latter analysis furnished the most intense peak with *m/z* 892.2 identified as the radical cationic molecule and a fragmentation at *m/z* 873.2 corresponding to the molecule having loss a fluoride. The presence of the triplet signal at δ = 1.31 ppm with a B-F coupling being 33.4 Hz in the ^{11}B NMR spectra proton decoupled, confirms the maintaining of the boron difluoride center.

The selective mono-condensation of the tetramethyl BODIPY **15** with the julolidine aldehyde **18** reaction might be explained because of the steric hindrance that the julolidine scaffold engender due to the methyl groups placed at 1,1,7,7-position of the julolidine core. The linkage of a second julolidine moiety becomes difficult due to overlapping between the methyl groups of both julolidine units. Hence, the rotation around the ethylene bridge allowing an optimized geometry gets stuck by the presence of the methyl groups and among others the O-hexyl chain. The dimethylaniline unit being obviously less steric, the condensation reaction occurs without any major constraint.

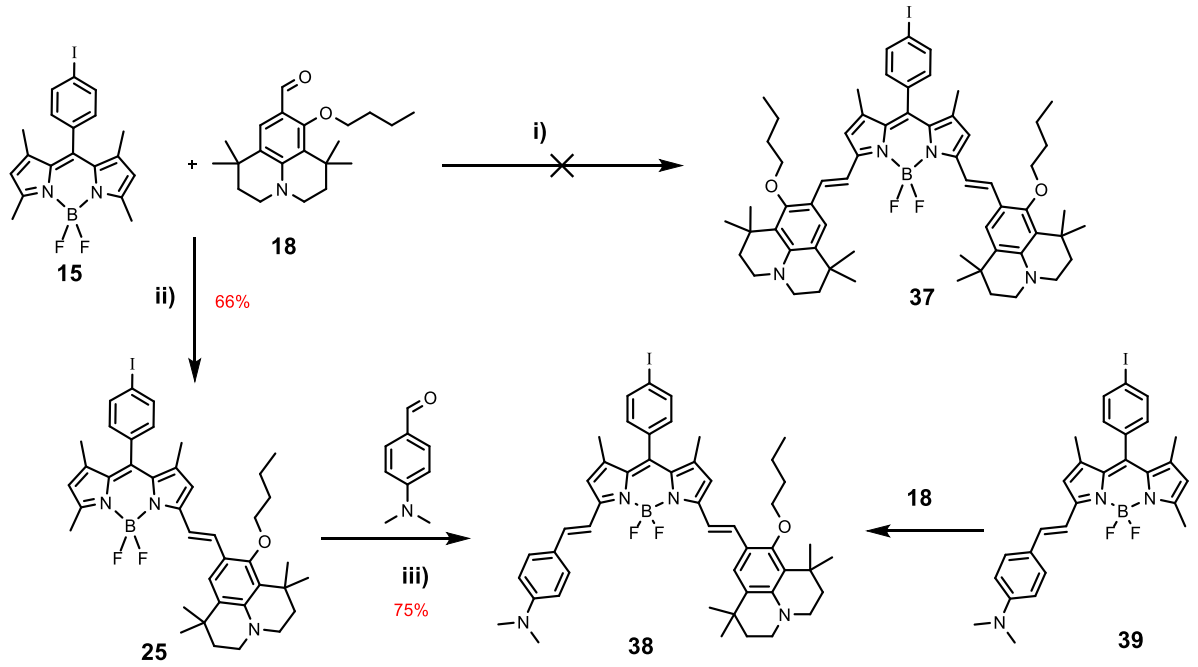

Scheme 2.9. Synthesis of compound **38**. For all the steps were employed the same reaction conditions: toluene, piperidine, p-TsOH cat., 140 °C until dryness.

2.2.1. ^{1}H NMR characterization of bis-styryl 38 and the mono-syryl 25

The proton NMR spectrum of product **38** was measured in deuterated chloroform and is presented in Figure 2.28. Its spectral profile is compared with proton NMR spectrum of mono-styryl **25** shown in the upper Figure 2.28. According the proton NMR analysis of **15,** the resonance signal of the β-pyrrolic protons is shifted at 6.0 ppm. The β-pyrrolic protons of **25**, herein numbered 6 and 7, are split at 6.0 ppm and 6.58 ppm as a result of the mono-condensation of the precursor tetramethyl BODIPY **15** with the corresponding aldehyde.

The spectral profile of dye **38** features one large signal for these protons at δ = 6.59 ppm. Hence the proton resonating at δ = 6.0 ppm is shifted downfield as a result of the second condensation of 4-*N*,*N*-dimethylbenzaldehyde with the methyl group at 5-position of BODIPY core. Furthermore the signal of the methyl (a, in Figure 2.28) appearing at δ = 2.58 ppm in the spectral profile of **25**, is missing in the spectrum of bis-hybrid **38** (lower side, Figure 2.28). The protons of the ethylene bridge in both dyes appear at *ca.* 7.5 ppm and are overlapped with other signals. However, the proton-proton coupling constant of dye **25** could be calculated as shown in the inserted figure in the upper Figure 2.28. The calculated $^{3}J_{H,H}$ = 16.3 Hz constant coupling confirms the maintaining of *trans*-configuration of ethylene bridging unit.

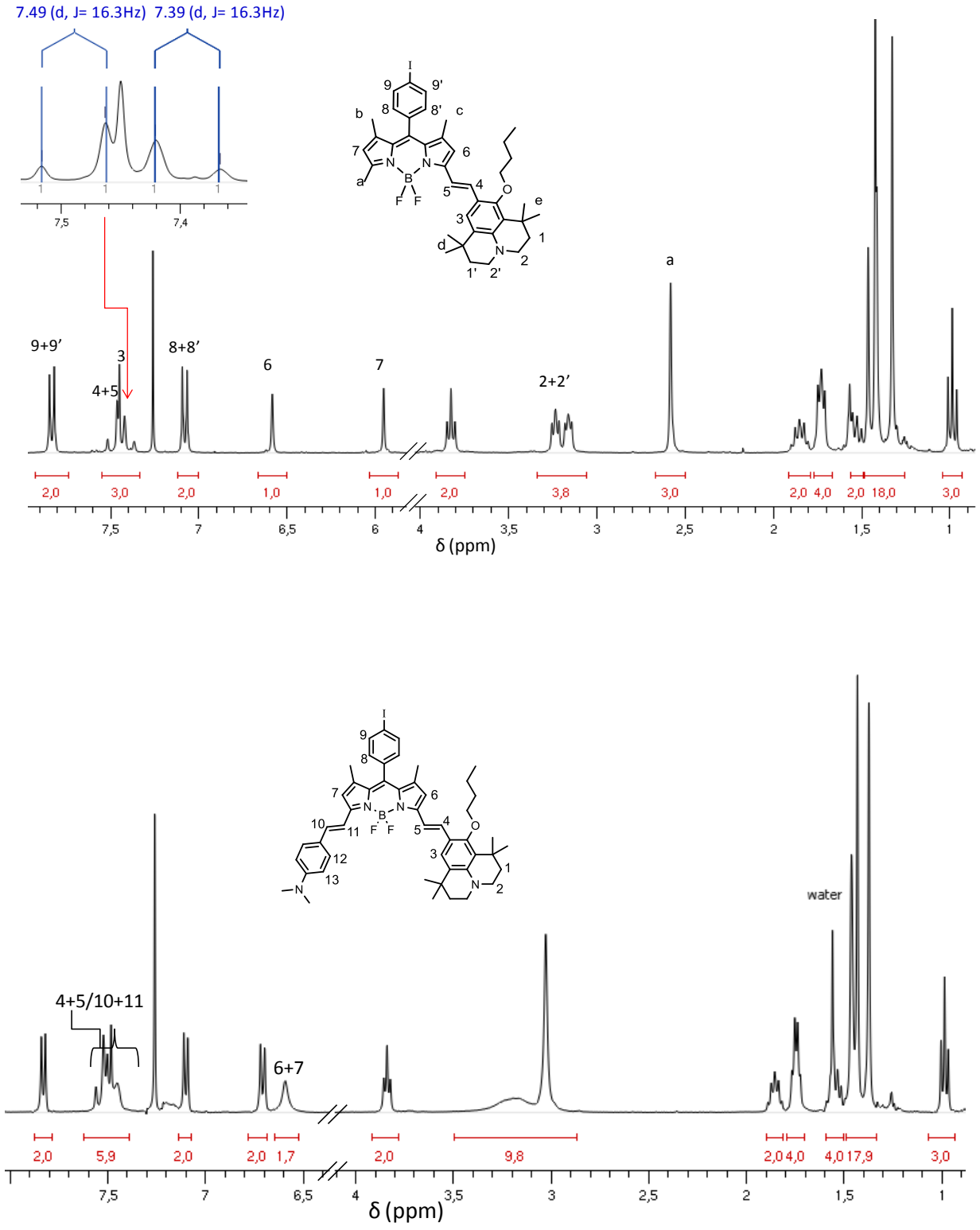

Figure 2.28. ^{1}H NMR spectra of bis-styryl **38** (upper side) and mono-styryl **25** (down side) in deuterated chloroform.

2.2.2. X-ray molecular structure analysis

The molecular structure of the bis-styryl was determined by single crystal X-ray diffraction obtained by slow diffusion of pentane into a concentrated solution of **38** in dichloromethane (Figure 2.29). The overall molecule shows a roughly planar structure. The iodophenyl group at the *meso*-position forms a dihedral angle of 79.7° with the BODIPY core, which is less orthogonal in comparison with that of compound **25** (*cf.* § 3.1.1, Figure 2.8). It appears from the X-ray structure that **38** have also a less planar dipyrrin core. In fact the introduction of a second molecular platform at the free methyl 5-position induces some distortion on the molecule core. The ethylene bridges between the BODIPY core and the terminal amine moieties adopt the (*E*)-configuration. The angles N-B-N and F-B-F are 107.8° (4) and 107.6° (4) respectively confirming the tetrahedral geometry of the boron centre.

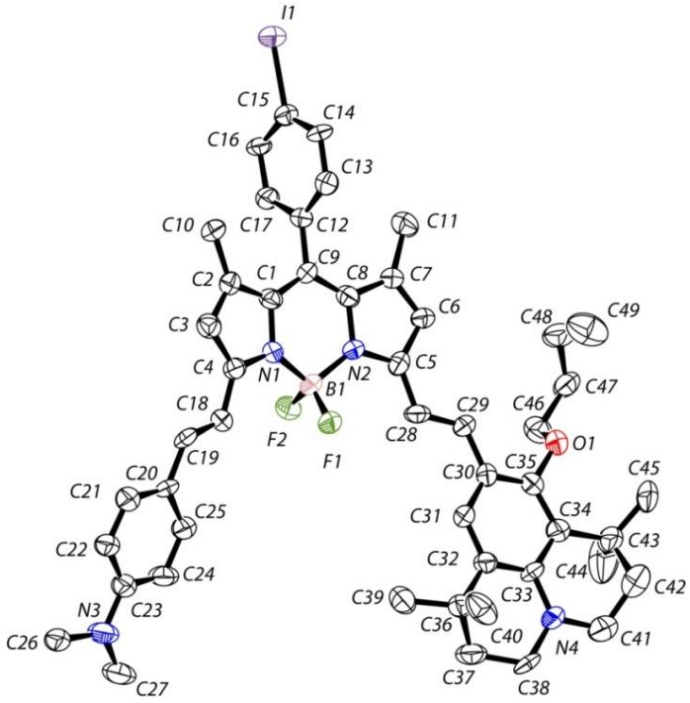

Figure 2.29. Molecular structure of compound **38**. ORTEP view with thermal ellipsoids plotted at 30 %. H atoms are omitted for clarity.

2.3. Electrochemical measurements

The electrochemical properties of compound **38** were measured by cyclic voltammetry in deoxygenated CH_2Cl_2 using $TBAPF_6$ as the supporting electrolyte. The data obtained are gathered in Table 2.7. The cyclic voltamogramm represented in Figure 2.30 displays three oxidative waves *quasi*-reversible with half-wave potential +0.26 V, +0.39 V and +1.27 V *vs.* SCE attributed to the oxidation of the BODIPY core and the amino moieties.

DFT calculations were made and localize the HOMO molecular orbital distributed over the whole molecule, such as it involves also the amino groups. According to these calculations we cannot distinguish which of the amino-moiety is oxidized first. Preferentially, we would think that the oxidation of the BODIPY core occurs after the oxidation steps of the two styryl-arms bearing the amino units. In negative scans a fully reversible reduction, with a half-wave potential -1.09 V *vs.* SCE is easily assigned to the formation of the π-radical anion of the BODIPY because according the DFT calculations LUMO is distributed only onto this latter moiety. This reduction is facilitated by 80 mV when compared with the mono-styryl lacking the dimethylaniline unit **25** (-1.17 V *vs.* SCE). When the solution of compound **38** in dichloromethane is treated with excess HCl vapor gas, the cyclic voltammogram (black curve, Figure 2.30) shows a fully reversible oxidation with a half-wave potential +0.53 V *vs.* SCE and an irreversible oxidation at +1.41 V *vs.* SCE corresponding to the oxidation of the BODIPY core. This oxidation is weakly shifted with respect to the non-protonated species as indicated by the cyclic voltamograms.

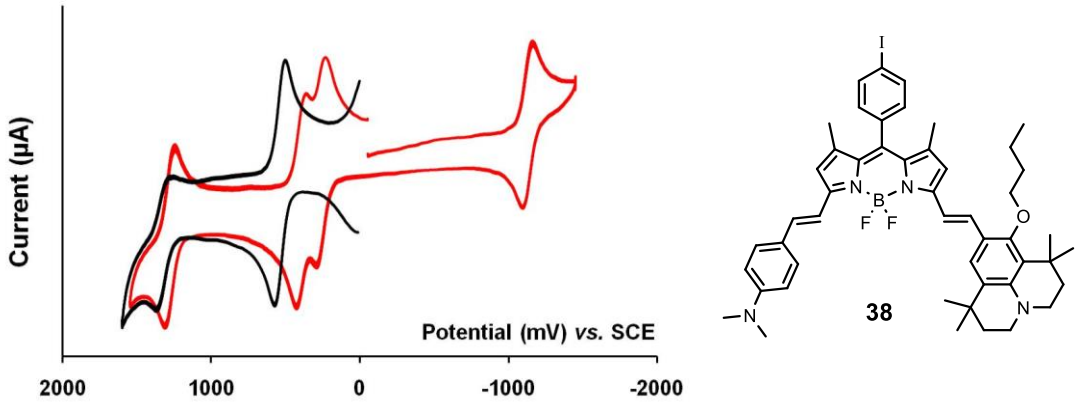

Figure 2.30. Cyclic voltamogramms of bis-styryl **38** in argon atmosphere (red curve) and the bis-styryl **38** under gaseous HCl (black curve). In acidic media the electrochemical window was restricted to positive potential to avoid proton reduction. Potentials are calibrated versus the SCE.

Table 2.7. Electrochemical data of the target compounds.

Compound	**$E°_{ox}$ [V] (ΔE [mV])**	**$E°_{red}$ [V] (ΔE [mV])**
38	+0.26 (60), +0.39 (60), 1.27 (70)	-1.09 (70)
38(HCl)*	+0.53 (80), +1.41 (irr.)	-1.08 (60)

Potentials determined by cyclic voltammetry in deoxygenated CH_2Cl_2/0.1 M $TBAPF_6$ [electrochemical window from +1.6 to -2.2 V], solute concentration approximately 1.5 mM, at rt. Potentials were standardized *vs.* ferrocene (Fc) an internal reference and converted to the SCE scale assuming that $E_{1/2}(Fc/Fc^+)$ = 0.38 V *vs.* SCE. The error in half-wave potential is ± 10 mV. * Values of the protonated **38** with excess of gaseous HCl.

2.4. Photophysical properties

The optical properties of bis-stryryl **38** were measured in different solvents and the data are gathered in Table 2.8. The absorption spectrum of **38** in CH_2Cl_2 (Figure 2.31) at room temperature exhibits an intense and broad absorption band centered at 736 nm (ε_{Max} = 84 000 M^{-1} cm^{-1}) having an internal charge transfer character. This band shows a dependence on the solvent polarity, since it undergoes a slight bathochromic shift passing from dibutyl ether as solvent (λ_{max} = 720 nm) to acetonitrile (λ_{max} = 736 nm). The next three high energy absorption bands are centered at 345 nm, 445 nm and 524 nm. The high energy absorption band occurring in the near UV region (λ_{max} = 345 nm) is assigned to the $S_0 \rightarrow S_2$ transition of the BODIPY core.

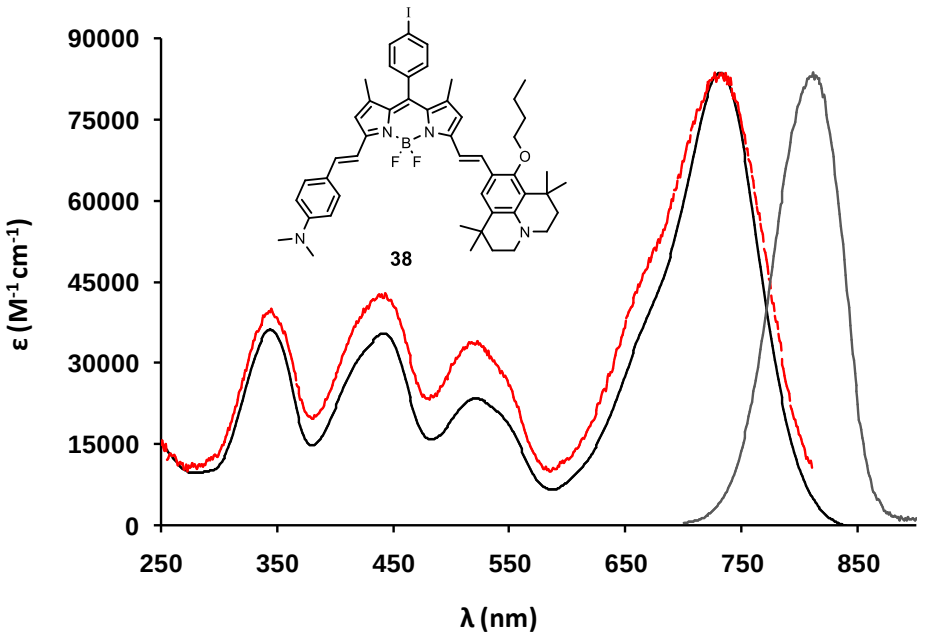

Figure 2.31. Absorption (full black line) emission spectra (grey line) and excitation (red line) recorded for dye **38** in dichloromethane solution at room temperature.

Table 2.8. Photophysical properties collected for **38** in various solvents in neutral or acidic conditions.

Solv.	λ_{abs} (nm)	ε ($M^{-1}cm^{-1}$)	λ_{em} (nm)	φ_F	τ_s (ns)	$\Delta\omega$ [c] (cm^{-1})	k_{Rad} [b] (10^7 s^{-1})
CH_2Cl_2	736	84 000	811	0.04	1.1	1260	3.6
CH_2Cl_2[a]	625	110 000	639	0.24	1.5	400	16.0
CH_3CN	736		820	0.02	1.0	1355	2.0
CH_3CN[a]	630		635	0.35	1.7	400	20.6
Bu_2O	720	84 000	748	0.15	2.8	520	5.4

[a]The optical parameters measured in CH_2Cl_2 or CH_3CN solution with amounts of gaseous HCl. [b] k_{Rad} was calculated following the equation $k_{Rad} = \varphi_F/\tau$. [c]$\Delta\omega$ is the Stokes shift.

The next two transitions are likely assigned to intramolecular charge-transfer process involving the amino-terminal moieties. The acidic treatment of CH_2Cl_2 solution causes the disappearance of these bands and a pronounced hypsochromic shift of the absorption/emission spectra (represented in Figure 2.32). This shift might be explained in terms of conjugation being decreased because the lone pairs of the N-atoms are not any more involved in the π-conjugation of the dye. The low-energy intense band centered at 736 nm is blue-shifted *ca.* 100 nm and it is well resolved after addition of vapour HCl in the dichloromethane solution. The intensity of the high-energy band centered at 345 nm is doubled but no shift is observed.

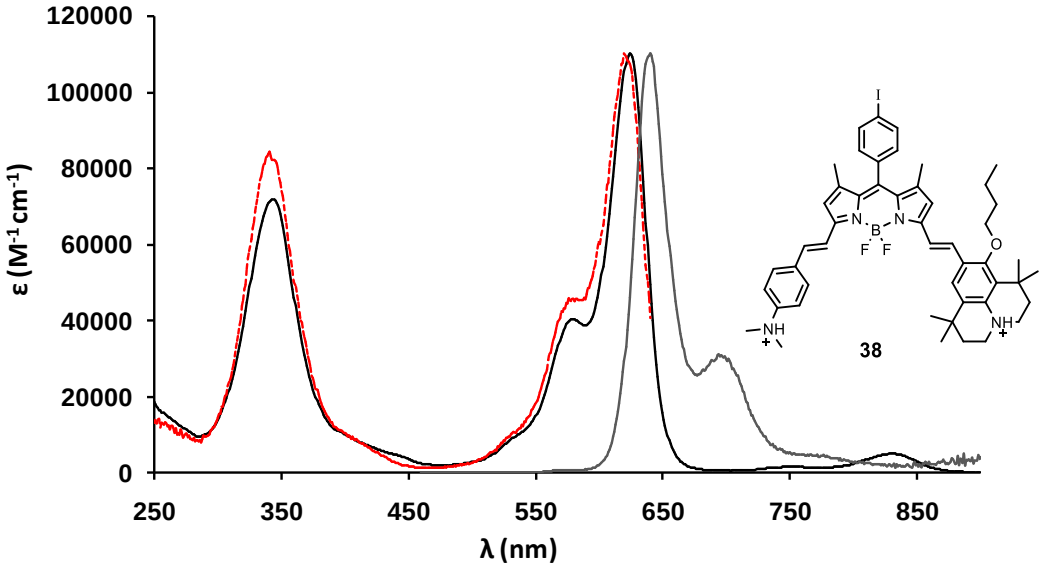

Figure 2.32. Absorption (full black line) emission spectra (grey line) and excitation (red pointed line) recorded for dye **38** in dichloromethane solution with addition of vapour HCl at room temperature.

The neutral bis-styryl **38** shows a broad fluorescence emission (Figure 2.31) centered at 811 nm with a low quantum yield φ = 0.04 and a rate coefficient of radiative decay k_{rad} = 3.3 10^7 s^{-1} in dichloromethane solution. Indeed the fluorescence is more affected from the polarity of the solvent contrary to the absorption (for values *cf.* Table 2.8). In dibutyl ether solution, λ_{em} = 740 nm is red shifted to λ_{em} = 820 nm in acetonitrile with a decrease on the luminescence quantum yield *i.e.* φ_F = 0.15 in dibutyl ether to 0.02 in acetonitrile. Furthermore, the Stokes' shift depends on solvent polarity and increases significantly on going from 520 cm^{-1} in dibutyl ether to 1355 cm^{-1} in acetonitrile indicating a slightly increase of the dipole moment after excitation. After acidification of **38** in acetonitrile or dichloromethane (Figure 2.32), the spectral emission profile of the protonated species features the narrow patterns of BODIPY-like dyes.[37-39] The fluorescence of the protonated bis-styryl increases significantly (for values see Table 2.8) and becomes sharper. The Stokes' shift decreases from 1260-1350 cm^{-1} for the neutral dye to 400

cm^{-1} for the bis-protonated dye. The different high energy absorption bands and the principal low energy band in the absorption spectra of the non-protonated and bis-protonated BODIPY dyes are well reproduced in their respective excitation spectra.

2.5. Spectral titration and pKa values determination

Absorption and fluorescence spectral titration were carried out for the compound **38** bearing two distinct terminal amino-arms in acetonitrile solution by gradual addition of amounts of HCl within a pH window going from 7.7 to 0.6. These studies were realised by Professor Anthony Harriman and his co-workers from the University of Newcastle.

The absorption (Figure 2.33) and emission (Figure 2.34) spectral titration indicate that the protonation process of dye **38** occurs in two successive steps. The addition of the first proton thus forming the mono-acid dye **38(H$^+$)** causes a slight blue-shift of the absorption spectra with retention of the transition bands observed for the neutral species. The addition of the second proton thus forming the di-acid species **38(H$^+$)$_2$** is accompanied with sharpened and pronounced blue-shift absorption spectra and an increase of the extinction coefficient. The analysis of the spectral data calculated with Spectfit[130] gave a pKa value of 5.75 for the first protonation and 2.75 for the second protonation.

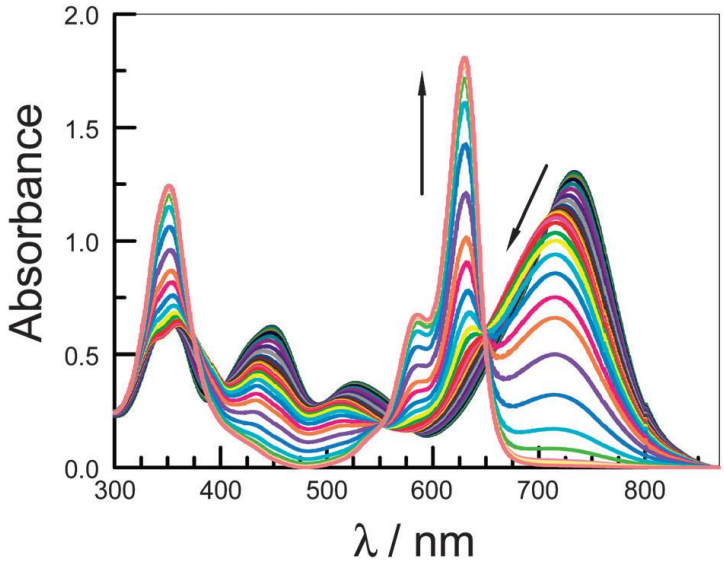

Figure 2.33. Absorption spectral titration of dye **38** (15 mM) in CH_3CN solution by progressive addition of HCl (effective pH decreasing from 7.7 to 0.6). The arrows indicate the major decrease/increase shifts during the addition of amount of HCl.

[130] Astron., K. G. *Astron. Soc. Pac. Conf. Ser.* **1994**, *61*, 437.

The fluorescence spectral titration were concomitantly measured by excitation at 365 nm which is an *isobestic point*; wavelength where the three species absorb similarly. Indeed three isobestic points are observed in the absorption spectra: 365 nm, 550 nm and 650 nm, but at 365 nm all the species absorb strongly than the two other points. Small addition of HCl causes a slight shift of the emission maximum from 820 nm to 810 nm which is ascribed to the fluorescence emission of the mono-protonated species. Further addition of HCl completely shifted the emission maximum at 635 nm corresponding to the fluorescence emission maximum of the di-protonated dye. The analyses of the fluorescence spectral data evaluate a pKa value of 5.80 for the mono-protonated form and 2.70 for the di-protonated species, which are in excellent agreement with the values found from absorption spectral titration.

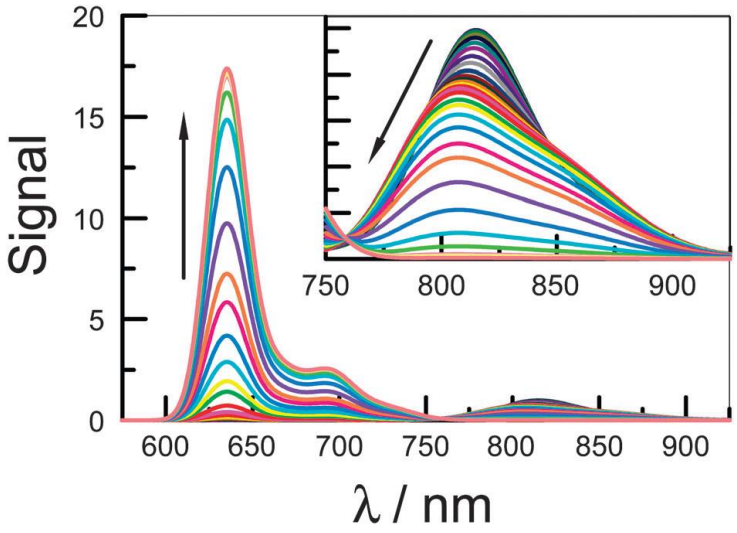

Figure 2.34. Fluorescence spectral titration of dye **38** (3μM) in CH_3CN by addition of increasing amount of HCl. The arrows indicate the reaction course by the addition of acid.

Considering the question of the first protonation step, theoretical analysis from DFT calculations (B3LYP/6-31G) were carried out and indicated in terms of Lowdin charges[131] for the N atoms of the amino units, that the first proton is added on the julolidine terminal. The second step of protonation is rendered difficult, so that the pKa of the conjugated di-acid is lower.

3.1. Conclusion

Herein we have synthesized and fully characterized a hybrid BODIPY dye bearing two different aromatic amino-moieties. They were introduced at 3,5-positions of the BODIPY core by means of a styryl arm generated using a Knoevenagel-type condensation. This is the first example of a

[131] Hollingsworth, C. A.; Seybold, P. G.; Hadad, C. M. *Int. J. Quantum Chem.* **2002**, *90*, 1396.

BODIPY derivative dye anchoring two disparate amino terminals at these positions. Interestingly this dye is likely to constitute a new class of fluorescent pH sensors operating in a broad pH range window *i.e.* 2-7. The electrochemical and photophysical analysis confirm the pronounced disparate character of the dimethylaniline and julolidine when they are linked to the BODIPY scaffold. The theoretical DFT calculations carried out for the synthesized dye indicate that julolidine moiety is protononated first, thus generating the acid conjugated species **38(H^+)** with a pKa value 5.75-5.80. The latter values are estimated from spectral titration in acetonitrile solution with addition of HCl. The first protonation step has a strong consequence in the addition of the second proton. It results that the formation of the di-protonated species becomes more difficult. The pKa of the di-protonated species were evaluated to be 2.78-2.70 by absorption and emission spectral titration.

Chapter III

Chapter III - Evaluation of julolidine-based ligands and its complexation with boron(III), iridium(III) and platinium(II). Design, synthesis and study of multichromophoric systems

1. Introduction

Chapter 1 introduced the julolidine in more details pointing out its intriguing chemical scaffold which obviously kept our attention during this doctoral thesis. *Due to the conformational rigidity, the electron lone pair of the nitrogen atom is fully conjugated within the aromatic π-system conferring to the julolidine core unusual reactivity.* Numerous julolidine-containing organic materials have been reported for various applications in biology and photonic devices (*vide supra*).

However, bibliographic investigations do not provide much information about julolidine derivatives being exploited as coordinating ligand in transition metal complexes. When this work was carried out, there were no reports in the literature about transition metal centers bearing a julolidine-based ligand. Recently, Borisov *et al.*[132] reported the synthesis and optical properties of palladium(II) and platinum(II) complexes with tetradentate Schiff bases, among them a tetradentate julolidine-based ligand chelating a Pd(II) center (Scheme 3.1). To the best of our knowledge, this was the only example, appearing in the literature until the moment of writing this thesis.

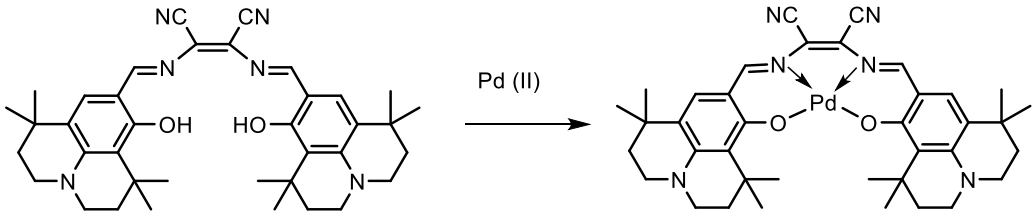

Scheme 3.1. The tetradentate ligand based on julolidine core and its Pd(II) metalation by Borisov *et al.*.[132]

[132] Borisov, S. M.; Saf, R.; Fischer R.; Klimant, I. *Inorg. Chem.* **2013**, *52*, 1206.

The lack of studies concerning the julolidine entity as ligand prompted us to explore the chemistry and optical properties of the transition metal complexes with julolidine-based ligands. Among the various transition metals we selected iridium(III) and platinum(II) which are well-known to provide emitting excited states. Alongside, complexation with boron(III) was explored.

Iridium is a robust metal of third row transition metal with a ground state electronic configuration $5d^7 6s^2$ and may have oxidative state -3 to +9.[133] The more common and largely utilized is Ir(III) $5d^6$ because of its higher stability. In general $4d^6$ and $5d^6$ metal complexes *e.g.* Ru(II), Os(II), Rh(III), Ir(III) have attracted much attention for photochemical applications because of their long lived-excited state and efficient photoluminescence. In this work we were concerned with the cyclometalating Ir(III) complexes.

1.1. Iridium^{III} cyclometalating complexes[134]

The intriguing chemistry of iridium(III) *ortho*-cyclometalating complexes was born with the pioneering works of Nonoyama[135] and Watts[136] independently. In 1974, Nonoyama reported the first dimeric dichloro-bridged iridium(III) complex, obtained upon reaction of benzo[*h*]quinoline base (*bhqH*) with an iridium(III) precursor $Na_3[IrCl_6]$, in refluxing 2-methoxyethanol (Figure 3.1a).[4] In 1977, Watts synthesized a cyclometalating complex from the reaction of 2,2'-bipyridine (*bpy)* with $IrCl_3.6H_2O$ in refluxing ethoxyethanol. The molecular structure of the complex was obtained in 1981 and revealed that one bipyridine cyclometalates the Ir center through the C3-carbon (Figure 3.1b). This coordination is unusual for 2,2'-bipyridines but it opened the way to the use of 2-phenylpyridine (*ppyH*) as potential cyclometalated ligands. In 1985 Watts *et al.* published the synthesis of a dimeric dichloro-bridged iridium complex (Figure 3.1c) from the reaction of 2-phenylpyridine with Ir(III) precursor following the same strategy proposed by Nonoyama.

---

[133] It was recently discovered that iridium can have an oxidative state +9, found in: Wang, G.; Zhou, M.; Goettel, J. T.; Schrobilgen, G. J.; Su, J.; Li, J.; Schlöder, T.; Riedel, S. *Nat.* **2014**, *514*, 475.

[134] Whitte, Victoria Louise (2008) *Synthesis and luminescence of iridium and rhodium complexes incorporating NCN-coordinating tetradentate ligands*, Durham thesis, Durham University. Available at Durham E-Thesis Online: http://etheses.dur.ac.uk/2126/.

[135] Nonoyama, M. *Bull. Chem. Soc. Jpn.* **1974**, *47*, 767.

[136] (a) Sprous, S.; King, K. A.; Spellane, P. J.; Watts, R. J. *J. Am. Chem. Soc.* **1984**, *106*, 6647. (b) King, K. A.; Spellane, P. J.; Watts, R. J. *J. Am. Chem. Soc.***1985**, *107*, 1421.

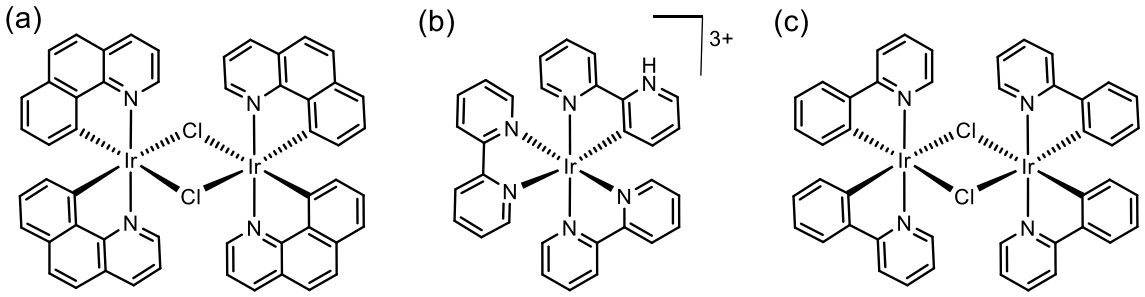

Figure 3.1. Chemical structure of (a) $[Ir(bhq)_2(\mu\text{-}Cl)]_2$, (b) $[Ir(bpy\text{-}NN')_2(Hbpy\text{-}C^3N')]^{3+}$ and (c) $[Ir(ppy)_2(\mu\text{-}Cl)]_2$.

The two cyclometalated ligands are in a *trans*-N,N-configuration as confirmed from the authors from ^1H, ^{13}C NMR analysis. The X-ray studies of various complexes reported in literature indicate that the iridium centre adopts an octahedral geometry by the coordination of two cyclometalating *ppy* ligands and two bridging chlorides. The dimeric species are largely used as intermediate for the preparation of *heteroleptic*[137] cationic or neutral complexes, including the work of this chapter. A wide range of compounds are used as ancillary ligands which cleave the chlorido-bridged dimer going from 2,4-pentadione derivatives[138] to amino acids (*e.g.* glycine) bipyridines derivatives. Some examples are shown in Scheme 3.1.

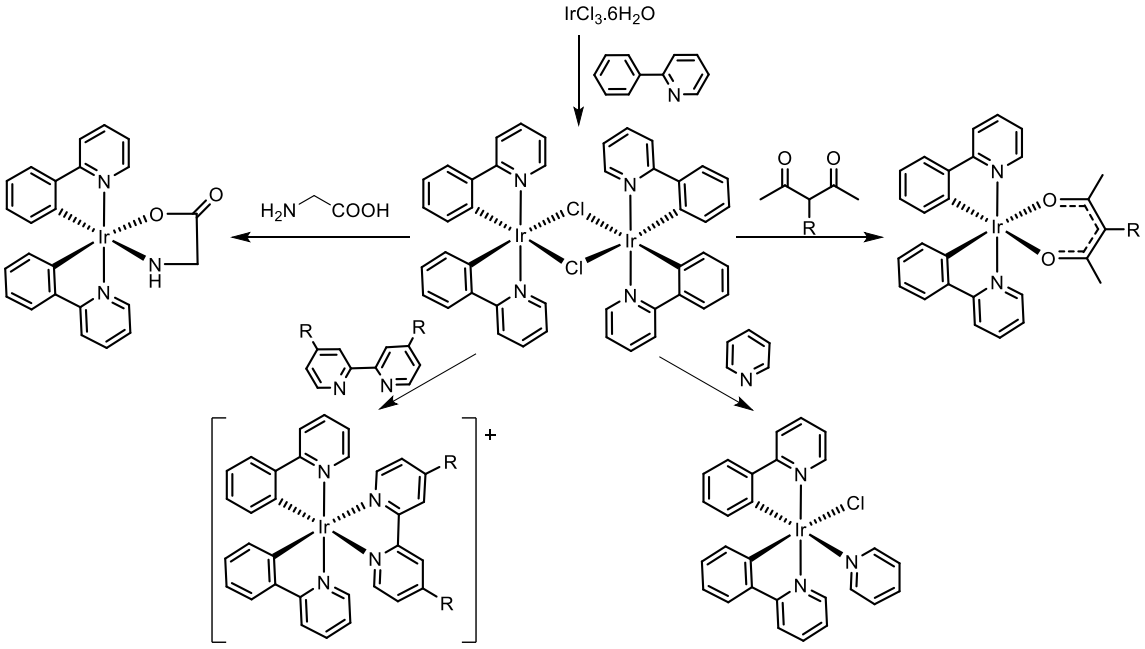

Scheme 3.1. Synthesis of various heteroleptic complexes from the chloro-bridged starting material.

[137] Heteroleptic is the definition given for an organometalic complex bearing two or more different ligands.

[138] Lamansky, S.; Djurovich, P.; Murphy, D.; Abdel-Razzaq, F.; Kwong, R.; Tsyba, I.; Bortz, M.; Mui, B.; Thompson, M. E. *Inorg. Chem.* **2001**, *40*, 1704.

1.2. Boranils

Following the research carried out in the LCOSA laboratory concerning the chemistry of *boranils*,[139,140] the julolidine scaffold was converted into the appropriate platform (*i.e.* anil, *vide supra*) in order to synthesize such derivatives. The chemistry of boranils was first introduced by Dr. D. Frath[141] during his doctoral work in this research group in 2011.[5] Boranils are the boron complexes of anil (Schiff base) derivatives. The latter consist of a bidentate N^O-coordinating ligands able to chelate boron(III) center, resulting in a stable 6-membered ring as depicted in Scheme 3.2. The chemistry of anil-derivatives is early known but their optical behavior is still exciting since these compounds are somewhat complex due to their multiple facets *i.e.* undergoing ESIPT process being photochromes, thermochromes and solvatochromes (*vide supra*).[142]

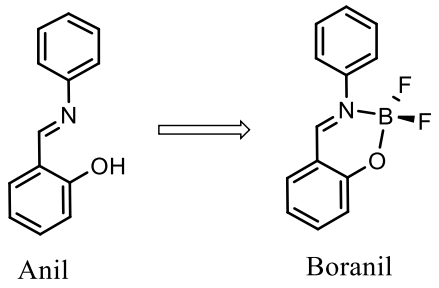

Scheme 3.2. General chemical structures of anil and boranil derivatives.

1.3. Multichromophoric systems

Multichromophoric compounds are molecular systems appending two or more photoactive units *i.e.* linking two or more metallic complexes or combining organic units with metallic complexes. They are of great interest because the appropriate combination of the modules may achieve a directed inter-component photoinduced electron transfer or electronic energy transfer process. Due to this ability they can be useful for the development of synthetic systems for artificial photosynthesis or applications in electroluminescence devices, information storage etc.

---

[139] Frath, D.; Azizi, S.; Ulrich, G.; Retailleau, P.; Ziessel, R. *Org. Lett.* **2011**, *13*, 3414.

[140] Dobkowski, J.; Wnuk, P.; Buczyńska, J.; Pszona, M.; Orzanowska, G.; Frath, D.; Ullrich, G.; Massue, J.; Mosquera-Vázquez, S.; Vauthey, E.; Rodzewicz, C.; Ziessel, R.; Waluk, J. *Chem. Eur. J.* **2015**, *21*, 1312.

[141] Frath, Denis (2013) *Nouveau complexes borate fluorescents. Synthèses, propriétés et applications*, Strasbourg thesis, University of Strasbourg. Available at Thesis Online: http://www.theses.fr/171614712.

[142] Hadjoudis, E. *Mol. Eng.* **1995**, *5*, 301.

Since several years, the Ziessel group has focused its researches toward the design and study of models for solar energy conversion and storage. Among the large library of such compounds are the series of multichromophoric systems featuring ruthenium(II) species and one or more BODIPY subunits.[143] For the target systems they remarked that photoinduced energy and electron transfer processes were occurring, leading to the quench of the luminescence of metallic complexes.[11c] For most of the hybrids Ru^{II}-BODIPY including the dyad **40** depicted in Scheme 3.3, the transient absorption spectra revealed an unusual observation.

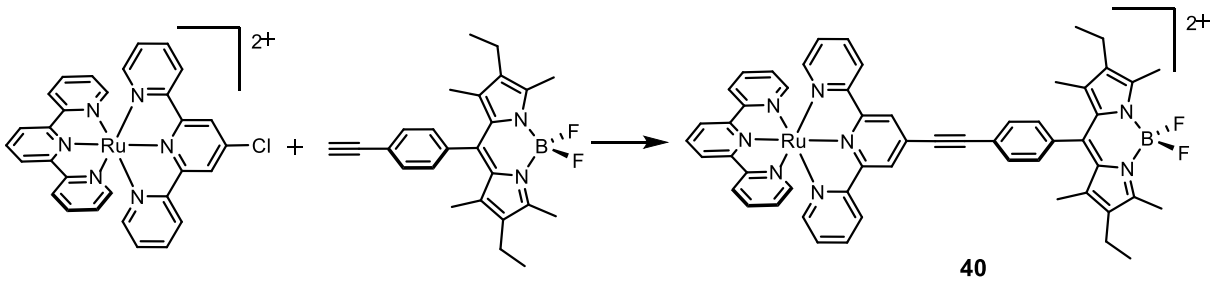

Scheme 3.3. Chemical structure of dyad **40** published by Ziessel *et al.*

The nanosecond transient absorption spectroscopy at 77 K revealed for the first time the existence of the triplet state of the BODIPY core. According to the authors, this phenomenon is due to the presence of the heavy metal (*i.e.* ruthenium) which facilitates the crossing from the ^{3}MLCT level to BODIPY $^3\pi$-π* level which is lower in energy relative to the former. An energy level diagram could be estimated and is shown in Figure 3.2. Certainly, observation of the phosphorescence luminescence from BODIPY core remains unusual.

[143] (a) Ulrich, G.; Ziessel, R. *J. Org. Chem.* **2004**, *45*, 1949. (b) Galletta, M.; Campagna, S.; Quesada, M.; Ulrich, G.; Ziessel, R. *Chem. Commun.* **2005**, 4222. (c) Galletta, M.; Puntoriero, F.; Campagna, S.; Chiorboli, C.; Quesada, M.; Goeb, S. ; Ziessel, R. *J. Phys. Chem.* A **2006**, *110*, 4348.

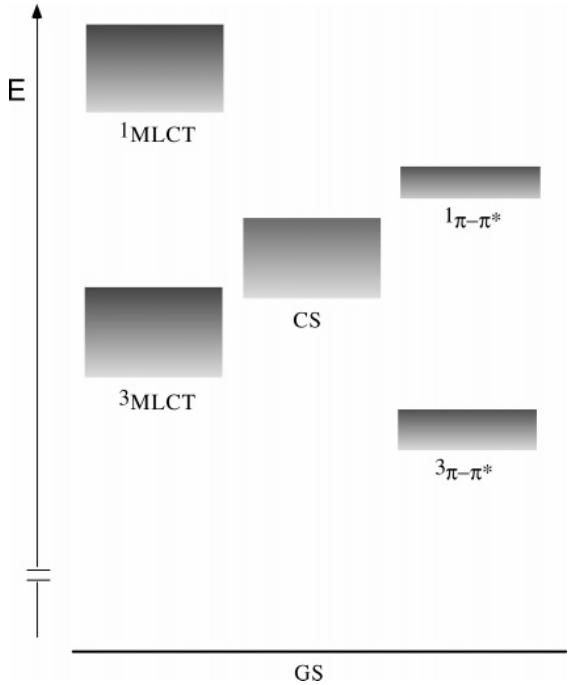

Figure 3.2. Estimated energy level diagram for the hybrid Ru-BODIPY molecular systems. On the left side are represented metal-based levels, on the right side BODIPY-centered levels. In the middle is represented the charge-separated (CS) state which is a multicomponent state and GS is the ground state. Figure printed from ref. [143c].

Further, in 2008 they reported a dyad combining a BODIPY (the same as the previous studies) and a platinum(II) terpyridine-acetylide subunits.[144] The title compound was obtained from a coupling reaction between the two components, catalyzed with CuI in inert atmosphere with excellent yield after purification (Scheme 3.4). Interestingly, the photophysical studies of this species showed different behavior comparing to the previous dyads bearing a Ru(II) metal. Fluorescence of the BODIPY entity was quenched neither by an energy transfer process, nor a photoinduced electron transfer process. Despite the favorable thermodynamic force, the system does not lead to a photoinduced electron transfer (PeT) process since the donor-acceptor coupling is very weak. In contrary the PeT process was observed for the previous Ru(II) species where the donor moiety *i.e.* the BODIPY was directly linked to the polypridine ligand unlike **41** where it is linked directly to the Pt(II) center. As Ru(II) hybrids, phosphorescence of the BODIPY core of Pt(II) dyads was observed at 77 K.

[144] Nastasi, F.; Puntoriero, F.; Campagna, S.; Dirig, S.; Ziessel, R. *Phys. Chem. Chem. Phys.* **2008**, *10*, 3982.

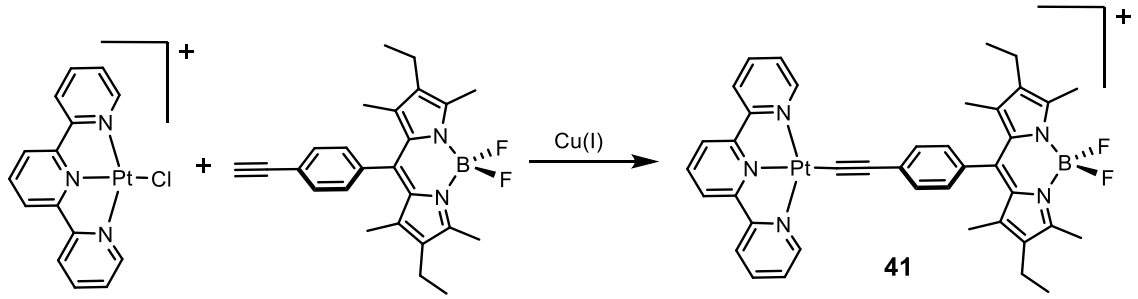

Scheme 3.4. The hybrid Pt(II)-Bodipy dyad **41**.

In 2012 Bronner *et al.* from the University of Strasbourg, published a neutral heterometallic dinuclear system (dyad **43**, Scheme 3.5), by connecting a platinium(II) and iridium(III) chromophore through a *dipyrrin-based* skeleton.[145] The latter has two different topological sites: a chelating site *i.e.* the dipyrrine and a monodentate site *i.e.* the pyridine, allowing to successfully obtain the dyad in two steps: i) reaction of the dipyrrine core with the bridged dimer Ir(III) and ii) a subsequent complexation of the pyridine fragment of monometallic complex **42** with [(dppyPt(dmso)] precursor as sketched in Scheme 3.5. The photophysical properties indicated a high directed efficient (*ca.* 90 %) *Electronic Energy Transfer* (EET) process form the platinum donor to the iridium acceptor at room temperature. The authors suggest that it occurs probably according to a Dexter-type mechanism.

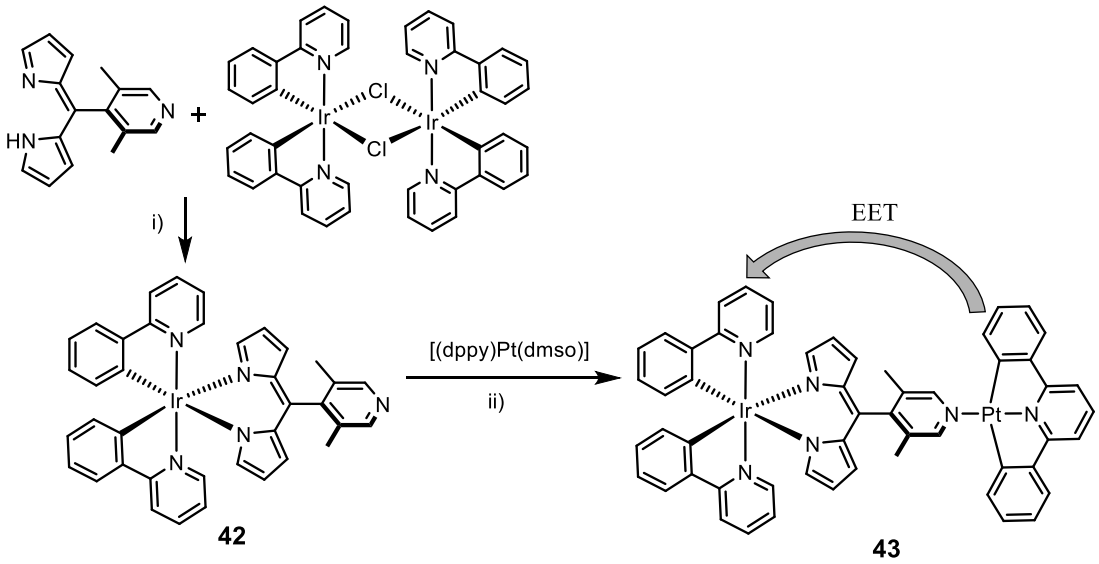

Scheme 3.5. The dinuclear complex Pt(II)/Ir(III) synthesized from Bronner *et al.*[145]

[145] Bronner, C.; Veiga, M.; Guenet, A.; De Cola, L.; Hosseini, M. W.; Strassert, C. A.; Baudron, S. A. *Chem. Eur. J.* **2012**, *18*, 4041.

- ***Objectives of the work***

Taking into account the various systems published in the literature and cited in the context of this work, the major goal of this chapter is the design and synthesis of julolidine-based ligands and their evaluation in coordinating with Ir(III) and Pt(II) transition metals as well as B(III). This work allows an extention of studies already reported in the laboratory on Ir(III) chemistry which is in continuous efforts for elaborating new complexes with innovative properties. Alongside, few examples of dinuclear heterometallic systems bearing Pt(II) and Ir(III) chromophores within the same ligand skeleton are reported. Herein we propose to link together a Pt(II) chromophore with a cyclometalating Ir(III) by using a anil-based ligand constructed around the julolidine motif as demonstrated schematically below. Having the julolidine entity **17** (described in the first chapter) we decided to convert it into a functionalizable chelating N^O-ligand capable to coordinate iridium(III) as well as boron(III) so as to provide a boranil complex. Moreover, hybrid systems combining the free ligands or the complexes with platinum(II) chromophore are designed and synthesized as summarized in Scheme 3.6.

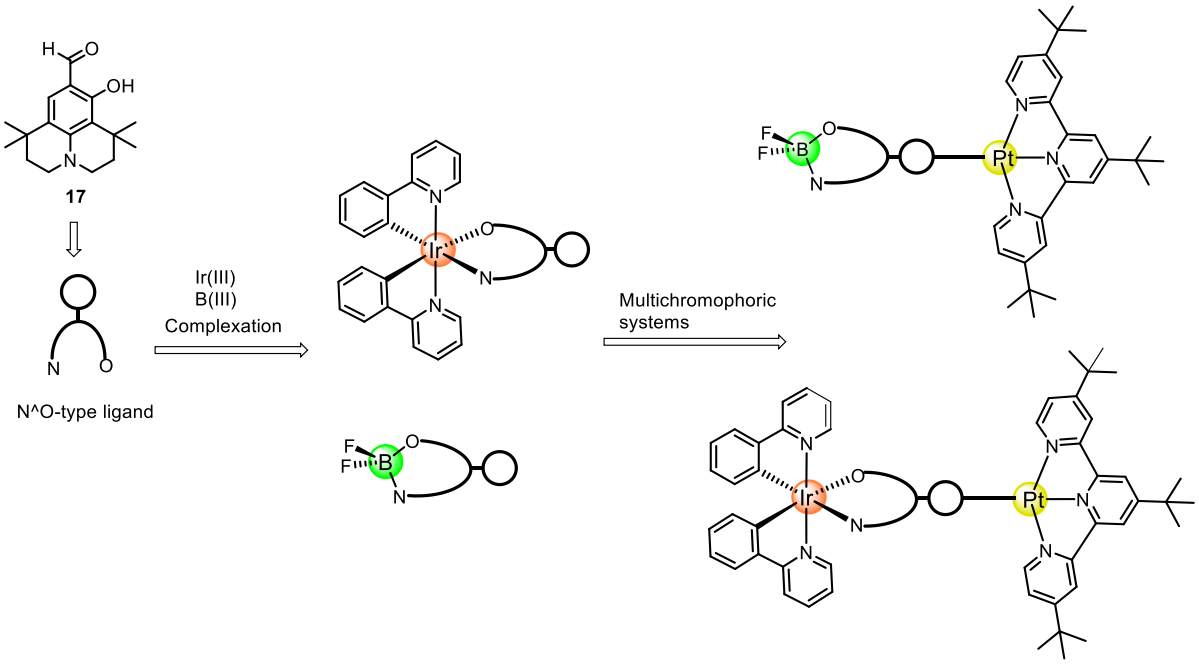

Scheme 3.6. Schematic representation of the work presented on this chapter.

2. Synthesis

2.1. Julolidine-based ligands

The 9-formyljulolidine **17** previously reported, was condensed with 4-iodoaniline in order to obtain a functionalizable N^O-type ligand (Scheme 3.7). The reactants were mixed in refluxing ethanol, according to previous procedures reported on anils,[146] in the presence of catalytic amounts of p-TsOH to yield the Schiff base **44**. The compound was obtained as yellow solid in 75 % yield following precipitation during the reaction and several washings with ethanol. The ^{1}H NMR pattern fits with the expected signals of the molecule fragments (*vide infra*). Electron ionization (EI) mass spectrometry analysis gave the radical cation molecular peak at *m/z* 474.0 as expected.

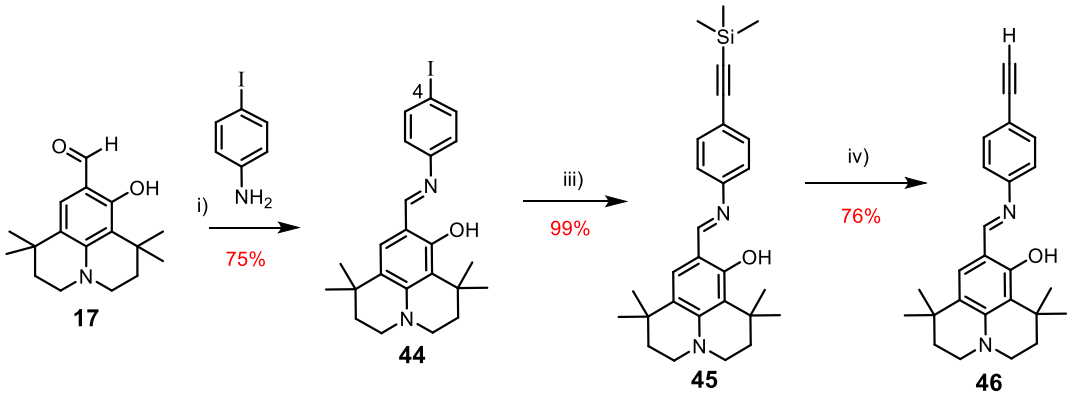

Scheme 3.7. Synthesis of julolidine-based ligands. Keys: i) p-TsOH cat., dry EtOH, 95 °C, 12 h. iii) $[Pd(PPh_3)_2Cl_2]$ 10 mol%, CuI 10 mol%, TMS acetylene, $^{i}Pr_2NH$, THF, rt, 12 h. iv) KF (100 eq.), $MeOH/H_2O$, THF, rt, 12 h.

The presence of an iodine atom at C4-position onto the phenyl ring of **44** opens various possibilities for tuning the chemical structure by way of metal-catalyzed cross-coupling reactions (*e.g.* Sonogashira, Suzuki, Stille etc.). Hence, we have investigated the possibility of *"chemistry on the ligand"* involving Sonogashira cross-coupling reactions. Compound **44** was transformed into trimethylsilyl (TMS)-aryl **45** quantitatively, following a Sonogashira cross-coupling reaction with TMS-acetylene catalyzed by $[Pd(PPh_3)_2Cl_2]$ and CuI. The latter was deprotected using large excess of KF at room temperature and gave the final N^O-chelating ligand **46** bearing a terminal acetylene. As a result, two sites are available and susceptible to undergo metalation: the N^O chelating site and the newly introduced terminal acetylide.

[146] Frath, D.; Azizi, S.; Ulrich, G.; Retailleau, P.; Ziessel, R. *Org. Lett.* **2011**, *13*, 3414.

The final ligand was characterized using the ^{1}H, ^{13}C NMR and infra-red spectroscopy (*vide infra*) as well as mass spectrometry and elemental analysis.

2.2. Boron complexes

The reaction of boron trifluoride etherate with iodo-anil **44** and acetylene-anil **46**, both containing a bidentate N^O-coordinating site, using large excess of *N,N*-diisopropylethylamine (DIPEA) in 1,2-dichloroethane for 3 hours, gave the tetrahedral boron difluoride complexes **48** and **47** in excellent yields (Scheme 3.8). Large excess of the base was necessary to neutralize the HF generated during the reaction. Both complexes were obtained in 89% and 94 % yield as highly pure orange solids highly pure following purification over column chromatography and crystallization. Their molecular structures were confirmed by X-ray crystallography (*vide infra)*.

The detailed experimental conditions are shown in Scheme 3.8 and described in the experimental section. As depicted in Scheme 3.8, we also attempted to synthesize **47** from **48** by investigating the possibility of *"chemistry on the complex"* in two steps: i) the cross-coupling reaction with TMS-acetylene, and ii) removal of the TMS group in basic conditions. We noted however, that it is more difficult to functionalize the iodide group after boron difluoride complexation has occurred.

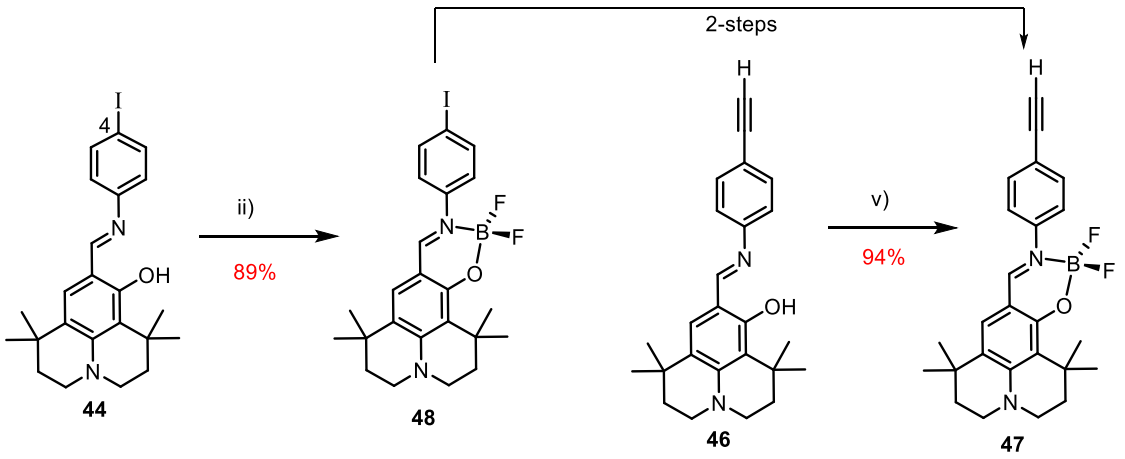

Scheme 3.8. Synthesis of boron difluoride complexes **48** and **47**. Keys: ii) BF_3Et_2O (6 eq.), 1,2-dichloroethane, rt, 30 min, DIPEA (6 eq.), 3 h. v) BF_3Et_2O (6 eq.), 1,2-dichloroethane, rt, 30 min.; DIPEA (6 eq.), 3 h.

2.2.1. X-ray crystallographic analysis of 48 and 47

The resolution of the molecular structures by X-ray cristallography of mono-crystals was realized from Dr. Pascal Retailleau at Gif-sur-Yvette. For boranil **48** and **47**, single crystals of suitable quality were obtained by slow evaporation of a concentrated solution in a dichloromethane/ethanol mixture. The compounds crystallize both in a monoclinic system but in different space groups, P 2/1n for **48** and P 2/1c for **47**. Considering compound **48**, the asymmetric unit of the crystal contains two independent molecules with a head-to-tail orientation. It should be note that the Figure 3.3 represents only one of two molecules for reasons of clarity. Hence the iodo-boranil adopts different orientations notably around the iodo-phenyl group. Crystallographic analysis indicates that only 12.5 % of the molecules of the crystal adopt a conformation such as the iodo-phenyl group is oriented in the same plane as the boranil core.

The 6-memered rings of quinolizidine entity of julolidines adopt an envelope conformation in both cases. The molecular structure of **48** is somewhat distorted comparing to **47** (Figure 3.3, right-side and Figure 3.3 right-side). This is a consequence of the important value of Van der Waals radii of the iodide and the interactions it might involve. The molecular structure of **47** shown in Figure 3.4 is more regular and highly planar. The acetylene-phenyl group is slightly twisted from the plane of the molecule with a dihedral angle being 2.8°, whereas the iodo-phenyl group of complex **48** is 35.7° out of plane. The boron center in both cases adopt a regular tetrahedral geometry with F-B-F, F-B-O and F-B-N angles being 107.7(2)°, 107.9(2)° and 110.6(2)° respectively for compound **47** and 109.7(5)°, 108.2(5)° and 110.3(5)° for compound **48.** As indicated from the values gathered in Table 3.1 and 3.2, boranil **47** shows equivalent B-F bond lengths [1.394(4) Å and 1.399(4) Å], whereas for **48** a slight difference exists between B-F1 and B-F2 [1.370(8) Å and 1.394(9) Å].

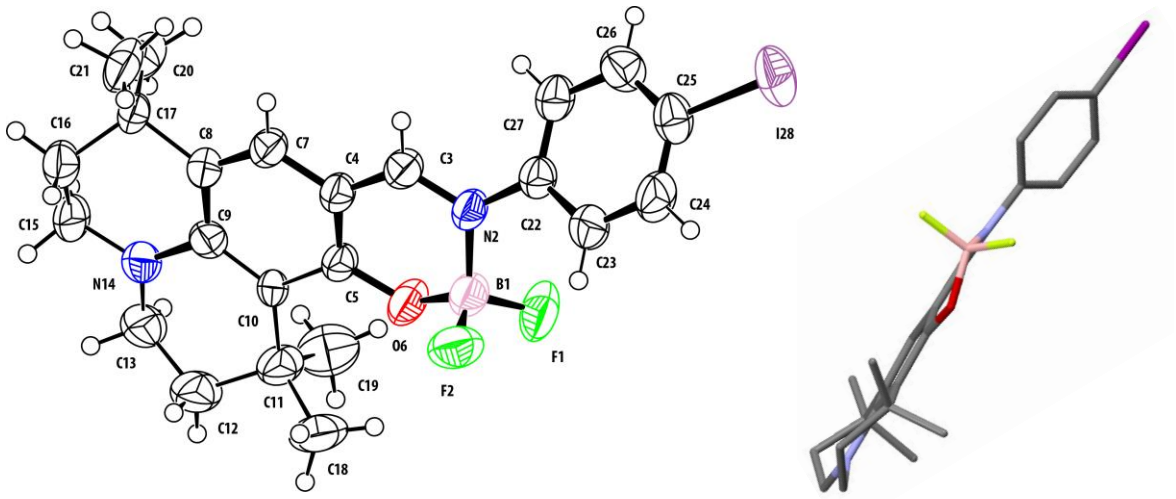

Figure 3.3. (Left) Ortep view of compound **48** with thermal ellipsoids plotted at the 50 % level. (Right) Profile view of the molecular structure showing its distortion.

Table 3.1. Selected bond lengths given in angstrom, angles and torsion angles given in degree for **48.**

Bond (Å)	**Angle (°)**	**Torsion angle (°)**
F1-B, 1.370(8)	F1-B-F2, 109.7(5)	C3-N1-B-O5, 24.5(7)
F2-B, 1.394(9)	F1-B-O6, 108.2(5)	C3-N2-C22-C23, 147.1(5)
O6-B, 1.444(7)	F1-B-N2, 110.3(5)	B-N2-C22-C27, 144.8(5)
N2-C3, 1.329(6)	N2-B-O6, 110.3(5)	N2-B-O6-C5, -12.8(8)
N2-B, 1.563(8)	F2-B-O6, 109.8(5)	
C9-N14, 1.404(6)	N2-B-F2, 108.7(5)	

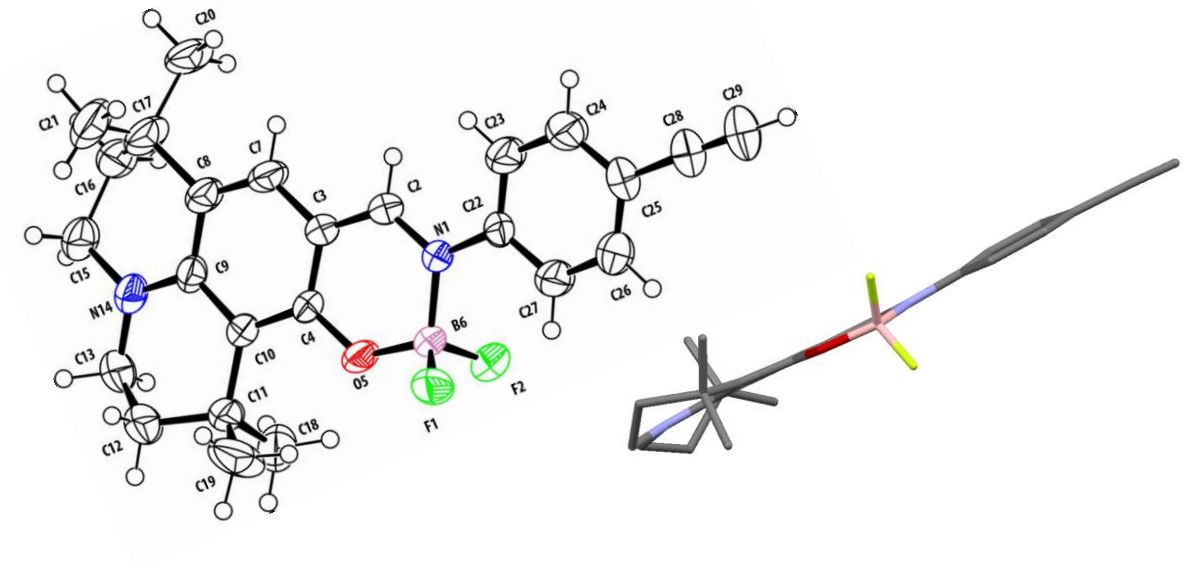

Figure 3.4. (Left) Ortep view of compound **47** with thermal ellipsoids plotted at the 50 % level. (Right) Profile view of the molecular structure showing its planarity.

Table 3.2. Selected bond lengths given in angstrom, angles and torsion angles given in degree for **47**.

Bond (Å)		Angle (°)		Torsion angle (°)	
F1-B,	1.394(4)	F1-B-F2,	107.7(2)	C2-N1-B-O5,	-7.1(3)
F2-B,	1.399(4)	F1-B-O5,	107.9(2)	C2-N1-C22-C23,	2.8(4)
O5-B,	1.436(3)	F1-B-N1,	110.6(2)	B-N1-C22-C27,	2.0(4)
N1-C2,	1.325(3)	N1-B-O5,	112.1(2)	C4-O5-B-N1,	4.0(4)
N1-B,	1.561(4)	F2-B-O5,	109.1(2)		
C9-N14,	1.350(3)	N1-B-F2,	109.3(2)		

2.3. ^{1}H NMR study of compound 44, 46, 47

The proton NMR spectra of the ligands **44**, **46**, and boranil **47** were recorded in $CDCl_3$ and are shown in Figure 3.5. For compound **44** and **46** a broad and weak signal at *ca.* 14.0 ppm is assigned to OH proton (Figure 3.5a, b). This signal is very downfield, due to the hydrogen bond that hydroxyl group forms with the free doublet of the nitrogen atom. The complexation of boron(III) with the chelating free N^O-site in **47** is accompanied with the absence of this peak in the ^{1}H NMR spectra (Figure 3.5b-c), thus indicating the deprotonation of OH group and its coordination to boron(III) center.

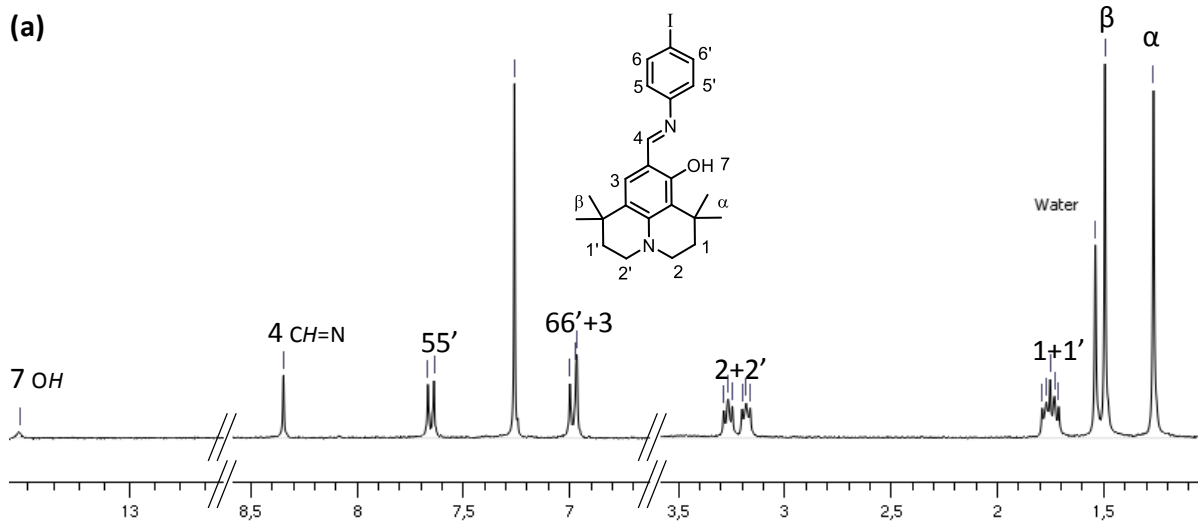

Figure 3.5a. ^{1}H NMR spectra of compound **44** in deuterated chloroform at room temperature.

Also, the singlet peak at *ca.* 8.40 ppm corresponding to the imine fragment proton (C*H*=N) in **44** and **46** becomes broad and is shifted upfield at δ = 7.90 ppm upon complexation. This shift is due to the shielding of the former from the boron center which has a high electron density. Indeed, this broad signal is a multiplet resulting from the coupling of the imine proton (C*H*=N)

with the boron center as has been demonstrated from previous studies by D. Frath according the non-decoupled proton ^{11}B NMR studies.[141]

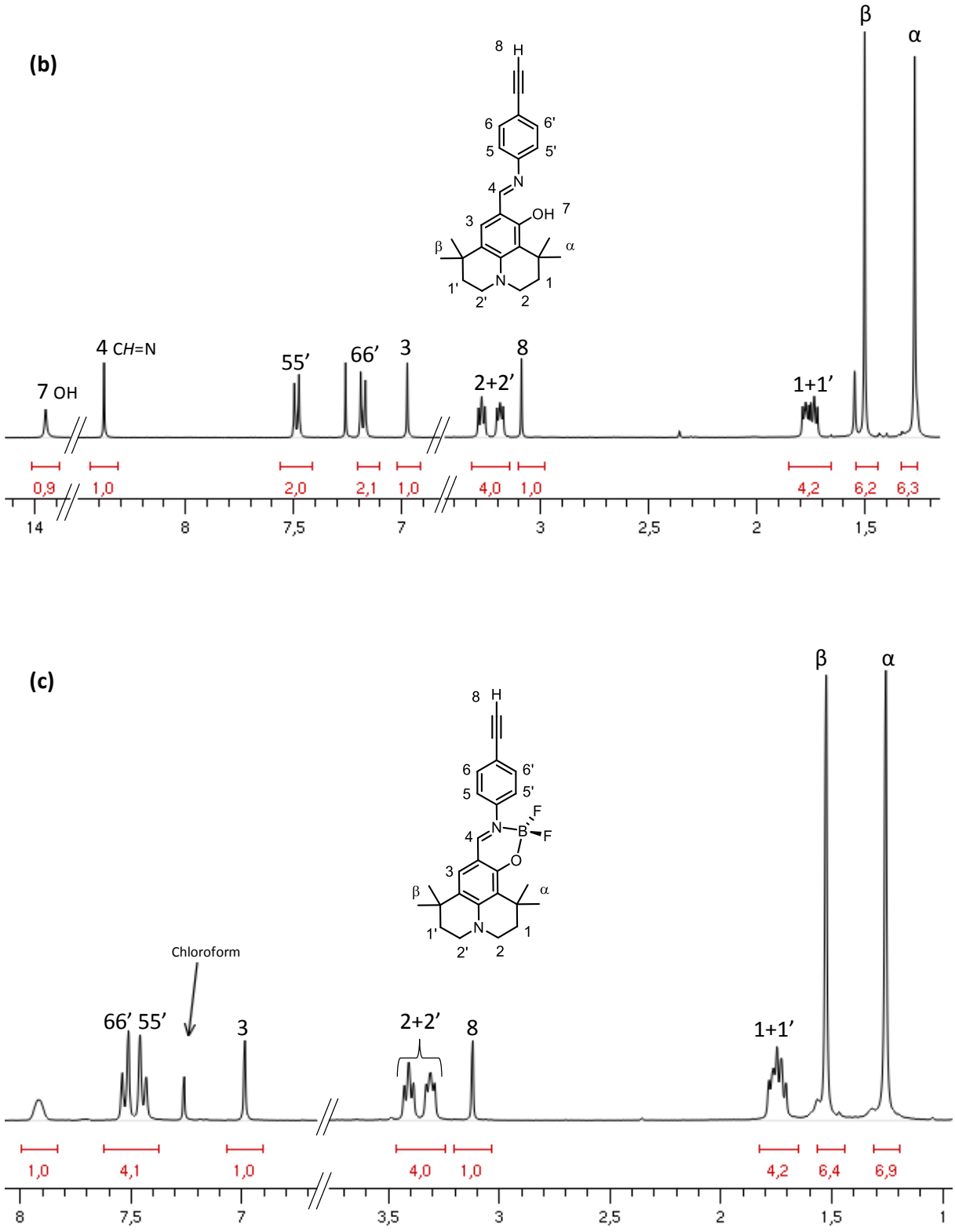

Figure 3.5b. ^{1}H NMR spectra of compound **46** (b) and **47** (c) in deuterated chloroforme at room temperature.

2.4. Fluoride substitution of the BF_2 entity

The substitution of the fluorine atoms on the boron center of BODIPY dyes with entities such as aryl, alkyne, alkoxide groups etc. (Scheme 3.9b) has been studied by several research groups including Ziessel group. It has been shown that adding steric constraints on the boron center increases the quantum yield of the dye. Also, adding aromatic substituents (*e.g.* pyrene, perylene etc.) makes possible energy transfer processes, thus the compounds can be regarded as energy transfer cassettes. In a recent publication, in analogy with BODIPYs, Ziessel and Waluk *et* co-workers studied the substitution of the fluoride of BF_2 entity on boranils (Scheme 3.9b).[140] The fluorides were displaced with phenyl groups and the optical properties were measured and compared in different solvents. In apolar solvents (*e.g.* toluene) the absorption spectra were very similar, however, an increase of the fluorescence quantum yield was observed for the phenyl substituted compared to the fluoride substituted compounds (Scheme 3.9b). The authors introduced the aryl group by reaction of the anil precursor with triphenylborane in toluene.

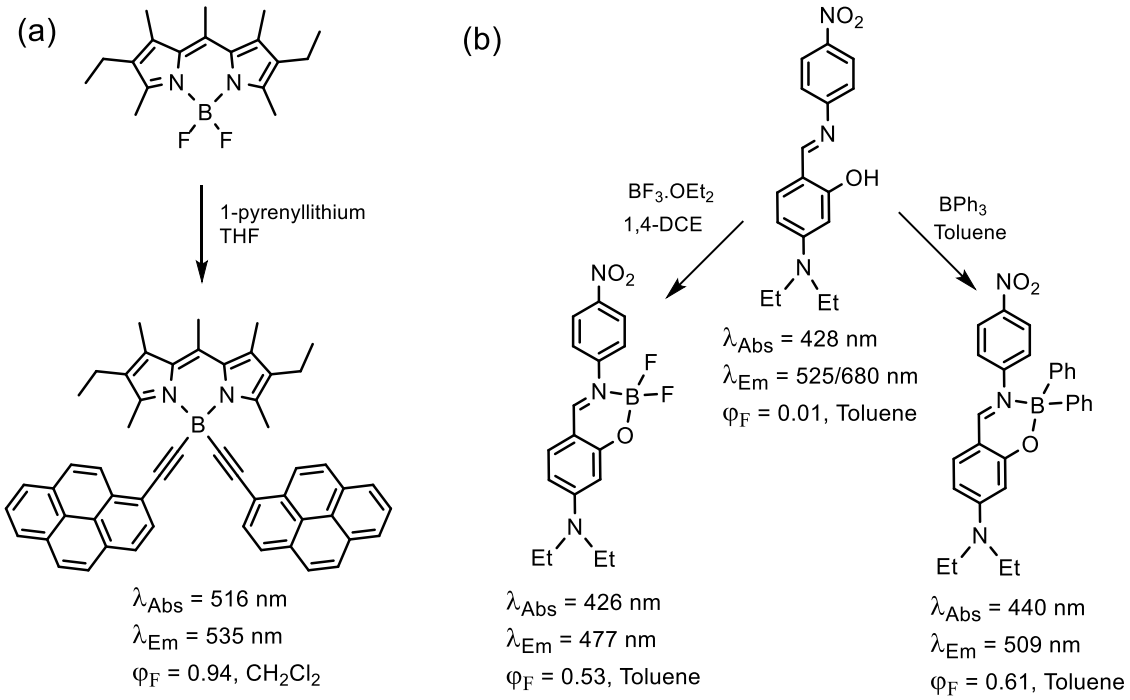

Scheme 3.9. Examples of fluoride substitution on (a) BODIPY core (b) boranils.

The present work consists on the substitution of the fluoride groups of boranil **48** directly onto the BF_2 entity by nucleophilic substitution with Grignard reagent according to similar procedures applied to BODPY dyes (Scheme 3.10).[147] In the first step, EtMgBr acting as a base reacts with the terminal acetylene-PEG chain in anhydrous THF during two hours to afford the new

[147] Mirloup, A.; Retailleau, P.; Ziessel, R. *Tetrahedron Lett.* **2013**, *54*, 4456.

Grignard reagent **49**. The latter was not isolated; it was allowed to react *in situ* with **48** in anhydrous THF at 60 °C during 12 hours. The nucleophilic substitution of the fluorine atoms with ethynylPEG chains by the Grignard reagent **49**, afforded **50** as yellow oil in 31% yield.

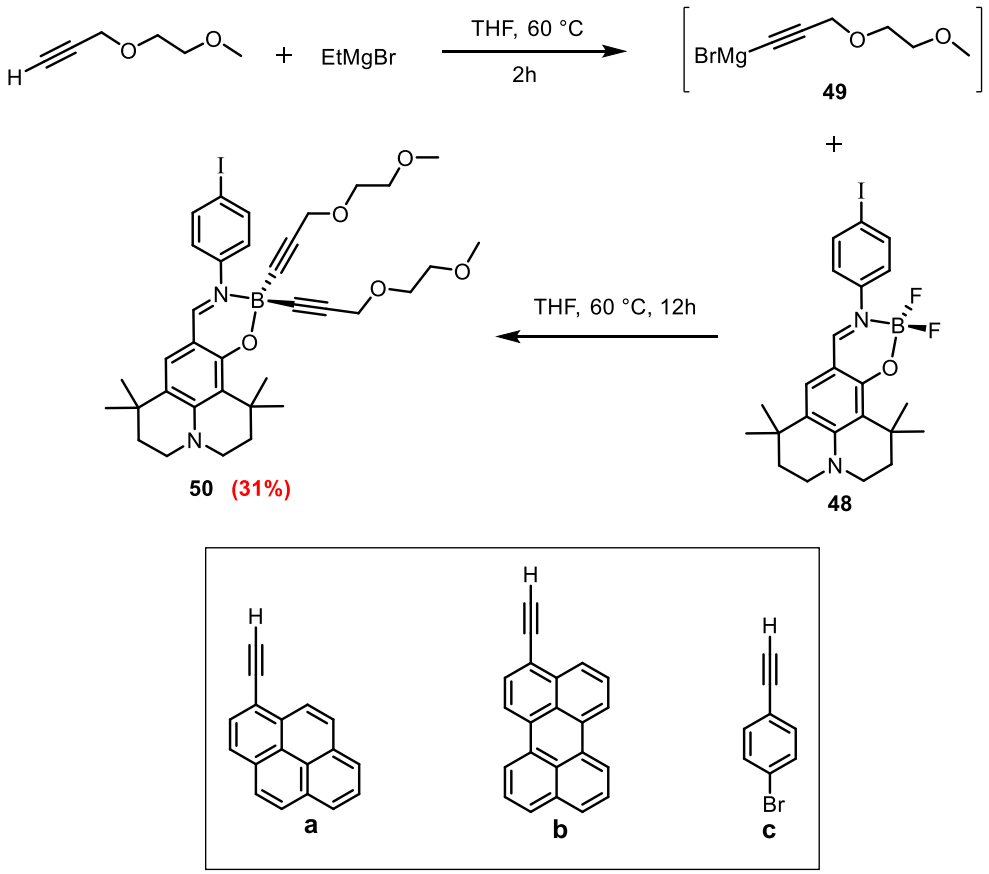

Scheme 3.10. Substitution of fluoride atoms of **48** by PEG-chains using Grignard reagent.

The PEG-chains were selected as a test for the substitution reaction of fluorides on the boron center. Indeed, our principle goal was to replace the fluorides with chromophores bearing functional groups in order to carry out chemistry directly on the boron center and study the optical properties of the resulting compounds. Few reactions attempted for displacing the fluorides with ethynylperylene (a), ethynylpyrene (b) and 1-bromo-4-ethynylbenzene (c) (Inset in Scheme 3.10) according to the same procedure as previously, showed no evidence of the formation of the product.

2.4.1. ^{11}B NMR spectra

Typically, the ^{11}B NMR spectrum of the boron difluoride complex **48** is characterized by a triplet at 0.9 ppm due to the coupling of boron (spin 3/2) with two fluorine atoms (spin 1/2) with a constant coupling of $J_{B\text{-}F}$ = 17.1 Hz (Figure 3.6, left-side). The substitution of fluorides shifts the boron signal at -7.0 ppm as a singlet due to the absence of the coupling with the PEG chains (Figure 3.6, right-side). The signal is shifted upfield, probably due to the shielding of the boron center resulting from its interaction with the π-orbitals of the PEG chains triple bonds. These results confirm the substitution of fluoride groups by alkyne derivatives.[148]

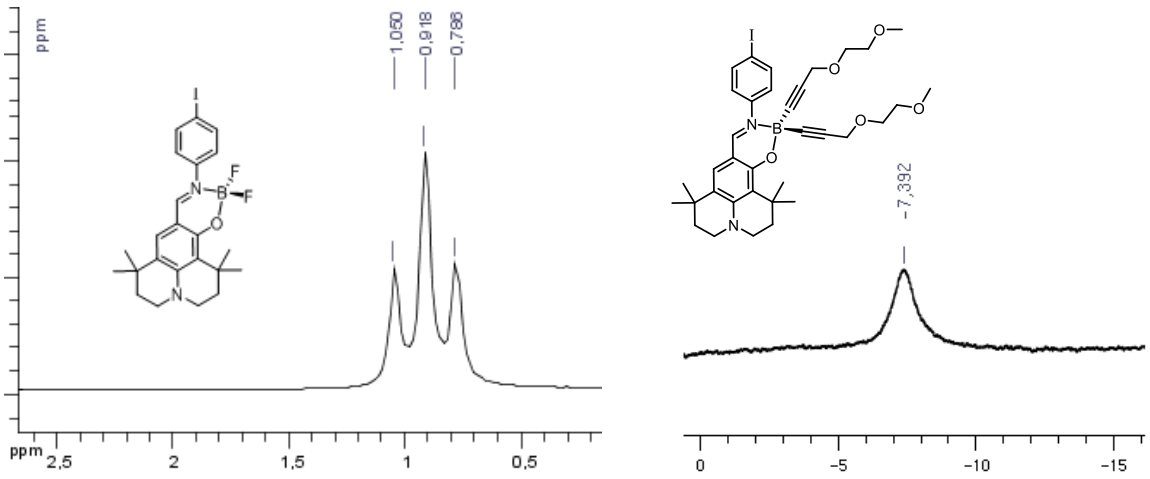

Figure 3.6. ^{11}B NMR (128 MHz, $CDCl_3$) ^{1}H decoupled spectra of compounds **48** (left) and **53** (right).

2.5. Synthesis of Iridium(III) N^O based-ligand complexes

Cyclometalating N^C type ligands derived from 2-phenylpyridine, phenanthroline or 2,2'-bipyridine, are widely used in the design and study of Ir(III) complexes. It is well established that the tuning ability of the optical properties of iridium complexes depends on the nature of the surrounding ligands. The need of innovation in this field is pushing researchers to turn toward the search of innovative ligands, which may allow having Ir complexes with innovative properties. More recently ligands such as triazoles, pyrazole, benzothiazole etc. were introduced, however Schiff bases N^O ligands were scarcely investigated. In 2001, Thomson *et al.* published a series of phosphorescent cyclometalated iridium complexes, alongside a complex bearing a bidentate monoanionic ancillary salen-type ligand (Figure 3.7).[149]

[148] Bura, T.; Ziessel, R. *Org. Lett.* **2011**, *13*, 3072.
[149] Lamansky, S.; Djurovich, P.; Murphy, D.; Abdel-Razzaq, F.; Kwong, R.; Tsyba, I.; Bortz, M.; Mui, B.; Bau, R.; Thomson, M. E. *Inorg. Chem.* **2001**, *40*, 1704.

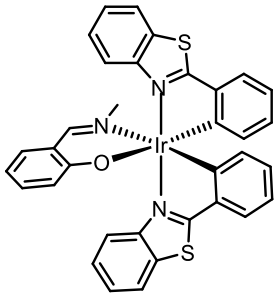

Figure 3.7. Complex [(bt)$_2$Ir(sal)] reported by Thomson *et al.*.[149]

Herein is described the synthesis of a new Ir(III) complex bearing two cyclometalating 2-phenylpyridine (*ppy*) ligands and an ancillary monoanionic N^O ligand which derives from the *julolidine* scaffold. The complex **51** was formed by cleavage of the chloride bridges of iridium(III) dimer [(*ppy*)$_2$Ir-(μ-Cl)]$_2$,[150] upon reaction with the bidentate ligand **44** in the presence of base and refluxing 1,2-dichloroethane/methanol mixture during two days (Scheme 3.11). The base triethylamine was necessary to quench the nascent acid and facilitate deprotonation of the phenol in **44**. Thus, the resulting complex is neutral and was obtained as an orange solid in 72 % yield following purification by column chromatography and precipitation.

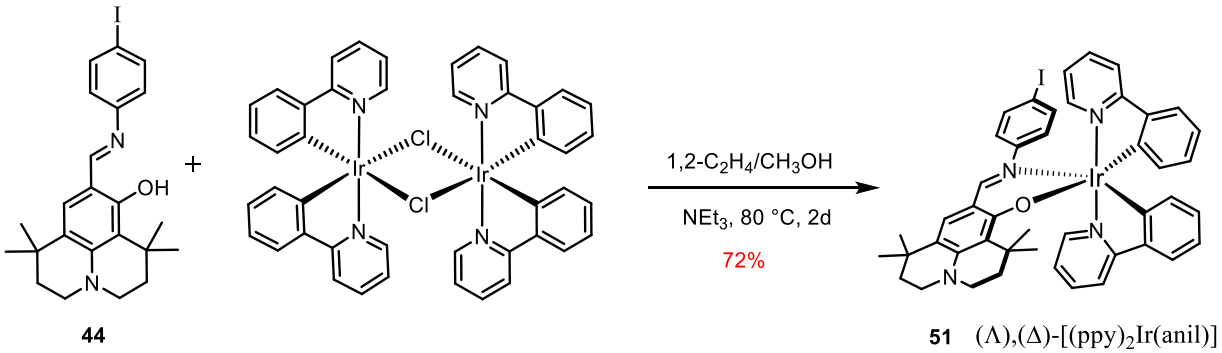

44 **51** (Λ),(Δ)-[(ppy)$_2$Ir(anil)]

Scheme 3.11. Synthesis of complex [(ppy)$_2$Ir(anil)], **51**.

Electron ionization (EI) mass spectrometry confirms the structure of **51** by the presence of *m/z* peak at 100 % intensity being 974.2 which is in agreement with the calculated *m/z* value. The compound was fully characterized by ^{1}H, ^{13}C NMR and infra-red spectroscopy (*vide infra*) and purity examined by way of elemental analysis.

It should be noted that complex **51** is isolated as a mixture of optical isomers Δ and Λ (Figure 3.8). Furthermore the complex **51** has a *N,N-trans*-configuration, which means that Ir-N bonds of the cyclometalating *ppy* ligands are disposed in *trans* position with respect to Ir-C bonds of the phenyl rings being in *cis*. This configuration has not been confirmed by X-ray study; however it

[150] King, K. A.; Spellane, P. J.; Watts, R. *J. Am. Chem. Soc.* **1985**, *107*, 1431.

results from various studies in the literature where the interaction of an ancillary ligand with the bridged dimer leads to the *trans*-isomer excusively.[151] This is due to the fact that the nitrogen atoms of the cyclometalating *ppy* ligands within the dimer [(*ppy*)$_2$Ir-(μ-Cl)]$_2$, are also disposed in a *trans*-configuration, while the weak Ir-Cl bonds in *cis* position.[152] This tendency was also observed and supported by X-ray analysis for other dichloride bridged iridium dimers and monomers.[149] This is commonly explained by the *trans*-effect, a well known concept in coordination chemistry.[153]

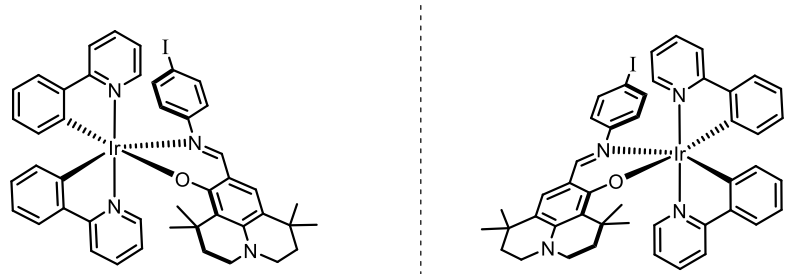

Δ-*trans*-[(ppy)$_2$Ir(anil)] Λ-*trans*-[(ppy)$_2$Ir(anil)]

Figure 3.8. Λ and Δ isomers of complex **51** resulting upon reaction with the dimeric Ir(III) precursor.

2.5.1. ^{1}H NMR study

The proton NMR spectrum of the heteroleptic compound **51** was determined in deuterated chloroform at room temperature and is represented in Figure 3.9. The spectrum clearly indicates the coordination of the julolidine-based ligand confirmed by the absence of the peak at *ca.* 14.0 ppm, assigned to the hydroxyl group of julolidine core. Alongside, the signals of the cyclometalating ligands are doubled, due to the loss of the C_2 symmetry of the dimer precursor [(*ppy*)$_2$Ir-(μ-Cl)]$_2$. The sharp singlet signal at δ = 7.70 ppm is assigned to CH_f=N proton of the ancillary ligand which is highfield compared to the free ligand (δ = 8.40 ppm) as a result of the metal shielding. Indeed all the peaks of the ancillary ligand are shifted upfield by *ca.* 1.0 to 2.0 ppm when metalated with the iridium center. One of the methyl groups is however the more affected after metalation and shifted at δ = 0.63 ppm probably because of its close proximity with the pyridinyl ring of the cyclometalating ligand.

[151] (a) Garces, F. O.; King, K. A.; Watts, R. J. *Inorg. Chem.* **1988**, *27*, 3464. (b) Garces, F. O.; Dedian, K.; Keder, N. L.; Watts, R. J. *Acta Crystallogr.* **1993**, *C49*, 1117.
[152] Sprous, S.; King, K. A.; Spellane, P. J.; Watts, R. J. *J. Am. Chem. Soc.* **1984**, *106*, 6647.
[153] Selected review for the *trans*-effect in transition metal complexes: Coe, B. J.; Glenwright, S. J. *Coord. Chem. Rev.* **2000**, *203*, 5.

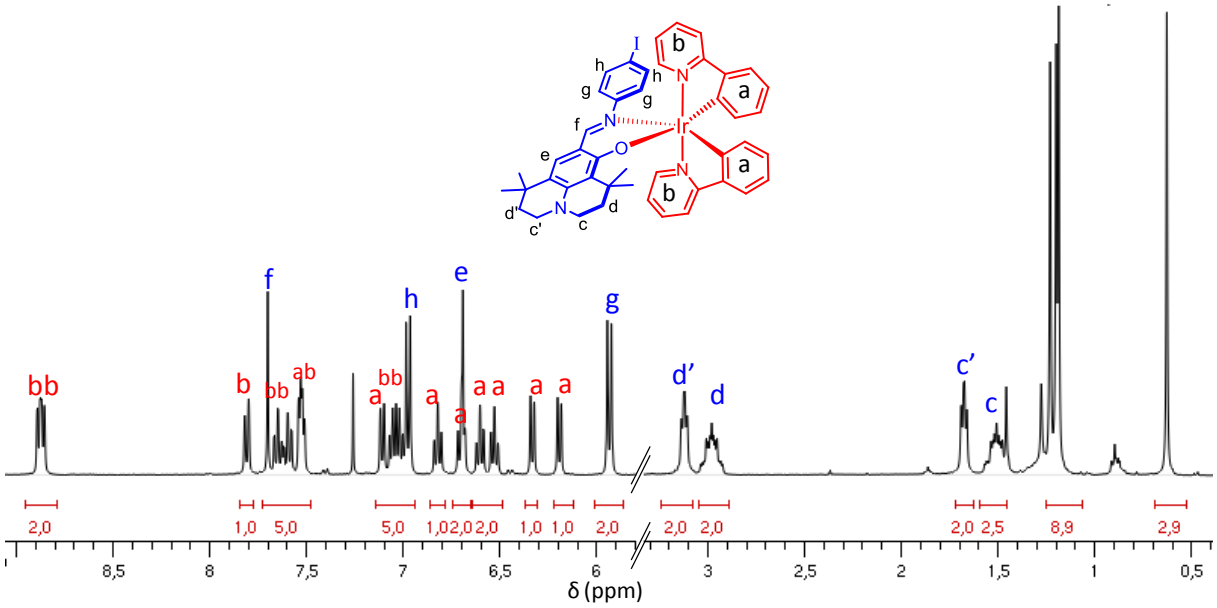

Figure 3.9. ^{1}H NMR (400 MHz, $CDCl_3$) spectrum of heteroleptic complex **51**.

2.6. Synthesis of multicomponent systems

2.6.1 Platinium(II)/Boranil dyad

A boranil subunit and a platinum(II) chromophore were linked within the same julolidine-based skeleton forming a dyad. To the best of our knowledge this is the first molecular framework combining a boranil derivative and a Pt^{II} chromophore; however an analogous system was reported in 2008 by Nastasi *et al.*, where a BODIPY subunit was anchored in place of the boranil (*vide supra*).[144]

Herein the target hybrid Pt^{II}-boranil based on a julolidine scaffold was designed and synthesized according procedures described for previous dyads. Two synthetic routes were applied for obtaining the target compound **53**. The first involves the coupling reaction of the terminal acetylide of ligand **46**, described in § 2.2, with $[(^{t}Bu_3tpy)PtCl]BF_4$[154] precursor (Scheme 3.12, route 1). The reaction was catalyzed with CuI in anhydrous THF and under an inert atmosphere. The final product **52** was obtained as brown powder in 70 % yield following ion exchange to the perchlorate salt and purification *via* column chromatography. The ^{1}H NMR spectra of **52** indicated the metalation of the Pt center through the ethynyl bond because the terminal acetylene proton at *ca.* 3.0 ppm (*cf.* Figure 3.5b) was absent.

[154] Yip, H.-K.; Cheng, L.-K.; Cheung, K.-K.; Che, C.-M. *J. Chem. Soc., Dalton Trans*. **1993**, 2933.

Subsequently the free chelating N^O site of **53** was coordinated to the boron difluoride entity by reacting with boron trifluoride etherate in basic conditions and anhydrous 1,2-dichloroethane solution. The hybrid Pt(II)-boranil **53** was isolated as red powder quantitatively following ion exchange to the ClO_4^- salt and column chromatography purification. The ClO_4^- was regularly selected as counter-anion for the cationic species because it ensures a better solubility of the complex and facilitates its purification by column chromatography. The anion exchange procedures are described in detail in the experimental section.

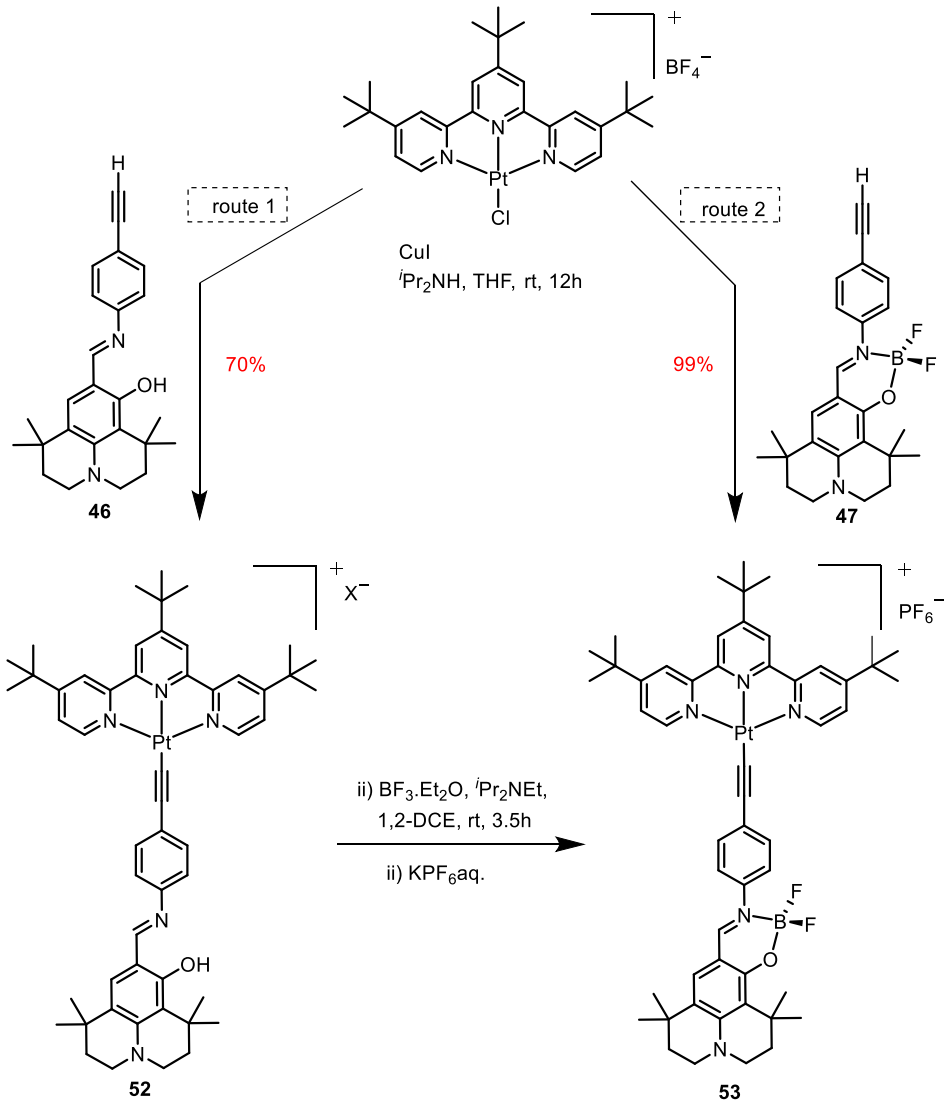

Scheme 3.12. Synthesis of dyad **52** and **53**.

Aside from the first procedure allowing the synthesis of **53** from the ligand **46**, synthesis from boron complex **47** was also investigated using the same reaction conditions as the former (Scheme 3.12, route 2). The coupling reaction of **47** with [(^{t}Bu$_3$tpy)PtCl](BF$_4$) following ion exchange and purification worked quantitatively.

The structure of Pt(II)-boranil dyad **53** was easily identified from electrospray (ES^+) mass spectrometry because of the positive charge of the complex. The *m/z* molecular peak at maximum intensity was assigned to the dyad having lost a perchlorate counter-anion. Elemental analyses were in good agreement with the calculated values thus confirming the purity of the synthesized compound. The proton NMR spectral profile appears consistent with the formation of the expected dyad. The spectrum is shown in Figure 3.10, where the peaks depicted in blue refer to the boranil component and in green to the platinum chromophore entity. We can easily distinguish the C*H*=N peak at δ = 7.90 ppm and the doublet at δ = 9.15 ppm which is characterized by two shoulders on the baseline due to the coupling of proton 7 and 7' with ^{195}Pt. The metalation of Pt(II) induces important shielding on the phenyl ring protons 5, 5' and 6, 6' (*ca.* 4.0 ppm), whereas the rest of the signals are apparently not affected.

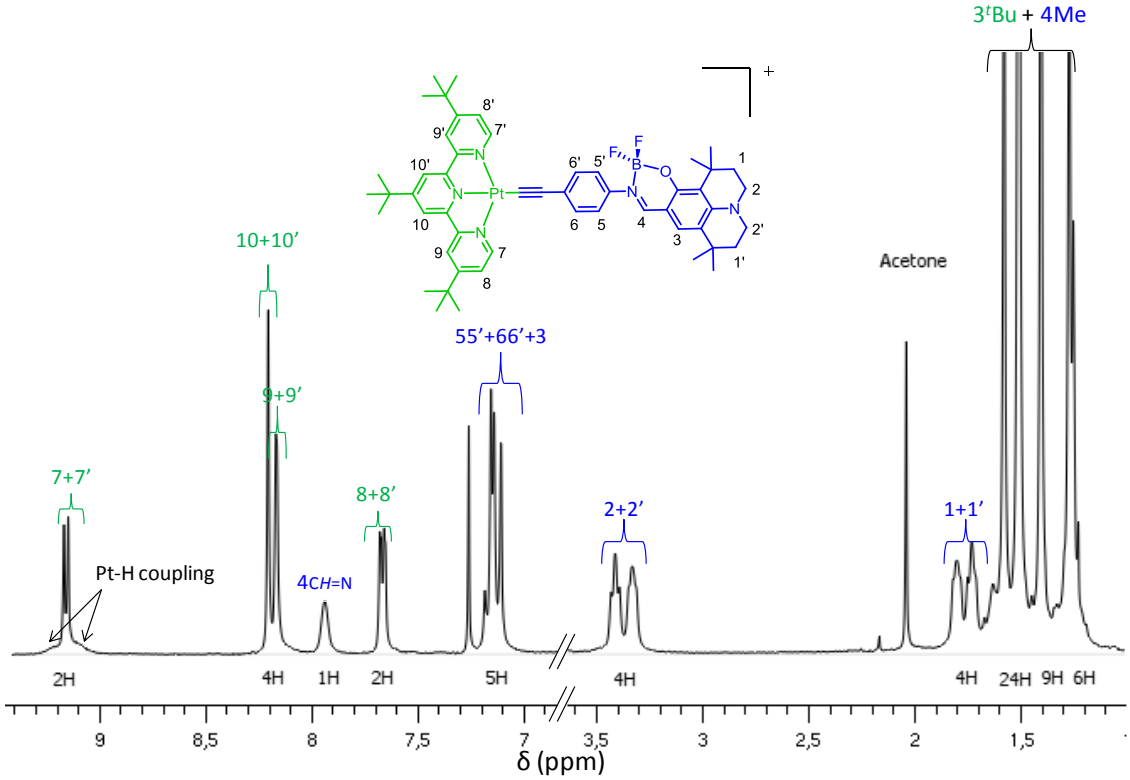

Figure 3.10. ^{1}H NMR spectrum of compound **53** in deuterated chloroform at room temperature.

2.6.2. Heterobimetallic Pt^{II}/Ir^{III} complex

The dinuclear complex Pt^{II}/Ir^{III} was synthesized using the approach of *"chemistry on the complex and the complex as ligand"*.[3] It consists of the creation of an appropriate coordination site onto the first monometallic complex using a cross-coupling reaction, then subsequent complexation of the former with a second metallic complex as schematically represented in Figure 3.11.

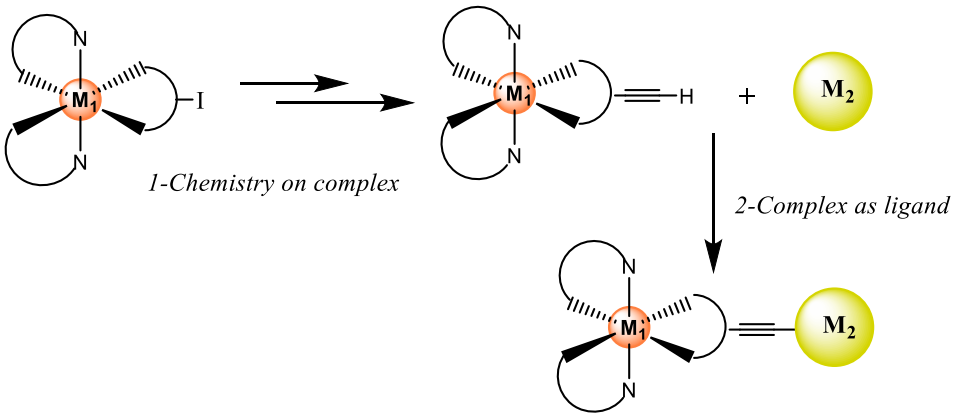

Figure 3.11. Schematic representation of "chemistry on the complex, complex as the ligand" approach.

The monometallic Ir(III) complex **51** incorporating an appended iodo-group onto the ancillary N^O ligand, was cross-coupled with TMS-acetylene Pd^{II}/Cu^{I}-catalyzed in anhydrous THF solution (Scheme 3.13). The desired complex **54** was obtained as orange powder in 72 % yield after purification by precipitation with methanol in dichloromethane solution. The presence of TMS peak at δ = 0.17 ppm in ^{1}H NMR spectra supported the formation of the desired product. Further the TMS group of **54** was removed with a large excess of KF in THF solution with addition of methanol and water to give **55,** bearing the terminal acetylene. The neutral complex was isolated as reddish-orange solids in quantitative yield.

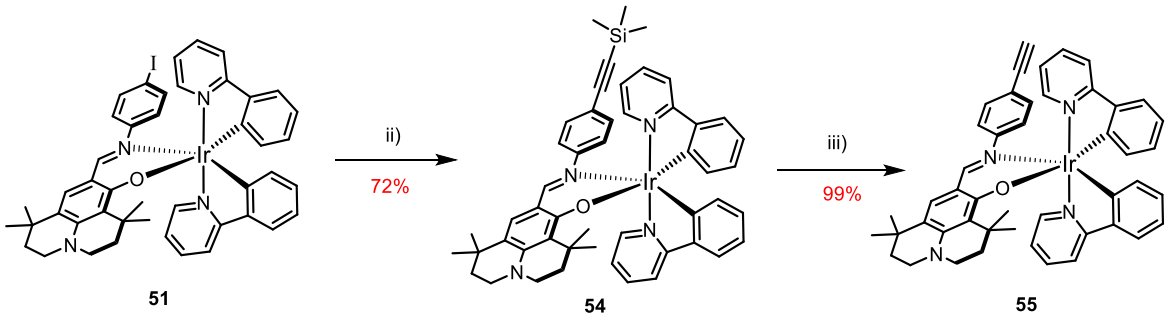

Scheme 3.13. i) $[Pd(PPh_3)_2Cl_2]$ 10 mol%, CuI 10 mol%, TMS acetylene, $^{i}Pr_2NH$, THF, rt, 12 h; ii) KF (100 eq.), THF, MeOH, H_2O, refluxing over night.

Note that the high yield reactions confirm the stability of iridium complexes when chemistry is carried out directly on the complex. Also, carrying out chemistry on the complex is a convenient method for extending the monometallic platform. It was noted however, that the products tend to decompose over the silica column, thus complex **54** and **55** were purified over aluminium column chromatography deactivated with 6% of water. Electrospray mass spectrometry analyses confirmed the nature of complexes **54** and **55**, where the calculated molecular peaks at 100 % intensity (respectively 872.3 and 944.2) were in agreement with the measured values. After

purification, the compounds were characterized using ^{1}H, ^{13}C NMR and IR spectroscopy and purity confirmed from elemental analysis.

The second metallic entity which is a platinum(II) chromophore was appended onto complex **55** by way of a coupling reaction, Cu(I)-catalyzed, in the presence of *N*,*N*-diisopropylamine in freshly distillated THF (Scheme 3.14). The cationic heterometallic dinuclear species was obtained as dark powder after purification under column chromatography, precipitation and several washings with pentane. The counter-anion was ClO_4^- which ensures a better solubility of the final dyad in conventional solvents.

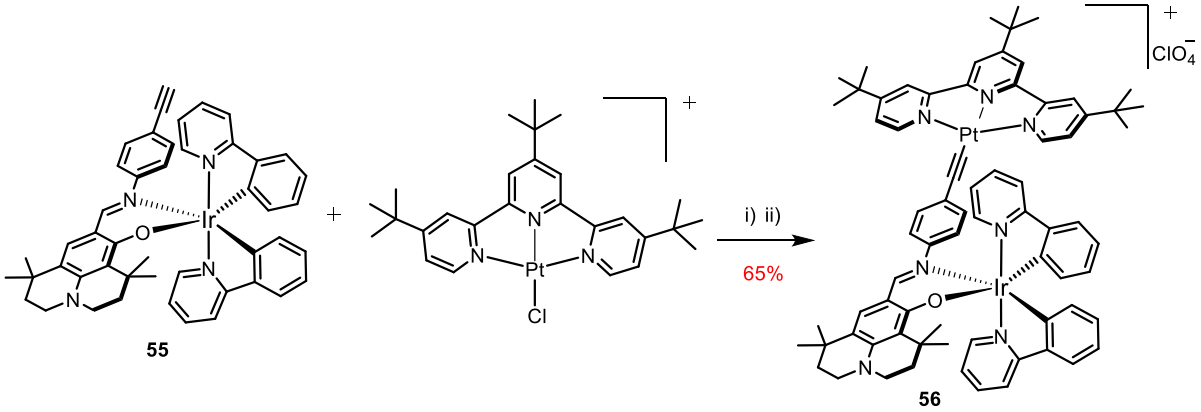

Scheme 3.14. Synthesis of dinuclear complex **56**. i): [(^{t}Bu$_3$tpy)PtCl]BF$_4$, ^{i}Pr$_2$NH, THF, CuI, rt, 12 h, anaerobic conditions ii) KClO$_4$, H$_2$O, rt, 1h30.

The proton NMR spectrum of the expected dinuclear complex was measured in deuterated acetonitrile at room temperature. The spectral profile shown in Figure 3.12 fits well with all the signal patterns of the three components composing compound **56** *i.e.* Pt chromophore, N^O-ligand and Ir chromophore. Furthermore, the singlet observed in the proton spectrum of **55** in deuterated benzene at $\delta = 2.64$ ppm corresponding to the terminal alkyne proton, disappear in the proton spectrum of **56** indicating the coordination of the platinum(II) through the carbon of ethynyl bond. Also, the anchoring of platinum entity splits two protons of pyridinyl rings in *trans* position in two doublet signals at $\delta = 9.0$ ppm and $\delta = 8.9$ ppm, whereas within the monometallic Ir complex **51** these signals are overlapped (*cf.* Figure 3.9). This is a consequence of the different chemical environment around both protons once the Pt entity is attached.

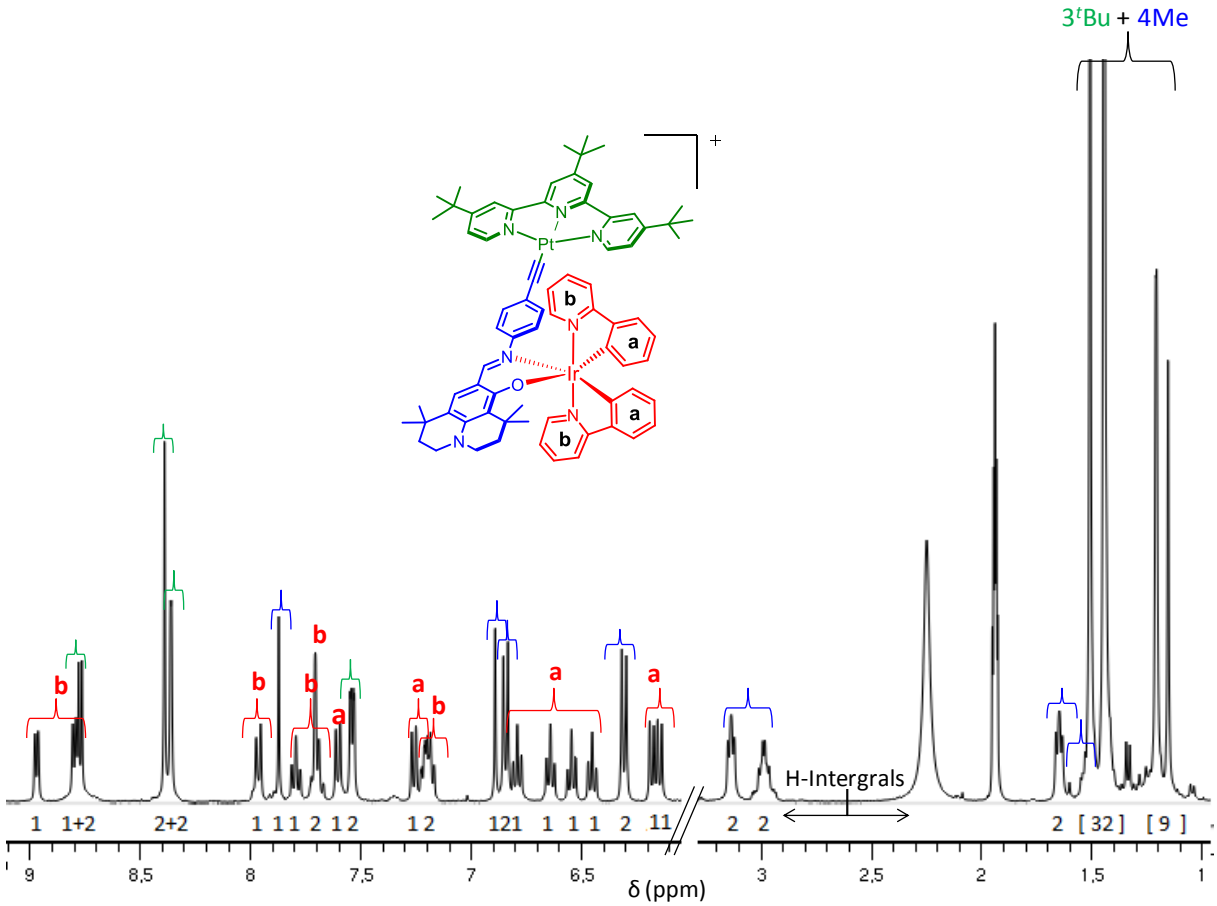

Figure 3.12. ^{1}H NMR (400 MHz) spectrum of dinuclear complex **56** in deuterated acetonitrile at room temperature. The letter "a" refers to the protons of the phenyl ring of *ppy* ligands, whereas "b" refers to the protons of the pyridinyl rings. A color code is used in order to distinguish the signals corresponding to each unity composing the dinuclear complex.

A second procedure was used for synthesizing the desired dinuclear complex by metalating the free N^O-site of **52** with Ir(III) by cleaving the dimer $[(ppy)_2Ir\text{-}(\mu\text{-}Cl)]_2$ following the same conditions as applied for **51** (Scheme 3.15). The product was obtained in 90 % yield following ion exchange and purification.

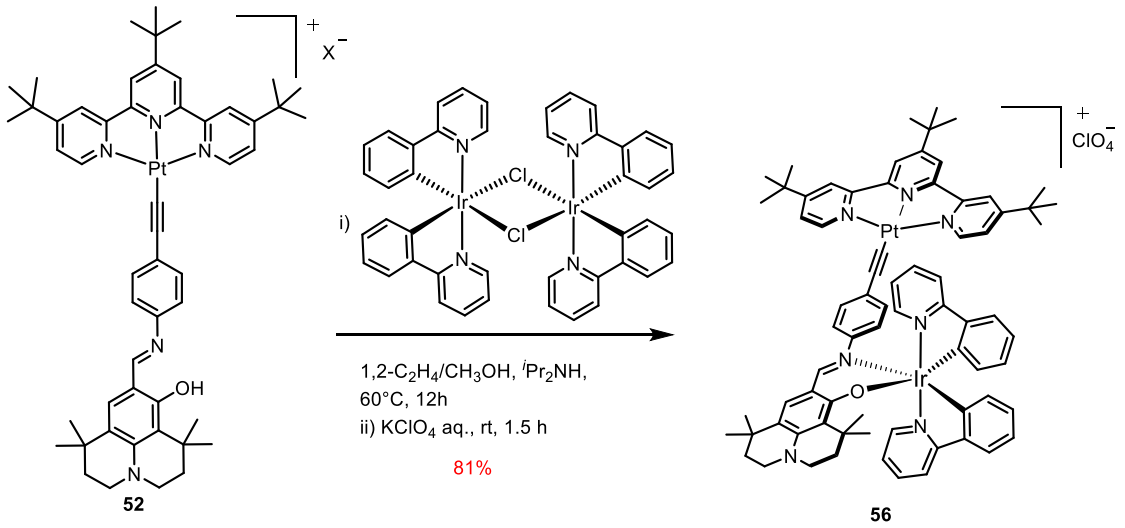

Scheme 3.15. Synthesis of dinuclear complex **56** starting from platinum(II)-N^O ligand **52**.

The dinuclear heterometalic complex was characterized from ^{13}C NMR and infra-red spectroscopy, mass spectrometry and the purity was examined by elemental analysis. In electrospray ionization (ESI) mass spectrometry analysis, the *m/z* peak at 100 % intensity was accurately assigned to the dinuclear complex.

2.7. IR study

The IR spectrum of **46** and **47** shows that alkyne C-H bond exhibit a strong absorption at around 3300 cm^{-1} due to the ν(C-H) stretching vibration. This band disappears in platinum (II) complexes **52**, **53** and **56** indicating the metalation to the ligand through the carbon of acetylene functions. Furthermore this is confirmed by the appearance of two sharp bands at 610 cm^{-1} and 620 cm^{-1} which can be assigned to ν(Pt-N) vibration. The IR spectrum of **55** suggest a weaker acetylene ν(C-H) stretching vibration, shifted at lower frequencies by ~47 cm^{-1} compared to that of the free ligand **46**. The absorption band of ν(C=N) appearing at 1620 cm^{-1} for **46** is shifted at lower frequencies in **55** (ν = 1604 cm^{-1}) and **56** (ν = 1605 cm^{-1}) indicating the coordination of the ligand to the Ir metal center through the nitrogen atom.

3. Photophysical measurements of the ligands and their boron complexes

The photophysical measurements for all compounds obtained in this chapter were realized by Dr. Andrea Barbieri and his co-workers in Italy.[155]

3.1. Absorption of 44, 46 and 48, 47

The absorption of the free ligands **44** and **46** (Figure 3.13) were measured in different solvents at room temperature and the spectra are shown in Figure 3.14. Both compounds are characterized by a broad and intense band centered at *ca.* 400 nm (ε_{max}: 37 000 to 50 000 $M^{-1}cm^{-1}$) which is not affected by the polarity of the solvents. This band is assigned to a $^1\pi$-π^* electronic transition and is usually observed for other anil derivatives reported in the literature.

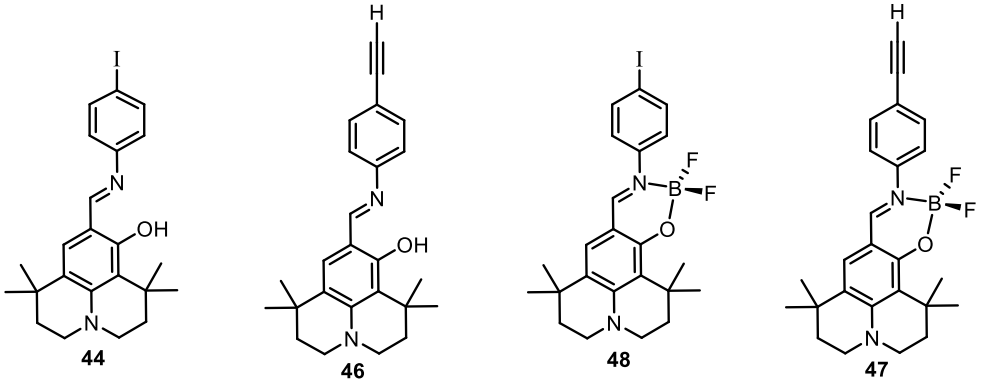

Figure. 3.13

The complexation of N^O-site of **44** and **46** with boron difluoride to give **48** and **47** (Figure 3.13) having a tetrahedral geometry, does not affect much the absorption profile of the molecules which resemble those of the free ligands (spectra shown in Figure 3.15). However, a slight bathochromic shift by *ca.* 20 nm is observed for the intense band which is centered at *ca.* 420 nm and an increase of the extinction coefficient *ca.* 64 000 $M^{-1}cm^{-1}$. This is probably due to the increase of the rigidity of the boranil core due to BF_2 complexation. As was previously the case for the free ligands, no spectral changes are observed in different polar solvents.

[155] Andrea Barbieri, Maria Pia Gullo, Barbara Ventura and Nicola Aarmaroli, "*Istituto per la Sintesi Organica e la Fotoreattività (ISOF)*", Consiglio Nazionale delle Ricerche, (CNR), Via P. Gobetti 101, 40129 Bologna BO, ITALY.

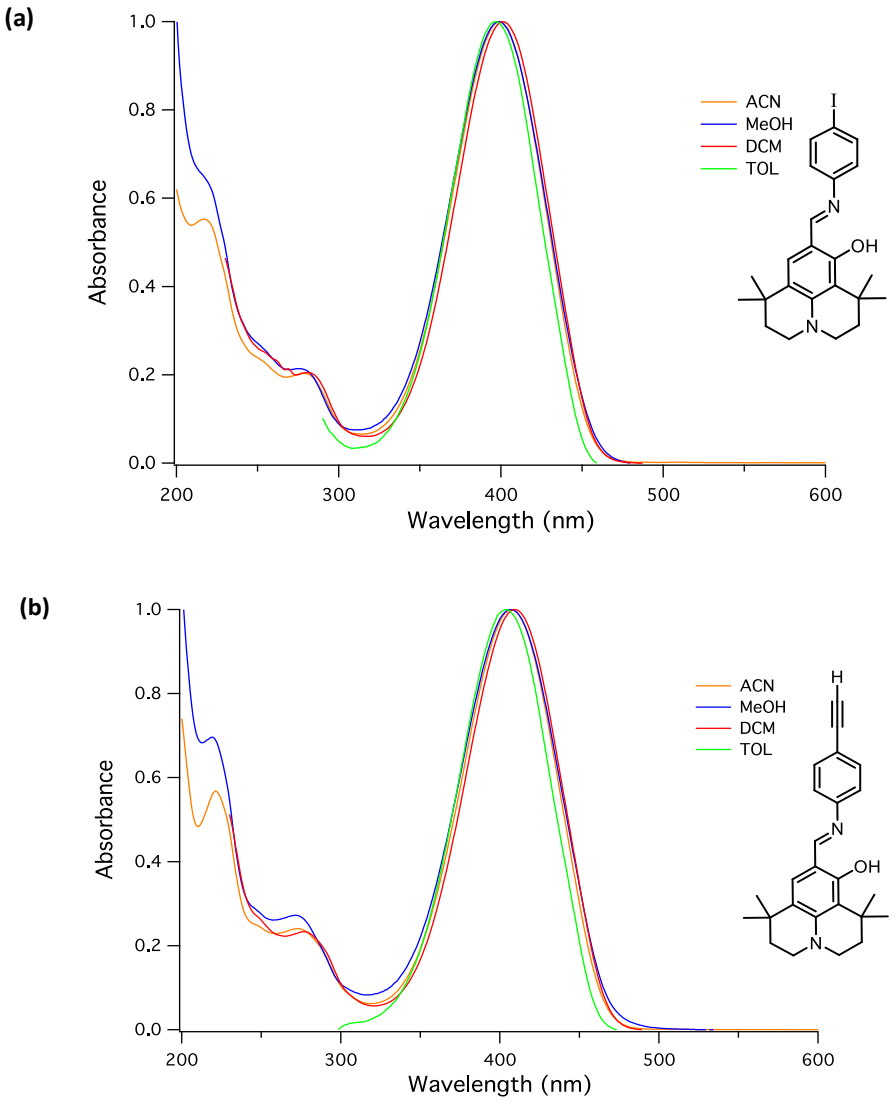

Figure 3.14. Normalized absorption spectra of compound **44** (a) and compound **46** (b) in various solvents at room temperature.

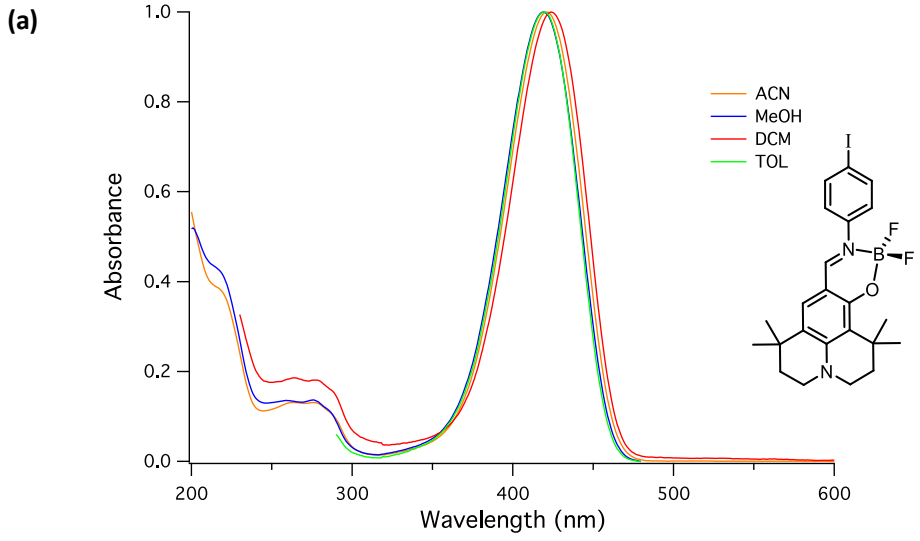

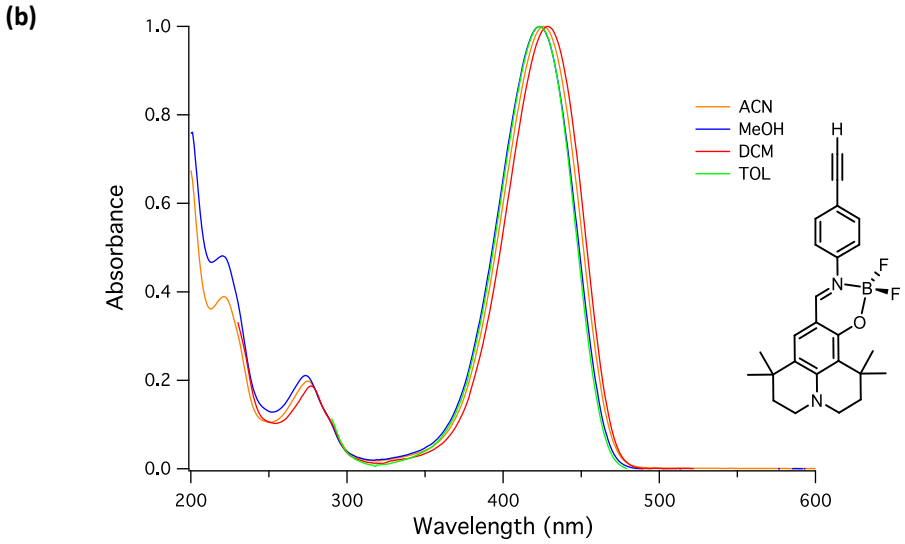

Figure 3.15. Normalized absorption spectra of compound **48** (a) and compound **47** (b) in various solvents at room temperature.

3.2. Photoluminescence of compounds 44, 46 and 48, 47

The emission of the free ligands and the corresponding boron(III) complexes are shown and compared in Figure 3.17 and data gathered in Table 3.3 and 3.4. The boron complexes **48** and **47** display an intense fluorescence emission which is characterized by a maximum at $\lambda = 480$ nm in acetonitrile and a shoulder at 500 nm. The latter is thought to result from the emission of the quinoidal form of the molecule. The increase of solvent polarity *i.e.* toluene to methanol, does not induce any shift in the spectral profile, but the intensity of the fluorescence emission is highly affected: for **48** the fluorescence quantum yield changes from $\varphi = 0.52$ in toluene to $\varphi = 0.75$ in acetonitrile whereas for **47** the quantum yield is increased from $\varphi = 0.48$ in toluene to 0.74 in acetonitrile. Furthermore the lifetime of the emissive species is fairly short in apolar solvents (*e.g.* in toluene $\tau = 1.10$ ns, 1.04 ns for **48** and **47** respectively) and is nearly doubled in polar solvent such as acetonitrile ($\tau = 1.91$ ns, 1.89 ns for **48** and **47** respectively). It might be explained in terms of stabilization by solvation of the polar excited species in the polar solvent.

Interestingly, the fluorescence quantum yield of boranil **48** and **47** are much higher than an analogue synthesized by D. Frath (φ = 0.09 in toluene) in this laboratory a few years ago (Figure 3.16a).[9] A red-shift of *ca.* 20 nm is observed for the absorption and emission maximum in our compounds relative to the *N*,*N*-diethylamino-boranil analogue. This is a clear evidence of the better conjugation of the nitrogen electron lone pair of the julolidine core with the π-system, due to the unusual tricyclic structure (*vide supra*).

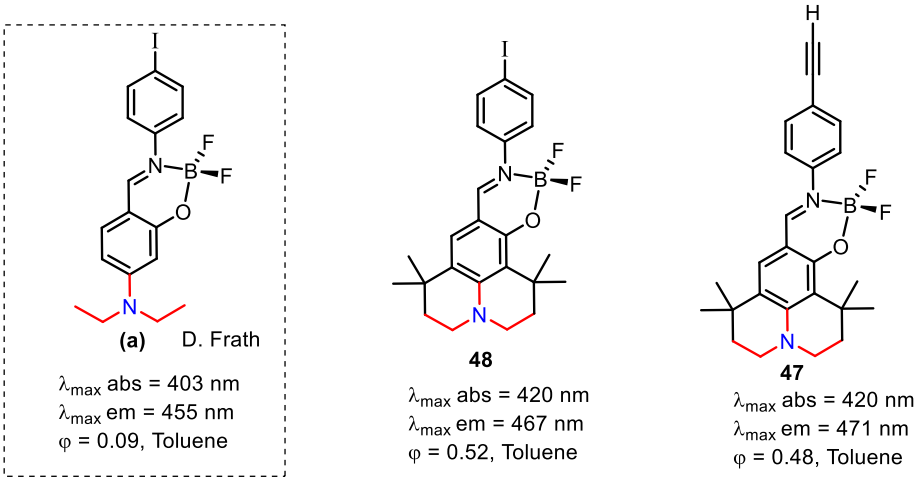

Figure 3.16. The chemical structures of the analogue compound synthesized by D. Frath (a) and the boranils synthesized within the context of this work.

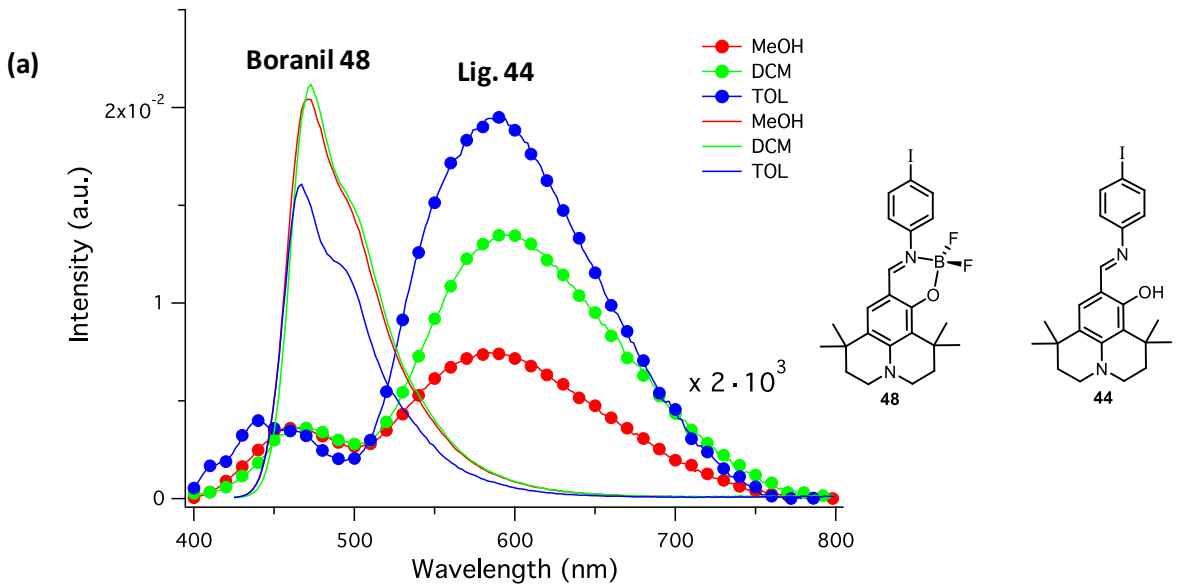

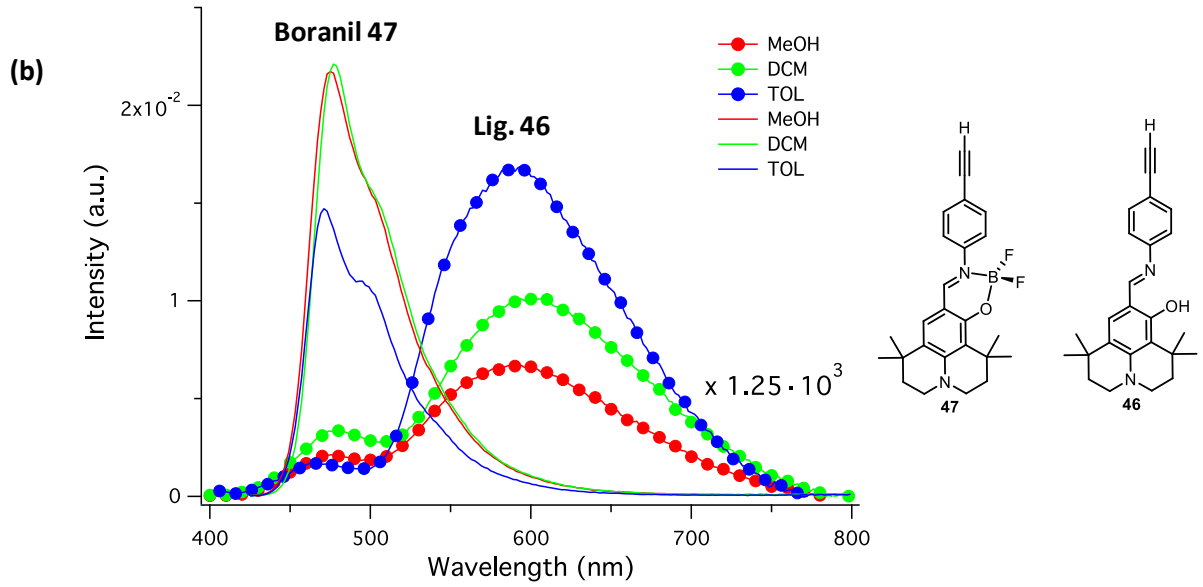

Figure 3.17. Emission spectra of boranils **48**, **47** and ligands **44**, **46** in various solvents at room temperature.

Considering the emission of the free ligands **44** and **46**, photophysical measurements revealed noteworthy results. As indicated from their spectral shape (Figure 3.17) a weak dual emission was observed. This is due to a *photoinduced excited state intramolecular proton transfer* ESIPT process (*vide infra*) already known for anil derivatives.[156] The ESIPT process causes a tautomerization from the enol form of the ligands to the keto form (Figure 3.18) by transferring a proton from the *ortho*-OH group to the nitrogen atom of the imine fragment. This process is favored by the intramolecular hydrogen bond between the *ortho*-hydroxyl group and the nitrogen atom; subsequently in the keto form a hydrogen bond stabilizes the tautomer in the *cis*-configuration. After the deactivation from radiation, the keto tautomer returns to the enol form by transferring back the proton onto the oxygen atom of the phenol unit. Thus, the presence of two bands in the luminescence spectrum comes from the enol and keto form. *However, in the absorption spectrum there is no evidence for the presence of keto tautomer because the tautomerization process is a high energy demanding process, hence not observed in the ground state.*[157]

[156] Shizuka, H.; Matsui, K.; Hirata, Y.; Tanaka, I. *J. Phys. Chem.* **1976**, *80*, 2070.
[157] Hadjoudis, E. *Mol. Eng.* **1995**, *5*, 301.

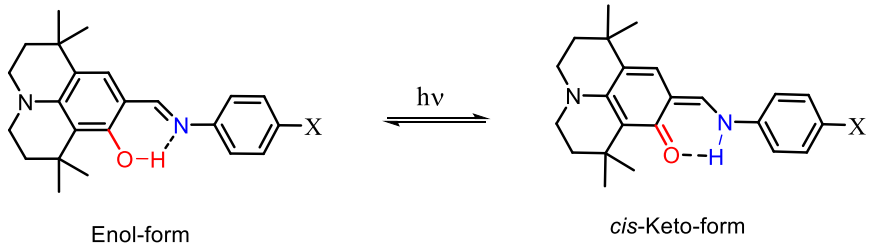

Figure 3.18. Enol-keto tautomer of julolidine-based anils.

As depicted by the luminescence spectra in Figure 3.17, the emission of the enol form is centered at 470-480 nm and the emission of the keto form is more intense, unusually broad and centered at 600 nm. The pronounced Stokes shift of the keto form ($\Delta\omega$ = 7950 cm^{-1} in methanol for **44** and **46**) is consistent with the fact that an important structural change has taken place in the excited keto form. *Even though luminescence is weak, it covers the overall visible spectral window. This observation is very exciting since a panchromatic emission from a unique small organic molecule is not common*. The global fluorescence quantum yield φ_F of the ligands are very weak (in the range of 0.001 in less polar and aprotic solvent and 0.0001 in methanol) and the excited state lifetime τ very short (for values see Table 3.3 and 3.4). Note that the keto tautomer band is more sensitive to the solvent polarity, whereas the enol emission band does not display such behavior. The excited state lifetime of the enol form is shorter than the limits of detection of the apparatus used for the optical measurements, *i.e.* less than 30 ps (see values reported in Table 3.4).

Table 3.3. Absorption and emission properties of ligands **44**, **46** and complexes **48**, **47** in acetonitrile solution.

			rt [a]			**77 K** [b]	
	λ_{abs}/nm	ε/$M^{-1}cm^{-1}$	λ_{em}/nm	φ	τ/ns	λ_{em}/ nm	τ/µs
46	407	40.300	E[c]: 480 K: 600	1.1×10^{-3} (1.1×10^{-3})	<0.02 0.13	multipeak 598	1.33×10^{-3} 54.6×10^{3}
44	399	49.000	E: 470 K[c]: 600	0.7×10^{-3} (0.7×10^{-3})	<0.02 0.12	460, 536 594	1.12×10^{-3} 11.6×10^{3}
47	426	64.500	479	0.75 (0.80)	1.89 (1.97)	463 572	1.84×10^{-3} 38.4×10^{3}
48	421	64.000	473	0.74 (0.82)	1.91 (2.01)	458 584	1.87×10^{-3} 17.1×10^{3}

[a] In air-equilibrated (de-aerated) CH_3CN solution. For quantum yield determination: λ_{exc} = 420 nm for **47** and **48**, λ_{exc} = 400 nm for **44** and **46**. For lifetime measurements: λ_{exc} = 373 nm. [b] In glassy solutions of CH_2Cl_2:CH_3OH (1:1) for both complexes and ligands. [c]E= enol form, K = Keto form.

Table 3.4. Emission properties of ligands **44**, **46** and complexes **48**, **47** in various solutions.

		TOL			DCM			MeOH		
		λ_{max}/nm	φ	τ/ps	λ_{max}/nm	φ	τ/ps	λ_{max}/nm	φ	τ/ps
46			9.4×10^{-4}			6.8×10^{-4}			4.4×10^{-4}	
	E[a]	464		< 20	478		< 20	466		< 20
	K[b]	590		131	602		143	592		81
46			7.1×10^{-4}			5.4×10^{-4}			3.3×10^{-4}	
	E[a]	440		< 20	468		< 20	462		30
	K[b]	588		116	596		128	586		72
48		467	0.52	$1.10\text{x}10^3$	473	0.69	$1.67\text{x}10^3$	471	0.69	$1.80\text{x}10^3$
47		471	0.48	$1.04\text{x}10^3$	477	0.71	$1.65\text{x}10^3$	475	0.72	$1.76\text{x}10^3$

For quantum yield determination in air-equilibrated solutions, λ_{exc} = 400 nm. For lifetime measurements, λ_{exc} = 407 nm for **46** and **46** and λ_{exc} = 373 nm for **48** and **47**.[a]E = enol form. [b]K = keto form.

3.3. Optical studies of the ligands in acidic media

The photophysical behavior of ligand **44** and **46** was studied also in acidic media, since the molecule has free doublet susceptible to be protonated. Herein is represented only the results of ligand **44**, but the same observation was made for **46**. The absorption spectrum measured in acetonitrile solution at room temperature (Figure 3.23a) indicates the lowering of the initial band (in blue, 0 equivalents of trifluoroacetic acid) and the appearing of a new band bathochromically shifted and increasingly intensity upon addition of acid. The nascent band is centered at *ca.* 480 nm and resembls the absorption profile of the corresponding closed cycle with boron difluoride entity. Regarding the emission profile (Figure 3.23b), measured by excitation at the isobestic point (λ = 420 nm) obtained in the absorption spectrum upon acidification, the emission band of the keto tautomer was gradually suppressed by the slow addition of acid. The emission of the enol form decreases and subsequently a new band appears slightly red-shifted compared to the enol band in neutral acetonitrile solution. This band is ascribed to the emission of a cationic species for which the spectrum is closely similar to those of the boranil complexes.

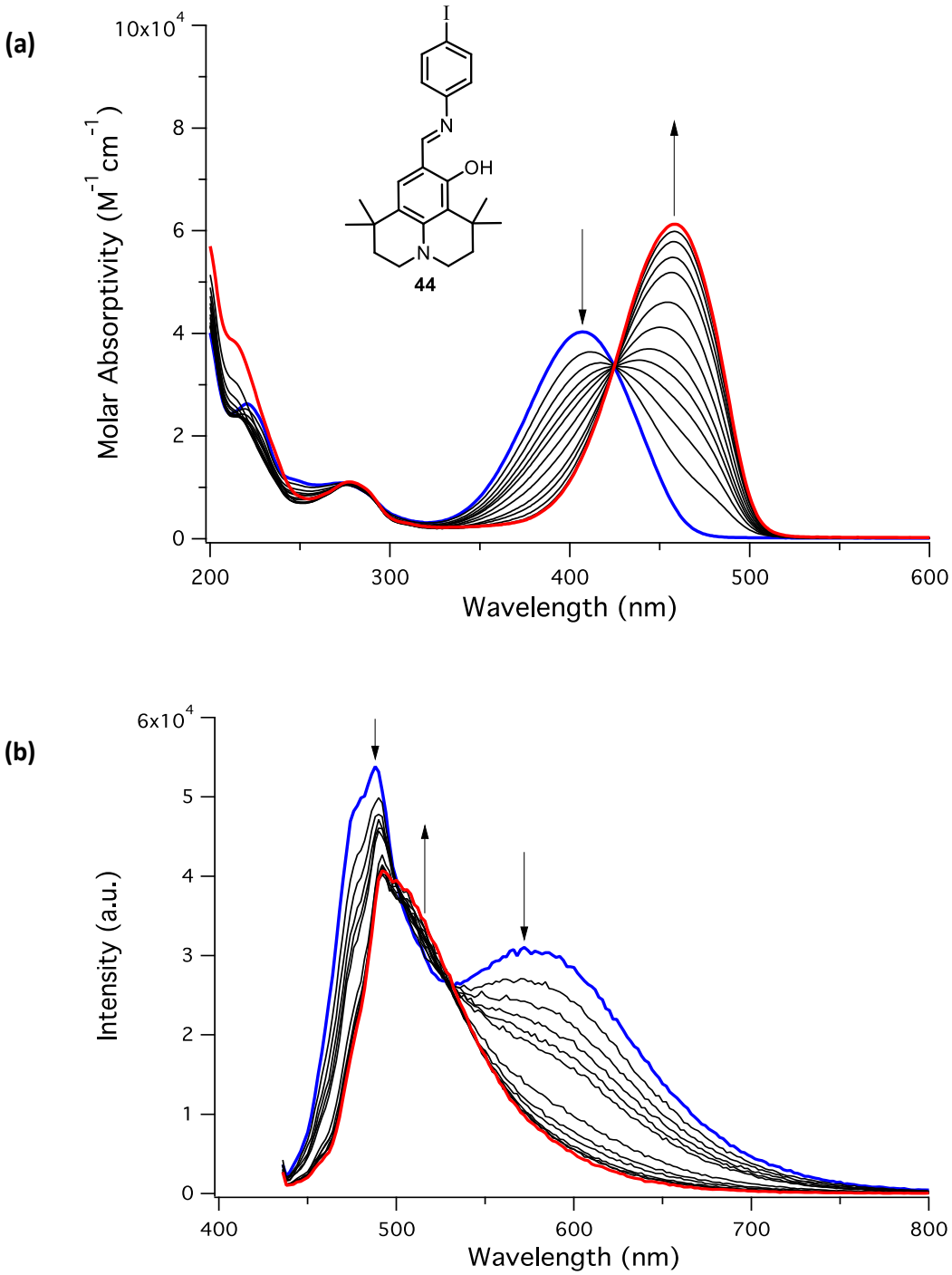

Figure 3.19. Absorption (a) and emission (b) spectra of ligand **44** in acetonitrile solution (c = 6.3×10^{-6} M) at room temperature upon addition of trifluoroacetic acid; starting from 0 eq. (blue line) to 1000 eq. (red line). The arrows indicate the progression of the reaction through addition of acid.

4. Photophysical measurements of the multichromophoric systems

4.1. Pt(II)-anil 52 and Pt(II)-boranil hybrid 53 complexes

The absorption and emission spectra of the dyads **52** and **53** were evaluated in acetonitrile solution at room temperature and at 77 K (for values see Table 3.5 and 3.6). The absorption profile of the dyad Pt(II)-anil **52** features the patterns of its subunits components as shown in Figure 3.20. An intense and broad band is observed centered at 408 nm with an extinction coefficient ε = 47 200 M^{-1} cm^{-1} and results from the absorption of the anil (julolidine-based) entity. At higher energies the absorption spectrum displays weak absorption bands: 223 nm (ε = 68.300 $M^{-1}cm^{-1}$), 310 nm (ε = 26.700 $M^{-1}cm^{-1}$), 339 nm (ε = 25.900 $M^{-1}cm^{-1}$), which are assigned to Pt chromophore relative to a Pt model.[158] Dyad **53** anchoring a BF_2 entity displays the same absorption bands but the maximum red-shifted *ca.* 20 nm (Figure 3.20). The same behaviour was observed previously for the compounds missing the Pt(II) chromophore *i.e.* anils **44**, **46** and boranils **48**, **47** (*cf.* Table 3.3).

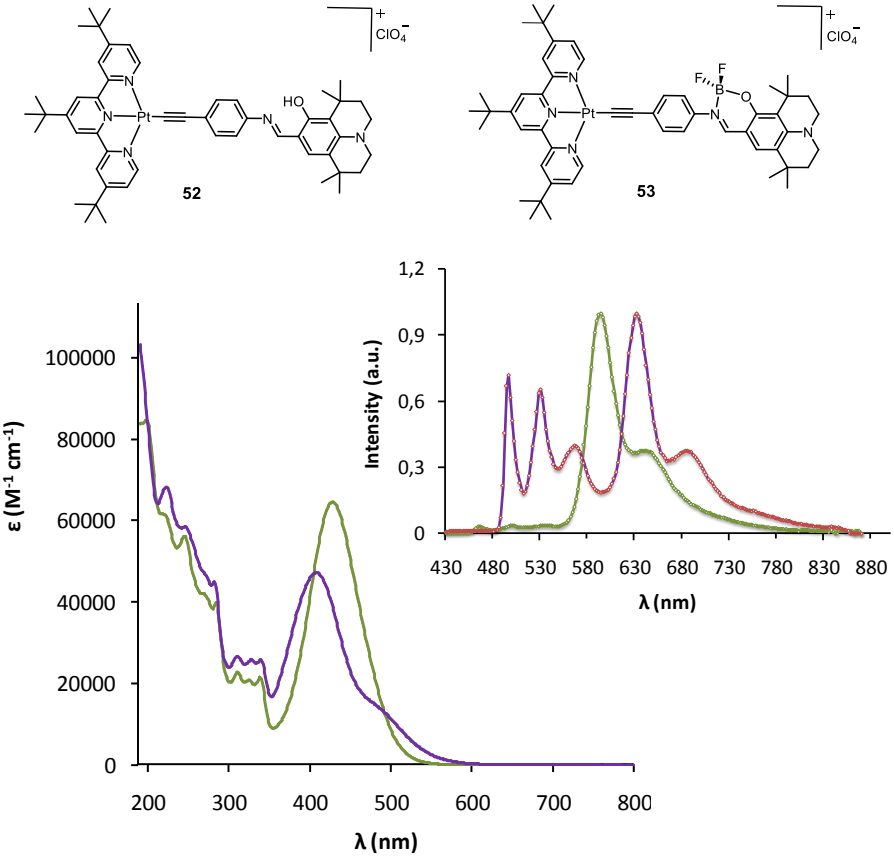

Figure 3.20. Lower side: absorption spectra of **52** (violet) and **53** (green) in acetonitrile solution at room temperature. Upper side: emission spectra of **52** (violet) and **53** (green) in CH_2Cl_2:CH_3OH (1:1) at 77 K.

[158] Ventura, B.; Barbieri, A.; Barigelletti, F.; Diring, S.; Ziessel, R. *Inorg. Chem.* **2010**, *49*, 8333.

Considering the emission spectrum of the dyads in de-aerated acetonitrile, no luminescence was observed at room temperature. Nevertheless, at 77 K in a mixture solution of dichloromethane and methanol, phosphorescence emission could be resolved. Figure 3.20 shows the emission spectra of dyad **52** and **53** whereas the data are gathered in Table 3.6. The spectral profiles seem to correspond to the overlapping phosphorescence of the model compounds *i.e.* anil **46** and boranil **47**. The emission of **52** is characterized by a low energy band peaking at 600 nm and two lower energy emission bands but well defined at 500 nm and 465 nm. The first band is thought to be due to the phosphorescence from the excited triplet state of julolidine-based ligand ^{3}LC such as it is the case for the free ligand **46** (phosphorescence was observed at 77 K, for values see Table 3.3).

The phosphorescence lifetimes of the dyads are 0.6 ms and 0.3 ms for the model **52** and 0.9 ms and 3.7 ms for the Pt-Boranil dyad **53**. These lifetimes are much lower than those of the free ligand **46** hence showing a mixing with a charge-transfer state. The band at 500 nm is assigned to ^{3}MLCT and the high energy band at 465 nm is assigned to ^{1}LC of julolidine-based ligand. These bands are well observed in case of Pt-julolidine-based ligand **52** but they are very weak in Pt-boranil **53** as shown in Figure 3.20. *An energy transfer process is thought to occur from Pt chromophore through the julolidine-based ligand.* This might be explained by the heavy atom effect of Pt which allows the spin-orbit coupling. Also the life-time phosphorescence emission of Pt(II) is shorter comparing to its Pt(II) model.

Table 3.5. Absorption features of ligands and complexes in acetonitrile at room temperature.

	λ_{max}, nm (ε_{max} 10^3, M^{-1} cm^{-1})
55	276 (58.8), 373 (23.6)
51	257 (55.3), 370 (23.5)
52	223 (68.3), 310 (26.7), 339 (25.9), 408 (47.2)
53	245 (56.3), 310 (22.7), 338 (21.5), 428 (64.6)
56	258(92.9), 340 (32.7), 373 (31.4)

Table 3.6. Emission properties of ligands and complexes.[a]

	rt [a]			77 K [b]		
	λ_{max}/nm	φ	τ/ns	λ_{max}/ nm	τ /µs	
55	576	0.5×10^{-3} (3.4×10^{-3})	34.5 (1310)	544	11.2	
51	584	0.4×10^{-3} (2.8×10^{-3})	30.8 (1140)	534	10.6	
52	n.d[d]	n.d.	n.d.	466 500 600	- 11.5 0.6×10^{3}, (52:48)	3.0×10^{3}
Pt [c]	605	4.7×10^{-3} (13×10^{-3})	313 (920)	523	20.0	
53	n.d.	n.d.	n.d.	464 500 594	- 11.2 0.9×10^{3}, (70:30)	3.7×10^{3}
56	n.d.	n.d.	n.d.	multipeak	multiexp.	

[a] In air-equilibrated (deaerated) CH_3CN solution. For quantum yield determination: λ_{exc} = 330 nm for **51** and **55**. For lifetime measurements: λ_{exc} = 331 nm for **51** and **55**. [b]In glassy solutions of CH_2Cl_2:CH_3OH (1:1) for all complexes. For lifetime measurements, λ_{exc} = 331 nm for **53**, **52, 51** and **55**.[c] Values found from ref. [27].[d] n.d. non determined.

4.2. Ir(III) monometallic complexes 51, 55

The absorption spectrum of the monometallic heteroleptic Ir complexes **51** and **55** in Figure 3.21, displays an absorption band at *ca.* 260 nm (ε = 60 000 M^{-1} cm^{-1}) and at lower energy band at *ca.* 370 nm (ε = 24 000 M^{-1} cm^{-1}). The emission spectra at room temperature in acetonitrile solution display a band peaking at 580 nm with very low quantum yield (for values see Table 3.6) and the lifetimes are τ = 30.8 ns and 34.5 ns for **51** and **55** respectively; in deaerated solution the lifetimes are much longer (values in Table 3.6).

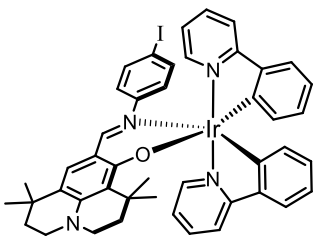

51

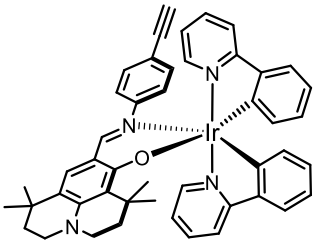

55

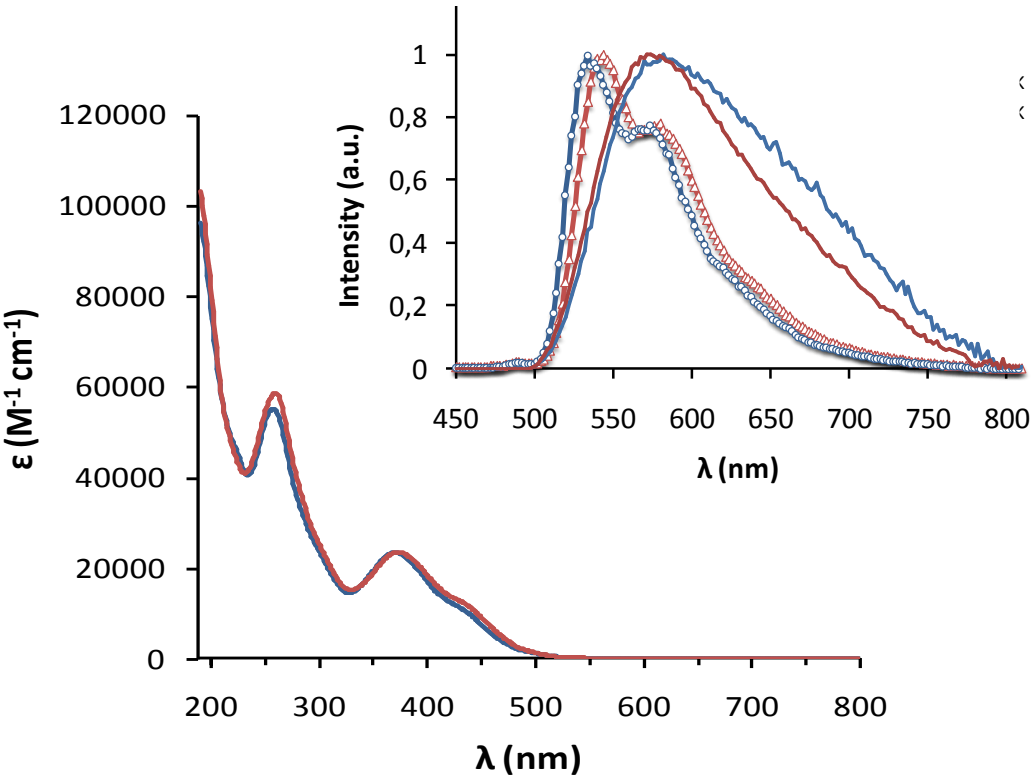

Figure 3.21. Lower side: absorption spectra of compound **51** (blue) and **55** (red) in acetonitrile solution at room temperature. Upper side: emission spectra of compound **51** (blue) and **55** (red) in deaerated acetonitrile solution at room temperature (continuous lines) and in CH_2Cl_2:CH_3OH (1:1) at 77 K (pointed lines).

In a glass matrix (a mixture of dichloromethane and methanol at 77 K) (inset Figure 3.21) the emission peaks are blue-shifed by *ca.* 50 nm and 30 nm and the lifetimes of the exited state much longer, 10.6 ns and 11.2 μs for **51** and **55** respectively comparing with the values at room temperature in acetonitrile solution. The radiative constant for **55** is k_r is 2.6 x 10^3 s^{-1} which appears 2-fold lower than expected value for a ^{3}MLCT transition. It might thus be assumed that the excited state species may have a contribution from the ^{3}LC of the julolidine-based ligand. Additional measurements have been conducted in film of **55**, prepared in the inert polymer matrix of polystyrene (Table 3.7). It shows a slightly red-shifted (20 nm) emission peak (λ_{max} = 564 nm) compared to the glassy matrix (λ_{max} = 544 nm) and the lifetimes (τ = 3.46 μs) has the same order of magnitude.

Table 3.7. Luminescence properties of **55** and **56** in polystyrene film at room temperature.
[a]Pt model see ref. [27].

	λ_{max}, nm	τ, ns
55	564	$3.5x10^3$
Pt[a]	538	$5.2x10^3$
56	630	multiexp

4.3. Pt(II)-Ir(III) dinuclear heterometallic complex 56

The absorption profile of the triad **56** is rather consistent with the sum of its own components as shown in Figure 3.22 pointing out the presence of a weak electronic coupling between the single subunits. Moving from higher to lower energy, it is possible to observe two sets of bands, as in the iridium(III) monometalic model **55**, and to recognize the distinct contributions of the single components. The specific features are listed below: (*i*) the most intense band, up to 350 nm, typical of $^1\pi,\pi^*$ terpy/ppy centered transitions ($\lambda_{max} \approx 258$ nm), (*ii*) the broad mixed iridium(III) **55** and Pt(II) ^{1}MLCT/^{1}LLCT transition band, extended from 350 to 500 nm; (*iii*) the ^{3}MLCT transition band, appearing as a tail with low intensity, up to 600 nm.

The emission of the dinuclear species is completely quenched at room temperature. But the emission spectrum (Figure 3.22) at 77 K displays a broad and multi-peak emission that covers all the visible range, with the contribution of all components. For understanding how much the single units affect the luminescence of the triad, emission profile was performed according two different ranges of excitation wavelengths *i.e.* λ_{exc} = 325 nm and λ_{exc} = 375 nm. Even exciting almost selectively the ligand and metal subunits, only slight differences in the relative intensities of the peaks were observed, without separation of the bands of the single components. The same behavior was observed when luminescence was measured on the inert polymer matrix of polystyrene.

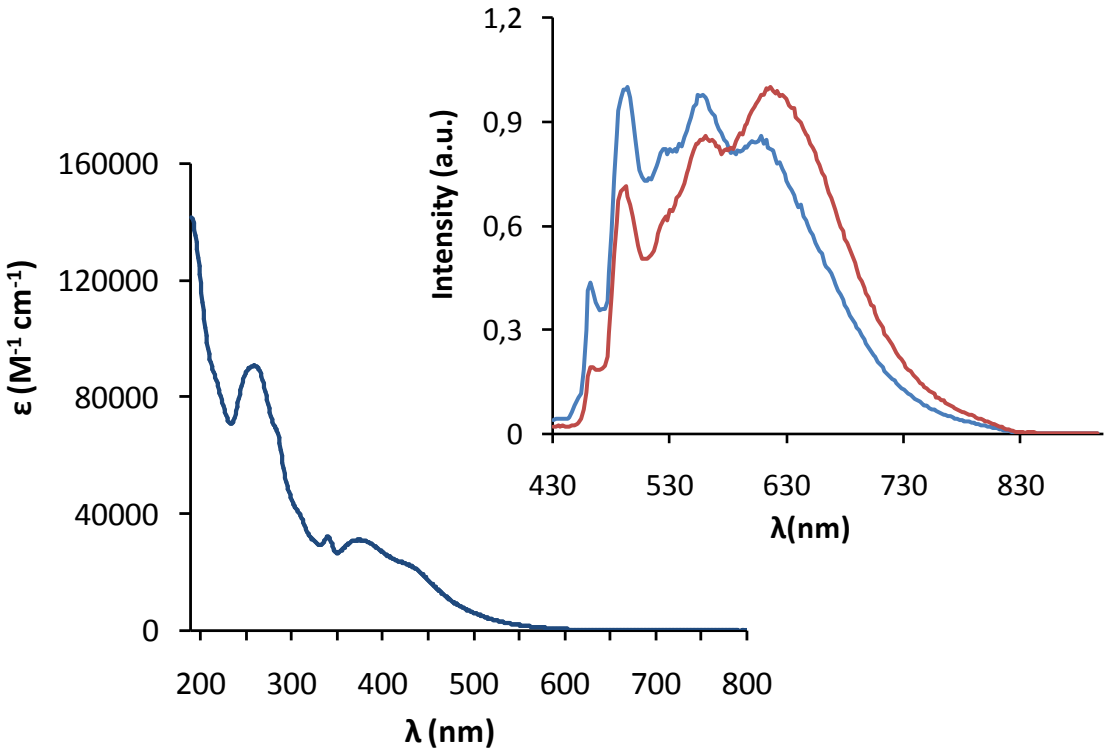

Figure 3.22. Lower side: absorption spectra of compound **56** in acetonitrile solution at room temperature. Upper side: emission spectra of compound **56** in CH_2Cl_2:CH_3OH (1:1) solution at 77 K, in blue (λ_{exc} = 325 nm) in red (λ_{exc} = 375 nm).

5. Conclusion

This work has focused on the synthesis and studies of a series of chelating N^O-type ligand based on the strong electron-donating julolidine motif. These compounds display ESIPT process due to the hydrogen bond of the hydroxyl group proton with the nitrogen atom of the imine fragment. Interestingly, their luminescence profiles exhibit broad luminescence band covering the whole spectrum. Although emission quantum yields are weak, these observations are prominent results since panchromatic emission form small organic molecules still remain a challenge. The complexation of N^O site with BF_2 entity suppresses the ESPIT processes and highly increases the fluorescence quantum yield of the corresponding boranil which is centered at *ca.* 470 nm. Alongside, the julolidine based ligands were metallated with Ir(III) center providing a new heteroleptic Ir(III) complexes. The low value k_r = 2.6 10^3 suggestss that the excited state of the complex is not a pure ^{3}MLCT state but has contribution from the triplet state of the julolidine based ligand ^{3}LC. The appending of a platinum(II) chromophore units onto julolidine core by way of palladium-catalyzed reaction provides a new hybrid dyad.

According the photophysical measurements upon photoexcitation the molecule exhibits an energy transfer process from the ^{3}MLCT of the platinium-containing chromophore through the lower energy triplet state of the julolidine-based ligand (see energy diagram levels in Figure 3.23). The process is observed even when the free N^O site is blocked with a boron difluoride unit. Finally, we designed and synthesized an original dinuclear heterometallic complex based on julolidine ligand which bears a Pt(II) chromophore and an Ir(III) cyclometallated center. The luminescence of this species at room temperature is completely quenched but at 77 K on glassy matrix it displays a broad emission covering the whole visible spectrum. The same behavior was observed when luminescence was measured on the inert polymer matrix of polystyrene.

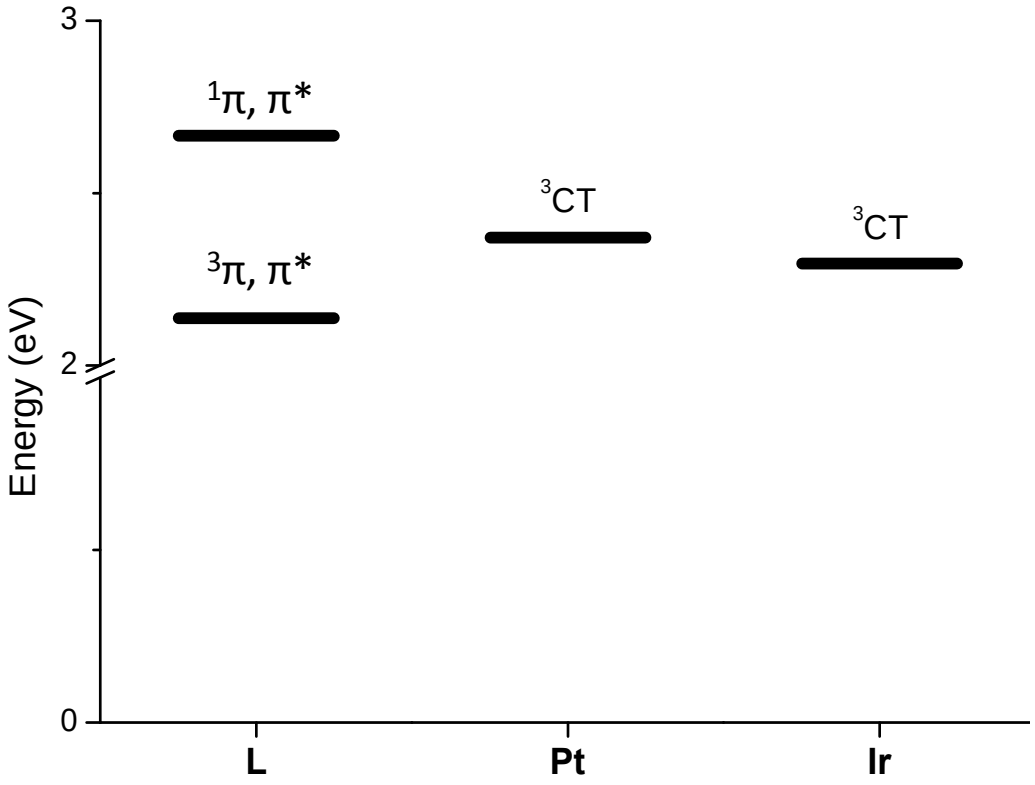

Figure 3.23. Estimated energy level diagram for the hybrid molecular systems. On the left side are represented julolidine-based (L) levels, on the right side metal-centered levels.

Chapter IV

Chapter IV- Fluorescent Photochromic Switches

One of the principle projects treated during this doctoral thesis concerns the design and synthesis of fluorescent switches based on photochromic units. Among the various types of photochromic module, we selected the [1,3]oxazine, a spiroheterocyclic compound, introduced by Tomasulo *et al.* from the University of Miami. This chapter will describe the route which conducted us to the synthesis and characterization of the final target compounds and the preliminary photophysical measurements.

1. Introduction– indolino[2,1-b][1,3]oxazine

In 2005, Tomasulo *et al.* designed and synthesized a new promising class of photochromic molecules, the [1,3]oxazines[159] which belong to the family of spiroheterocyclic compounds (*vide supra*). Their 3*H*-indoline moiety is fused with benzo[1,3]oxazine cycle through the nitrogen atom and a tetrahedral carbon at 2-position (Figure 4.1). As the other spiroheterocyclic *(i.e.* spiropyrans and spiro[1,4]oxazines reviewed in Chapter I) the tetrahedral carbon at 2-position confers to the molecule a particular non planar skeleton and is named spiro carbon (C_{spiro}). In addition, [1,3]oxazines are chiral due to the asymmetric C_{spiro} center. To our knowledge, no crystallographic structure of photochromic [1,3]oxazines are reported until the moment of writing this thesis. However, during this thesis work we could obtain the molecular structure of an [1,3]oxazine derivative which will be discussed further.

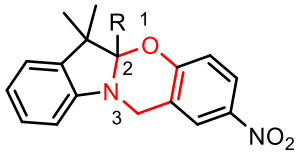

[1,3]oxazine

Figure 4.1. New photochromic compounds introduced by Raymo *et al.*

[1,3]oxazine containing a phenyl ring attached to the sp^3 carbon center, undergoes photoinduced opening of the oxazine ring after laser excitation as confirmed by Tomasulo *et al.* (Scheme 4.1).[159] The zwitterionic open form containing an indolium cationic fragment and an anionic phenolate fragment (merocyanine-type) was estimated to be formed in a time scale of *ca.* 6 ns and switched back thermally in 25 ns.

[159] Tomasulo, M.; Sortino, S.; Raymo, F. M. *Org. Lett*. **2005**, *7*, 1109.

The transient absorption spectrum was characterized by the appearance of a band at 440 nm assigned to the $S_0 \rightarrow S_1$ electronic transition of the 4-nitrophenolate fragment. Whereas the steady state absorption spectrum of the closed oxazine showed a band centered at 308 nm assigned to the $S_0 \rightarrow S_1$ of 4-nitrophenoxy moiety. An outstanding point is that *the photo-conversion process was not accompanied with any degradation of the product even in the air-saturated solution and after 3000 cycles*. The quantum yield of the photo-conversion reaction from oxazine form to indolium form was estimated *ca.* 0.1.

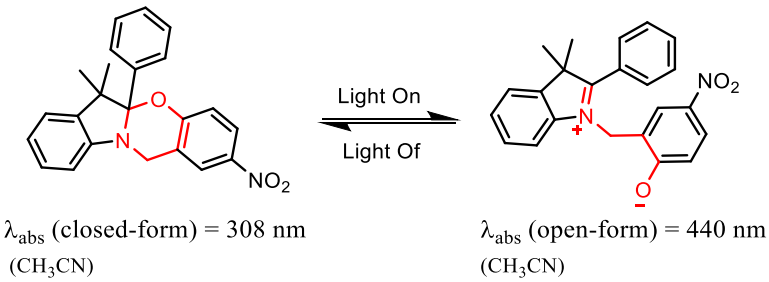

Scheme 4.1. The first photochromic [1,3]oxazine synthesized and reported by Raymo *et al.*.

In 2008, Tomasulo *et al.* reported on the synthesis and investigation of a series of 1,3[oxazine] derivatives. The main point being the study of the photochromism by introducing extended π-conjugated substitutions at three different positions of the oxazine core (inset figure in Scheme 4.2).[160] In particular, they investigated the anchoring of a π-conjugated fragment at the chiral carbon center (Scheme 4.2) so as to generate an extended indolium chromophore absorbing in the visible range after photoinduced cleavage of the oxazine ring.

They noted that the laser excitation induces only the opening of the molecule **2a** and **3a** with a quantum yield (φ) 0.08 and 0.25 and lifetime (τ) of the open forms being 38 ns and 140 ns respectively. Indeed, the absorption band of the zwitterionic products of **2a**, **3a** was centered at 420 and 430 nm respectively and was the sum of the absorption of the two independent fragments of the open species *i.e.* the extended indolium chromophore and 4-nitrophenolate chromophore. The interesting point herein is the bathochromic shift in the absorption spectrum after addition of the π-conjugated arm compared to compound **1a** shown in the Scheme 4.2.

[160] Tomasulo, M.; Sortino, S.; Raymo, F. M. *J. Photochem. Photobiol. A: Chem.* **2008**, *200*, 44.

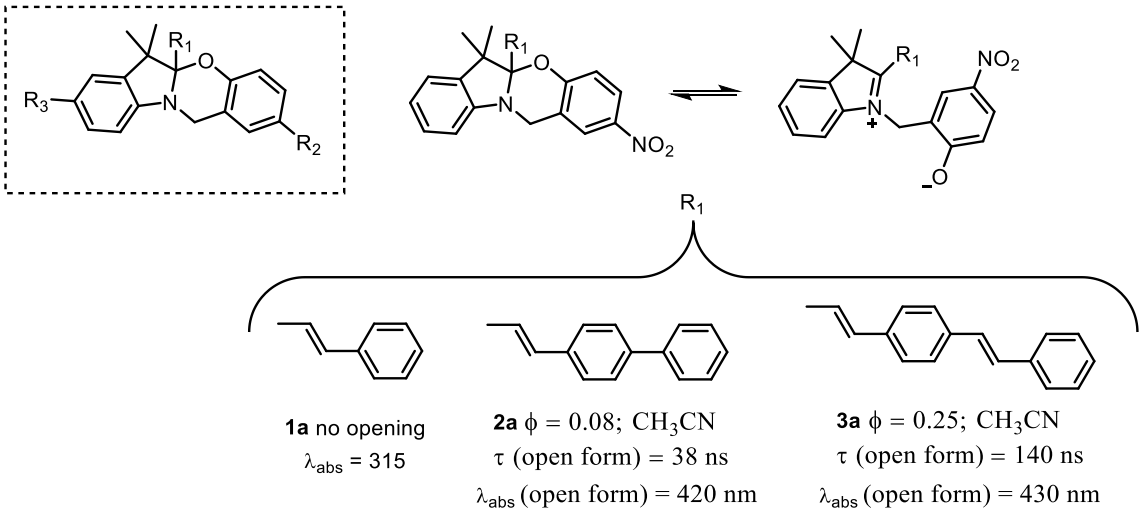

Scheme 4.2. Study of photochromisme by extending the R_1 group.

Notice that the appendage of a *trans*-stilbenylvinyl arm at the R_3-position (Scheme 4.3) induces no opening of the [1,3]oxazine ring upon irradiation at λ = 355 nm, in spite of the introduction of the extended π-system. Indeed the spectral pattern measured 80 ns after irradiation with λ = 355 nm causes the appearing of a band centered at 510 nm. According to the authors this band corresponds to a transition of the *trans*-stilbenylvinyl-3*H*-indole entity, not to the open oxazine.[2] These observations are consistent with previous experimental results reported on spiropyrans and spiroxazines, where the substitution of the half left part of the molecule does not influence the photoinduced opening of the oxazine/pyran core.

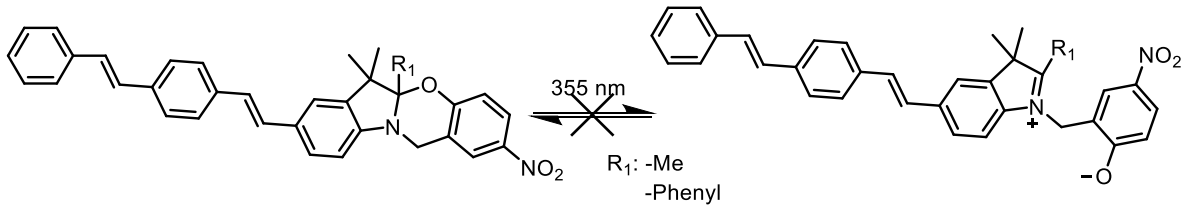

Scheme. 4.3. Study of extending the R_3 position on [1,3]oxazine.

When an electron-donor as 2-(4-dimethylaminophenyl)-ethylene group is introduced at R_1 position (Scheme 4.4), the ultraviolet irradiation of the oxazine core induces the photogeneration of a merocyanine open isomer which has an additional intense absorption band centered at 550 nm. The transient absorption spectrum reveals the band at 440 nm which is assigned to 4-nitrophenolate anion entity and the band centered at 550 nm assigned to 3*H*-indolium fragment with the extended π-system. The solution containing the open isomer becomes highly colored.

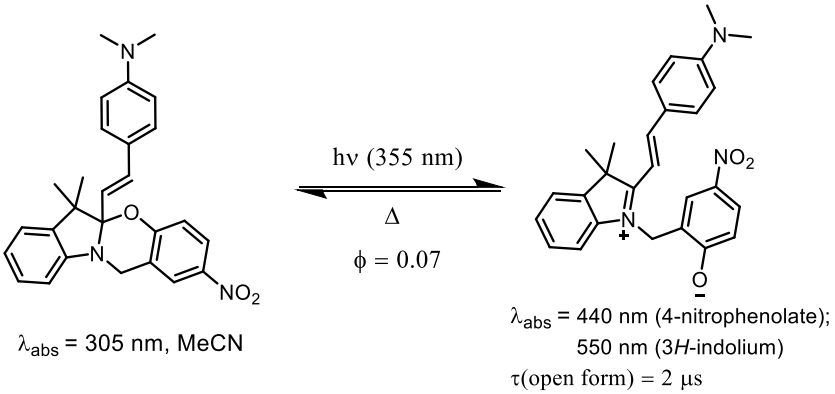

Scheme 4.4. Photochromism of dimethylamino-styryl[1,3]oxazines.

Indeed the chemistry around the [1,3]oxazine core has taken inspiration from another class of spiro-photochromic compounds: the styryl-indolino[2,1-b]oxazolidines (Scheme 4.5), not commonly used in literature but highly protected by patterns. The skeleton is based on a substituted styryl entity attached to the indole moiety through the spiro carbon. In the closed form their solution is colorless or slightly colored, while the open form becomes colored due to the extended π-conjugation spread over the molecule. Such heterocycles have appeared during the 1970's and were utilized first by the Japanese Society Matsushita Electric Industrial Co.[161]

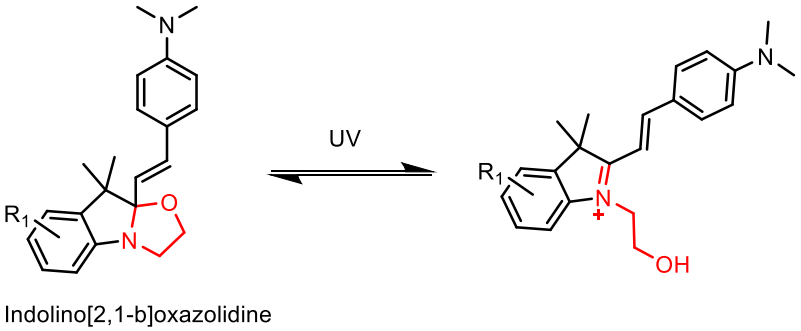

Scheme. 4.5. Photochromism of indolino[1,2-b]oxazolidines.

Oxazolidine as well as oxazines are photochromes and acidochromes. The addition of acid shifts the equilibrium of the solution through the colored thermally stable open form. The latter returns back to the closed form after addition of a base or by irradiation.

[161] Found in : Sevez, Guillaume «*Conception, synthèse et étude de nouveaux switches multimodulables*», Thesis dissertation, Université de Bordeaux, 2009, pp 73.

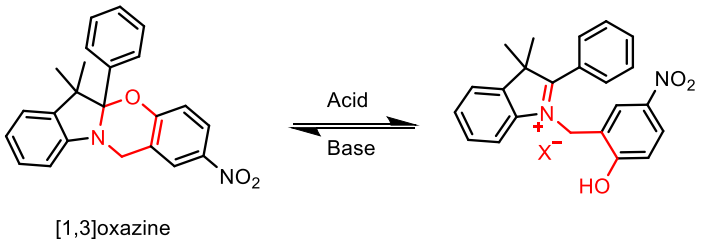

Scheme 4.6. Acidochromism of [1,3]oxazines.

1.1. Selection of indolino[1,3]oxazine

There are several parameters, which have been discussed in the first chapter characterizing a photochromic species. Among others we mentioned the *fatigue resistance* and the *number of cycles* supported by a molecule without any loss of efficiency. When the photochromism is utilized for designing optical molecular switches, these parameters are to be considered very carefully. In designing molecular switches, Raymo's oxazines appeared very attracting to us compared to spiro[1,4]oxazine, one of the most popular member of spiroheterocyclic compounds, or the oxazolidine derivatives. Indeed, Raymo's oxazine chemical structure appears as a nice combination of indolino[1,4]oxazine and indolino[2,1-b]oxazolidine taking advantages of both structures (Figure 4.2). They were designed such as to overcome some problems persisting on the common spirocompounds and which limit considerably their uses in optical devices applications.

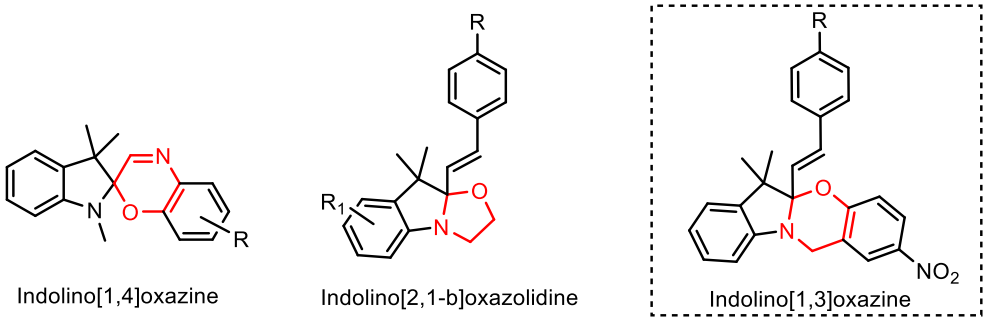

Figure 4.2.

1.2. Objectives of the present work

The [1,3]oxazine photochrome has already been studied as fluorescent switching in pairing with a fluorescent dye as reported by Deniz *et al.*.[162] However, the convenient combination of two fluorescent dyes within the same photochromic skeleton such as to control an energy transfer

[162] (a) Deniz, E.; Sortino, S.; Raymo, F. M. *J. Phys. Chem. Lett.* **2010**, *1*, 1690. (b) Deniz, E.; Shuvasree, R.; Tomassulo, M.; Impellizzeri, S.; Sortino, S.; Raymo, F. M. *J. Phys. Chem. A.* **2010**, *114*, 11567.

process through switching of the *indolino[1,3]oxazine* core has not been studied so far. Additionally, the triad systems tuning an energy transfer process by employing an addressable switching bridge are still small comparing to the usual molecular systems *i.e.* donor-normal bridge-acceptor. Hence the primary objective of our work was the design and synthesis of a functionalizable photochromic core which upon optical and/or chemical stimuli, may lead to open oxazine absorbing in the visible window of the electromagnetic spectrum. Furthermore, the work consists on the construction of a triad by covalently attaching the optimal fluorescent dyes onto a photochromic scaffold (Figure 4.3). In order to achieve an optimum output, the careful selection of each components of the triad is very important. For the first molecular switch our attention was turned toward boranil (already presented in Chapter II) as energy-donor and a BODIPY dye as energy-acceptor.

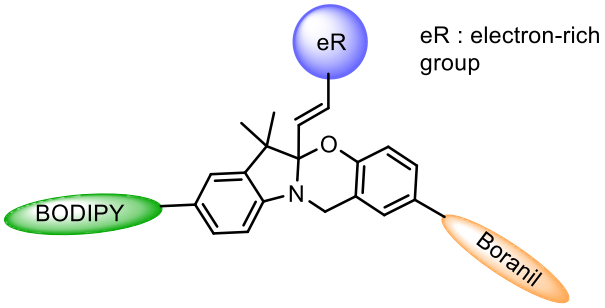

Figure 4.3. The designed triad.

2. Retrosynthetic strategy of triad BODIPY-[1,3]oxazine-Boranil

The method which was applied for the synthesis of the target triad consists on a step-by-step procedure starting from a [1,3]oxazine **60** appending two functional sites *i.e.* a bromide group and an iodo group. Both sites have different reactivity toward metal-catalyzed reaction. This property is used for introducing in a first step the BODIPY moiety (energy-acceptor) through Sonogashira cross-coupling reaction then the Boranil moiety (energy-donor) through a second cross-coupling reaction. The final step consists on a Knoevenagel-type condensation which allows to covalently attach an electron-rich platform with the activated methyl group at the chiral center. This step is crucial for ensuring the switching behavior of our molecular framework as it introduces the photochromic property of the [1,3]oxazine central unit.

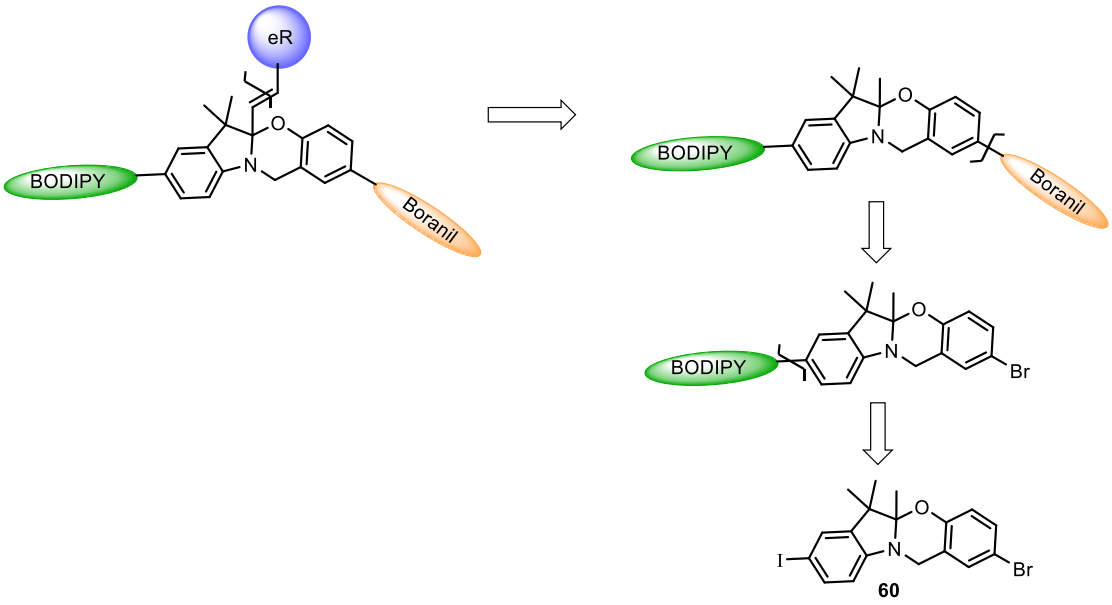

Scheme 4.7. Retrosynthetic pathway for the designed triad.

3. Synthesis of I-indolin[1,3]oxazine-Br 60

In order to reach the goal described above, we synthesized the molecule **60**, appending two different functional sites for various possibilities of selective metal-catalyzed cross-coupling reactions (*e.g.* Sonogashira, Suzuki, Heck). Compound **60** was prepared in two steps starting with the preparation of the Fisher indole **57**[163] from 4-iodophenyl hydrazine and isopropyl methyl ketone in refluxing glacial acetic acid overnight (Scheme 4.8).[164] After purification over silica column chromatography, 3*H*-indole fragment was obtained as yellowish oil.

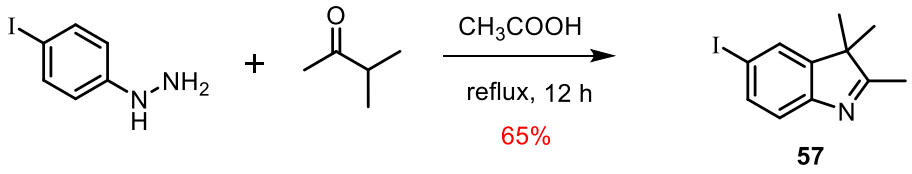

Scheme 4.8. Synthesis of the Fisher indole precursor **57**.[164]

Afterwards, 5-bromo-2-hydroxybenzyl alcohol in the presence of phosphorus tribromide in anhydrous acetonitrile gave the intermediate **58** which has not been isolated. Condensation *in situ* with 3*H*-indole during 3-4 days at room temperature provided **60**.

[163] The Fisher indole synthesis allows the preparation of aromatic heterocyclic indole from a substituted (or not) phenylhydrazine with an aldehyde or ketone in acidic conditions.

[164](a) Tomasulo, M.; Sortino, S.; Raymo, F. M. *J. Org. Chem.* **2008**, *73*, 118. (b) Petersen, M. A.; Deniz, E.; Bronsted Nielsen, M.; Sortino, S.; Raymo, F. M. *Eur. J. Org. Chem.* **2009**, *2009*, 4333.

The compound was purified by silica column chromatography and obtained as colorless oil in low yields, 9 to 20%. Characterized by NMR spectroscopy, mass spectrometry elemental analysis confirmed the structure and the purity of **60**. EI mass spectrometry displays two intense molecular peaks at *m/z* 469.0 and 471.0 with equivalent intensity because the bromine atom has two isotopes, ^{79}Br and ^{81}Br in approximately 1:1 ratio.

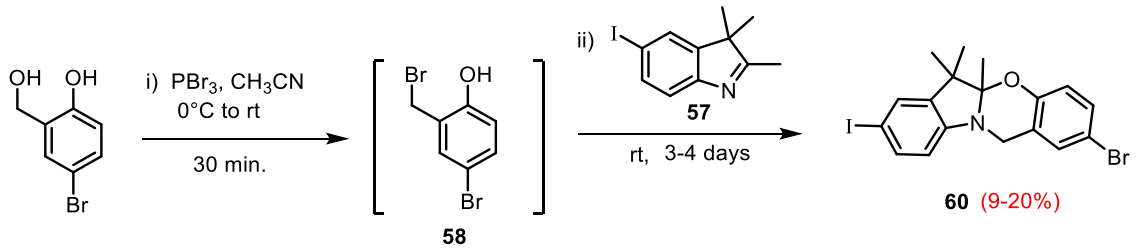

Scheme 4.9. Synthetic pathway of [1,3]oxazine **60** according literature.[164]

3.1. Optimization of I-indolin[1,3]oxazine-Br reaction yield

[1,3]oxazine **60** bearing an iodide and a bromide functional group is our pivotal module for the synthesis of all the target compounds, thus large quantities of this product was necessary. The procedure described above provides restricted amount of the oxazine **60** and consumes important amounts of the initial 4-iodo-phenylhydrazine which is a highly expensive starting material. In order to avoid draining the stock very rapidly and wasting much time in remaking the product, improving the synthesis pathway was necessary. After several attempts we could estabilished the method using the thionyl chloride which gave satisfactory yields compared to the previous method. In short, 5-bromo-2-hydroxybenzyl alcohol was reacted with thionyl chloride over short time before addition of 4-iodo-3*H*-indole **57** at room temperature (Scheme 4.10). Oxazine **60** was obtained in acceptable yields (40-50 %) comparing to the previous method allowing only 9-20 % yield.

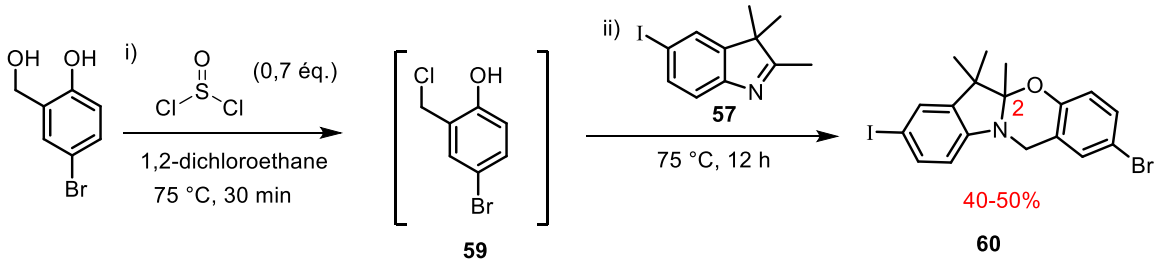

Scheme 4.10. The optimized synthetic pathway of [1,3]oxazine **60** core.

3.2. Synthesis of photochromic styryl indolino[1,3]oxazine derivatives

As discussed in the introduction section, the functionalization of the methyl group in position 2 with electron-rich modules through a vinylic bond has a direct consequence on the absorption of the open oxazine form. The initial dihalogenated oxazine does not absorb in the visible range of the electromagnetic spectrum (λ_{abs} : 240-330 nm with λ_{max} = 256 nm, ε_{max} =10 000 $M^{-1}cm^{-1}$in THF). The methyl group being acidic enough it can undergo a Konevenagel-type condensation with aromatic aldehyde which may allow to tune the color of the open merocyanine *e.g.* from λ_{abs} = 320 nm to 530 nm.[165]

The condensation of oxazine **60** with the julolidinyl **17** in anhydrous ethanol solution with trifluoroacetic acid furnished the photochrome **72** in excellent yield following purification (Scheme 4.11). The solution of the reaction media at the beginning of the reaction is colorless and becomes deep blue after several minutes. The color is a good indicator of formation of the photochromic oxazine, since it was mentioned before that in the presence of acid, the C-O bond of styryl-[1,3]oxazine undergoes opening. However, during the work up, when the organic phase is washed several times with water, the deep blue color of the solution becomes colorless or yellowish.

Inspired by a similar study realized by Deniz *et al.*[165] and following a similar synthetic procedure as for **72,** eleven other aldehydes were condensed with the methyl group at the spiro center thus generating a library of new functional photochromic oxazines (Scheme 4.11). The reaction yields for the various compounds are low *i.e.* in the range 22-69 %, because the reaction was not completed in spite of large excess of aldehyde employed. The low yield may also be explained because the purification over silica or aluminum column chromatography was very complicated due to the proximity of the final and starting materials. Moreover, all the oxazine derivatives appear to trail along the chromatographic column.

[165] Deniz, E.; Cusido, J.; Swaminathan, S.; Battal, M.; Impellizzeri, S.; Sortino, S.; Raymo, F. M. *J. Photochem. Photobiol. A,* **2012**, *229*, 20.

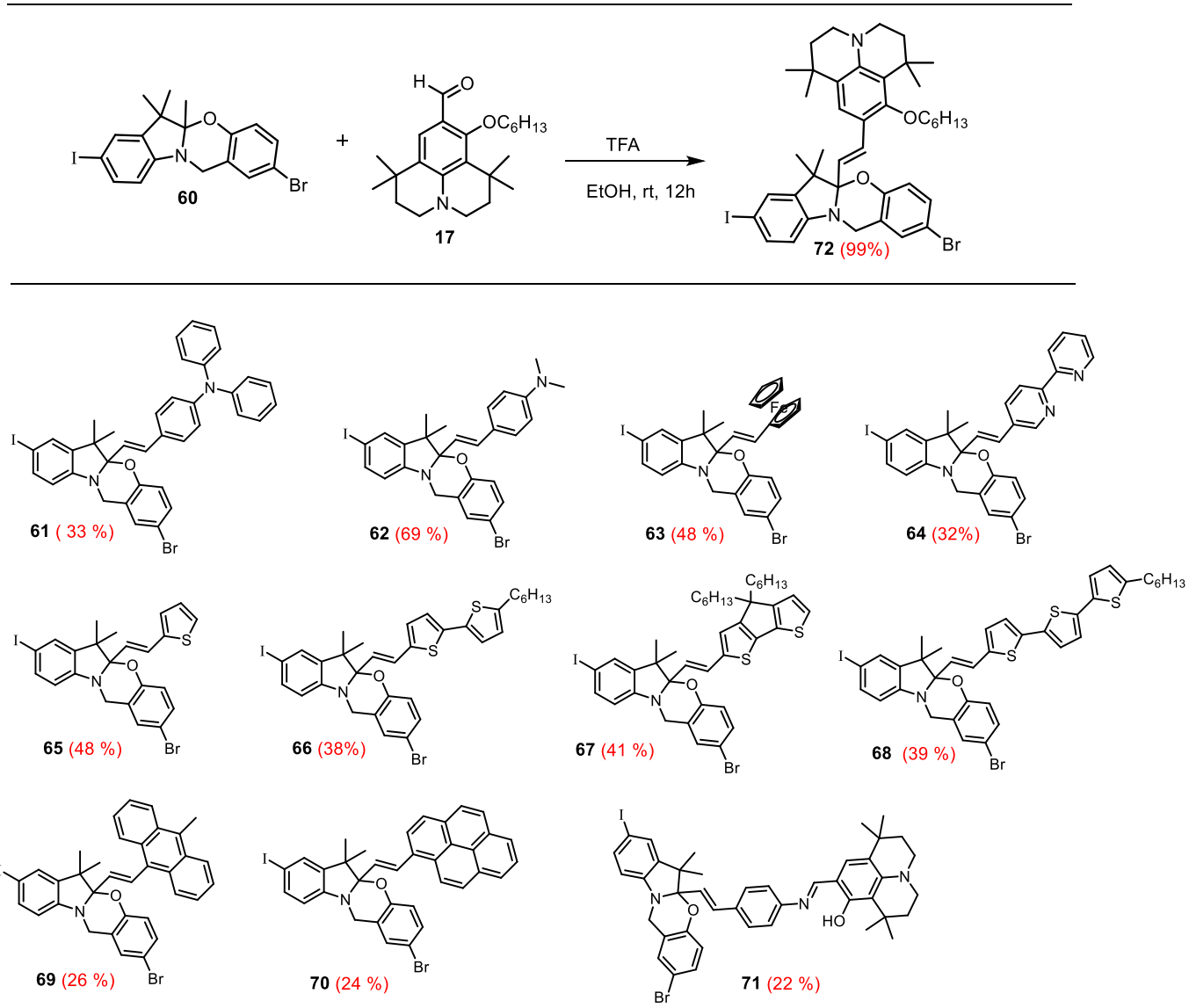

Scheme 4.11. Synthesis of large library of styryl-[1,3]oxazine derivatives.

3.2.1. ^{1}H NMR characterization of compounds 60 and 72

The proton NMR spectra of the various photochromes synthesized were measured in deuterated benzene. The spectral profiles feature the patterns of each compound as expected. It can be easily identified the AB quartet at *ca.* δ = 4.0 ppm corresponding to the diastereotopic methylene protons noted "g" and "h". Herein is shown only the spectrum of photochrome **72** (Figure 4.4) which was selected for further investigations and the spectral profile of **60** (Figure 4.5). The presence of the AB quartet in the spectral profile of **60** indicates that the [1,3]oxazine core is in the closed form and the molecule retains its chirality.

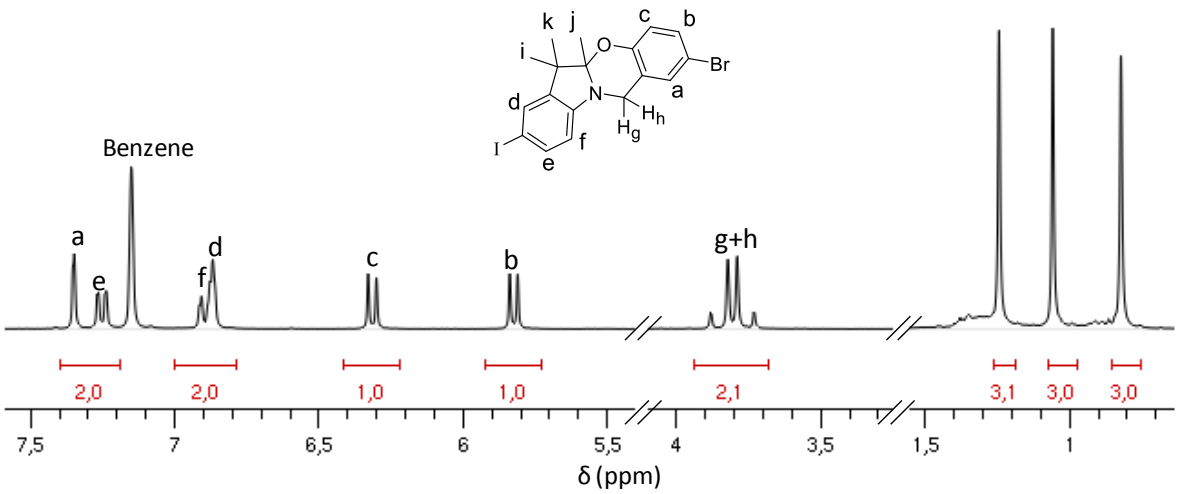

Figure 4.4. ^{1}H NMR spectrum of compound **60** in deuterated benzene at room temperature.

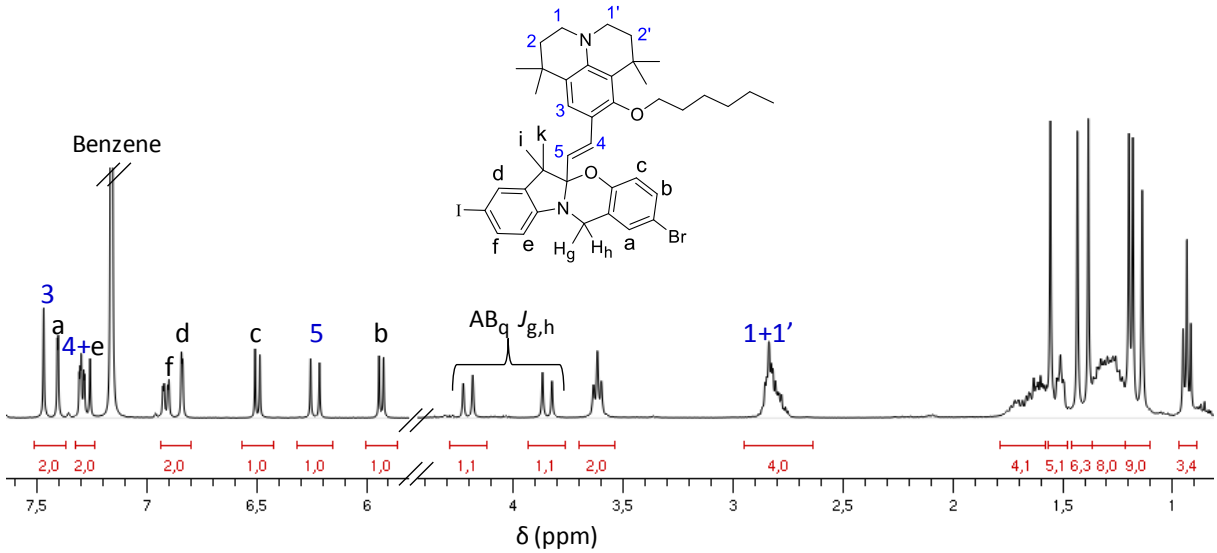

Figure. 4.5. ^{1}H NMR spectrum of compound **72** in deuterated benzene at room temperature.

The presence of the chirality into the molecule affects also the chemical shifts of the methyl group protons noted "i", "j", and "k" which are not equivalent but splited at δ = 0.82 ppm, 1.06 ppm and 1.24 ppm. The addition of the styryl-julolidine arm in **60** thus providing **72** increases the chemical shift of protons "b" and "c" by *ca.* 0.1-0.2 ppm while the remaining aromatic protons are not subjected to a chemical shift (Figure 4.4). The constant coupling of the vicinal protons "4" and "5" in the Figure 4.5 is $^{3}J_{H,H}$ = 16.3 Hz and confirms the (*E*)-configuration of the vinylic bond covalently attached to the asymmetric carbon. The presence of the AB system in the spectrum of **72** is maintained, but more splited that in the case of **60**.

3.3. Synthesis of dyad 74

In order to test first the chemical reactivity of the halogenated sites onto [1,3]oxazine we employed the BODIPY-acetylene dye **73**. The iodinated BODIPY dye is already reported in the literature,[166] whereas the terminal alkyne not reported was prepared in the context of this work. In fact, this compound is not the most pertinent choice concerning its optical characteristics (λ_{max} abs ($S_0 \rightarrow S_1$) = 570 nm, λ_{max} abs ($S_0 \rightarrow S_2$) = 340 nm in THF), but it is used for understanding the reactivity behavior of **60**. A cross coupling Sonogashira reaction, Pd(II)/Cu(I) catalyzed in a degazed THF solution gave the dyad **74** in 89 % yield. The presence of a polyethylene glycol chain (PEG) in the BODIPY dye introduces some polarity into the dyad making feasible and easy its separation by TLC and column chromatography.

Indeed, under these conditions Sonogashira coupling occurs selectively onto iodo group. In particular ^{13}C NMR spectra recorded for dyad **74** and precursor **60,** and comparison with literature data allowed us to determine the C-I at δ = 81.9 ppm and C-Br δ = 112.3 ppm chemical shifts and thus confirmed the cross coupling reaction on the iodo-aryl side. The final molecule is characterized also by ^{1}H, ^{11}B NMR spectroscopy, mass spectrometry and elemental analysis. Moreover the molecular structure of **74** was determined by X-ray diffraction crystallography technique (*vide infra*).

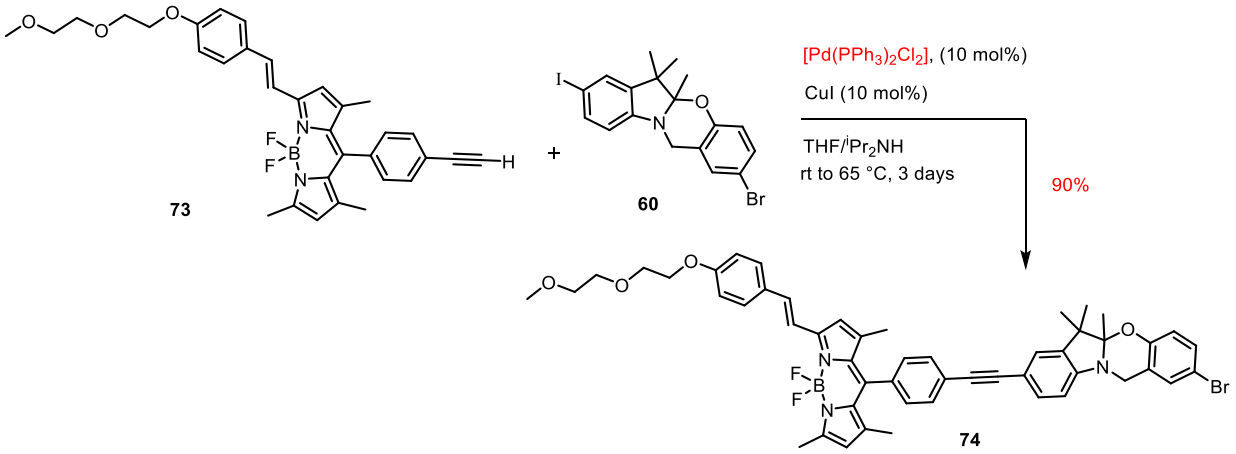

Scheme 4.12. Synthesis of compound **74**.

[166] Bura, Thomas (2013) *Construction de nouveau Bodipys solubles pour la concentration d'énergie et les cellules photovoltaïques*, Strasbourg thesis, University of Strasbourg.

3.3.1. ^{1}H NMR characterization of 74

The proton NMR spectral profile of compound **74**, measured in deuterated dichloromethane at room temperature fits the patterns of the desired dyad. The integral patterns account for the expected number of protons. The signals of the PEG chain are identified as multiplets from δ = 3.50 ppm to 4.15 ppm. The peak at δ = 2.53 ppm is assigned to methyl protons noted "1" of the BODIPY core and the signal at 6.0 ppm was ascribed to the β-pyrrolic proton, while the β' is overlapped with other signals.

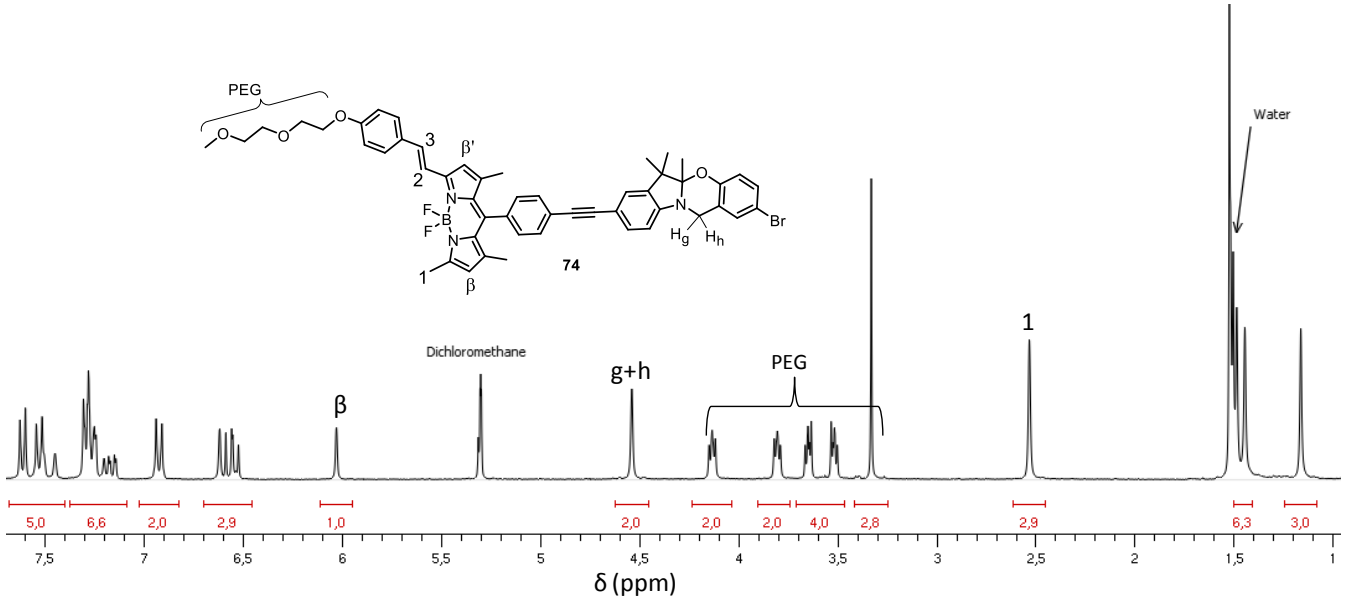

Figure 4.6. ^{1}H NMR spectrum of compound **74** in deuterated dichloromethane at room temperature.

The methylene protons of oxazine ring "g" and "h" do not appear as AB quartet contrary to the previous molecules **60** and **72** in Figure 4.4 and 4.5.This is probably due to the fact that the diclorometh ane is somewhat acid, so that the equilibrium might be shifted toward the open form oxazine ring. It is well known that the photochromism of the spirocompounds is dependent on the polarity and the proticity of the solvent (*vide supra*). The spectral patterns of the previous compounds **60** and **72** were measured in deuterated benzene, an apolar and protic solvent which favor the closed form of the oxazine ring.

3.3.2. X-Ray structure of 74

The resolution of the molecular structures by X-ray cristallography of mono-crystals was realized from Dr. Pascal Retailleau at Gif-sur-Yvette. Single crystals of suitable quality were obtained by slow evaporation of a concentrated solution of **74** by slow diffusion of pentane in dichloromethane solution. The molecular structure is represented in Figure 4.7.

To the best of our knowledge, this is the first crystallographic structure of an *[1,3]oxazine* derivative obtained in the closed form. The structure allows confirming of the regioselectivity of the palladium-catalyzed cross-coupling reaction. The most interesting information which can be pointed out from this structure concerns the oxazine core. The angle between the plane containing the 3*H*-indoline moiety and the plane containing the benzoxazine moiety is 115.93° while this angle is *ca.* 109 ° for the [1,4]oxazine derivative (Figure 4.7-lower side). The C_{spiro}-O bond length is 1.470 Å. the value of this bond length is in the range 1.45-1.47 Å identified for other photochromic spiro-compounds from their X-ray structure. The bond lengths N15A-C16A and N15A-C12A are 1.49(2), 1.44(3) respectively. The phenyl of the BODIPY core is roughly in the same plane with the indole fragment of oxazine core and it conserves the orthogonality with the dipyrrin fragment forming a dihedral angle 84.1°.

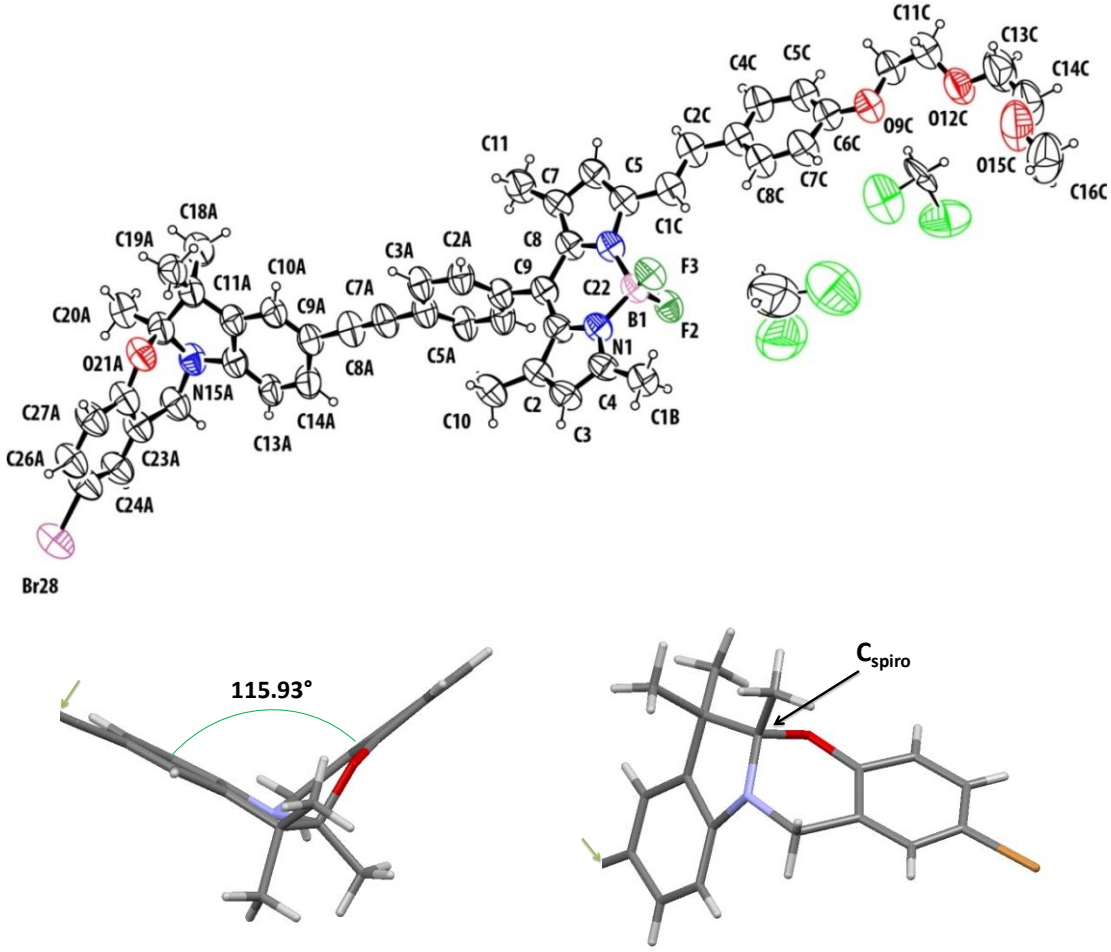

Figure 4.7. (Upper side) Ortep view of oxazine **74** bearing a BODIPY dye onto 3*H*-indole fragment. The molecular structure is shown with two molecules of dichloromethane. (Lower side) Partial views of the molecular structure showing the tetrahedral carbon spiro and the angle between the plane containing the 3*H*-indole and benzoxazine fragment.

4. Synthesis of triad BODIPY-[1,3]oxazine-Boranil 83

The triad that we have designed was obtained according a seven-step procedure from [1,3]oxazine **60** core bearing an iodo and a bromide group. The first step consists of a selective Sonogashira cross-coupling reaction of **60** with excess of TMS-acetylene in toluene at room temperature (Scheme 4.13). The base used is *N*,*N*-diisopropylamine (DIPA) which was regularly employed in the following cross-coupling reactions. According to experimental studies on Sonogashira cross-coupling reaction reported in the literature, DIPA gives better reaction yields than triethylamine which is more commonly used for these types of procedures.[167] The reaction was catalyzed with $[Pd(PPh_3)_2Cl_2]$ and CuI as co-catalyzer. Under these conditions, the mono-coupled product **75** (Scheme 4.13) was obtained in high yield following routine purification. In the following step, the TMS-group was removed with stochiometric amount of KOH in THF and methanol solution and water as proton source during 2 to 3 hours. The terminal alkyne **76** was provided as colorless oil which solidifies under vacuum in excellent yield.

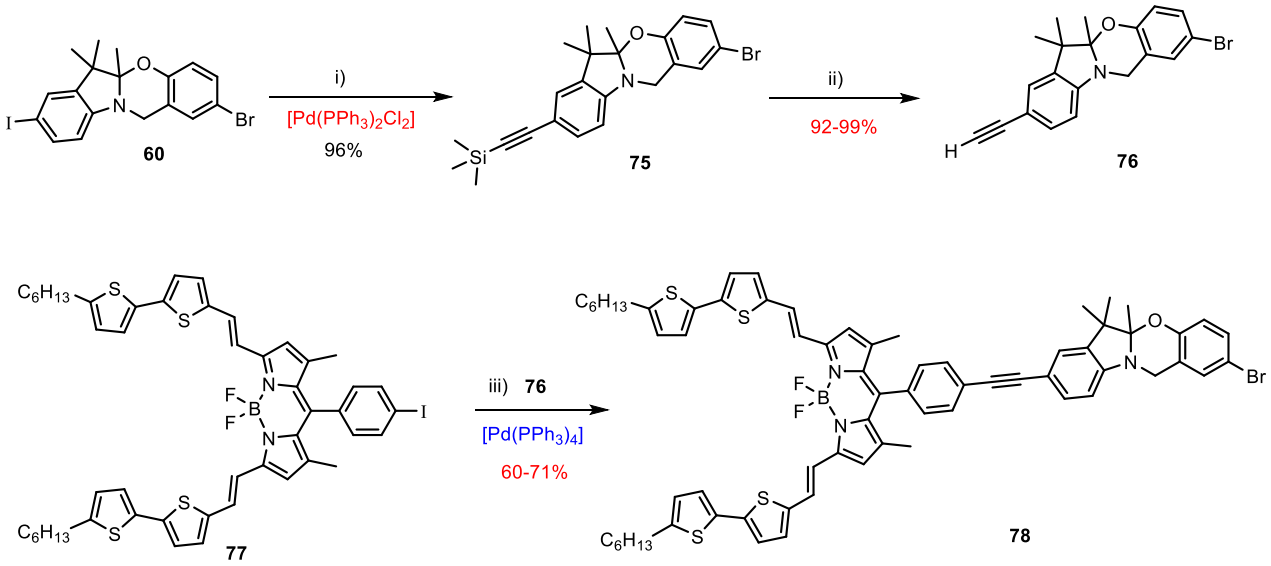

Scheme 4.13. i) TMS-acetylene, $[Pd(PPh_3)_2Cl_2]$ 10 mol%, CuI 10mol%, DIPA, toluene, 1.5 h, rt. ii) KOH, THF, MeOH/H_2O, 2-3 h, rt. iii) $[Pd(PPh_3)_4]$ 10 mol%, toluene, DIPA, 70 °C, 12 h.

[167] Severin, R.; Reimer, J.; Doye, S. *J. Org. Chem*. **2010**, *75*, 3518.

Afterwards, the energy-acceptor BODIPY dye[168] was cross-coupled with the terminal alkyne **76** in toluene solution in presence of excess DIPA. Degassing the solution before addition of Pd/Cu might be very important in most of cases when copper(I) salt is used as co-catalyzer. In order to avoid as much as possible the possibility of Glaser homocoupling side-product,[169,170] we catalyzed the reaction with [$Pd(PPh_3)_4$] at 70 °C during 12 hours. In this case CuI is not necessary but conserving an inert atmosphere is demanded since Pd^0 is very air sensitive. Finally, the dye **78** bearing an oxazine core in *para*-position of the phenyl ring was obtained as dark green solids after purification over column chromatography and several precipitations. Compound **78** was isolated in 60-71% yields and was confirmed from ^{1}H, ^{13}C and ^{11}B NMR spectroscopy (*vide infra*) and purity examined by elemental analysis. Because the bromine atom has two isotopes, ^{79}Br and ^{81}Br in approximately 1:1 ratio, the EI mass spectrometry displays two *m/z* molecular peaks with values 1212.2 [M+2] and 1210.3 [M] with equal intensity and a fragmentation peak at 35 % intensity corresponding to the molecule having loss an hexyl chain.

In the next steps, the bromide group of **78** has been transformed into terminal alkyne which has been further functionalized *via* a second Sonogashira cross-coupling reaction with the energy-donor module. As expected and as revealed by other published procedure, the reactivity of aryl bromide is rather low, thus demanding harsh reaction condition. Furthermore, TMS-acetylene being not electron-rich group, it does not favor the transmetallation step during the catalytic cycle.[171] Hence, the dyad previously obtained was allowed to react with large excess of TMS-acetylene, Pd(II)/Cu(I)-catalyzed in toluene solution and DIPA at 95 °C. The first attempts catalyzed by [$Pd(PPh_3)_2Cl_2$] did not afford the desired compound **79**. Replacing the diphenylphosphine by diphenylphosphinoferrocene in [$Pd(dppf)_2Cl_2$] (chemical structure shown in Scheme 4.15) was indeed more efficient because the metal center is more electron-rich due to a stronger σ-donating effect of the ferrocene ligand, hence favoring the oxidative addition of the substrate. Finally the TMS-aryl compound **79** was obtained as dark solid in 70-85% yields after flash chromatography and precipitations.

[168] Bura, T.; Leclerc, N.; Fall, S.; Lévêque, P.; Heiser, T.; Retailleau, P.; Rhin, S.; Mirloup, A.; Ziessel, R. *J. Am. Chem. Soc.* **2012**, *134*, 17404.
[169] Glaser, C. *Ann. Chem. Pharm.* **1870**, *154*, 137.
[170] Siemens, P.; Livingston, R.; Diedrich, F. *Angew. Chem. Int. Ed.* **2000**, *39*, 2632.
[171] Amatore, C.; Jutand, A. *Acc. Chem. Res.* **2000**, *33*, 314.

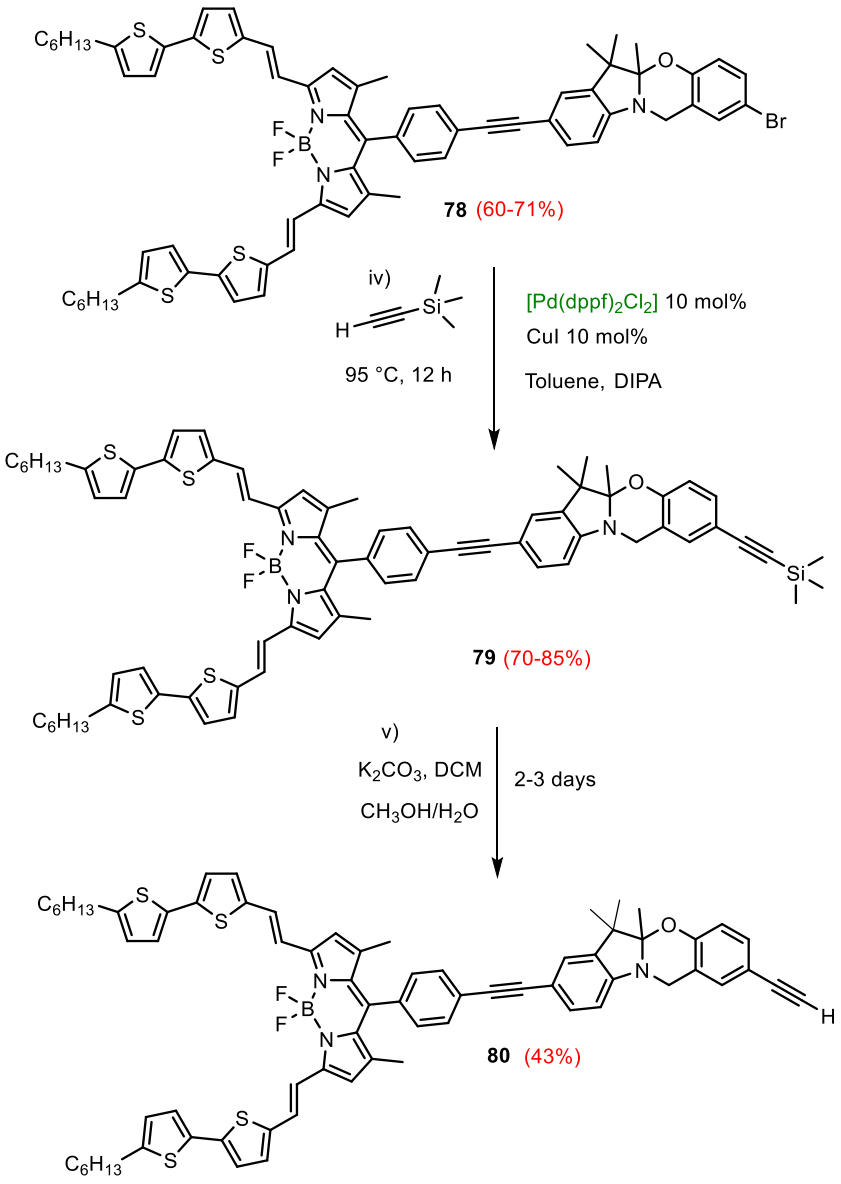

Scheme 4.14. Step iv) Substitution of the bromide group of **78** by TMS-acetylene. Step v) Deprotection of TMS group of **79** to give **80**.

It was also noted that bromide substitution is rendered much more difficult once the donor-energy is appended onto oxazine entity by substituting the iodo-group. When non-functionalized dihalogenated oxazine is reacted with excess TMS-acetylene in the presence of $[Pd(dppf)_2Cl_2]$ at room temperature during 2 hours, disubstituted compound was afforded quantitatively (Scheme 4.15).

Removing of TMS protecting group of **79** was achieved with large excess of K_2CO_3 in dichloromethane with methanol and water as proton source. The deprotection was very slow; after three days under stirring the initial product was still persisting. Nevertheless no degradation was observed. Heating under reflux did not change the kinetics of the reaction but degradation became present. The inconvenience is the separation of the final product **80** from the protected TMS product **79** having the similar polarity as the former. Deprotection of **79** with stochiometric amount of KOH at room temperature gave the product in same yields as the method employing K_2CO_3. No initial product was observed after 2-3 hours but the degradation was very consequent. Indeed, under these conditions the boron difluoride entity probably undergoes fluoride substitution with hydroxyl group from the reaction media as already known and observed for other BODIPY dyes.

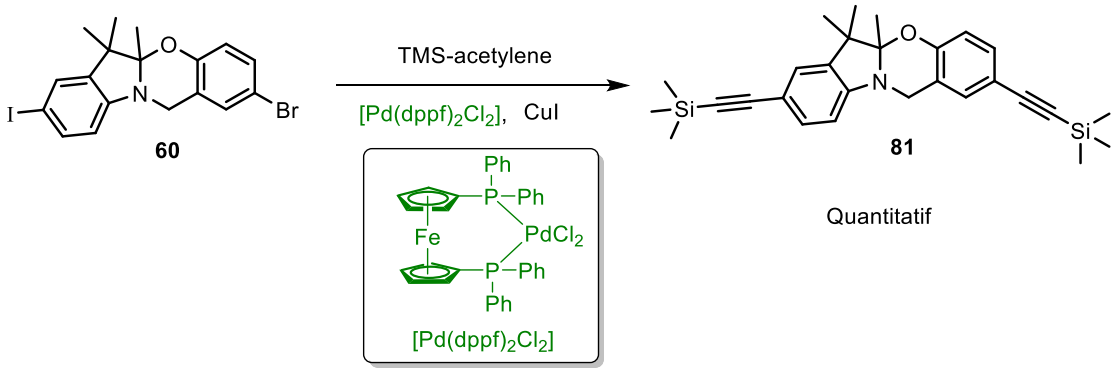

Scheme 4.15. Bis-functionalization of di-halogenated oxazine core catalyzed by $[Pd(dppf)_2Cl_2]$.

The aryl acetylide **80** previously obtained was functionalized *via* a second Sonogashira coupling with the boranil **48** (the synthesis was described in Chapter III) in toluene solution using DIPA as base, $[Pd(PPh_3)_4]$ –catalyzed at 60 °C overnight (Scheme 4.16). The choice of $[Pd(PPh_3)_4]$ is justified as previously to avoid the use of copper salts which may encourage the homocoupling byproduct of aryl alkyne in the presence of oxygen. The desired product **82** bearing a BODIPY-acetylene in *para*-position relative to nitrogen of indole moiety and a boranil-acetylene in *para*-position relative to oxygen of benzoxazine fragment was isolated as dark green solid in 75% yield. The product was purified over a silica column chromatography and by several precipitation and washing with pentane. The compound was characterized by ^{1}H, ^{13}C and ^{11}B NMR spectroscopy (*vide infra*). ES^+ mass spectrometry gives the most intense peak with a *m/z* value 1550.5 corresponding the cationic molecular peak and a fragmentation peak with *m/z* 1530.5 at 35 % intensity being assigned to the molecule missing a fluoride.

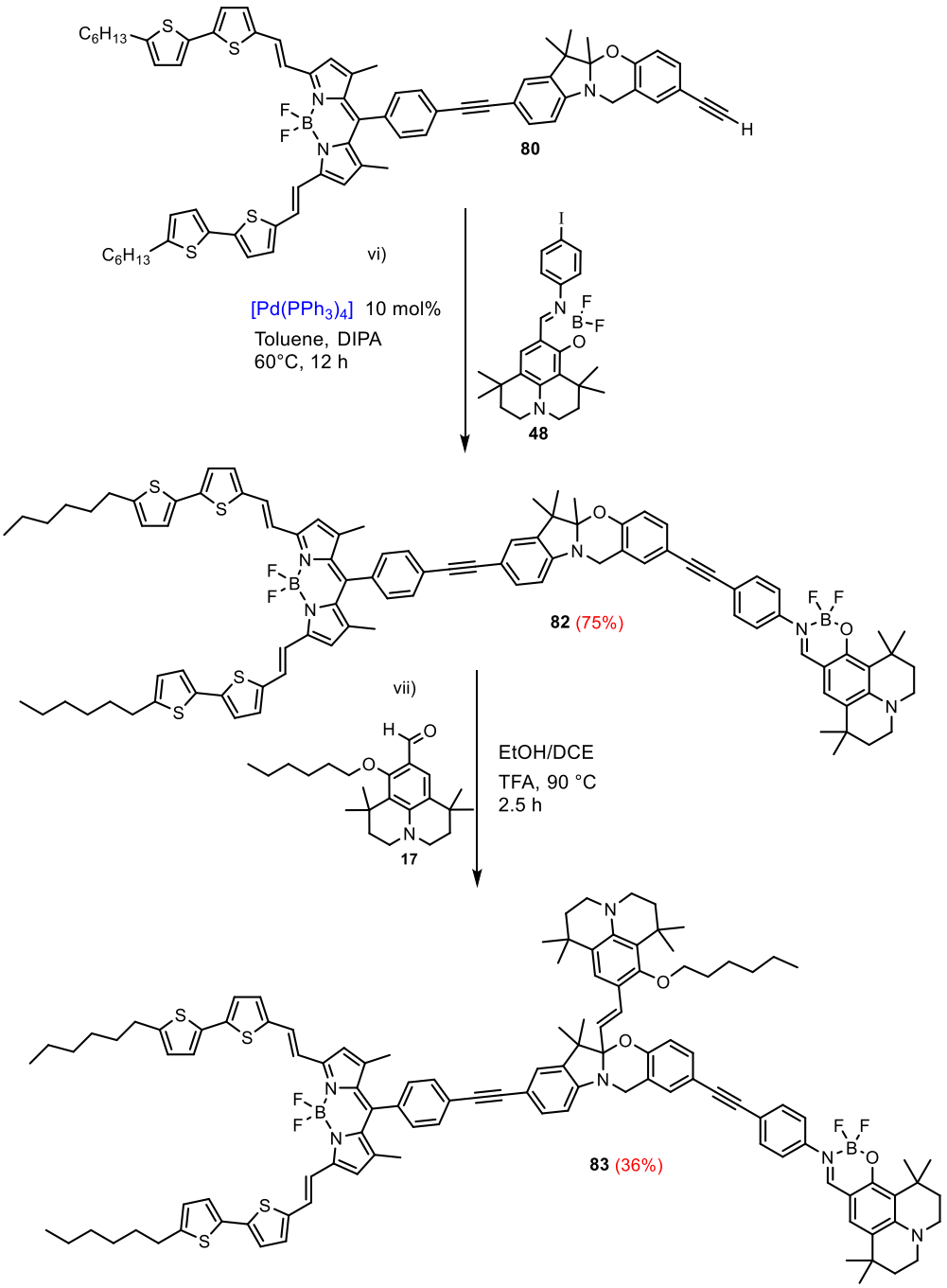

Scheme 4.16. Step vi) Sonogashira coupling of boranil with aryl acetylide **80**. Step vii) synthesis of the final triad **83**.

Finally, the Knoevenagel-type condensation of julolidinyl –aldehyde **17** with precursor **82** gave the triad **83** appending the julolidine moiety to the asymmetric carbon center through a vinylic fragment. The anchoring of the latter ensures the photochromism of the [1,3]oxazine core. The reaction was catalyzed by addition of trifluoroacetic acid in an anhydrous mixture of ethanol and 1,2-dichloroethane under an inert atmosphere. It was isolated as a dark green solid after

purification over silica column chromatography and several washings with pentane in 36 % yield. The triad precursor is insoluble or less soluble in most of organic solvents. The spectrum of high-resolution mass spectrometry displayed an intense peak at *m/z* 1890.8979 corresponding to the cationic molecular triad. The structure of triad was confirmed by the usual techniques of NMR spectroscopy high-resolution mass spectrometry and elemental analysis.

4.1. ^{1}H NMR study of triad 83 and its intermediates

Herein are represented the spectra profiles of the final triad and the key intermediate compounds. The measurements were realized in deuterated chloroform at room temperature. The spectrum of [1,3]oxazine **76** fits the expected resonance signals (Figure 4.8). We can note the presence of a narrow signal at δ = 2.95 ppm assigned to terminal alkyne proton and a large, not well defined AB system signal at δ = 4.50 ppm ascribed to oxazine methylene protons noted "g" and "h". These protons are diastereotopic because of the presence of the asymmetric carbon center in the closed oxazine form. The chirality of the molecule imposes different environments to the two methyl groups "i", "k" where one has a chemical shift *ca.* 1.50 ppm (with the methyl "j") and the second is shielded upfield at 1.15 ppm as described for similar compound by F. Raymo *et al.*.[1]

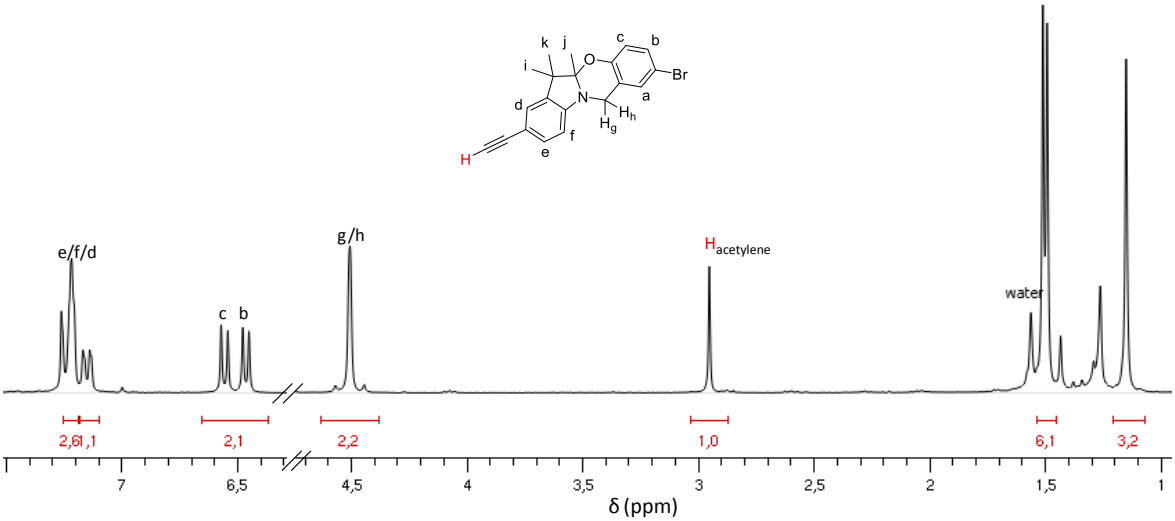

Figure 4.8. ^{1}H NMR spectrum of **76** in $CDCl_3$ at room temperature

After coupling of this compound with the BODIPY dye **77**, the proton spectrum of **78** (Figure 4.9) indicates the disappearance of the terminal alkyne proton. Also we can easily identify the β-pyrrolic protons of BODIPY core resonating at 6.60 ppm with an intense signal accounting for two protons.

The functionalization of bromide group into terminal acetylene is supported by the appearance of a resonance signal at 2.98 ppm in the spectral profile of dyad **80** (Figure 4.10). This

transformation does affect the resonance of aromatic protons on benzoxazine fragments noted "b" and "c" whereas the others remains at the same chemical shifts. The signals of "b" and "c" appear overlapped when the phenyl ring is *para*-subsituted with a bromide and they undergo splitting in the spectral pattern of **80**.

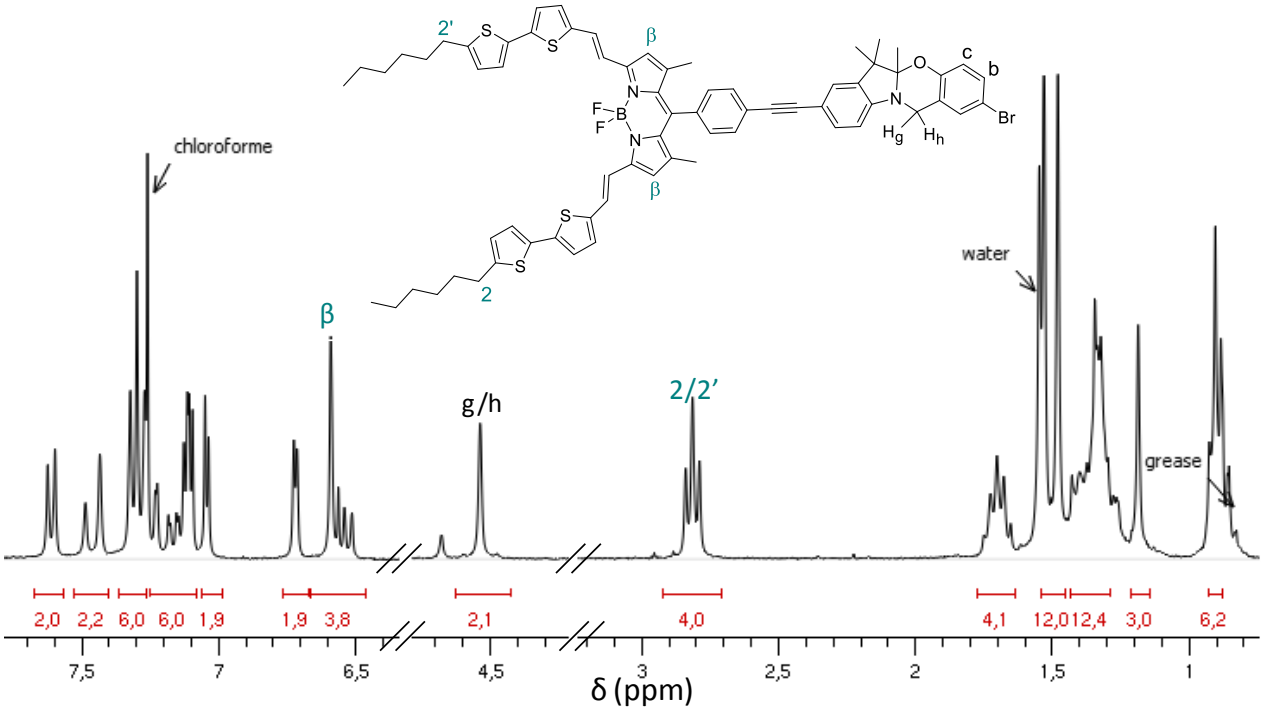

Figure 4.9. ^{1}H NMR spectrum of **78** in $CDCl_3$ at room temperature.

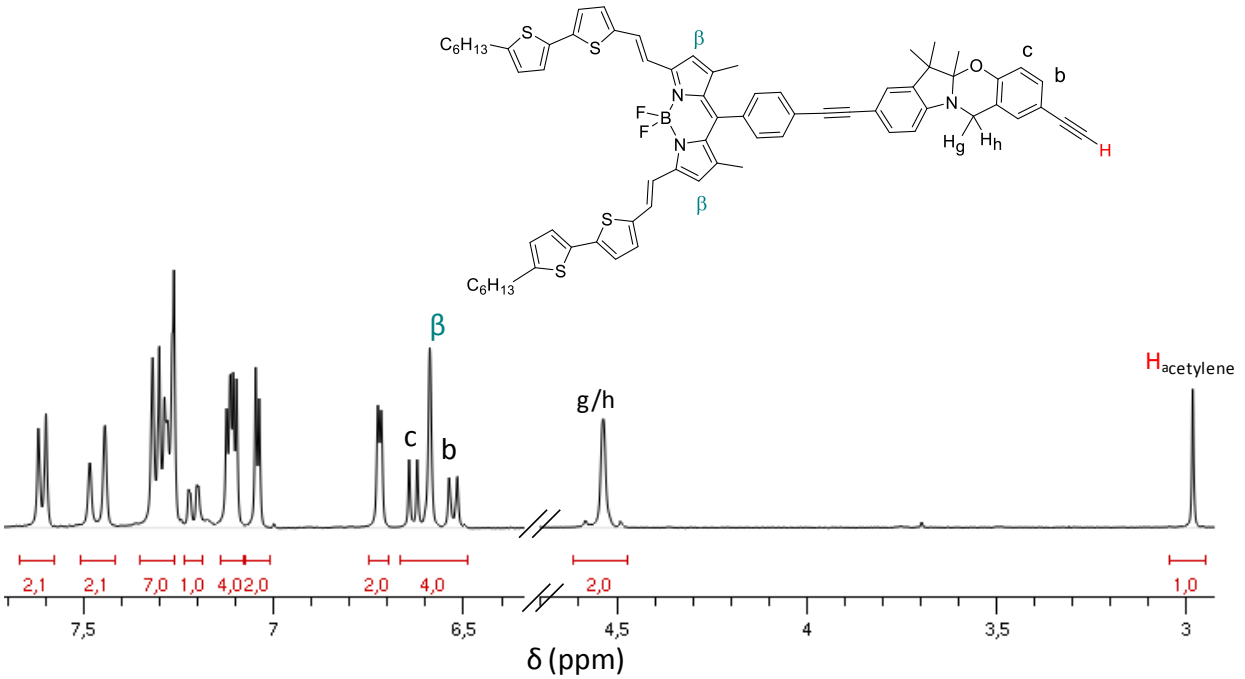

Figure 4.10. ^{1}H NMR spectrum of **80** in $CDCl_3$ at room temperature partially presented for clarity.

The spectral analysis of **82** features the signal patterns of its three components *i.e.* the BODIPY core, indolino[1,3]oxazine core and boranil (Figure 4.11). For clarity reasons the spectrum is shown only partially. The broad and weak signal of imine fragment proton, noted "3" at δ = 7.93 ppm and two triplets ascribed to methylene protons (1 and 1') of julolidine core can be easily identified.

In the final triad (Figure 4.12) the addition of a second julolidine fragment is identified by the appearance of a second set of multiplets at 3.15 ppm and 3.07 ppm corresponding to protons 4 and 4'. These multiplets are upfielded *ca.* 0.25 ppm compared to the previous one. Moreover the additional doublets at 6.15 ppm and 7.00 ppm (noted in blue in Figure 4.12) can be easily ascribed to the vinylic protons "5" and "6" due to constant coupling being J = 16.2 Hz. This value indicates that ethylene bridge adopts the *(E)*-configuration (as was demonstrated with the vinylic protons of BODIPY dyes). Contrary to the previous intermediates, the AB system of the diastereotopic methylene protons "g" and "h" in the final trial is well resolved and confirms the maintaining of the chirality of the molecule.

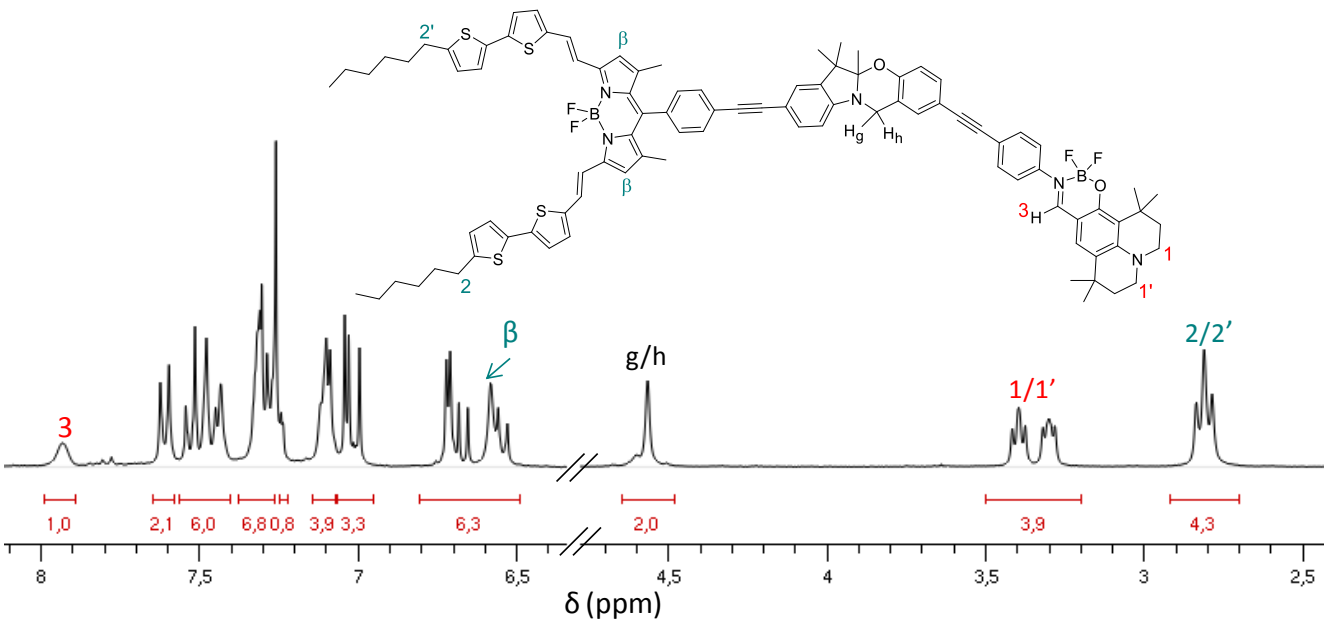

Figure 4.11. ^{1}H NMR spectrum of **82** in $CDCl_3$ at room temperature partially presented for clarity.

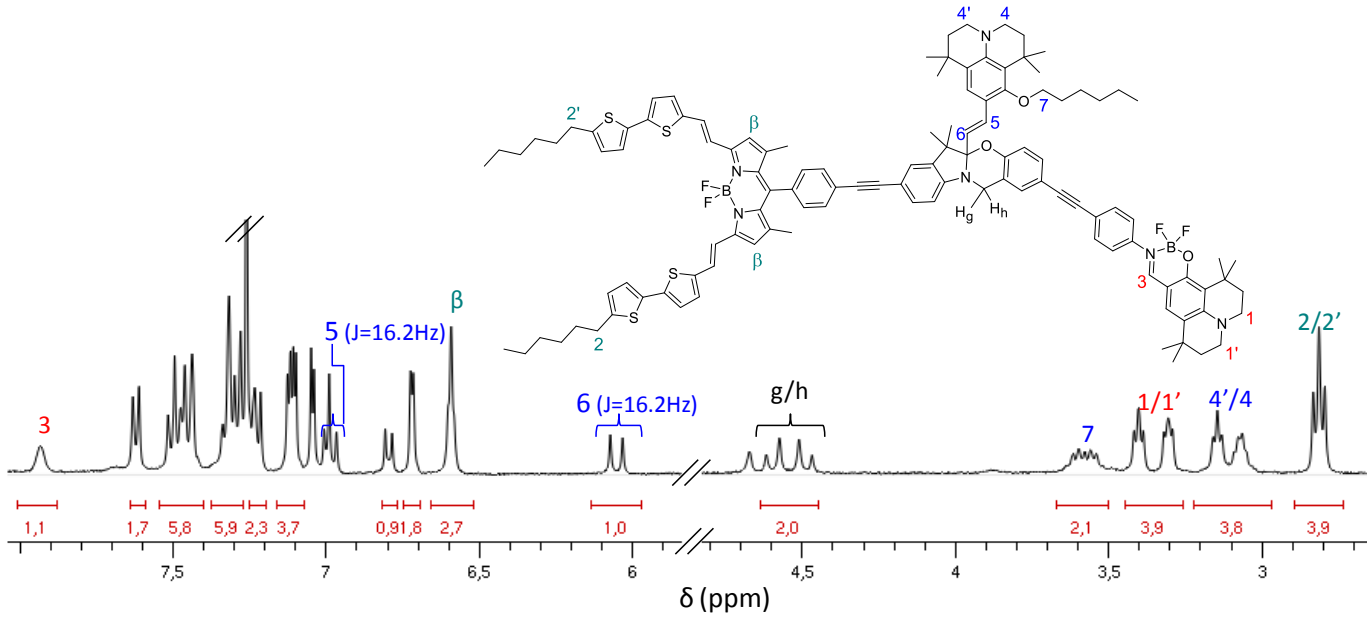

Figure 4.12. ^{1}H NMR spectrum of **83** in $CDCl_3$ at room temperature partially presented for clarity reasons.

5. Photophysical measurements

The advanced photophysical studies concerning our switches are under investigation in collaboration with Professor Salvatore Sortino from the University of Catania in Italy.[172] Herein are presented the preliminary results obtained during this collaboration.

5.1. Absorption and luminescence of triad 83 and its models

The absorption spectrum of the triad **83** in the closed form was measured in THF solution at room temperature and is represented in Figure 4.14-black curve. The spectral profile has the features of the units composing it, *i.e.* the BODIPY core, boranil and [1,3]oxazine core with maxima pointing respectively at 711 nm (ε_{max} =77 260 $M^{-1}cm^{-1}$), 440 nm (ε_{max} = 136 400 $M^{-1}cm^{-1}$) and 320 nm (ε_{max} = 63 750 $M^{-1}cm^{-1}$). The absorption profile confirms that **83** is in the closed form as previously stated by NMR spectroscopy (Figure 4.12). The absence of an intense and broad band centered at *ca.* 600-630 nm accounting for the open styryljulolidine-[1,3]oxazine switch, confirms the closed state of the donor-[1,3]oxazine-acceptor system. Figure 4.14 indicates that the maxima of the triad fit closely those of the models donor and acceptor, therefore suggesting that no pronounced electronic communication take place between the respective modules within the molecular triad.

[172] Salvatore Sortino, Laboratory of Photochemistry, Dipartimento di Scienze Chimiche, Università di Catania, viale Andrea Doria, Catania, I-95125, Italy.

The steady state emission spectrum of the triad **83** after excitation within the energy-donor band at λ_{exc} = 440 nm revealed the characteristic emission of the isolated BODIPY model **84** (Figure 4.15 and chemical structure shown in Figure 4.13). In contrast, emission from the Boranil energy-donor was not observed. These results are consistent with the fact that in the closed form our system achieves a highly efficient energy transfer process from the Boranil donor to the BODIPY acceptor. Above all, there exists an important integral overlap between donor emission and the acceptor absorption.

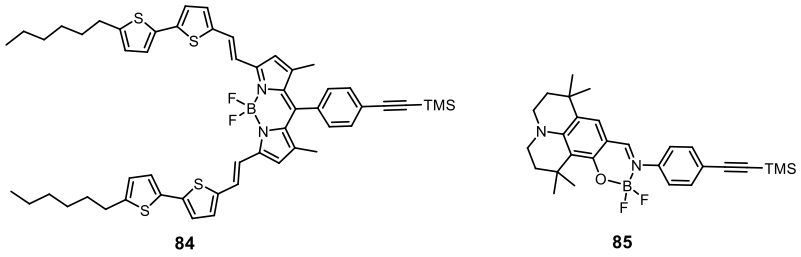

Figure 4.13. Chemical structures of models BODIPY dye **84** and **85**.

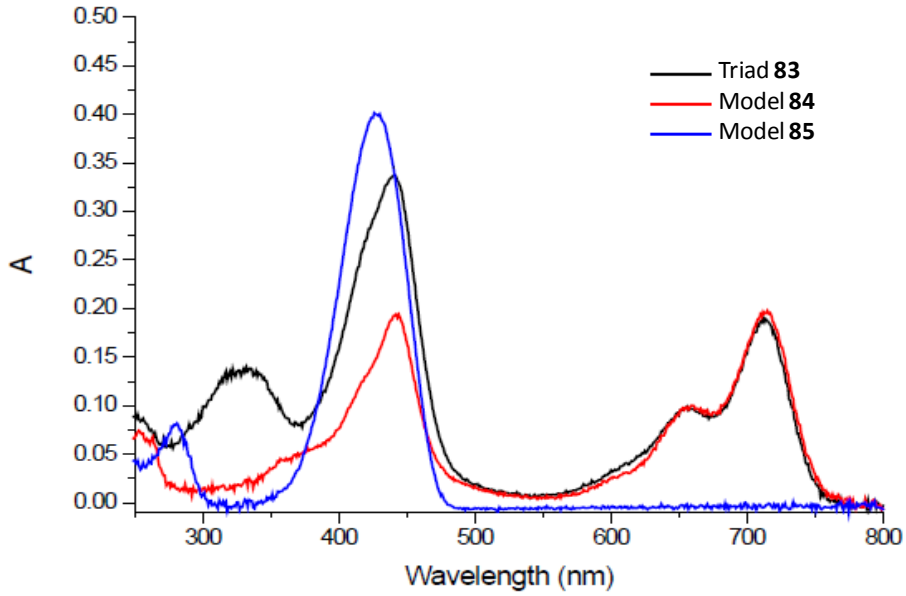

Figure 4.14. Absorption spectra of the triad **83** (black curve), BODIPY **84** energy-acceptor (red curve) and boranil **85** energy-donor (blue curve). Spectra measured in THF solution at room temperature.

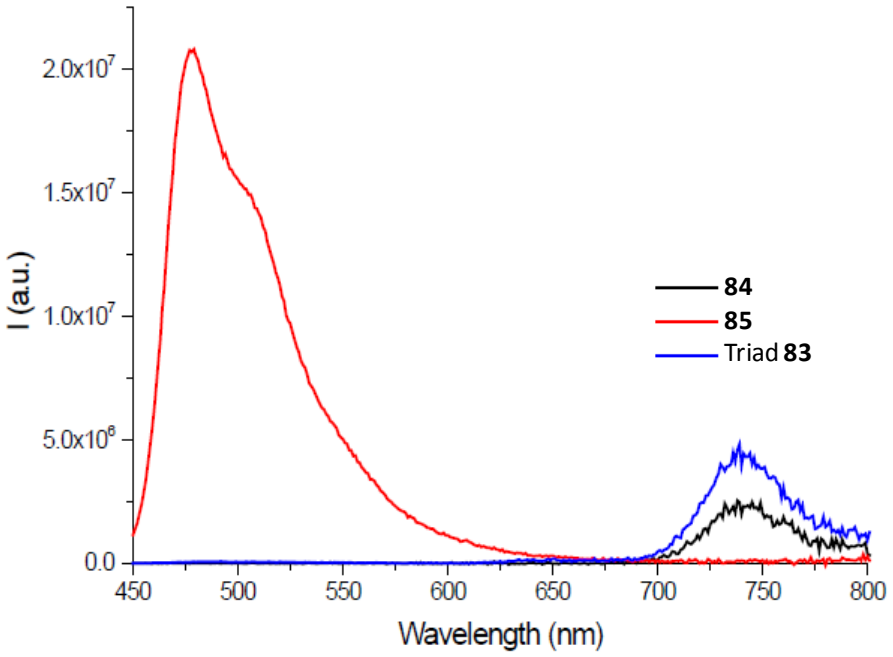

Figure 4.15. Emission spectra of the triad **83** (blue curve), the boranil **85** energy-donor (red curve) and the BODPIPY **84** energy-acceptor (black curve). Spectra measured in THF solution at room temperature. λ_{exc} = 440 nm.

The process of electronic energy transfer is successfully achieved also within the model compound **82** lacking the julolidine arm. As shown in the Figure 4.16-left, the normalized absorption profile of the triad-precursor **82** fits perfectly the spectrum of the triad **83** and that of a mixture of the isolated donor and acceptor units. The low energy band at *ca.* 320 nm in the spectrum of the spectral profile of the triad and pre-triad is ascribed to the $\pi \rightarrow \pi^*$ transition of oxazine core. This band is absent in the spectral pattern of the energy donor/acceptor mixture (Figure 4.16). As previously, the emission spectrum of the molecule where the donor and the acceptor are covalently attached to the oxazine core, obtained after excitation with λ_{exc} = 440 nm resemble that of the BODIPY energy acceptor.

Alongside, the irradiation of the mixture solution with λ_{exc} = 440 nm displays a dual emission; one at *ca.* 470 nm having the characteristic of the donor (Boranil) and a second at *ca.* 740 nm having the characteristic of the acceptor model (BODIPY). This observations point out the fact that no fluorescence modulation occurs from the non-covalentyl attached model dyes. More importantly, the intensity of the BODIPY emission at 740 nm in the mixture is much lower than the intensity of the triad **83** and pre-triad **82**. In both systems, the oxazine core with or without the julolidine scaffold, serves as a bridging unit which brings in proximity the donor and the acceptor and direct EET through spectral overlap between the formers.

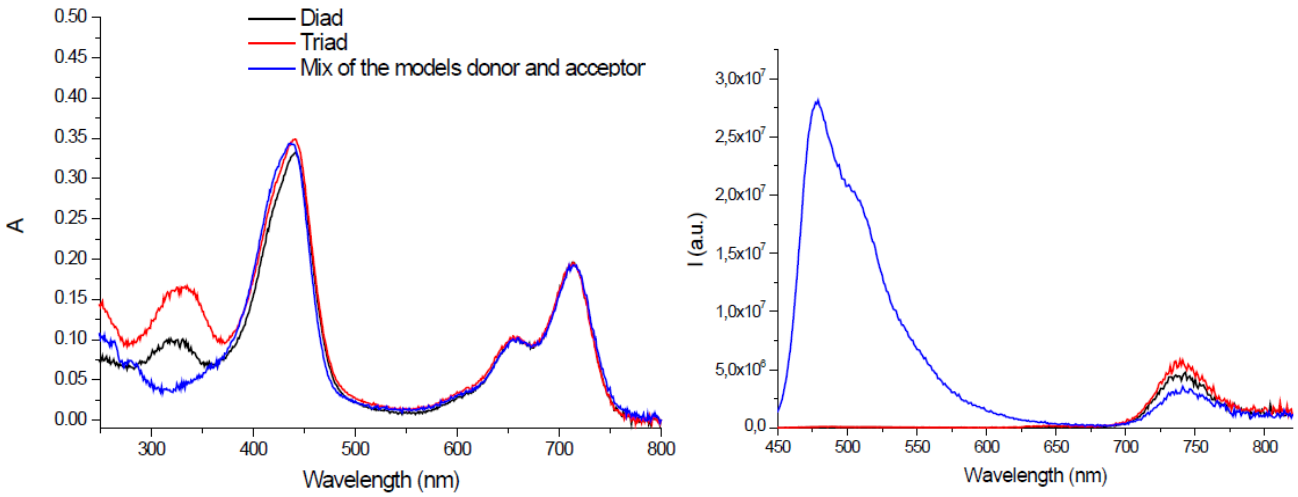

Figure 4.16. Absorption and emission spectra (λ_{exc} = 440 nm) of triad **83**, dyad **82** and a mixture of the BODIPY **84** and boranil **85** in THF solution at room temperature.

Further, several attempts of opening the oxazine cycle of the triad **83** by irradiation with λ = 330 nm and λ = 350 nm did not afford any trace of the mercyanine open photochrome form even after 45 minutes under continuous irradiation (Figure 4.17). In contrary the UV irradiation of the photochromic core **72** missing the BODIPY and the boranil arm with a Xenon lamp (300 W) leads to the merocyanine open form (λ_{abs} = 600 nm in acetonitrile) in acetonitrile solution successfully (Figure 4.18).

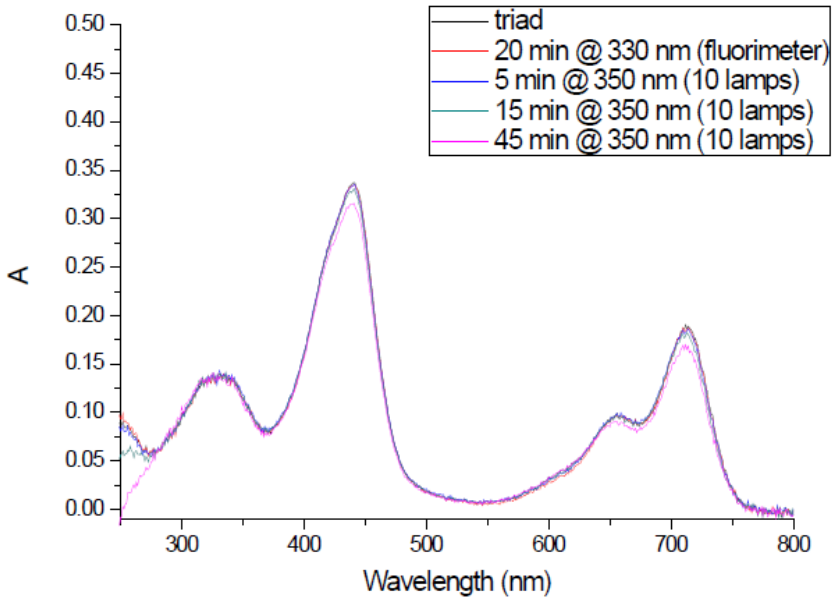

Figure 4.17. Attempts of opening the oxazine ring in the triad **83** upon UV irradiation in a THF solution at room temperature.

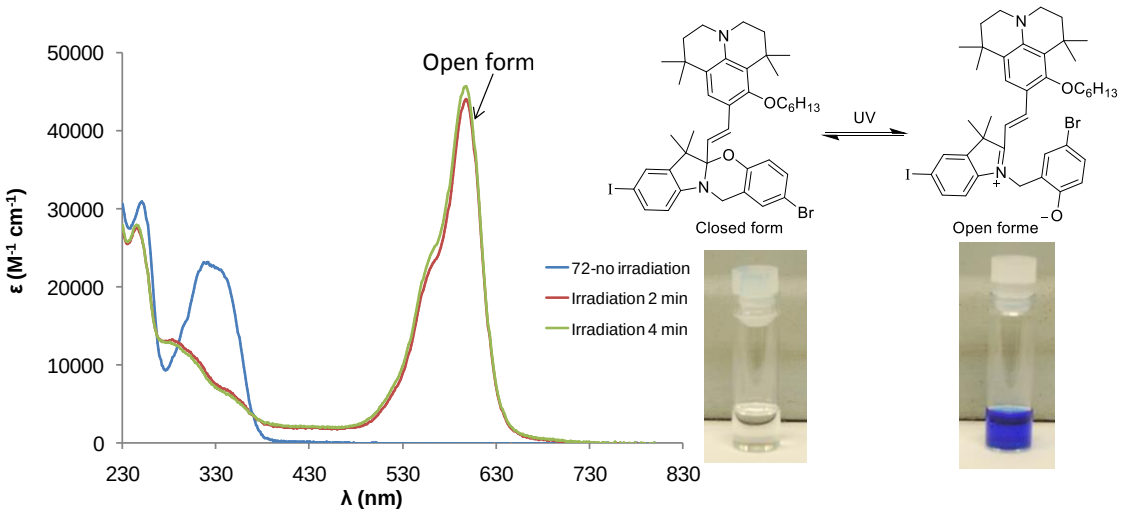

Figure 4.18. Absorption spectra of **72** in THF at room temperature before irradiation and after 2 minutes and 4 minutes of irradiation upon UV light with a Xenon lamp (300 W).

5.1.1. Acidi treatment

Although the first attempts of opening the triad **83** upon UV illumination were unsuccessful, treatment of a THF solution of the target compound with HCl vapors subsequently modifies its spectral pattern (Figure 4.19). A nascent intense band centered at 620 nm appeared in the absorption spectrum, without affecting the maxima of the Boranil and BODIPY components centered at 440 nm and 710 nm respectively. Relative to the absorption maximum of the styryljulolidine-indolino[1,3]oxazine **72** core after acidic treatment (Figure 4.20), the nascent band at 620 nm clearly confirms the chemical opening of the oxazine ring in Figure 4.19. The band was carefully assigned to an indolinium-styryljulolidine π-extended fragment. Alongside, acidic treatment of a THF solution of the BODIPY model **84** and a THF solution of **82** have no impact on their spectral profile relative to the neutral solutions (Figure 4.21).

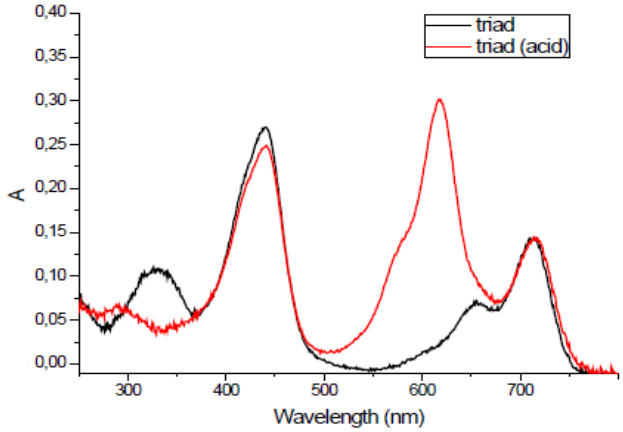

Figure 4.19. Absorption spectra of a THF solution of triad **83** without addition of acid (black curve) and triad **83** after treatment with HCl (red curve) at room temperature.

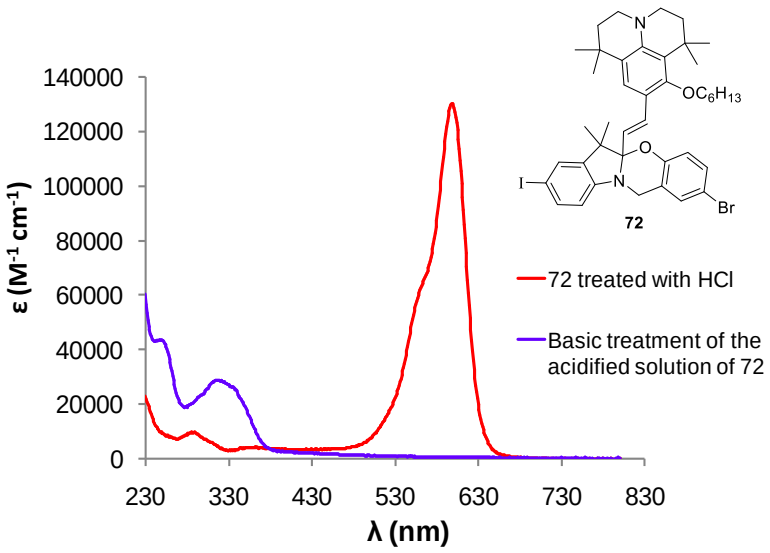

Figure 4.20. Absorption spectrum of compound **72** in acetonitrile solution after treatment with HCl vapors at room temperature.

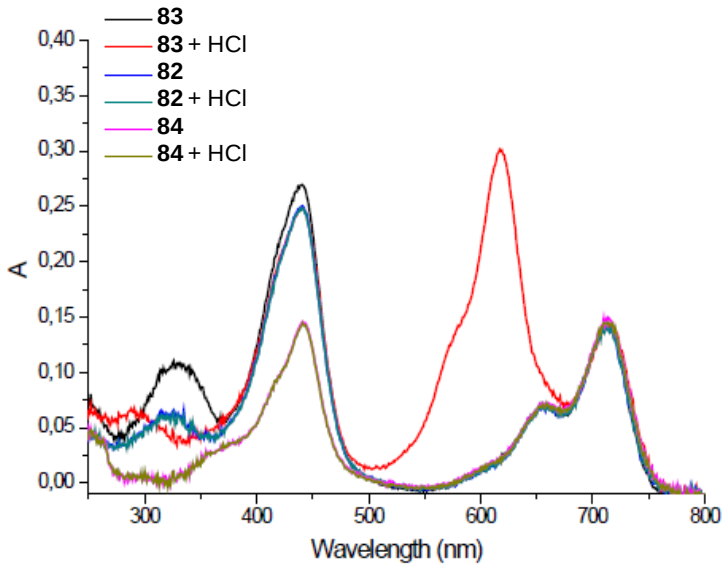

Figure 4.21. Absorption spectra of the target compounds in THF solution at room temperature before and after acidic treatment with HCl.

The emission of BODIPY **84** and triad-precursor **82** measured before and after acidic treatment overlap perfectly, indicating no change in their emission efficiency (Figure 4.22). Things are different when considering the final triad. Indeed the chemical opening of the oxazine ring, thus generating a merocyanine, strongly decreases the intensity of the characteristic emission form the BODIPY component (Figure 4.22). This is consistent with the deactivation of the energy transfer process from the energy-donor to the BODIPY acceptor. Indeed the band of the open oxazine core centered at 620 nm overlaps very well with the emission band of energy-donor component *i.e.* the boranil, thus successfully quenching its emission through activation of energy transfer

process. Moreover the latter process is encouraged by the close proximity of the donor and the photochrome entity.

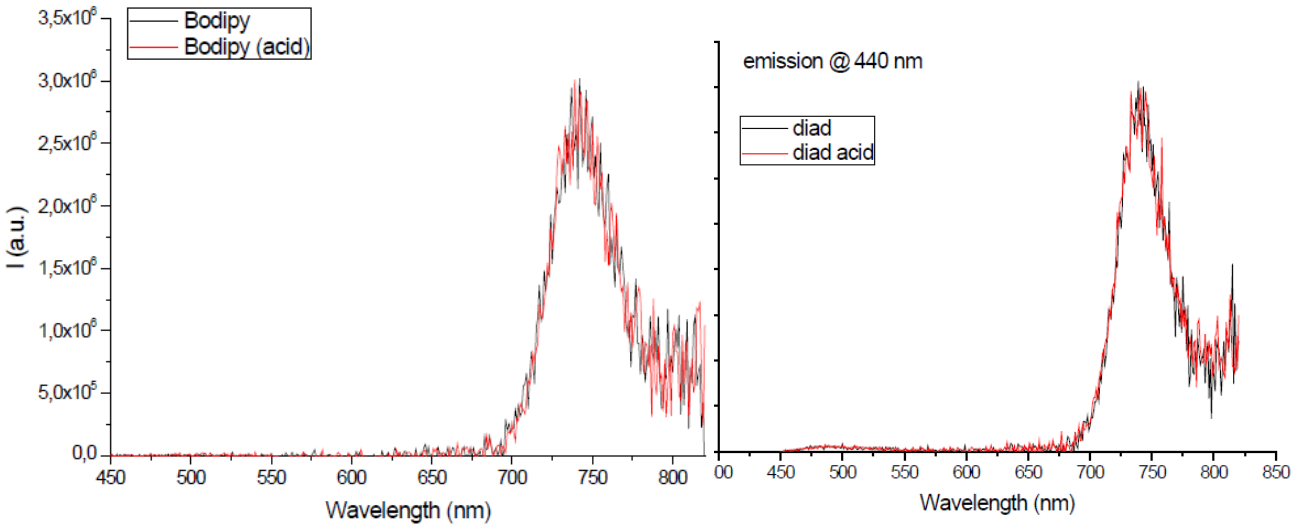

Figure 4.22. Emission spectra of BODIPY **84** and triad-precursor **82** in THF solution before and after acidic treatment room temperature. λ_{exc} = 440 nm

In other terms, in the presence of acid the closed styryl-indolin[1,3]oxazine follows transformation to the open merocyanine photochrome which acts as an energy "sink" relative to boranil energy-donor. We could demonstrate that the addition of a base such as tetramethylammonium hydroxide (NMe_4OH) allows the ring closing back process and re-activation of the long path energy transfer mechanism, *i.e.* from the boranil to the BODIPY. Figure 4.23-right shows that the spectra of triad treated with acid and then with the base overlaps perfectly indicating that acidification and the subsequent basification does not induce any degradation in the solution.

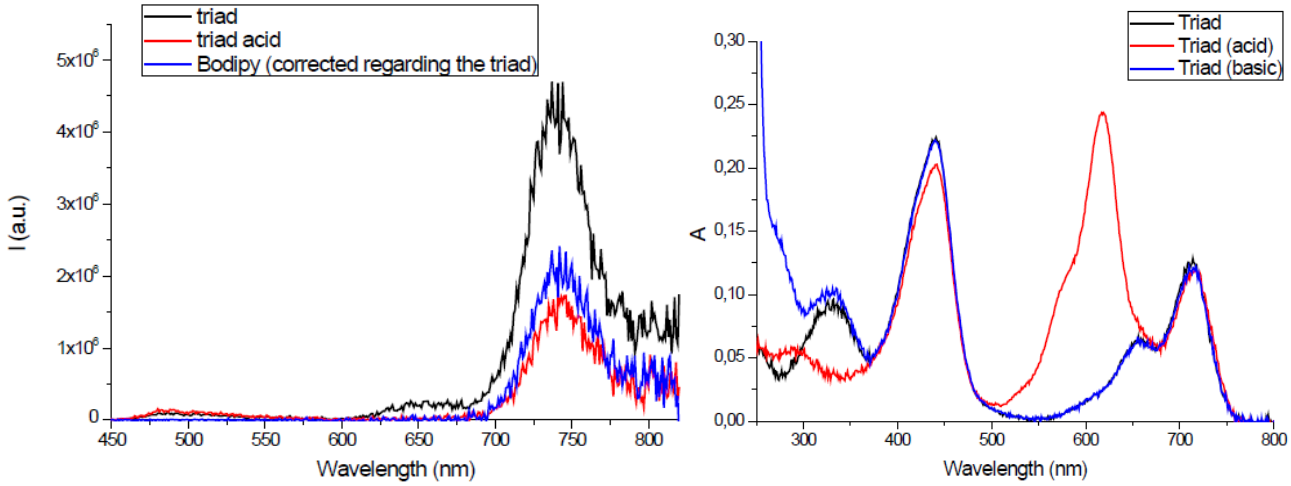

Figure 4.23. (Left) Emission spectra of triad **83** without acidic treatement (black curve), triad **83** after acidic treatment (red curve) and BODIPY model **84**, λ_{exc} = 440 nm. (Right) Absorption spectra of a neutral solution of the triad **83** (black) after addition of HCl (red) and after basification of the acidic solution with an aqueous solution of Me_4NOH. THF at room temperature.

The triad we have designed and synthesized shows interesting properties since it allows switching of the emission of energy-donor entity through the opening and closing of the photochromic core. The energy transfer is directed through the energy-acceptor BODIPY when the ring is closed but when the photochromic core is open the EET is directed over the photochromic energy sink (Figure 4.24). The process is among others enhanced by the close proximity between the energy-donor module and the photochrome. Irradiation into the open form of the photochrome at 610 nm might generate an energy transfer process from the dark state of the open photochromes unit to the BODIPY acceptor *via* the Dexter mechanism. This has to be confirmed by further works which are currently in progress.

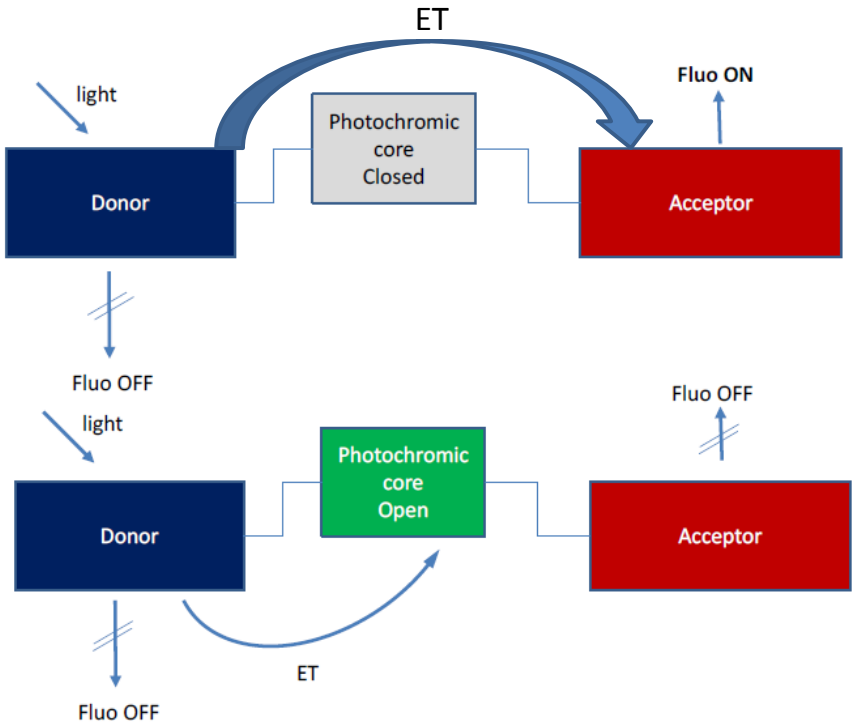

Figure 4.24. Schematic representation of the EET mechanism within donor-switch-acceptor triad. Upper: Energy transfer occurs from the donor to the acceptor while the photochromic core is closed. Down: Opening of the photochromic core quenches the emission of the donor, thus deactivating the acceptor emission path.

6. Design of a triad based on squarine energy-acceptor module

The triad BODIPY-[1,3]oxazine-Boranil **83** which was synthesized and discussed in the previous section, presents interesting switching properties, however the choice of the energy-acceptor module *i.e.* BODIPY is not the most convenient for this system. The BODIPY dyes in general present an intense low energy absorption band corresponding to $S_0 \rightarrow S_1$ transition of BODIPY core and a high energy weak band corresponding to $S_0 \rightarrow S_2$ transition. Furthermore, the $\pi \rightarrow \pi^*$

transition of the styryl fragment is very intense at *ca.* 450 nm and overlaps with the $S_0 \rightarrow S_2$ transition (see Figure 4.14, red curve). In fact, the latter electronic transitions overlaps completely with the absorption band of the energy-donor unit *i.e.* boranil at *ca.* 400 - 440 nm. This might complicate the behavior of our systems if considering a selective addressable input *i.e.* only effective irradiation of the donor without perturbing the acceptor.

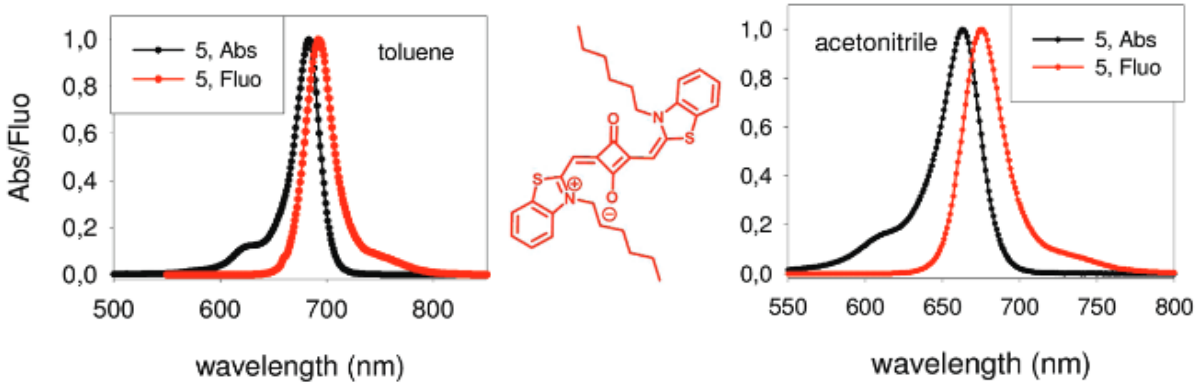

Figure 4.25. Absorption and emission spectra of the target squarine in toluene and acetonitrile solution. Figure partially printed from ref. [174].

Table 4.1. Spectral properties of squarine in air-equilibrated solutions measured by Rappozi *et al.*[174]

Solvent	λ_{abs} (max), nm	ε_{max}, $M^{-1}cm^{-1}$	λ_{em} (max), nm	Φ_F
Toluene	682	295 000	705	0.85
Acetonitrile	663	280 000	675	0.21

In order to avoid such problems, the most suitable module would be a dye which has only a characteristic absorption pattern within a range *ca.* 630-700 nm and high fluorescence quantum yield. Indeed after bibliographic researche, *squarine*[173] dyes seem as the most optimal dyes for our triad molecular framework. More particularly attention was turned on N-alkylbenzothiazole-based squarines presented in Figure 4.25.[174] These molecules feature a unique absorption band at 660-680 nm depending on the solvent as presented in the spectra above and show high fluorescence emission (Table 4.1). Hence we have designed the triad presented in Figure 4.26 bearing a squarine as energy-acceptor unit and boranil as energy-donor unit.

[173] (a) Sprenger, G. E.; Ziegenebien, W. *Angew. Chem. Int. Ed. Engl.* **1968**, *7*, 530. (b) Keil, D.; Hartmann, H. *Dyes Pigm.* **2001**, *49*, 161. (c) Beverina, L.; Ruffo, R.; Salamone, M. M.; Ronchi, E.; Binda, M.; Natali, D.; Sampietro, M. *J. Mater. Chem.* **2012**, *22*, 6704.

[174] Rappozi, V.; Beverina, L.; Salice, P.; Pagani, G. A.; Camerin, M. ; Xodo, L. E. *J. Med. Chem.* **2010**, *53*, 2188.

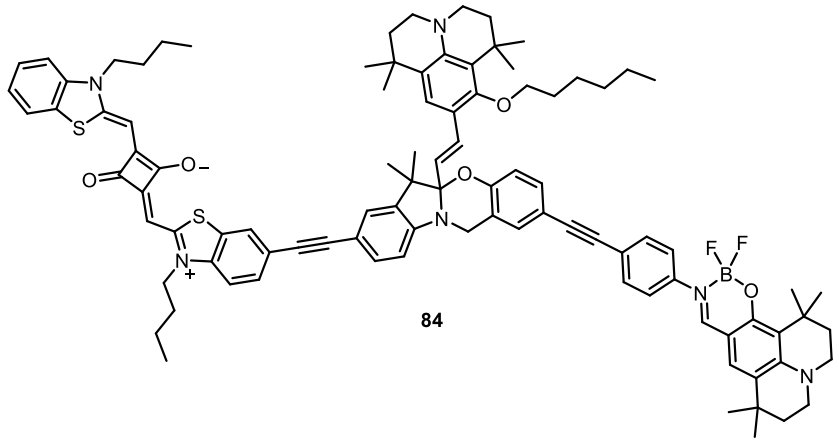

84

Figure 4.26. Design of a triad bearing a squarine dye as energy-acceptor entity. The synthesis of this compound is an undergoing project.

6.1. Attempting to synthesize a functional semi-squarine dye

The synthesis of the triad involves first the synthesis of a squarine bearing a functional group *e.g.* iodide, which allows its coupling with the oxazine core utilizing the usual metal-catalyzed cross-coupling reaction *e.g.* Sonogashira reaction. The synthesis of symmetrical squarines is almost easy, but synthesis of asymmetrical one is much more tedious. Obviously we are concerned foremost with the latter squarine-types.

We attempted to provide first a mono-iodinated squariylium dye as sketched in the retrosynthetic pathway (Scheme 4.17) from the condensation of 6-iodo-2-methyl-1,3-benzothiazole with semi-squarine **90**. The iodinated benzothizole was prepared following reported methods from 2-aminothiophenol in five steps.[175] Several efforts were conducted without success for providing the semi-squaric acid **90** from the hydrolysis of the corresponding ester **89** (obtained in good yield (51%) in one step) applying methods reported for similar compounds.[176] The synthesis of the final molecule remains currently an undergoing project.

[175] Santos, P. F.; Reis, L. V.; Duarte, I. ; Serrano, J. P.; Almeida, P.; Oliveira, A. S.; Ferreira, L. F. V. *Helv. Chim. Acta*, **2005**, *88*, 1135.

[176] Kim, S.; Mor, G. K.; Paulose, M.; Varghese, O. K.; Baik, C.; Grimes, C. A. *Langmuir*, **2010**, *26*, 12486.

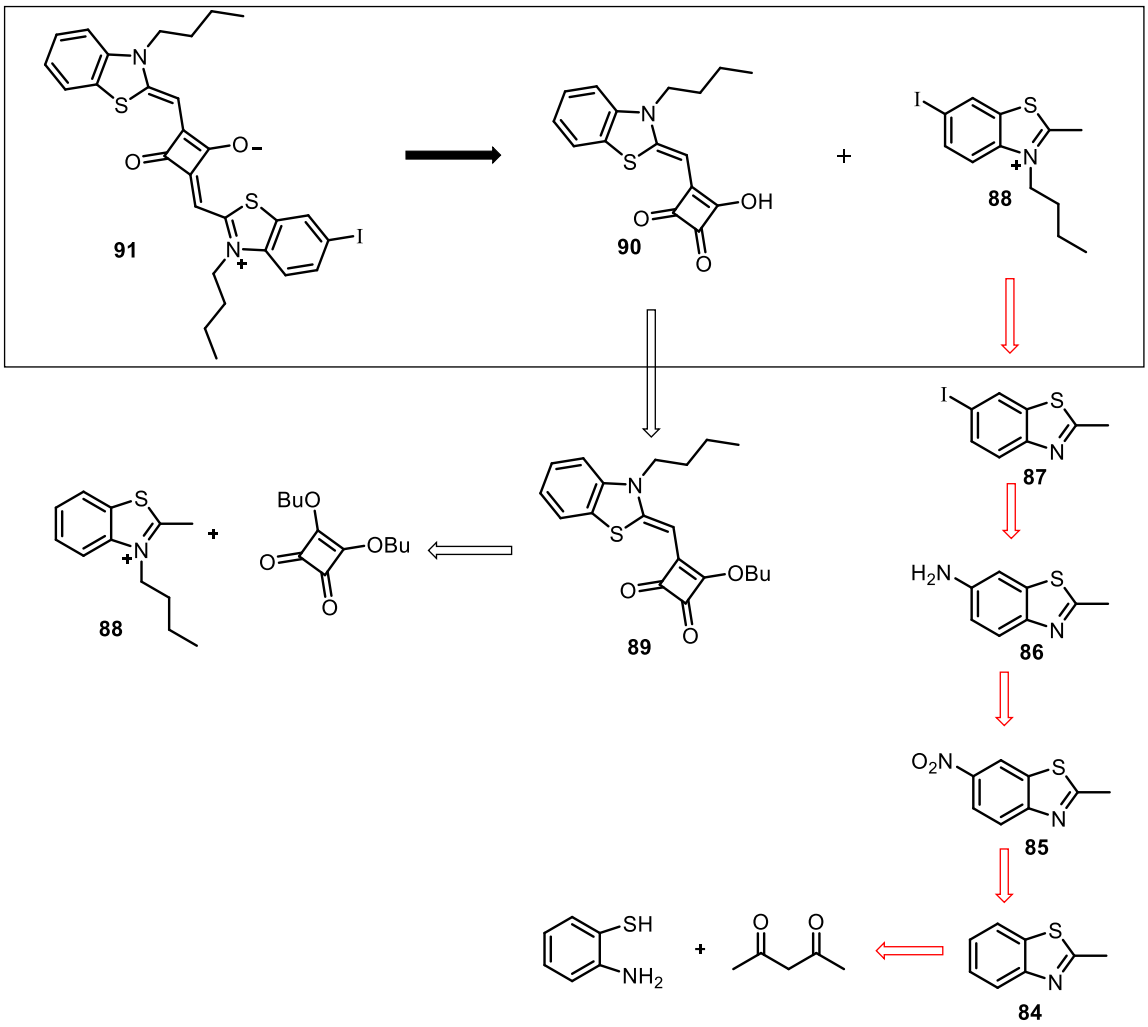

Scheme 4.17. Retrosynthetic pathway of designed asymmetric squarine.

7. Tuning energy transfer in phosphorescent switches

In Chapter I, we introduced some examples combining the photochromic units with metallic complexes. In most of the cases the models reported are based on diarylethene photochromic switches due to their numerous advantages, notably the high fatigue resistance and the thermal stability. Such hybrid systems are regularly investigated for obtaining a non-destructive readout capability. Contrary to the systems proposed by Lehn, Branda or De Cola (*vide supra*), our objective consists on anchoring two different metal centers connected through [1,3]oxazine moiety. This latter would serve as a "*lift bridge*" such as the optically or chemically opening/closing of oxazine ring may control the electronic energy transfer from the high energy metal center (Ir^{III}) to the second lower energy metal center (Os^{II}).

7.1. Synthesis of indolino[1,3]oxazine bearing two identical iridium(II) centers

The general procedure applied for the synthesis of the homonuclear complex involves first the preparation of the free ligand bearing two chelating bipyridine coordinating sites (Scheme 4.18). The Sonogashira cross-coupling of dihalogenated [1,3]oxazine **60** with large excess of TMS-acetylene was catalyzed with $[Pd(PPh_3)_2Cl_2]$ and CuI at elevated temperature because of the bromide functionality. The reaction gave a mixing of products according to TLC which are difficult to separate over column chromatography. However, as was previously mentioned, using a more electron-rich complex such as $[Pd(dppf)_2Cl_2]$ indeed provided the bis-coupled product **81** after 4.5 hours at room temperature in excellent yields.

Deprotection of TMS groups with stochiometric amount of KOH in THF, methanol and the water as proton source gave the terminal alkyne **92**. [1,3]oxazine appending two terminal alkynes onto the 3*H*-indole fragment and benoxazine ring was collected as slightly yellow oil which solidifies under vacuum in 91% yield. Characterization from ^{1}H, ^{13}C NMR spectroscopy (*vide infra*), elemental analysis and mass spectrometry confirmed the structure of compound **92**. ESI mass spectrometry provides the highest peak with *m/z* value 314.1 corresponding to cationic molecular peak [M+H].

Further, the homonuclear complex **94** was formed by cleavage of the chloride bridges of iridium(III) dimer $[(ppy)_2Ir\text{-}(\mu\text{-}Cl)]_2$, upon reaction with the free ligand **93** in 1,2-dichloroethane/methanol mixture as sketched in Scheme 4.18. The product was isolated as deep orange solids in 51% yield following anion exchange with hexafluorophosphate and purification *via* aluminium column chromatography. Analysis from ^{1}H and ^{13}C NMR spectroscopy confirmed the structure of **94**.

Finally, in order to ensure the photochromism of the oxazine core, julolidinyl-aldehyde was condensed with the activated methyl group of the chiral center in acidic conditions as depicted in Scheme 4.18-Step v. After a few minutes stirring at room temperature, the orange color of the reaction media changes and is transformed into deep blue overnight. Excess trifluoroacetic acid leads to chemical opening of the photochrome bearing the juloldine group, thus explaining the change in color. During the work up, washing of the organic phase with water eliminates the excess acid and favors ring closing; the deep blue color reverts back to orange. Purification of the triad over column chromatography gave the product as solids in *ca.* 40 %. So far the product could not be fully characterized. The proton NMR spectrum of triad **95** in deutreated acetonitrile was not well resolved, due to solubility problems.

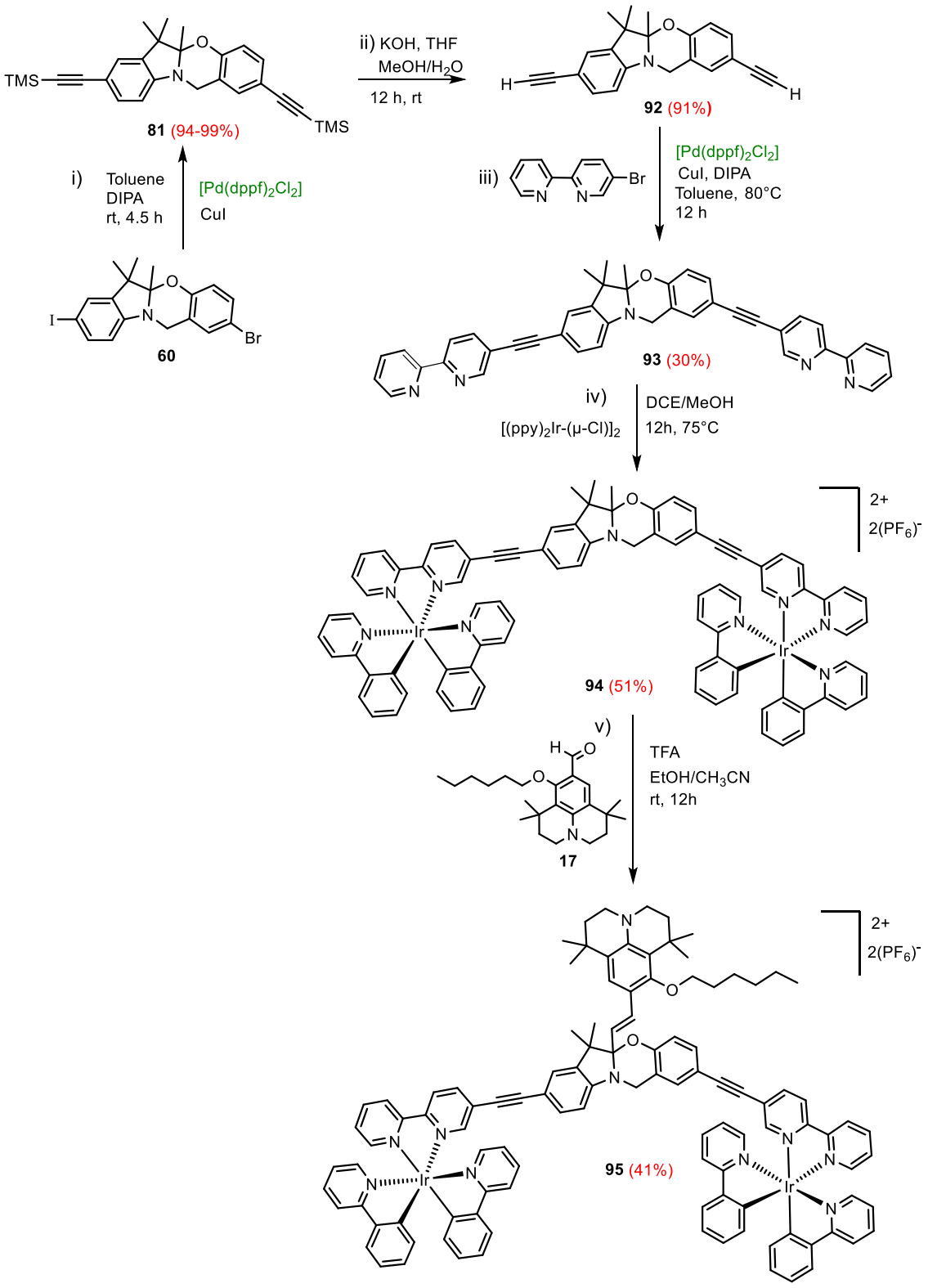

Scheme 4.18. Synthetic pathway of triad **95**.

The triad **95**, which serves as a model for the investigation of the optical properties of the next designed dinuclear complex **102**, was provided without any major complication from synthetic point of view. Regioselectivity is not required for anchoring the Ir(III) centers, thus the halogenated sites of precursor **60** are simultaneously transformed into two free chelating *2,2'-bpy* ligands before the unique metallation step occurs. As will be described below, the synthesis of a triad bearing two different metal centers needs the elaboration of a step-by-step synthetic procedure for the introduction of the metals regioselectively.

7.1.1. ^{1}H NMR characterization of compound 92, 93 and 94

The proton NMR spectral profile of compound **92** and **93** were measured in deuterated chloroform whereas for compound **94** in deuterated acetonitrile at room temperature. The presence of two terminal alkynes in **92** is easily identified by the appearing of two singlet signals at δ = 2.84 ppm and 2.86 ppm relative to its halogenated precursor **60** (Figure 2.27). After the cross-coupling reaction of **92** with 5-bromo-2,2'-*bpy*, the protons "1" and "2" are replaced by the aromatic signals of *bpy* ligands in the spectrum of **93** (Figure 2.28). The resonance signals of the [1,3]oxazine entity are shielded downfield by *ca.* 0.15 ppm after the covalent linkage of *bpy* chelating ligands.

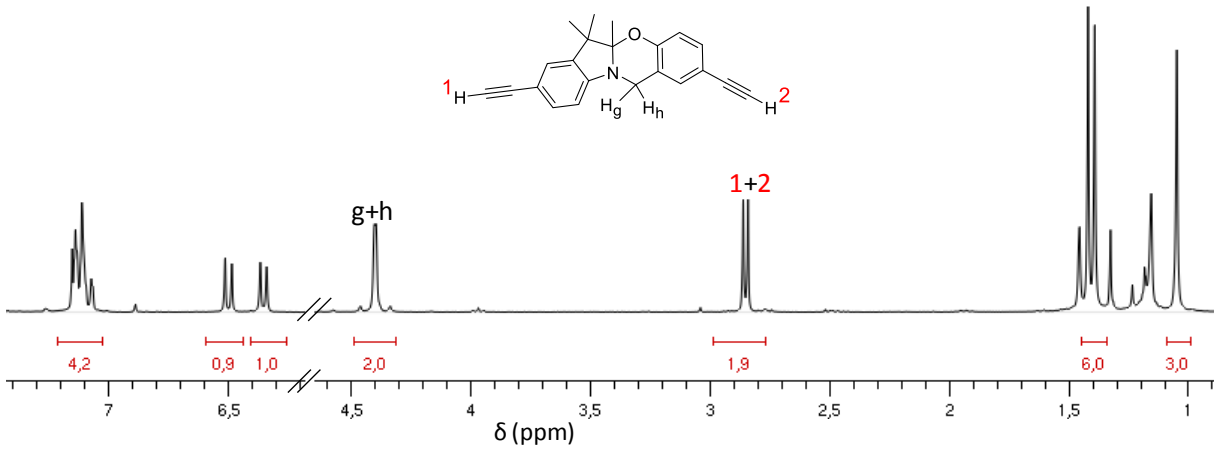

Figure 2.27. ^{1}H NMR spectrum of compound **92** in deuterated chloroform at room temperature.

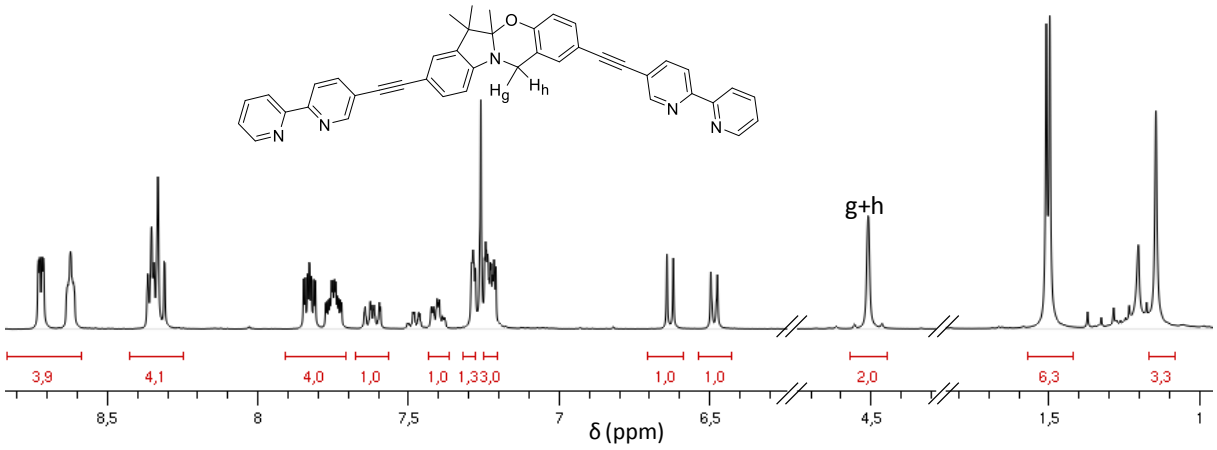

Figure 2.28. [1]H NMR spectrum of compound **93** in deuterated chloroform at room temperature.

The coordination of two Ir(III) centers thus providing the dinuclear complex **94** is accompanied by the appearance of the resonance signals of 2-phenylpyridine cyclometalated ligands in the aromatic window. Moreover, we can identify the AB system of the diastereotopic protons "g" and "h" which confirms the keeping of the chirality of the oxazine center. Due to the presence of the chirality of the oxazine center and the chirality of the iridium center the molecule exists as a mixing of several diastereoisomers which is manifested by the doubling of the resonance signals. This is more evident with the signals of AB quartet and the methyl groups in the spectrum Figure 2.29

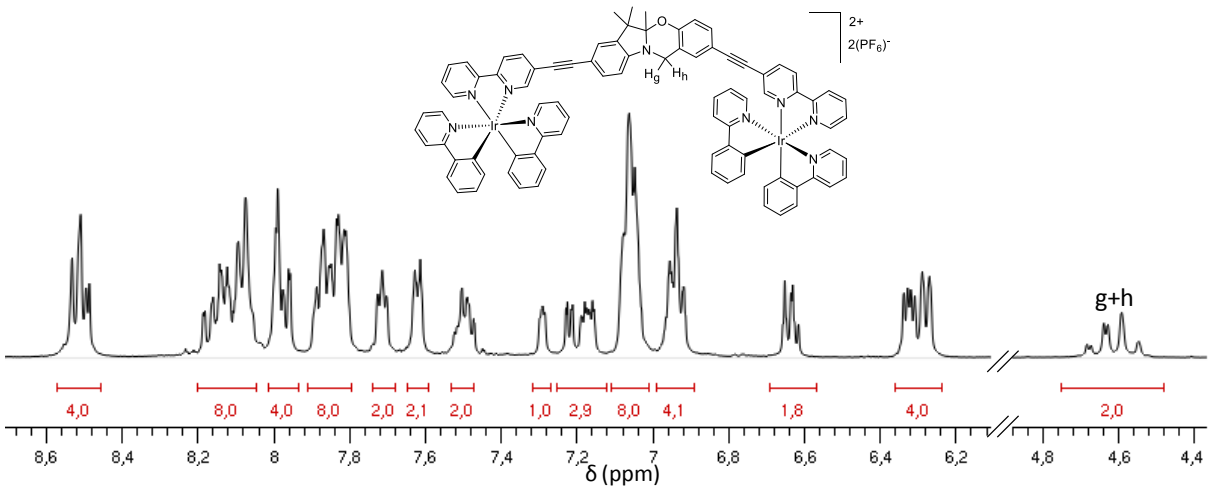

Figure 2.29. [1]H NMR spectrum of compound **94** in deuterated acetonitrile at room temperature. The spectrum is shown partially for clarity.

7.2. Synthesis of indolino[1,3]oxazine bearing an iridium(II) and osmium(II) center

Herein we have designed a triad where a cylometallating iridium(III) complex and a polypyridine osmium(II) complex are covalently attached onto [1,3]oxazine core **102** (Scheme 4.20). A synthetic strategy somewhat long was established and will be described below. It consists of a linear method which allows to regioselectively attach the Ir(III) and Os(II) metal centers in 8-step procedure.

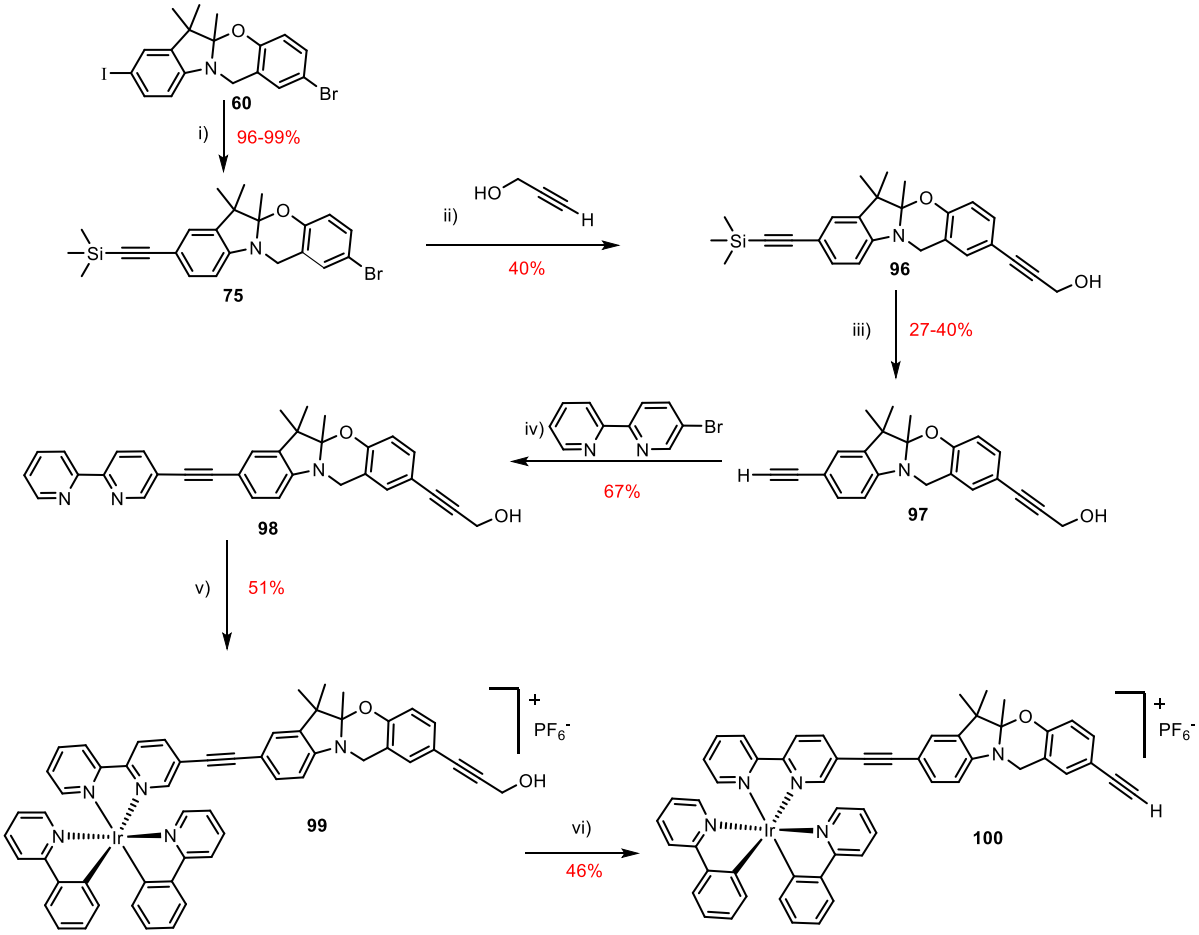

Scheme 4.19. Synthesis of mononuclear intermediate **100**.i) TMS-acetylene, $[Pd(PPh_3)_2Cl_2]$10mol%, CuI 10mol%, DIPA, toluene, 1.5 h, rt. ii) $[Pd(PPh_3)_4]$ 10 mol%, DIPA, toluene, 70 °C, 20 h. iii) KOH, THF, MeOH, H_2O, rt. iv) $[Pd(PPh_3)_4]$ 10 mol%, DIPA, toluene, 75 °C, 12 h. v) $[(ppy)_2Ir\text{-}(\mu\text{-}Cl)]_2$, DCE, MeOH, 75 °C, 12 h than anion exchange with KPF_6 aq. vi) MnO_2, KOH, THF, rt, 20 h than anion exchange with KPF_6 aq.

[1,3]oxazine core **60** was first converted in intermediate **75** having a TMS-acetylene group as discussed previously. In the next step, the bromine site was transformed into propargylic alcohol fragment such as the two sites may be deprotected applying different conditions (Scheme 4.19). The product **96** was obtained as white solids following purification in 40% yield. The TMS group was removed using the usual procedure *i.e.* KOH in THF/methanol and water and

subsequently the terminal alkyne was coupled with the 5-bromo-2,2'-bipyrydine catalyzed with Pd^0 in toluene solution and DIPA as base as sketched in Scheme 4.19. The product **98** bearing a free chelating site was obtained as yellowish oil in acceptable yield (67%) following purification. Complexation of the free *bpy* ligand of **98** with Ir(III) center by cleavage of the choro bridged Ir(III) precursor leads to the corresponding complex **99** in 51 % yield following anion exchange and purification. We already demonstrated in the third chapter that tuning the chemical structure of the ligand directly onto the Ir complex does not induce any degradation. But the deprotection of the propargylic alcohol group was difficult yielding the product in low amounts. At the end of the procedure we could obtain only 10 mg of the product **100** which is not enough for continuing the next step. As shown in Scheme 4.20 compound **101** would be generated by the coupling of intermediate **100** with the Os(II) precursor. Finally the Knoevenagel condensation of **100** would lead to the dinuclear triad **102** as previously obtained with the Ir(III) homocomplex.

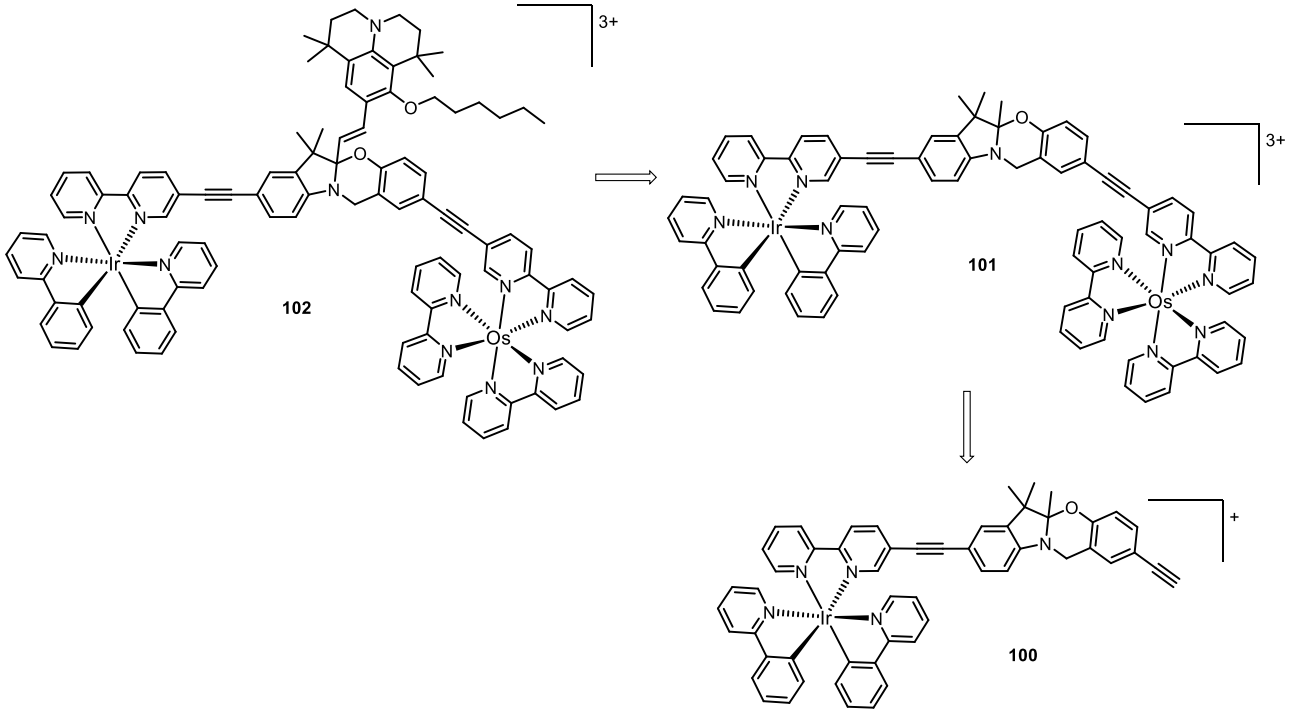

Scheme 4.20. Retrosynthesis of the dinuclear complex **102** bearing an Ir(III) and Os(II) center.

7.2.1. ^{1}H NMR characterization of compound 97 and 99

The NMR spectra of compounds **97** and **99** were measured in deuterated chloroform at room temperature. The resonance signal at δ = 2.94 ppm was accurately assigned to the terminal alkyne of compound **97**. The methylene protons of the propargylic alcohol fragment appear at

ca. 4.5 ppm and are overlapped with the methylene protons “g” and “h” of the oxazine ring. The absence of a peak at *ca.* 3.0 ppm in the spectrum of **99** indicates that the *bpy* ligand was successfully coupled with the terminal acetylide **97**. The integral of the multiplets appearing within the aromatic region of the spectrum account for the expected number of protons provided by the bipyridine ligand and 2-phenylpyridine cyclometallating ligands around Ir(III) center. The chemical shift of the protons of oxazine core seems not affected by the appendage of the metal center onto the 3*H*-indole part of the molecule.

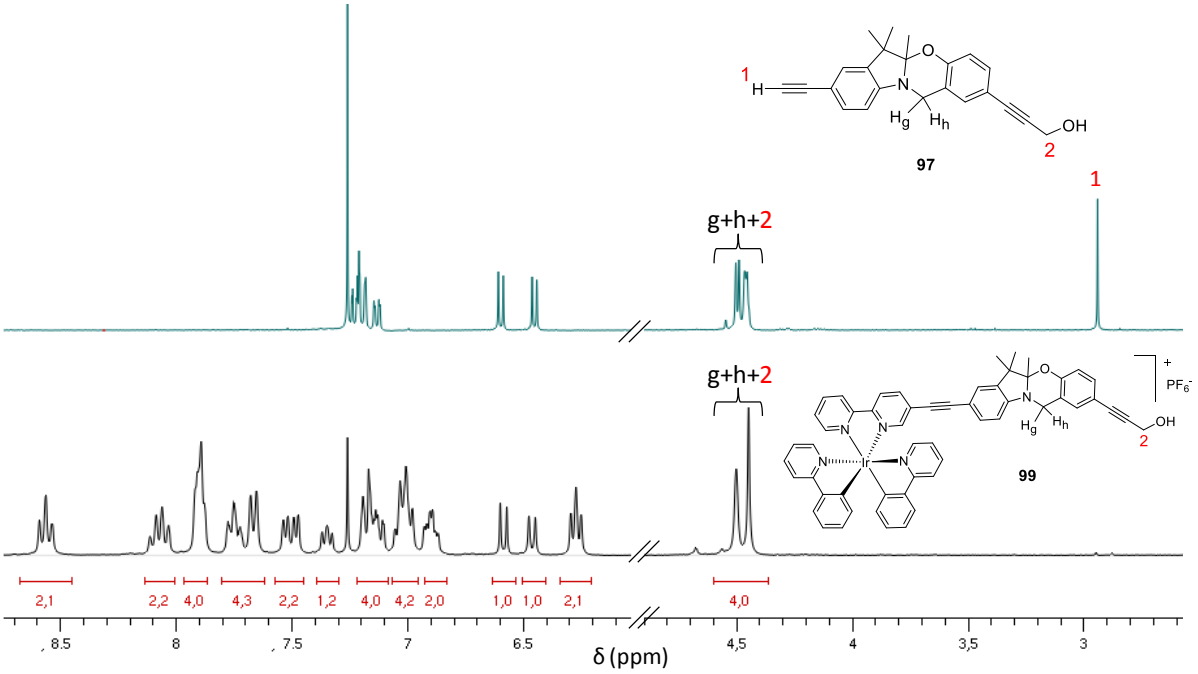

Figure 2.30. ^{1}H NMR spectra of compound **97** and **99** in deuterated chloroform at room temperature. The spectra are partially shown for clarity.

8. Conclusion

A new florescent switching triad **83** was successfully designed and synthesized after long efforts. It is constructed around [1,3]oxazine as the photochromic entity which is covalently linked with an energy-donor and an energy-acceptor. Among the large library of photochromes synthesized, oxazine bearing a styryl-julolidine was used for further investigations. BODIPY dye **84** was selected as the acceptor and attached onto the 3*H*-indole fragment and Boranil **85** as the donor attached onto benzoxazine core. The irradiation of the donor moiety with λ_{exc} = 440 nm allows an efficient electronic energy transfer from the Boranil-donor to the BODIPY acceptor when the oxazine is in the closed form, favored by an important integral overlap between the donor and the acceptor. The chemical opening of the triad by acidification of the THF solution with HCl

vapors, leads to the activation of a short path energy transfer process. Thus emission provided from the irradiation of the donor is successfully directed through the open [1,3]oxazine sink. The closing of the oxazine ring was realized by basification of the acidic solution which subsequently re-activates the long path of energy transfer process from the boranil moiety through the BODIPY moiety. Extension of this work with designing and synthesizing a triad bearing a squarine module could not be finished within the context of this doctoral thesis due to limited remaining time. Furthermore, we wished to introduce another metallic-based triad which bears two distinct metallic centers *i.e.* Ir(III) and Os(II) in order to activate a switchable energy transfer process form iridium through osmium platform by controlling of the opening/closing of the photochromic oxazine entity.

General conclusion and perspectives

During these years of doctoral thesis we were interested in the design and synthesis of organic and/or organometallic molecular frameworks for triggering important phenomena such as the photoinduced electron transfer or electronic energy transfer process. The foregoing chapters have illustrated the numerous compounds targeted for the purposes. First, our attention was turned toward the organic push-pull chromophores because they are useful model systems for studying the mechanism of photoinduced electron transfer process. One of the principle axes of researches in the Ziessel group concerns the BODIPY chemistry. Surprisingly, BODIPY derivatives have not been widely exploited as photoactive bridges in D-π-A chromophores. Also photoinduced electron transfer involving BODIPY dyes is not so common.

This conducted us to design and synthesize new push-pull systems bearing a dicyanovinyl fragment as the electron-acceptor and a strong electron-donor such as the julolidine and triazatruxene scaffolds covalently linked through a BODIPY dye bridge. Electrochemical, DFT calculations and photophysical studies confirmed their strong push-pull behavior. These compounds, although presenting high charge-transfer character, do not promote an excited charge-separation state. However, for the model compound lacking the donor unit, we could observe the emission from an exiplex state which does not evolve into a CS state. Therefore a modest driving force for photoinduced charge-transfer (ΔG_{CT} = -0.17 eV) exists for this model in MTHF at 20 °C.

Further, we explored the intriguing chemistry of julolidine motif which particularly retained our attention. Numerous julolidine-containing organic materials have been reported for various applications in biology and photonic devices (*vide supra*), but the small organic molecule is less exploited in conjunction with transition metal complexes. First, the julolidine platform was transformed into chelating N^O-type ligands. These compounds display ESIPT process and interestingly, their luminescence profiles exhibited panchromatic luminescence. The complexation of N^O site with BF_2 entity suppressed the ESPIT processes and highly increased the fluorescence quantum yield of the corresponding boranil centered at *ca.* 470 nm. The molecular structure of boranil derivatives was confirmed from X-ray diffraction technique. Furthermore we appended a platinum(II) chromophore units onto julolidine core

by way of palladium-catalyzed reaction. According to the photophysical measurements, an energy transfer process was observed from the ^{3}MLCT of the platinum(II) chromophore through the lower energy triplet state of the julolidine-based ligand. Aside, we synthesized an original dinuclear heterometallic complex based on the julolidine ligand which bears a Pt(II) chromophore and an Ir(III) cyclometallated center. Its luminescence spectral profile showed a broad emission covering the whole visible spectrum at 77 K on glassy matrix. In contrary, the luminescence was quenched at room temperature.

We could successfully obtain a new florescent switching triad constructed around an [1,3]oxazine core bearing a styryl-julolidine arm which ensures its photochromic ability. As energy-donor was selected a boranil dye (λ_{max} abs = 430 nm, λ_{max} em = 475 nm in THF) and as energy-acceptor a BODIPY dye (λ_{max} abs = 714 nm, λ_{max} em = 743 nm). The preliminary optical results indicate a highly efficient energy transfer from the donor to the acceptor when the [1,3]oxazine ring is in the closed state, whereas its chemical opening with addition of acid direct the energy transfer toward the styryl-indolenium energy sink through spectral overlap. Hence, the fluorescence emission form the acceptor is switched ON when the oxazine ring is closed and the fluorescence is switched OFF when the oxazine ring is open. Further advanced studies attempting to open the oxazine ring with UV light are currently in progress.

It was already mentioned that although the obtained triad shows interesting switching properties, it presents some intrinsic drawback points. The BODIPY component displays a low energy absorption band and a high energy absorption band which overlap completely with the absorption band of the boranil energy-donor component. Moreover the fluorescence quantum yield of the selected BODIPY is weak (*ca.* 0.07 for the isolated dye). Hence, in perspective we envisage the synthesis and study of fluorescent switching where the acceptor is a squarylium cyanine dye (introduced in the previous chapter) which readily absorbs within the optimum spectral window relative to the components composing the triad *i.e.* the styryl-julolidine[1,3]oxazine core and the boranil energy-donor. Aside, we might consider demonstrating the tuning of EET process within a switch which is covalently linked to two different metal centers carefully selected for the purpose.

Conclusion générale et perspectives

Durant ces années de thèse nous nous sommes intéressés au design, à la synthèse et à la caractérisation des systèmes moléculaires organiques et organométallique pour l'étude des phénomènes importants tels que le transfert photoinduit d'électron ou le transfert électronique d'énergie. Les chapitres précédents ont illustrés les nombreux composés cibles dans ce but. Tout d'abord, notre intérêt s'est porté vers les chromophores organiques de type push-pull parce qu'elles constituent des modèles très utiles pour l'étude du mécanisme de transfert photoinduit d'électron. L'un des principaux axes de recherche dans le group Ziessel est focalisé sur l'étude et la chimie des dérivés BODIPYs. En effet, les derivésBODIPYs sont peu exploités dans les systèmes D-π-A en tant qu'espaceurs π-conjugués photoactives. De même, l'étude du processus de transfert photoinduit d'électron dans des composés contenant le motif BODIPY n'est pas très courant.

Ces constatations nous ont conduits vers le design et la synthèse des systèmes push-pull contenant un bras dicyanovinyl comme unité électron-acceptrice et une unité julolidine ou triazatruxène comme électron-donneur fort, liés de manière covalente avec un espaceur BODIPY. Les études électrochimiques, les études théoriques par DFT ainsi que les mesures photophysiques ont mises en évidence un caractère push-pull très fort pour ces composés. Malgré leurs forts caractères push-pull, ces molécules ne présentent pas un état à charge séparé à l'état excité. Néanmoins, pour l'un des composés modèles, dont l'unité donneur d'électrons est absente, nous avons pu observer une émission de luminescence depuis un état exciplex. Ce système est caractérisé par une force motrice modeste de transfert de charge photoinduit (ΔG_{CT} = -0.17 eV) dans une solution de MTHF à 20 °C.

Entre autre nous avons exploité la chimie très fascinante de la julolidine, un motif qui à attiré particulièrement notre attention. De nombreux matériaux organiques contenant ce motif ont été reportés dans la littérature pour diverses applications dans le domaine de la biologie et les dispositifs optiques. Néanmoins, elle est peu étudiée dans des combinaisons avec des métaux de transitions. Ainsi, ici elle a été d'abord transformée en ligand chélatant de type anil N^O. Ces composés subissent un processus de *transfert de proton intramoléculaire à l'état excité* (ESIPT, acronyme utilisé pour *Excited State Intramolecular Proton Transfer*) et leurs spectres d'absorptions montrent une *luminescence panchromatique*, les rendant très intéressants du point de vue optique. La complexation des sites de chélation N^O des ligands anils avec BF_2 supprime le processus ESIPT et augmente de façon appréciable le rendement quantique de

fluorescence pour ces composés. Les structures moléculaires des boranils obtenues dans cette thèse de doctorat sont confirmées par la technique de diffraction aux rayons-X. Par la suite, les ligands dérivés de la julolidine sont combinés avec un chromophore Pt(II) par des réactions catalysées au palladium. Les mesures photophysiques ont mis en évidence un transfert d'énergie depuis l'état ^{3}MLCT du chromophore Pt vers le niveau de plus bas énergie de l'état triplet du ligand contenant la julolidine. Entre autre, le ligand dérivé de la julolidine à été utilisé pour combiner deux centres métalliques différents, un Pt(II) et un Ir(III). Le spectre de luminescence du complexe hétérobimétallique présente une bande d'émission assez large couvrant l'ensemlre de la fenêtre du spectre visible à 77 K sur une matrice solide. En revanche, sa luminescence est entièrement supprimée à température ambiante.

L'un des sujets principaux de cette thèse consistait dans le design et la synthèse des molécules commutables par des stimuli optiques ou chimiques. Dans le Chapitre IV nous avons présenté une triade construite autour de l'unité photochrome [1,3]oxazine connecté à un bras styryl-julolidine et pouvant contrôler l'émission de fluorescence de façon adressable. Le donneur d'énergie est un boranil et l'accepteur d'énergie est un dérivé BODIPY. Les résultats préliminaires obtenus jusqu'à présent indiquent un processus de transfert électronique d'énergie très efficace depuis le donneur vers l'accepteur lorsque le cycle oxazine est fermé. De l'autre côté, l'ouverture du cycle oxazine par traitement acide dirige le transfert d'énergie vers l'unité styryl-indolenium par un mécanisme de recouvrement spectrale. Ainsi, l'émission de fluorescence a pu être activée de manière contrôlée lorsque le photochrome est fermée et supprimée dans le cas contraire. Des études supplémentaires visant à ouvrir optiquement le cycle oxazine sont au moment d'écrire cette thèse, en cours.

Malgré que notre triade présente des propriétés de commutation intéressantes, elle n'est intrinsèquement pas très optimale. Le spectre d'absorption du BODIPY présente une bande à basse énergie et une bande vers les hautes énergies qui se superpose entièrement avec la bande d'absorption du donneur d'énergie, le boranil. Entre autre le rendement quantique de fluorescence est très faible. Ainsi dans la perspective, nous envisageons la synthèse et l'étude des molécules photocommutables ou l'accepteur d'énergie est un dérivé squarine ayant une fenêtre optique optimale. Entre autre nous envisageons d'appliquer le concept de commutation de luminescence également aux systèmes ou le photochrome est lié de manière covalente avec deux centres métalliques choisis de manière appropriée.

Chapter V

Chapter V - Experimental section

➢ Instrumentation

NMR Spectroscopy

^{1}H, ^{13}C, and ^{11}B NMR spectra were recorded on Brucker Spectrometers (200, 300 and 400 MHz). ^{1}H , ^{13}C chemical shifts were reported to the delta scale in ppm relative to the residual peak of the perdeuterated used solvent as internal standards: benzene-d_6 (^{1}H: δ = 7.16 ppm; ^{13}C: δ =128.00), chloroform-d_1 (^{1}H: δ = 7.26 ppm; ^{13}C: δ = 77.16), methanol-d_4 (^{1}H: δ = 3.31 ppm; ^{13}C: δ = 49.00), dichloromethane-d_2 (^{1}H: δ = 5.32 ppm; ^{13}C: δ = 54.00), acetonitrile-d_3 (^{1}H: δ = 7.26 ppm; ^{13}C: δ = 1.94 ppm, 118.26 ppm) . The ^{11}B NMR spectra were calibrated with the borosilicate of the NMR tubes.

IR and UV-Visible Spectroscopy and Luminescence Spectroscopy

FT-IR spectra were recorded as solid sample on a Perkin Elmer Spectrum One equipped with ATR diamond apparatus. UV-visible spectra were recorded using Schimadzu UV-300 dual-beam grating spectrophotometer with a 1 cm quartz cell. Steady-state emission and excitation spectra were recorded at 25 °C on a HORIBA Jobin-Yvon FluoroMax 4P spectrofluorimeter. All the fluorescence spectra were corrected. The fluorescence quantum yield (φ_F) was calculated from the following equation:

$$\varphi_{exp} = \varphi_{ref} \frac{F\left[1 - \exp(-A_{ref}\ ln10\right]n^2}{F_{ref}[1 - \exp(A\ ln10]n_{ref}^2}$$

Where *F* denotes the integral of the corrected emission spectrum, *A* is the absorbance at the excitation wavelength and n is the refractive index of the medium. The reference systems used were rhodamine 6G (φ_F = 0.88 in EtOH, λ_{exc} = 488 nm), Cresyl Violet (φ_F = 0.50 in EtOH, λ_{exc} = 546 nm) or a reported BODIPY dye (φ_F = 0.49 in CH_2Cl_2, λ_{exc} = 650 nm) in regards to the emission wavelength of the studied compounds.[177] Luminescence lifetimes were measured on a FL 920 Edimburgh Instruments spectrofluorimeter equipped with a R928 photomulitplier and a PicoQuant PDL 800-D pulsed diode connected to a G^{w}Instect GFG-8015G delay

[177] Ulrich, G.; Goeb, S.; De Nicola, A.; Retailleau, P.; Ziessel, R. *Synlett.* **2007**, 1517.

generator. Emission wavelengths were selected by a monochromator. Lifetimes were deconvulted with FS-900 software using a light-scattering solution (LUDOX) for instrument response.

Cyclic voltammetry

Electrochemical studies employed cyclic voltammetry with a conventional 3-electrode system using a BAS CV-50W voltammetric analyser equipped with a Pt a microdisk (2 mm^2) working electrode and a silver wire counter electrode. Ferrocene was used as an internal standard and was calibrated against a saturated calomel reference electrode (SCE) separated from the electrolysis cell by a glass frit presoaked with electrolyte solution. Solutions contained the electro-active substrate in deoxygenated and anhydrous dichloromethane containing tetra-n-butylammonium hexafluorophosphate (0.1 M) as supporting electrolyte. The quoted half-wave potentials were reproducible within ~ 10mV.

- **General methods, Reagents and Materials**

Chromatography

Chromatographic purifications were conducted by using standardized Silica gel (SiO_2) 60 (0.063-0.200 mm) or de-activated aluminium oxide (Al_2O_3) with 6 % of water w/w. Thin layer chromatography was performed on silica gel or alumina plates coated with fluorescent indicators.

Anhydrous solvents

CH_2Cl_2, 1,2-dichloroethane and acetonitrile were distillated from P_2O_5 under an argon atmosphere. THF was distillated over sodium/benzophenone and toluene was distillated over sodium under argon atmosphere. DMF was distillated over KOH under reduced pressure, while $CHCl_3$ was neutralized on basic alumina prior to use.

Reagents

$[Pd(PPh_3)_2Cl_2]$,[178] $[Pd(dppf)_2Cl_2]$,[179] $[(^tBu_3tpy)PtCl]BF_4$,[180] $[(ppy)_2Ir\text{-}(\mu\text{-}Cl)]_2$,[181] $[Pd(PPh_3)_2Cl_2]$[182] were prepared according to literature procedure. Purification of Et_3N, $^iPr_2NH$, N-Bromosuccinimide (NBS) were performed according to reported literature.[183]

[178] Dangles, O.; Guibe, F.; Balavoine, G.; Lavielle, S.; Marquet, A. *J. Org. Chem.* **1987**, *52*, 4984.

Experimental procedures - Chapter II

Compound **15** (4,4-Difluoro-8-(4-iodo) phenyl-1,3,5,7-tetramethyl-4-bora-3a,4a-diaza-s-indacene) was prepared according to Ulrich, G.; Ziessel, R. *J. Org. Chem*. **2004**, *69*, 2070.

Compound **17** (9-formyl-1,1,7,7-tetramethyl-2,3,6,7-tetrahydro-1H,5H-pyrido[3,2,1-ij]quinolizidine) Lee, C.-C.; Hu, A. T. *Dyes Pigm.* **2003**, *59*, 63.

Compound **22** and compound **29** were prepared according Bura, T.; Leclerc, N.; Fall, S.; Lévêque, P.; Heiser, T.; Ziessel, R. *Org. Lett.* **2011**, *13*, 6030.

Compound **24** 2-(2-*tert*-Butyl-6-methyl-4*H*-pyran-4-ylidene) malonitrile was synthesized inspired by Chang, Y. J.; Chow, T. J. *J. Mater. Chem.* **2011**, *21*, 3091.

General Procedure A: in a round bottomed flask, piperidine and a crystal of p-TsOH were added to a solution of BODIPY **15** (1 equiv.) and 9-formyl-10-butoxy-1,1,7,7-tetramethyl-2,3,6,7-tetrahydro-1*H*,5*H*-pyrido-[3,2,1-ij]quinolizidine **17** (1.5 equiv.) in toluene. The solution was heated at 140°C until it had evaporated to dryness. The solids were purified by silica gel chromatography before being re-crystallized.

General Procedure B: in a two-neck flask equipped with a reflux condenser, a gas bubbler and a magnetic stirring bar, $[Pd(PPh_3)_2Cl_2]$ (10 mmol%) and sodium formate (1.2 equiv) were added to a solution of halogenated dye (1 equiv.) in anhydrous DMF (8 ml). The reaction mixture was degassed under a continuous flow of CO at atmospheric pressure and stirred at 90 °C for 3 hours. After cooling to room temperature, the mixture was extracted with dichloromethane and washed several times with water. The organic phase was dried over hygroscopic cotton wool and evaporated. The crude residue was then purified by flash chromatography.

---

[179] (a) Housecroft, C. E.; Owen, S. M.; Raithby, P. R.; Shaykh, B. A. M. *Organometallics*, **1990**, *9*, 1617. (b) Four, P. *J. Org. Chem.* **1981**, *146*, 4439.

[180] Yip, H.-K.; Cheng, L.-K.; Cheung, K.-K.; Che, C.-M. *J. Chem. Soc., Dalton Trans*. **1993**, 2933.

[181] King, K. A.; Spellane, P. J.; Watts, R. *J. J Am. Chem. Soc.* **1985**, *107*, 1431.

[182] Dangels, O.; Guibe, F.; Balavoine, G.; Lavielle, S.; Marquet, A. *J. Org. Chem.* **1987**, *52*, 4984.

[183] Armarego, W. L. F.; Perrin, D. D. *Purification of laboratory chemicals fourth edition*, Oxford, Butterworth Hinemann, **2000**.

General Procedure C: in a Schlenk tube equipped with a stir bar, malonitrile (1.2 equiv.) and several drops of piperidine/acetic acid were added to a suspension of the aldehyde precursor (1 equiv.) in methanol (2.5 ml). The mixture was stirred at 85-95 °C during 0.5-1 hour.

Compound 18

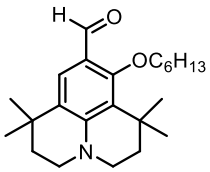

18

An aliquot of NaH (46 mg, 1.92 mmol) was added slowly to a solution of 9-formyl-1,1,7,7-tetramethyl-2,3,6,7-tetrahydro-1H,5H-pyrido[3,2,1-ij]quinolizidine **17** (314 mg, 1.279 mmol) in DMF under argon. The mixture was stirred for 1 h before addition of 1-bromohexane (0.2 mL, 1.53 mmol). After stirring for 2 days at 95°C, the solution was quenched with water and extracted several times with dichloromethane. The isolated product was purified by column chromatography, eluting with dichloromethane/petroleum ether (7/3, v/v) (388 mg, 85%). R_f = 0.19 (dichloromethane/petroleum ether). ^{1}H NMR ($CDCl_3$, 300 MHz) δ: 0.9 (t, ^2J = 6,9 Hz, 3H), 1.26 (s, 6H), 1.32-1.37 (m, 4H), 1.42 (s, 6H), 1.45-1.51 (m, 2H), 1.70 (dd, ^3J = 12.1 Hz, ^2J = 6.2 Hz, 4H), 1.9 (td, ^3J = 11.0 Hz, ^2J = 7.2 Hz, 2H), 3.22 (t, ^2J = 5.8 Hz, 2H), 3.28 (t, ^2J = 6.1 Hz, 2H), 3.95 (t, ^2J = 6.9 Hz, 2H), 7.58 (s, 1H), 9.95 (s, 1H); ^{13}C NMR ($CDCl_3$, 75 MHz) δ: 14.0, 22.6, 25.7, 29.7, 30.0, 30.3, 31.8, 32.1, 32.5, 35.7, 39.4, 46.9, 47.5, 79.0, 117.3, 120.7, 125.3, 126.1, 148.2, 162.2, 187.8; MS (EI neat matter): *m/z* (intensity, %) Calc. for [M]: 357.2 found: 357.1 (100); 329.1 (35), [M-CHO]; Anal. Calc. for $C_{23}H_{35}NO_2$: C, 77.27; H, 9.87; N, 3.92 found: C, 77.04; H, 9.62; N, 3.77.

Compound 25

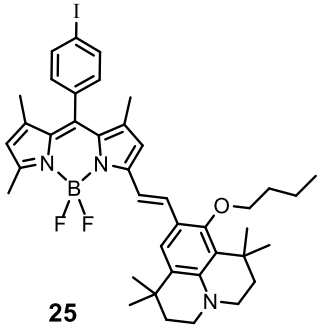

25

It was synthesized according to General Procedure A, starting from 4,4-difluoro-8-(4-iodo)-phenyl-1,3,5,7-tetramethyl-4-bora-3a,4a-diaza-s-indacene **15** (226 mg, 0.50 mmol). Column chromatography (SiO_2, CH_2Cl_2/petroleum ether: 4/6, v/v) and recrystallization from an ethanol/CH_2Cl_2 mixture gave **25** (220 mg, 58%) as a dark blue solid. R_f = 0.30 (CH_2Cl_2/petroleum ether: 4/6); ^{1}H NMR ($CDCl_3$, 300 MHz) δ: 0.99 (t, ^3J = 7.3 Hz, 3H), 1.33 (s, 6H), 1.41-1.42 (m, 9H), 1.46 (s, 3H), 1.52-1.57 (m, 2H), 1.70-1.74 (m, 4H), 1.80-1.90 (m, 2H), 2.58 (s, 3H), 3.16 (t, ^3J = 5.7 Hz, 2H), 3.23 (t, ^3J = 5.7 Hz, 2H), 3.83 (t, ^3J = 6.6 Hz, 2H), 5.95 (s, 1H), 6.58 (s, 1H), 7.08 (d, ^3J = 8.2 Hz, 2H), 7.32 (d, ^3J = 16.2 Hz, 1H), 7.37 (s, 1H), 7.42 (d, ^3J = 16.2 Hz, 1H), 7.83 (d, ^3J = 8.2 Hz, 2H); ^{13}C NMR ($CDCl_3$, 50 MHz) δ: 14.3, 14.1, 14.7, 14.7, 15.2, 19.6, 30.2, 31.0, 32.4, 32.4, 32.8, 36.6, 40.1, 47.0, 47.6,

94.6, 113.2, 113.3, 113.3, 113.3, 117.4, 118.3, 120.3, 120.3, 122.0, 123.6, 126.9, 130.7, 135.3, 136.4, 138.3, 139.5, 142.7, 144.7, 152.2, 156.6, 157.6; ^{11}B NMR ($CDCl_3$, 128 MHz) δ: 1.07 (t, $J_{B\text{-}F}$ = 32.6 Hz); MS (EI neat matter): *m/z* (intensity, %) calc. for [M]: 761.2 found: 761.1 (100); 688.2 (30), [M-(OC_4H_9)]; Anal. calc. for $C_{40}H_{47}BF_2IN_3O$: C, 63.09; H, 6.22; N, 5.52 found: C, 62.76; H, 6.04; N, 5.38.

Compound 26

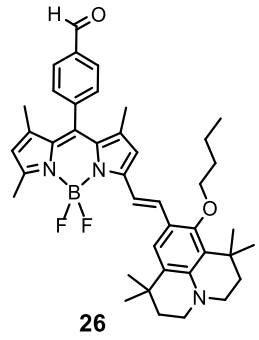

26

It was synthesized according to General Procedure B, starting from compound **25** (155 mg, 0.203 mmol). The crude residue so obtained was purified by column chromatography (SiO_2), eluting with toluene/CH_2Cl_2 (8/2, v/v) to give the desired compound as a dark blue solid (95 mg, 71%). R_f = 0.46 (toluene/ CH_2Cl_2: 8/2); ^{1}H NMR ($CDCl_3$, 300 MHz) δ: 0.98 (t, ^3J = 7.2 Hz, 3H), 1.33-1.42 (m, 18H), 1.51-1.57 (m, 2H), 1.73 (t, ^3J = 6.0 Hz, 4H), 1.81-1.88 (m, 2H), 2.59 (s, 3H), 3.16-3.24 (m, 4H), 3.83 (t, ^3J = 6.7 Hz, 2H), 5.96 (s, 1H), 6.59 (s, 1H), 7.46-7.48 (m, 3H), 7.54 (d, ^3J = 8.1 Hz, 2H), 8.02 (d, ^3J = 8.1 Hz, 2H), 10.12 (s, 1H); ^{13}C NMR ($CDCl_3$, 50 MHz) δ: 14.2, 14.4, 14.6, 15.0, 19.5, 29.74, 30.1, 30.8, 30.9, 32.3, 32.7, 36.4, 40.0, 46.9, 47.5, 113.1, 117.3, 118.4, 120.3, 121.9, 123.5, 125.3, 126.9, 128.3, 129.1, 129.8, 130.2, 132.8, 135.6, 135.8, 136.5, 137.9, 139.1, 142.2, 142.3, 142.4, 144.7, 152.3, 156.8, 157.6, 191.7; ^{11}B NMR ($CDCl_3$, 128 MHz) δ: 1.07 (t, $J_{B\text{-}F}$ = 33.2 Hz); MS (EI neat matter): *m/z* (intensity, %) calc. for [M]: 663.3 found: 663.2 (100); 590.2 (35), [M-(OC_4H_9)]; IR (cm^{-1}) ν: 701, 763, 976, 1061, 1116, 1156, 1194, 1254, 1290, 1317, 1464, 1497, 1532, 1581, 1702 (νCHO), 2869, 2927, 2957; Anal. calc. for $C_{41}H_{48}BF_2N_3O_2$: C, 74.20; H, 7.29; N, 6.33 found: C, 73.92; H, 6.98; N, 6.12.

Compound 27

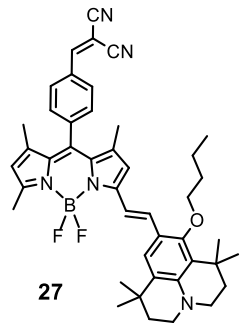

27

It was synthesized according to General Procedure C, starting from compound **29** (39 mg, 0.056 mmol). After cooling to room temperature, the precipitate formed during the reaction was isolated by centrifugation and washed several times with methanol, giving the product as a dark blue powder (20 mg, 50%). ^{1}H NMR ($CDCl_3$, 300 MHz) δ: 0.98 (t, ^3J = 7.3 Hz, 3H), 1.33-1.42 (s, 18H), 1.50-1.55 (m, 2H), 1.71-1.75 (m, 4H), 1.80-1.90 (m, 2H), 2.59 (s, 3H), 3.17 (t, ^3J =

5.8 Hz, 2H), 3.25 (t, ^{3}J = 5.8 Hz, 2H), 3.82 (t, ^{3}J = 6.7 Hz, 2H), 5.96 (s, 1H), 6.60 (s, 1H), 7.73-7.48 (m, 3H), 7.55 (d, ^{3}J = 8.2 Hz, 2H), 7.84 (s, 1H), 8.05 (d, ^{3}J = 8.3 Hz, 2H); ^{13}C NMR ($CDCl_3$, 100 MHz) δ: 14.3, 14.5, 14.6, 15.1, 19.5, 29.4, 29.7, 30.0, 30.8, 32.3, 32.3, 32.7, 36.4, 39.9, 46.9, 47.5, 75.9, 83.9, 112.5, 112.9, 113.5, 117.2, 118.7, 120.4, 121.9, 123.5, 126.9, 129.8, 130.0, 130.5, 131.1, 131.2, 132.7, 134.7, 135.9, 138.7, 142.2, 142.6, 144.8, 152.3, 157.1, 157.7, 158.9, 165.5; MS (EI neat matter): *m/z* (intensity, %) calc. for [M]: 711.4 found: 711.2 (100); 692.2 (30), [M-F]; ^{11}B NMR ($CDCl_3$, 128 MHz) δ: 1.04 (t, $J_{B\text{-}F}$ = 32.9 Hz); IR (cm^{-1}) ν: 702, 795, 854, 984, 1014, 1156, 1196, 1257, 1294, 1320, 1465, 1496, 1533, 1583, 2228 (νCN), 2963, 2961, 2926; Anal. calc. for $C_{44}H_{48}BF_2N_5O$: C, 74.26; H, 6.80; N, 9.84 found: C, 73.94; H, 6.62; N, 9.62.

Compound 30

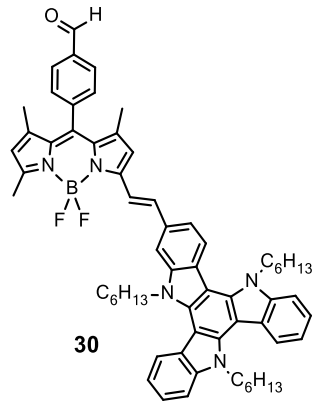

30

This compound was synthesized according to General Procedure B, starting from compound **29** (101 mg, 0.077 mmol). Flash chromatography from silica gel (toluene/ petroleum ether: 7/3, v/v) gave the product as a dark blue solid (78%, 73 mg). R_f = 0.48 (toluene/ petroleum ether: 7/3); ^{1}H NMR ($CDCl_3$, 300 MHz) δ: 0.78-0.85 (m, 9H), 1.19-1.43 (m, 25H), 1.93-2.04 (m, 6H), 2.66 (s, 3H), 4.88-4.96 (m, 6H), 6.04 (s, 1H), 6.73 (s, 1H), 7.35 (t, ^{3}J = 7.4 Hz, 2H), 7.43-7.50 (m, 3H), 7.55 (d, ^{3}J = 8.0 Hz, 2H), 7.62-7.70 (m, 3H), 7.71 (s, 1H), 7.85 (d, ^{3}J = 16.0 Hz, 1H), 8.04 (d, ^{3}J = 8.0 Hz, 2H), 8.22-8.29 (m, 3H), 10.12 (s, 1H); ^{11}B NMR ($CDCl_3$, 128 MHz) δ: 1.10 (t, $J_{B\text{-}F}$ = 32.6 Hz); MS (EI neat matter): *m/z* (intensity, %) calc. for [M]: 959.5 found: 959.3 (100); 940.3 (35), [M-F]; IR (cm^{-1}) ν: 706, 727, 794, 984, 1015, 1075, 1157, 1193, 1260, 1298, 1372, 1464, 1499, 1538, 1705 (νCHO), 2852, 2923, 2958; Anal. calc. for $C_{63}H_{68}BF_2N_5O$: C, 78.82; H, 7.14; N, 7.29 found: C, 78.54; H, 6.72; N, 6.82.

Compound 31

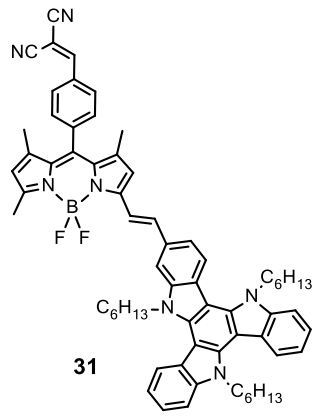

31

In a Schlenk tube equipped with a stir bar and charged with a solution of the aldehyde precursor **30** (68 mg, 0.056 mmoles) in THF (3 ml) was added the malonitrile (7 mg, 0.112 mmoles) and several drops of piperidine/acetic acid. The mixture was stirred at 95 °C during 20-30 minutes. After purification by column chromatography (SiO_2, toluene/CH_2Cl_2: 8/2, v/v), the product was obtained as a dark blue solid (22 mg, 50%). R_f = 0.64 (toluene/CH_2Cl_2: 8/2); ^{1}H NMR ($CDCl_3$, 400 MHz) δ: 0.78-0.85 (m, 9H), 1.21-1.33 (m, 18H), 1.41 (s, 3H), 1.47 (s, 3H), 1.94-2.03 (m, 6H), 2.65 (s, 3H), 4.91-4.98 (m, 6H), 6.05 (s, 1H), 6.76 (s, 1H), 7.36 (t, ^3J = 7.4 Hz, 2H), 7.46 (t, ^3J = 8.1 Hz, 2H), 7.54 (d, ^3J = 7.6 Hz, 1H), 7.58 (d, ^3J = 8.3 Hz, 2H), 7.36-7.66 (m, 2H), 7.69 (d, ^3J = 8.5 Hz, 1H),7.75 (s, 1H), 7.85 (d, ^3J = 16.2 Hz, 1H), 7.86 (s, 1H), 8.08 (d, ^3J = 8.3 Hz, 2H), 8.26 (d, ^3J = 8.5, 1H), 8.29 (d, ^3J = 7.9 Hz, 2H); ^{13}C NMR ($CDCl_3$, 50 MHz) δ: 13.9, 13.9, 14.1, 14.6, 14.9, 22.4, 22.5, 22.7, 26.3, 26.4, 29.3, 29.7, 31.4, 31.4, 31.4, 31.9, 47.1, 84.2, 110.3, 110.6, 119.3, 119.8, 119.8, 119.8, 121.4, 121.5, 121.6, 122.7, 123.3, 123.4, 124.6, 129.7, 130.2, 130.9, 131.3, 138.5, 138.8, 139.4, 140.9, 141.0, 141.2, 142.0, 154.5, 155.1, 158.7; ^{11}B NMR ($CDCl_3$, 128 MHz) δ: 1.07 (t, $J_{B\text{-}F}$ = 32.0 Hz); MS (EI neat matter): *m/z* (intensity, %) calc. for [M]: 1007.5 found: 1007.3 (100); 988.3 (20), [M-F]; IR (cm^{-1}) ν: 710, 727, 800, 984, 1018, 1039, 1077, 1158, 1194, 1299, 1373, 1409, 1463, 1500, 1540, 1589, 2229 (νCN), 2853, 2923, 2954; Anal. calc. for $C_{66}H_{68}BF_2N_7$: C, 78.63; H, 6.80; N, 9.73 found: C, 78.42; H, 6.62; N, 9.42.

Compound 33

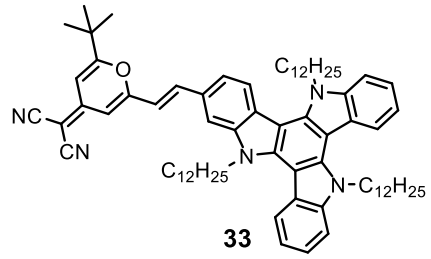

33

This compound was synthesized according to General Procedure A from a mixture of **22** (196 mg, 0.223 mmol) and 2-(2-*tert*-Butyl-6-methyl-4*H*-pyran-4-ylidene)malonitrile **24** (57 mg, 0.267 mmol). Flash Chromatography on silica gel (CH_2Cl_2/toluene: 2/8) and precipitation in cold pentane gave the desired product as a red thin powder (90 mg, 38%). R_f = 0.41 (CH_2Cl_2/toluene: 2/8); ^{1}H NMR ($CDCl_3$, 300 MHz) δ: 0.84-0.88 (m, 9H), 1.14-1.26 (m, 54H), 1.92-2.03 (m, 6H), 4.87-4.99 (m, 6H), 6.60 (d, ^4J = 1.9 Hz, 1H), 6.77 (d, ^4J = 1.9 Hz, 1H), 6.87 (d, ^3J = 15.3 Hz, 1H), 7.34-

7.38 (m, 2H), 7.47 (t, ^3J = 7.5 Hz, 2H), 7.54 (d, ^3J = 8.7 Hz, 1H), 7.63-7.65 (m, 3H), 7.70 (d, ^3J = 15.3 Hz, 1H), 8.25-8.30 (m, 3H); ^{13}C NMR ($CDCl_3$, 75 MHz) δ: 14.1, 22.7, 26.6, 26.6, 28.2, 29.2, 29.3, 29.5, 29.5, 29.5, 29.6, 29.8, 31.9, 36.7, 47.0, 58.9, 76.6, 102.6, 103.1, 103.3, 103.6, 106.5, 109.9, 110.6, 110.7, 115.4, 115.6, 116.3, 119.6, 119.9, 121.5, 121.6, 123.0, 123.2, 123.3, 125.5, 128.7, 138.5, 138.9, 139.6, 140.3, 140.9, 140.9, 141.0, 156.7, 159.5, 172.1; MS (EI neat matter): *m/z* (intensity, %) calc. for [M]: 1073.8 found: 1073.9 (100); 904.5 (25), [M-($C_{12}H_{25}$)]; IR (cm^{-1}) ν: 729, 795, 840, 926, 965, 1120, 1187, 1333, 1419, 1465, 1494, 1547, 1638, 2204 (νCN), 2852, 2922; Anal. calc. for $C_{74}H_{99}N_5O$: C, 82.71; H, 9.29; N, 6.52 found: C, 82.54; H, 8.97; N, 6.22.

Compound 34

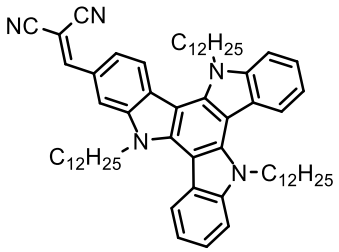

34

This compound was synthesized from a mixture of **22** (50 mg, 0.057 mmol) and malonitrile (8 mg, 0.114 mmol) following the General Procedure C. The reaction mixture was stirred for 10 minutes. Flash chromatography (SiO_2, CH_2Cl_2/petroleum ether: 3/7) and then precipitation into cold pentane gave the desired compound as a red thin powder (42 mg, 80%). R_f = 0.54 (CH_2Cl_2/petroleum ether: 3/7); ^{1}H NMR ($CDCl_3$, 300 MHz) δ: 0.88 (m, 9H), 1.17-1.26 (m, 51H), 1.84 (m, 2H), 1.98 (m, 4H), 4.67-4.76 (m, 4H), 4.85-4.91 (m, 2H), 7.33-7.40 (m, 2H), 7.46-7.56 (m, 3H), 7.60-7.64 (m, 2H), 7.73 (s, 1H), 7.97 (d, ^3J = 8.5 Hz, 1H), 8.16 (m, 2H), 7.97 (d, ^3J = 8.5 Hz, 1H); ^{13}C NMR ($CDCl_3$, 100 MHz) δ: 14.2, 22.7, 26.6, 29.2, 29.2, 29.3, 29.5, 29.6, 29.9, 30.1, 31.9, 47.1, 102.8, 103.3, 103.9, 110.9, 110.9, 111.7, 114.3, 115.1, 120.4, 120.5, 121.2, 121.5, 121.7, 123.1, 123.1, 123.4, 123.4, 123.7, 124.7, 128.4, 138.4, 140.1, 140.6, 140.9, 141.8, 159.7; MS (EI neat matter): *m/z* (intensity, %) calc. for [M]: 925.7 found: 925.5 (100); IR (cm^{-1}) ν: 724, 742, 806, 853, 1031, 1160, 1211, 1283, 1332, 1372, 1407, 1465, 1539, 1557, 1607, 2221 (νCN), 2851, 2920, 2952; Anal. calc. for $C_{64}H_{87}N_5$: C, 82.97; H, 9.47; N, 7.56 found: C, 82.75; H, 9.14; N, 7.35.

Compound 35

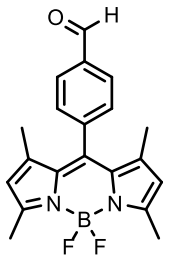

In a two-neck flask equipped with a reflux condenser, a gas bubbler and a magnetic stirring bar, [$Pd(PPh_3)_2Cl_2$] (10 mmol%) and sodium formate (1.2 equiv) were added to a solution of BODIPY **15** (112 mg, 0.248 mmol) in anhydrous DMF (8 ml). The reaction mixture was degassed under a continuous flow of CO at atmospheric pressure and stirred at 90°C for 3 hours. After cooling to room temperature, the mixture was extracted with dichloromethane and washed several times with water. The organic phase was dried over hygroscopic cotton wool and evaporated. The crude residue was then purified by flash chromatography using toluene/CH_2Cl_2: 8/2, v/v, as mobile phase and afforded the desired compound **35** as an orange solid (75 mg, 85%). R_f = 0.30 (toluene/CH_2Cl_2: 8/2); ^{1}H NMR ($CDCl_3$, 400 MHz) δ: 1.35 (s, 6H), 2.56 (s, 6H), 6.00 (s, 2H), 7.51 (d, ^3J = 8.1 Hz, 2H), 8.03 (d, ^3J = 8.0 Hz, 2H), 10.11 (s, 1H); ^{13}C NMR ($CDCl_3$, 100 MHz) δ: 14.6, 14.7, 121.6, 129.2, 130.4, 130.8, 136.7, 139.7, 141.4, 142.8, 156.3, 191.5; IR (cm^{-1}) ν: 702, 760, 800, 971, 1043, 1152, 1189, 1259, 1303, 1407, 1464, 1505, 1541, 1606, 1704 (νCHO), 2849, 2920, 2961; ^{11}B NMR ($CDCl_3$, 128 MHz) δ: 0.77 (t, J_{B-F} = 33.0 Hz); MS (EI neat matter): *m/z* (intensity, %) calc. for [M]: 352.2 found: 352.1 (100); 333.1 (20), [M-F]; Anal. calc. for $C_{20}H_{19}BF_2N_2O$: C, 68.21; H, 5.44; N, 7.95 found: C, 67.91; H, 5.24; N, 7.72.

Compound 36

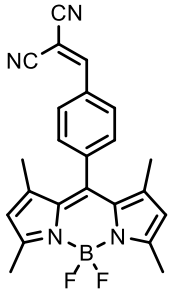

In a Schlenk tube equipped with a stirbar, malonitrile (1.2 equiv.) and several drops of piperidine/acetic acid were added to a suspension of the aldehyde **35** (40 mg, 0.113 mmol) in methanol (2.5 ml). The mixture was stirred at 95 °C for 20-30 minutes. The residue was purified by flash chromatography (SiO_2, CH_2Cl_2/petroleum ether: 7/3, v/v) and recrystallization from CH_2Cl_2/etchanol mixture yielding compound **36** as an orange solid (39 mg, 86%). R_f = 0.26 (CH_2Cl_2/petroleum ether: 7/3); ^{1}H NMR ($CDCl_3$, 300 MHz) δ: 1.38 (s, 6H), 2.56 (s, 6H), 6.01 (s, 2H), 7.52 (d, ^3J = 8.2 Hz, 2H), 7.84 (s, 1H), 8.06 (d, ^3J = 8.2 Hz, 2H); ^{13}C NMR ($CDCl_3$, 50 MHz) δ:14.8, 14.8, 29.8, 84.5, 112.5, 113.5, 121.9, 121.9, 129.9, 131.4, 131.5, 138.9, 141.8, 142.7, 156.7, 158.8; ^{11}B NMR ($CDCl_3$, 128 MHz) δ: 0.74 (t, J_{B-F} = 33.0 Hz); MS (EI neat matter): *m/z* (intensity, %) calc. for [M]: 400.2 found: 400.1 (100); 381.1 (15), [M-F]; IR (cm^{-1}) ν: 705, 759, 804, 833, 913, 967, 1047, 1153, 1183,

1263, 1306, 1362, 1407, 1463, 1508, 1540, 1593, 2229 (νCN), 2864, 2926, 2964; Anal. calc. for $C_{23}H_{19}BF_2N_4$: C, 69.02; H, 4.78; N, 14.00 found: C, 68.74; H, 4.56; N, 13.69.

Compound 38

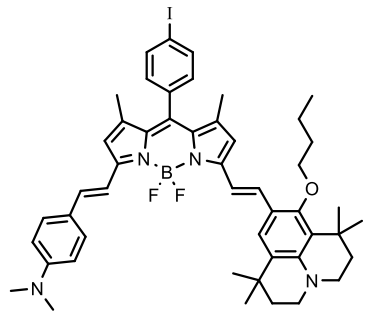

It was synthesized by reacting compound **39** (73 mg, 0.124 mmol) and julolidine aldehyde **17** (43 mg, 0.130 mmol) following General Procedure A. The dark green solids were purified by silica gel chromatography, eluting with toluene/CH_2Cl_2 (3/7), and recristallized from a pentane/CH_2Cl_2 mixture (73 mg, 75%). R_f = 0.76 (toluene/CH_2Cl_2: 3/7) ^{1}H NMR ($CDCl_3$, 300 MHz) δ: 0.99 (t, ^3J = 7.4 Hz, 3H), 1.37-1.46 (m, 18H), 1.52-1.59 (m, 2H), 1.72-1.77 (m, 4H), 1.82-1.89 (m, 2H), 3.03 (s, 6H), 3.20 (m, 4H), 3.84 (t, ^3J = 6.6 Hz, 2H), 5.95 (s, 1H), 6.59 (s, 2H), 6.71 (d, ^3J = 8.7 Hz, 2H), 7.01 (d, ^3J = 8.1 Hz, 2H) 7.45-7.56 (m, 7H), 7.83 (d, ^3J = 8.1 Hz, 2H); ^{13}C NMR ($CDCl_3$, 50 MHz) δ:14.3, 14.9, 15.1, 19.6, 29.8, 30.2, 31.2, 32.4, 32.7, 36.7, 40.2, 40.4, 47.0, 47.6, 94.4, 112.2, 113.9, 115.1, 117.2, 117.3, 122.0, 123.6, 125.3, 126.9, 129.1, 131.1, 134.0, 135.6, 136.1, 138.1, 139.9, 140.9, 144.3, 150.9, 152.3, 154.6, 157.4; ^{11}B NMR ($CDCl_3$, 128 MHz) δ: 1.31 (t, J_{B-F} = 33.4 Hz); MS (EI neat matter): *m/z* (intensity, %) calc. for [M]: 892.4 found: 892.2 (100); 873.2 (25), [M-F]; IR (cm^{-1}) ν: 697, 760, 800, 953, 990, 1062, 1106, 1162, 1256, 1286, 1319, 1362, 1489, 1533, 1586, 2858, 2925, 2952; Anal. calc. for $C_{49}H_{56}BF_2IN_4O$: C, 65.93; H, 6.32; N, 6.28 found: C, 65.72; H, 6.05; N, 5.93.

- **Experimental procedure - Chapter III**

Compound 44

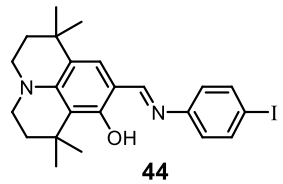

44

9-formyl-1,1,7,7-tetramethyl-2,3,6,7-tetrahydro-*1H,5H*-pyrido [3,2,1-ij] quinoline **17** (300 mg, 1.10 mmol) and 4-iodoaniline (360 mg, 1.64 mmol) were placed in a Schlenk tube and solubilized in anhydrous ethanol (15 mL). Then a crystal of p-TsOH was added under an argon flow. The resulting solution was stirred at 95 °C over night. After evaporation of the solvent the crude was treated with CH_2Cl_2 and washed several times with water. The organic layer was dried over anhydrous cotton wool, concentrated under vacuum and purified by column chromatography (SiO_2, CH_2Cl_2/petroleum ether: 5/5, v/v). The product was obtained as a yellow powder (300 mg, 75 %). ^{1}H NMR

($CDCl_3$, 300 MHz) δ: 1.27 (s, 6H), 1.49 (s, 6H), 1.71-1.79 (m, 4H), 3.18 (t, ^3J = 5.6 Hz, 2H), 3.27 (t, ^3J = 5.9 Hz, 2H), 6.96 (s, 1H), 6.98 (d, ^3J = 8.7 Hz, 2H), 7.65 (d, ^3J = 8.6 Hz, 2H), 8.34 (s, 1H), 13.87 (s, 1H); ^{13}C NMR ($CDCl_3$, 100 MHz) δ: 28.4, 30.9, 31.8, 32.2, 36.3, 39.9, 47.1, 47.5, 89.0, 109.1, 114.6, 122.7, 123.0, 128.4, 138.2, 146.7, 149.0, 160.6, 161.6; IR-ATR (cm^{-1}) ν: 488, 818, 944, 1029, 1216, 1309, 1514, 1576, 1619, 2854, 2926; EI-MS *m/z* (intensity, %) calc. for [M]: 474.1 found: 474.0 (100); Anal. calc. for $C_{23}H_{27}IN_2O$: C, 58.23; H, 5.74; N, 5.91 found: C, 57.98; H, 5.39; N, 5.59;

Compound 45

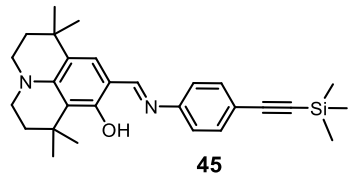

45

To the solution of **44** (300 mg, 0.63 mmol), [$Pd(PPh_3)_2Cl_2$] (44 mg, 0.06 mmol) and CuI (12 mg, 0.06 mmol) in THF (10 mL), TMS-acetylene (0.27 mL, 1.90 mmol) and DIPA (2 mL) were added. The reaction media was stirred at room temperature over night. After removing the solvent, the crude was solubilized in dichloromethane and washed with water. The organic phase was dried over hydrophilic cotton and concentrated under vacuum following purification from flash chromatography (SiO_2) eluting with petroleum ether/CH_2Cl_2, 7/3, v/v). The product was obtained as a brown powder quantitatively. ^{1}H NMR ($CDCl_3$, 400 MHz) δ: 0.26 (s, 9H), 1.27, (s, 6H), 1.50 (s, 6H), 1.72-1.79 (m, 4H), 3.19 (t, ^3J = 5.5 Hz, 2H), 3.27 (t, ^3J = 5.5 Hz, 2H), 6.97 (s, 1H), 7.16 (d, ^3J = 8.0 Hz, 2H), 7.46 (d, ^3J = 8.0 Hz, 2H), 8.38 (s, 1H), 13.94 (s, 1H,); ^{13}C NMR ($CDCl_3$, 100 MHz) δ: 0.0 [-Si(*C*H_3)$_3$], 28.3, 30.8, 31.7, 32.2, 36.3, 39.8, 47.0, 47.4, 94.1, 105.3, 109.2, 120.7, 122.7, 128.4, 132.9, 146.7, 149.1, 160.8, 161.3; 444.3; EI-MS *m/z* (intensity, %) calc. for [M]: 444.7 found: 444.1 (100); 372.1 (100); Anal. calc. for $C_{28}H_{36}N_2OSi$: C, 75.63; H, 8.16; N, 6.30 found: C, 75.43; H, 7.84; N, 6.01.

Compound 46

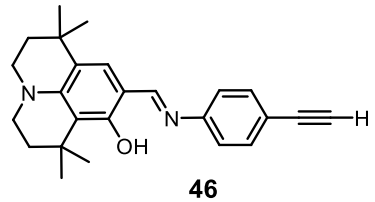

46

The solution of **45** (172 mg, 0.39 mmol) and KF (2.25 g, 38.67 mmol) in a mixture of THF (20 mL), MeOH (2 mL) and water (0.5 mL) was refluxed during 12 hours. Afterwards, the solvents were removed from under vacuum and the crude was solubilized in dichloromethane, neutralized with aqueous HCl (2M) and washed several times with water. The organic phase was dried under hydrophilic cotton and evaporated under vacuum. The crude was purified by silica flash chromatography, eluting with petroleum ether/CH_2Cl_2: 6/4 to 5/5, v/v) to give the

46 as a yellow powder (110 mg, 76 %). ^{1}H NMR ($CDCl_3$, 400 MHz) δ: 1.27 (s, 6H), 1.50 (s, 6H), 3.09 (s, 1H), 3.19 (t, ^{3}J = 5.8 Hz, 2H), 3.27 (t, ^{3}J = 5.8 Hz, 2H), 6.97 (s, 1H), 7.18 (d, ^{3}J = 4.2 Hz, 2H), 7.49 (d, ^{3}J = 4.2 Hz, 2H), 8.38 (s, 1H), 13.95 (s, 1H, O*H*); ^{13}C NMR ($CDCl_3$, 100 MHz) δ: 28.4, 30.8, 31.8, 32.2, 36.3, 39.9, 47.0, 47.5, 83.8, 109.2, 114.6, 118.5, 120.9, 122.7, 128.5, 133.2, 146.8, 149.6, 160.8, 161.6; DEPT 135 ($CDCl_3$, 100 MHz) CH_3, CH positive mode δ: 28.4, 30.8, 120.8, 128.5, 133.2 CH_2 negative mode δ: 36.3, 39.9, 47.0, 47.5; IR-ATR (cm^{-1}) ν: 781, 1156, 1193, 1236, 1305, 1501, 1585, 1609, 1739, 2096 [ν(C≡C), vw], 2923, 3239 [ν(Csp-H), m]; EI-MS *m/z* (intensity, %) calc. for [M]: 372.2 found: 372.1 (100); Anal. calc. for $C_{25}H_{28}N_2O$: C, 80.61; H, 7.58; N, 7.52 found: C, 80.24; H, 7.21; N, 7.04.

Compound 47

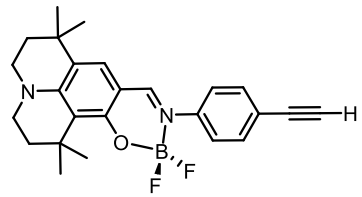

47

BF_3Et_2O (0.14 mL, 0.97 mmol) was added dropwise to a solution of **46** (120 mg, 0.32 mmol) in 1,2-dichloroethane (4 mL) under an argon flow. Afterwards the mixture was stirred for 20-30 minutes at room temperature, DIPEA (0.16 mL, 0.97 mmol) was added and the reaction mixture was stirred for additional 40 minutes at room temperature. After evaporation of the solvent, the crude was purified by column chromatography (SiO_2, CH_2Cl_2/petroleum ether: 8/2, v/v) and re-crystallized from a CH_2Cl_2/ethanol mixture giving the compound as orange solids (127 mg, 94 %). ^{1}H NMR ($CDCl_3$, 400 MHz) δ: 1.26 (s, 6H), 1.52 (s, 6H), 1.71-1.78 (m, 4H), 3.12 (s, 1H) 3.29-3.32 (m, 2H), 3.41 (t, ^{3}J = 6.1 Hz, 2H), 6.99 (s, 1H), 7.49 (ABq, ^{3}J = 32.3 Hz, ^{4}J = 8.5 Hz, 4H), 7.92 (s, 1H); ^{13}C NMR ($CDCl_3$, 100 MHz) δ: 28.1, 29.8, 31.7, 32.0, 35.2, 38.8, 47.5, 47.9, 83.1, 107.4, 114.8, 12.7, 122.9, 125.7, 127.5, 133.1, 143.6, 151.7, 157.2, 158.5; ^{11}B NMR (CD_3Cl, 128 MHz) δ: 0.95 (t, $J_{B\text{-}F}$ = 16.9 Hz); IR-ATR (cm^{-1}) ν: 507, 544, 781, 838, 979, 1021, 1156, 1192, 1236, 1305; 1454, 1500, 1585, 1609, 1739, 2095 [ν(C≡C), vw], 2849, 2923, 2955, 3239 [ν(Csp-H), m]; EI-MS: *m/z* (intensity, %) calc. for [M]: 420.2 found: 420.1 (100); 371.1 (80), [M-F]; Anal. calc. for $C_{25}H_{27}BF_2N_2O$: C, 71.44; H, 6.47; N, 6.67 found: C, 71.22; H, 6.27; N, 6.44.

Compound 48

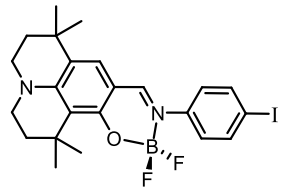

48

BF_3Et_2O (0.28 mL, 1.90 mmol) was added dropwise to a solution of **44** (150 mg, 0.32 mmol) in 1,2-dichloroethane (6 mL) under an argon flow. After this mixture had been stirred for 20-30 minutes at room temperature, DIPEA (0.16 mL, 0.966 mmol) was added and the reaction mixture was stirred for 3 hours at room temperature. After evaporation of the solvent, the crude was purified by silica column chromatography eluting with CH_2Cl_2 and re-crystallized from a slow evaporation of a mixture of CH_2Cl_2/ethanol providing **48** as yellow solids (155 mg, 89 %).^{1}H NMR ($CDCl_3$, 300 MHz) δ: 1.25 (s, 6H), 1.52 (s, 6H), 1.71-1.78 (m, 4H), 3.31 (t, ^{3}J = 5.7 Hz, 2H), 3.41 (t, ^{3}J = 6.0 Hz, 2H), 6.97 (s, 1H), 7.24 (d, ^{3}J = 8.6 Hz, 2H), 7.72 (d, ^{3}J = 8.6 Hz, 2H), 7.88 (s, 1H); ^{13}C NMR ($CDCl_3$, 100 MHz) δ: 28.1, 29.8, 31.7, 32.0, 35.2, 38.9, 47.5, 47.9, 91.8, 107.4, 114.8, 124.9, 125.7, 127.5, 138.3, 143.2, 151.6, 157.2, 158.4; DEPT ($CDCl_3$, 100 MHz) CH_3, CH positive mode δ: 28.1, 29.8, 124.9, 127.5, 138.3, 157.2, negative mode (CH_2) δ: 35.2, 38.9, 47.5, 47.9; ^{11}B NMR (CD_3Cl, 128 MHz) δ: 0.91 (t, $J_{B\text{-}F}$ = 17.4 Hz); IR-ATR (cm^{-1}) ν: 488 (Csp^2-I), 780, 818, 944, 1029, 1216, 1309 vs, 1514 vs, 1576, 1620, 2924; EI-MS: *m/z* (intensity, %) calc. for [M]: 522.1 found: 522.1 (80), 473.0 (100) [M-BF_2]; Anal. calc. for $C_{23}H_{26}BF_2IN_2O$: C, 52.90; H, 5.02; N, 5.36 found: C, 51.60; H, 5.39; N, 5.04.

Compound 50

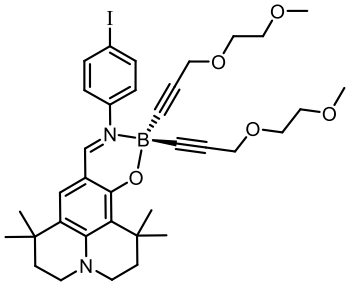

50

Ethyl magnesium bromide (0.6 mL, 0.54 mmol) and ethylene glycol methyl ether acetylene (90 µL, 0.72 mmol) were added to freshly distilled THF and stirred for 2 hours at 60 °C. After cooling to room temperature, the solution was added *via* cannula to a solution of compound **48** (100 mg, 0.18 mmol), in THF. The mixture was stirred overnight at 60 °C. After cooling to room temperature, the solution was quenched with a solution of HCl (1M) before being washed several times with water. The combined organic layer was collected and purified by column chromatography (Al_2O_3 de-activated with 6% (w/w) of H_2O, dichloromethane). The product was obtained as yellow oil (40 mg, 31 %). R_f = 0.4 (dichloromethane). ^{1}H NMR (CD_3CN, 300 MHz) δ: 1.29 (s, 6H), 1.49 (s, 6H), 1.99-2.01 (m, 4H), 3.32 (s, 6H), 3.52-3.93 (m, 2H), 3.42-3.46 (m, 10H), 4.05 (s, 4H), 7.15 (s, 1H), 7.43 (d, ^{3}J = 8.7 Hz, 2H), 7.82 ((d, ^{3}J = 8.7 Hz, 2H), 7.95 (s, 1H); ^{13}C NMR (CD_3CN, 100 MHz) δ:

27.7, 28.9, 31.4, 31.6, 34.9, 38.3, 46.9, 47.5, 57.9, 58.5, 68.1, 71.4, 90.9, 108.2, 114.9, 125.1, 125.4, 128.5, 137.7, 145.2, 151.7, 157.2, 158.2; ^{11}B NMR (CD_3Cl, 128 MHz) δ: - 0.7 (s); MS-EI *m/z* (intensity, %) calc. for [M]: 710.24 found 710.1; Anal. calc. for $C_{35}H_{44}BIN_2O_5$: C, 59.17; H, 6.24; N, 3.94 found: C, 58.88; H, 5.91; N, 3.70.

Compound 51

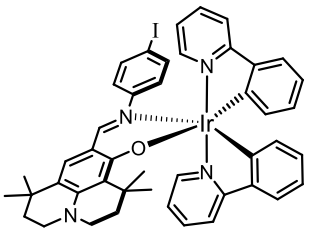

51

To the suspension of $[(ppy)_2Ir\text{-}(\mu\text{-}Cl)]_2$ (145 mg, 0.14 mmol) in MeOH (1mL) and 1,2-dichloroethane (4 mL) were added compound **44** (80 mg, 0.17 mmol) and NEt_3 (71 µL, 0.51 mmol). The mixture was placed at 80 °C during 2 days. After cooling down to ambient temperature, dichloromethane was added and the organic phase was washed with water. The organic layer was dried over hydrophilic cotton and concentrated under vacuum. The crude was purified by precipitation in a CH_2Cl_2/MeOH mixture giving **51** as an orange powder (118 mg, 72 %). ^{1}H NMR ($CDCl_3$, 400 MHz) δ: 0.63 (s, 3H), 1.19 (s, 3H), 1.20 (s, 3H), 1.23 (s, 3H), 1.48-1.57 (m, 2H), 1.68 (t, ^3J = 5.8 Hz, 2H), 2.93-3.04 (m, 2H), 3.12 (t, ^3J = 5.8 Hz, 2H), 5.94 (d, *J* = 8.4 Hz, 2H), 6.19 (d, *J* = 7.5 Hz, 1H), 6.33 (d, *J* = 7.5 Hz, 1H), 6.53 (t, ^3J = 7.2 Hz, 1H), 6.60 (t, ^3J = 7.2 Hz, 1H), 6.68-6.72 (m, 2H), 6.82 (t, ^3J = 7.5 Hz, 1H), 6.98 (d, ^3J = 8.4 Hz, 2H), 7.00-7.07 (m, 2H), 7.11 (d, *J* = 7.6 Hz, 1H), 7.51-7.54 (m, 2H), 7.58-7.67 (m, 2H), 7.70 (s, 1H), 7.81 (d, *J* = 8.0 Hz, 1H), 8.85-8.89 (m, 2H); ^{13}C NMR ($CDCl_3$, 100 MHz) δ: 27.5, 28.5, 31.1, 31.2, 31.6, 32.1, 36.9, 40.6, 47.2, 47.4, 87.6, 113.1, 117.5, 117.6, 118.3, 119.3, 119.8, 120.6, 120.9, 121.5, 123.2, 123.6, 125.3, 128.7, 128.9, 131.0, 132.7, 133.0, 136.0, 136.1, 144.3, 145.1, 147.6, 148.5, 149.7, 152.6, 153.4, 159.2, 164.7, 168.7, 169.5; DEPT ($CDCl_3$, 100 MHz) CH_3, CH positive mode δ: 27.5, 28.5, 31.1, 31.2, 117.6, 118.3, 119.3, 120.6, 120.9, 121.5, 123.2, 123.6, 125.3, 128.7, 128.9, 131.1, 132.7, 133.0, 136.0, 136.1, 148.5, 149.7, 159.2, negative mode (CH_2) δ: 36.9, 40.6, 47.2, 47.4; IR-ATR (cm^{-1}) ν: 488, 728, 753, 1003, 1183, 1308, 1422, 1475, 1564, 2849, 2920, 3039; MS-EI: *m/z* (intensity, %) calc. for [M]: 974.2 found: 974.2; Anal. calc. for $C_{45}H_{42}IIrN_4O$: C, 55.49; H, 4.35; N, 5.75 found: C, 55.38; H, 4.18; N, 6.72.

Compound 52

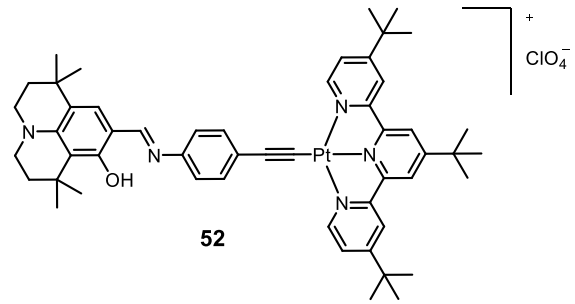

52

$^{i}Pr_2NH$ (1 mL) was added to a solution of **46** (25 mg, 0.067 mmol) and [(^{t}Bu-*ter*-Pyr)$_3$PtCl](BF$_4$) (48 mg, 0.067 mmol) in THF (5mL). After stirring 10 minutes at room temperature, a small pearl of CuI was added to the solution under an atmosphere of argon and the mixture was continued stirring at room temperature over night. After evaporation of the solvents, a solution of lithium perchlorate $LiClO_4$ (285 mg, 2.68 mmol) in water (15 mL) was added dropwise to a stirring DMF (5 mL) solution of the crude. Finally the mixture was stirred at room temperature for an additional hour and filtered through a filter paper. The crude was purified from aluminum (activated with 6 % H_2O w/w) column chromatography, eluting with CH_2Cl_2/MeOH to give the title compound as a brown powder (50 mg, 70 %). ^{1}H NMR ($CDCl_3$, 400 MHz) δ: 1.12 (t, ^{3}J = 7.0 Hz, 4H), 1.23 (s, 5H), 1.36 (s, 17H), 1.49-1.52 (m, 2H), 1.59 (s, 8H), 1.66-1.68 (m, 2H), 1.78 (s, 5H) 2.82-2.88 (m, 4H), 3.01-3.02 (m, 2H); 3.27 (dd, *J* = 14.2 Hz, *J* = 7.1 Hz, 3H), 6.44 (d, *J* = 6.0 Hz, 2H), 6.91 (s, 1H), 7.95 (d, *J* = 8.3, 2H), 8.18 (s, 1H, -C*H*N), 8.63 (s, 2H), 8.66 (s, 2H), 8.91 (d, *J* = 6.0 Hz, 2H), 14.7 (s, 1H, -O*H*); ^{13}C NMR ($CDCl_3$, 100 MHz) δ:28.4, 29.7, 30.2, 30.4, 30.5, 31.8, 32.3, 36.3, 36.5, 37.5, 39.9, 47.1, 47.5, 97.7, 104.7, 109.3, 114.6, 120.6, 120.8, 121.6, 121.9, 122.7, 123.0, 123.2, 123.3, 124.9, 125.5, 125.6, 128.3, 129.7, 132.9, 133.0, 146.6, 147.4, 151.0, 153.9, 154.0, 154.2, 158.4, 158.8, 160.7, 160.8, 167.3, 167.9, 168.3, 168.4; DEPT ($CDCl_3$, 100 MHz) positive (CH_3, CH) δ: 28.4, 30.2, 30.4, 30.5, 30.9, 120.6, 121.6, 123.0, 123.1, 125.0, 125.4, 128.3, 132.9, 154.0, 160.7 negative (CH_2) δ: 36.3, 40.0, 47.0, 47.5; IR-ATR (cm^{-1}) ν: 608, 621, 727, 841, 1080, 1197, 1312, 1614, 1668, 1723, 2916, 2958; MS-ES: *m/z* (intensity, %) calc. for [M]: 1066.4 found: 967.3 (100), [M-ClO_4]; 371.1 (80), [M-F]; Anal. calc. for $C_{52}H_{62}ClN_5O_5Pt$: C, 58.50; H, 5.85; N, 6.56 found: C, 58.32; H, 5.64; N, 6.27.

Compound 53

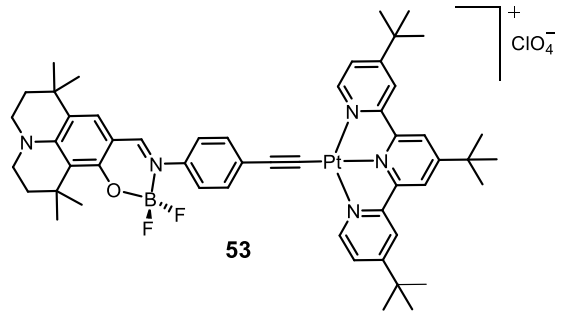

53

DIPA (1 mL) was added to the solution of **46** (20 mg, 0.047 mmol) and [Pt(^{t}Bu-^{t}Pyr)$_3$Cl](BF$_4$) (34 mg, 0.049 mmol) in THF (5mL). After 10 minutes under stirring at room temperature, a small pearl of CuI was added to the solution under an argon atmosphere and the mixture was continued stirring at room temperature over night. After evaporation of the solvents, a solution of Lithium perchlorate $LiClO_4$ (200 mg, 1.880 mmol) in water (13 mL) was added dropwise to a stirring DMF (2 mL) solution of the crude. The mixture was stirred for an additional hour and filtered through a filter paper. The crude was purified from aluminum (activated with 6 % H_2O) column chromatography, eluting with CH_2Cl_2/EtOH 1 % to give the desired product as a red powder quantitatively. ^{1}H NMR ($CDCl_3$, 400 MHz) δ: 1.27 (s, 6H), 1.40 (s, 9H), 1.51 (s, 18H), 1.58 (s, 6H), 1.71-1.72 (m, 2H), 1.78-1.82 (m, 2H), 3.31-3.35 (m, 2H), 3.39-3.43 (m, 2H), 7.11-7.19 (m, 5H), 7.65-7.76 (m, 2H), 7.94 (s, 1H), 8.16-8.17 (m, 2H), 8.21 (s, 2H), 9.16 (d, ^3J = 6.0 Hz, 2H); ^{13}C NMR ($CDCl_3$, 100 MHz) δ: 28.3, 29.7, 29.8, 30.3, 30.4, 30.4, 31.8, 32.0, 35.4, 36.4, 37.1, 39.0, 47.4, 47.9, 53.4, 101.5, 104.4, 107.4, 114.3, 121.4, 122.4, 122.9, 125.3, 125.7, 128.3, 132.7, 141.3, 151.4, 153.7, 157.5, 157.9, 158.8, 166.5, 167.2 ^{11}B NMR (CD_3CN, 128 MHz) δ: 0.92 (t, $J_{B\text{-}F}$ = 17.6 Hz); IR-ATR (cm^{-1}) ν: 622, 843, 1084, 1209, 1312, 1501, 1584, 1618, 2109 [ν(C≡C), vw], 2959; MS-ES: *m/z* (intensity, %) calc. for [M]: 1114.4 found: 1015.4 (100), [M-ClO_4]; Anal. calc. for $C_{52}H_{61}BClF_2N_5O_5Pt$: C, 55.99; H, 5.51; N, 6.28 found: C, 55.74; H, 5.21; N, 6.04.

Compound 54

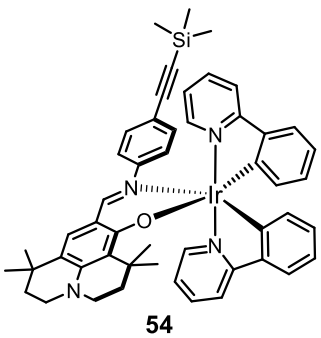

54

Compound **51** (70 mg, 0.07 mmol), [Pd(PPh$_3$)$_2$Cl$_2$] (18 mg, 0.01 mmol) and CuI (1.5 mg, 0.01 mmol) were placed in a THF (5 mL) solution before addition of ^{i}Pr$_2$NH (0.5 mL) and TMS-acetylene (26 µL , 0.18 mmol) under an argon flow. The reaction media was stirred at room temperature over night. Than evaporation of the solvent and purification of the crude by aluminum column chromatography activated with 6 % of water and eluting with petroleum ether/CH_2Cl_2: 8/2, v/v. The desired compound was obtained

quantitatively as an orange powder. ^{1}H NMR (C_6D_6, 400 MHz) δ: 0.17 (s, 9H), 1.05 (s, 3H), 1.17 (s, 3H), 1.18 (s, 3H), 1.27-1.31 (m, 2H), 1.40 (t, ^{3}J = 5.9 Hz, 2H), 2.66-2.81 (m, 4H), 6.21 (t, ^{3}J = 6.7 Hz, 1H), 6.26 (d, ^{3}J = 8.3 Hz, 2H), 6.31 (t, ^{3}J = 6.7 Hz, 1H), 6.55-6.66 (m, 3H), 6.72 (d, ^{3}J = 7.3 Hz, 1H), 6.89 (t, ^{3}J = 7.6 Hz, 1H), 6.94 (d, ^{3}J = 8.2 Hz, 1H), 6.97 (d, ^{3}J = 8.3 Hz, 1H), 7.09 (d, ^{3}J = 8.3 Hz, 2H), 7.35 (d, ^{3}J = 8.2 Hz, 1H), 7.50 (d, ^{3}J = 7.4 Hz, 1H), 7.76 (s, 1H), 8.89 (d, ^{3}J = 5.5 Hz, 1H), 8.96 (d, ^{3}J = 5.5 Hz, 1H); ^{13}C NMR (C_6D_6, 100 MHz) δ: 0.01, 28.1, 29.1, 31.2, 31.7, 32.6, 37.1, 41.2, 47.3, 93.4, 106.2, 113.9, 117.7, 118.0, 118.2, 118.8, 119.8, 120.4, 120.7, 121.2, 121.3, 123.7, 123.9, 124.1, 129.3, 129.4, 131.3, 131.5, 133.2, 133.6, 135.7, 135.9, 144.5, 145.4, 148.1, 148.4, 149.7, 153.0, 153.7, 153.8, 159.3, 165.2, 169.1, 169.9; IR-ATR (cm^{-1}) ν: 728, 753, 1003, 1182, 1308, 1422, 1475, 1565, 2824, 2916, 3039; MS-ES: *m/z* (intensity, %) calc. for [M]: 944.3 found: 944.2 (100), 872.3 (30) [M-Si(CH_3)$_3$]; Anal. calc. for $C_{50}H_{51}IIrN_4OSi$: C, 63.60; H, 5.44; N, 5.93 found: C, 63.42; H, 5.18; N, 5.77.

Compound 55

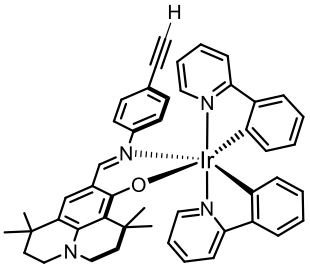

55

The desired compound **55** was prepared following the same procedure as applied to compound **46**. Purification of the crude by column chromatography Al_2O_3 (6 % water w/w), eluting with petroleum ether/CH_2Cl_2: 7/3, v/v gave the complex as deep orange solids. ^{1}H NMR (C_6D_6, 400 MHz) δ: 1.05 (s, 3H), 1.18 (s, 3H), 1.19 (s, 3H), 1.38-1.42 (m, 2H), 1.53-1.60 (m, 2H; s, 3H); 2.64 (s, 1H), 2.67-2.82 (m, 4H), 6.20-6.24 (m, 3H), 6.29-6.32 (m, 1H), 6.55 (dd, ^{3}J = 7.4 Hz, ^{4}J = 1.2 Hz, 1H), 6.60 (td, ^{3}J = 7.2 Hz, ^{4}J = 1.3 Hz, 1H), 6.72 (dd, ^{3}J = 7.4 Hz, ^{4}J = 1.2 Hz, 1H), 6.77-6.91 (m, 5H), 6.93-6.97 (m, 2H), 7.00 (d, ^{3}J = 8.4 Hz, 2H), 7.35 (d, ^{3}J = 8.3 Hz, 1H), 7.51 (d, ^{3}J = 7.6 Hz, 1H), 7.76 (s, 1H), 8.89 (d, ^{3}J = 5.5 Hz, 1H), 8.96 (d, ^{3}J = 5.5 Hz, 1H); ^{13}C NMR (C_6D_6, 100 MHz) δ: 27.9, 28.9, 31.0, 31.4, 32.4, 36.9, 41.0, 47.1, 76.9, 83.8, 113.6, 117.4, 117.5, 117.8, 118.0, 119.5, 120.1, 120.5, 120.9, 121.1, 123.4, 123.6, 123.8, 129.1, 131.1, 131.3, 133.0, 133.4, 135.6, 144.2, 145.1, 147.9, 147.2, 149.4, 152.8, 153.5, 153.6, 156.0, 164.9, 168.8, 169.6; IR-ATR (cm^{-1}) ν: 728, 753, 824, 1029, 1193, 1308, 1475, 1568, 1604, 2106 [ν(C≡C), vw], 2843, 2920, 3037, 3285 [ν(Csp-H]; MS-ES: *m/z* (intensity, %) calc. for [M]: 872.3 found: 872.3 (100); Anal. calc. for $C_{47}H_{43}IrN_4O$: C, 64.73; H, 4.97; N, 6.42 found: C, 64.50; H, 4.66; N, 6.30;

Compound 56

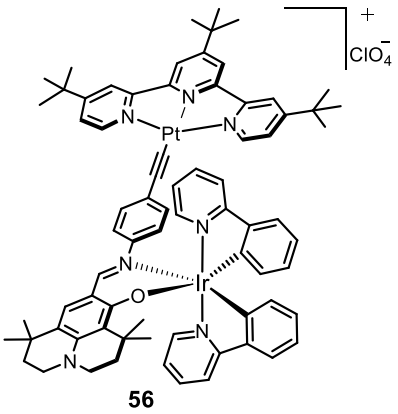

56

To the suspension of $[(ppy)_2Ir\text{-}(\mu\text{-}Cl)]_2$ (20 mg, 0.02 mmol) and **52** (40 mg, 0.04 mmol) in a MeOH (2 mL) and 1,2-dichloroethane (6 mL) mixture, $^{i}Pr_2NH$ was added and the mixture was stirred at 60 °C over night. After concentration of the solvents, the crude was purified by column chromatography Al_2O_3 (6 % water w/w), eluting with CH_2Cl_2/MeOH 5% to give **56** as dark fine powder (53 mg, 90 %). ^{1}H NMR (CD_3CN, 400 MHz) δ: 0.58 (s, 3H), 1.16 (s, 3H), 1.20 (s, 3H), 1.21 (s, 3H), 1.45 (s, 19H), 1.51-1.55 (s, 9H; m, 2H), 1.65 (t, ^3J = 5.8 Hz, 2H), 2.93-3.04 (m, 2H), 3.14 (t, ^3J = 5.8 Hz, 2H), 6.14-6.19 (m, 2H), 6.31 (d, ^3J = 8.3 Hz, 1H), 6.45 (t, ^3J = 7.2 Hz, 1H), 6.55 (t, ^3J = 7.2 Hz, 1H), 6.64 (t, ^3J = 7.2 Hz, 1H), 6.79 (t, ^3J = 7.2 Hz, 1H), 6.84 (d, ^3J = 8.2 Hz, 2H), 6.89 (s, 1H), 7.17-7.23 (m, 2H), 7.26 (d, ^3J = 7.6 Hz, 1H), 7.54 (dd, ^3J = 6.0 Hz, ^4J = 1.8 Hz, 2H), 7.60 (d, ^3J = 7.8 Hz, 1H), 7.67-7.73 (m, 2H), 7.80 (t, ^3J = 7.9 Hz, 1H), 7.87 (s, 1H), 7.96 (d, ^3J = 7.8 Hz, 1H), 8.36 (s, 1H), 8.36 (s, 1H), 8.39 (s, 2H), 8.77 (d, ^3J = 6.0 Hz, 2H), 8.80 (d, ^3J = 5.7 Hz, 1H), 8.97 (d, ^3J = 5.7 Hz, 1H); ^{13}C NMR (CD_3CN, 100 MHz) δ: 27.0, 28.1, 29.3, 29.7, 30.2, 30.3, 31.3, 31.8, 36.1, 36.7, 37.1, 40.4, 46.6, 47.0, 54.2, 113.1, 118.6, 119.2, 119.9, 120.7, 121.4, 122.0, 123.2, 123.6, 125.8, 128.3, 128.5, 130.7, 131.6, 132.2, 133.1, 136.9, 137.0, 144.8, 145.6, 147.7, 148.0, 149.9, 152.4, 152.7, 153.6, 153.8, 154.1, 158.8, 159.8, 164.1, 167.0, 167.5, 168.6, 169.1; IR-ATR (cm^{-1}) ν: 556, 729, 755, 835, 1030, 1192, 1309, 1422, 1476, 1573, 1605, 1662, 1729, 2922 ; MS-ESI: *m/z* (intensity, %) calc. for [M]: 1574.14 found: 1532.3 (100); Anal. calc. for $C_{74}H_{77}ClIrN_7O_5Pt$: C, 56.71; H, 4.95; N, 6.26 found: C, 56.81; H, 5.28; N, 6.48;

- **Experimental procedures - Chapter IV**

Compound 57 was prepared according to ref. 164a: Tomasulo, M.; Sortino, S.; Raymo, F. M. *J. Org. Chem*. **2008**, *73*, 118.

Compound 60 (Procedure I) was prepared inspired by ref 164a and 164b: (b) Petersen, M. A.; Deniz, E.; Bronsted Nielsen, M.; Sortino, S.; Raymo, F. M. *Eur. J. Org. Chem*. **2009**, *2009*, 4333.

Compound 60

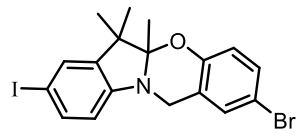

60

Procedure I:[164] PBr_3 (0.15 mL, 1.603 mmol) was added dropwise to a solution of 5-bromo-2-hydroxybenzyl alcohol (217 mg, 1.069 mmol) in CH_3CN under argon, maintained at 0 °C and stirring for 30 min. Than a solution of 3*H*- indol **57** (305 mg, 1.069) in CH_3CN was added and the final mixture was cooled down to ambient temperature and stirred for 3-4 days. Sodium phosphate buffer (pH = 7) was added to the reaction mixture which was then extracted with CH_2Cl_2. Organic phase was washed one more time with sodium phosphate buffer, brine and water. It was dried under anhydrous cotton wood, concentrated under vacuum and purified by column chromatography (SiO_2, CH_2Cl_2/petroleum ether: 5/5, v/v) giving the product as colorless oil (100 mg, 21 %).

Procedure II: 5-bromo-2-hydroxybenzyl alcohol (1 eq) was solubilised in anhydrous 1,2-dichloroethane and dropwise addition of thionyl chloride (0.7 eq) was followed under an argon flux. The solution was stirred at 75 °C during 30 min. After cooling down to room temperature, a solution of 3*H*- indol **57** (1.2 eq) in anhydrous 1,2-dichloroethane was added within the reaction media and the final mixture was stirred at 75 °C during 5 to 12h. After cooling down to room temperature, dichloroethane was added to the reaction mixture and washed with a saturated solution of $NaHCO_3$ and water (3 times). The organic phase was dried with anhydrous Na_2SO_4 and evaporated under vacuum. The crude was purified over a silica column chromatography as described in Procedure I. ^{1}H NMR (C_6D_6, 300 MHz) δ: 0.67 (s, 3H), 0.91 (s, 3H), 1.09 (s, 3H), 3.66 (ABq, ^2J = 15.0 Hz, 2H), 5.67 (d, , ^3J = 8.1 Hz, 1H), 6.16 (d, ^3J = 8.3 Hz, 1H), 6.72-6.76 (m, 2H), 7.1 (dd, , ^3J = 8.1 Hz, , ^4J = 1.5 Hz, 1H), 7.19-7.20 (m, 1H); ^{13}C NMR (C_6D_6, 100 MHz) δ: 15.6, 18.6, 25.5, 39.8, 47.9, 82.0, 100.6, 110.8, 112.4, 119.7, 120.6, 127.7, 128.0, 128.3, 129.7, 131.2, 131.4, 136.6, 141.5, 147.4, 152.3; EI-MS *m/z* (intensity, %) calc. for [M]: 468.9 and [M+2] 470.95 found: 469.0 and 471.0(100); Anal. calc. for $C_{18}H_{17}BrINO$: C, 45.98; H, 3.64; N, 2.98 found: C, 45.72; H, 3.41; N, 2.77.

Compound 72

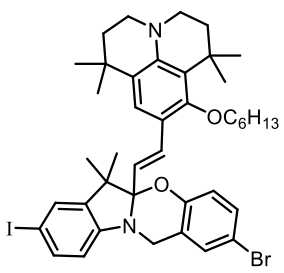

The solution of compounds **2** (25 mg, 0.056 mmol) and 9-formyl-10-hex oxy-1,1,7,7-tétramethyl-2,3,6,7-tetrahydro-*1H,5H*-pyrido [3,2,1-ij] quinolizidine **18** (24 mg, 0.068 mmol) and TFA (40 µl, 0.392 mmol) was stirred at room temperature during 12 hours. After cooling down to ambient temperature the solvent was evaporated under reduced pressure. The crude was dissolved in CH_2Cl_2 and washed several times with water. The organic phase was dried over anhydrous Na_2SO_4, the solvent evaporated under reduced pressure and the residues purified over a short column chromatography (de-activated Al_2O_3 with 6% H_2O w/w) eluting with CH_2Cl_2 than CH_2Cl_2/MeOH 1%. The product was obtained as oil solidifying under vacuum (43 mg, 95%). ^{1}H NMR (C_6D_6, 400 MHz) δ: 0.93 (t, ^3J = 7.1 Hz, 3H), 1.14 (s, 3H), 1.18 (s, 3H), 1.20 (s, 3H), 1.22-1.36 (m, 8H), 1.38 (s, 3H), 1.43 (s, 3H), 1.49-1.53 (m, 2H), 1.56 (s, 3H), 1.58-1.75 (m, 4H), 2.75-2.88 (m, 4H), 3.62 (t, ^3J = 7.1 Hz, 2H), 3.84, 4.20 (ABq J_{AB} = 17.3 Hz, 2H), 5.93 (d, ^3J = 8.7 Hz, 1H), 6.23 (d, ^3J = 16.3 Hz, 1H), 6.50 (d, ^3J = 8.7 Hz, 1H), 6.84 (d, ^2J = 2.2 Hz, 1H), 6.91 (dd, ^3J = 8.8 Hz, ^2J = 2.4 Hz, 1H), 7.28 (d, ^3J = 16.3 Hz, 1H), 7.29 (dd, ^3J = 8.2 Hz, ^2J = 1.7 Hz, 1H), 7.40 (d, ^2J = 1.7 Hz, 1H), 7.47 (s, 1H); ^{13}C NMR (C_6D_6, 100 MHz) δ: 14.0, 18.1, 22.8, 25.8, 26.0, 30.1, 30.0, 30.1, 30.3, 31.1, 31.4, 32.0, 32.0, 32.7, 36.9, 40.3, 40.6, 46.7, 47.1, 49.8, 75.0, 81.8, 102.5, 110.9, 112.0, 117.7, 118.0, 118.9, 121.5, 122.5, 123.0, 126.6, 126.9, 126.9, 128.3, 128.5, 129.4, 130.8, 131.1, 133.0, 136.3, 141.6, 143.4, 147.1, 152.6, 156.6; DEPT 135 (C_6D_6, 100 MHz) δ CH_2: 14.0, 18.1, 26.1, 30.2, 30.4, 31.1, 31.4 ; δ CH_3, CH : 22.8, 25.8, 30.1, 32.0, 40.3, 40.6, 46.7, 47.2, 75.0, 110.9, 118.0, 118.9, 122.9, 129.4, 130.8, 131.1, 133.0, 136.3; EI-MS: *m/z* (intensity, %) calc. four [M] 808.2 and [M+2] 810.21 found 808.1and 810.1 due to ^{79}Br and ^{81}Br; 681.1 (30) [M-I]; Anal. calc. Four $C_{41}H_{50}BrIN_2O_2$: C, 60.82; H, 6.22; N, 3.46 found: C, 60.66; H, 5.84; N, 3.22.

Compound 61 to **71** were prepared following the same general procedure as **72**

Compound 61

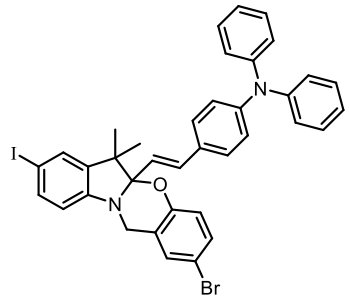

(35 mg, 33%). ^{1}H NMR ($CDCl_3$, 400 MHz) δ: 1.17 (s, 3H), 1.47 (s, 3H), 4.43 (ABq, J_{AB} = 17.3 Hz, 2H), 6.14 (d, ^{3}J = 16.0 Hz, 1H), 6.38 (d, ^{3}J = 8.0 Hz, 1H), 6.70 (d, ^{3}J = 24.0 Hz, 1H), 6.69 (s, 1H), 6.70-6.09 (m, 8H), 7.12-7.17 (m, 2H), 7.23-7.25 (m, 4H), 7.35-7.38 (m, 2H); RMN ^{13}C ($CDCl_3$, 100 MHz) δ: 18.4, 26.4, 29.7, 40.7, 49.9, 81.6, 101.9, 110.9, 112.2, 119.1, 121.4, 121.7, 123.2, 124.6, 127.7, 129.3, 129.6, 130.8, 131.2, 135.5, 136.2, 141.4, 147.0, 147.4, 148.1, 152.4; DEPT 135 δ: CH_3, CH: 18.1, 26.0, 110.9, 118.8, 121.9, 123.1, 123.7, 124.5, 127.8, 128.0, 129.3, 129.5, 130.8, 131.1, 135.4, 136.4; CH_2 δ: 40.2; MS-EI: *m/z* (intensity, %) calc. for [M]: 724.1 and [M+2] 726.06 found 724.0 and 724.0; Anal. calc. four $C_{37}H_{30}BrIN_2O$: C, 61.26; H, 4.17; N, 3.86 found: C, 60.92; H, 3.82; N, 3.62.

Compound 62

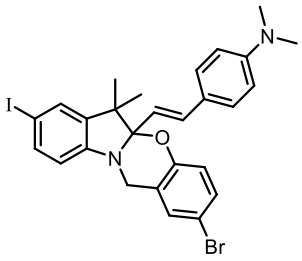

(30 mg, 69%). RMN ^{1}H (C_6D_6, 300 MHz) δ: 1.05 (s, 3H), 1.38 (s, 3H), 2.43 (s, 6H), 3.95 (ABq, J_{AB} = 17.1 Hz, 2H), 5.92 (d, ^{3}J = 8.2 Hz, 1H), 6.09 (d, ^{3}J = 15.9 Hz, 1H), 6.45-6.50 (m, 3H), 6.81 (d, ^{4}J = 2.3 Hz, 1H), 6.90 (d, ^{3}J = 15.9 Hz, 1H), 6.93 (dd, ^{3}J = 8.6 Hz, ^{4}J = 2.2 Hz, 1H), 7.28 (d, ^{3}J = 8.8 Hz, 2H), 7.30 (dd, ^{3}J = 8.2 Hz, ^{4}J = 1.5 Hz, 1H), 7.41 (d, ^{4}J = 1.4 Hz, 1H); RMN ^{13}C (C_6D_6, 100 MHz) δ: 18.1, 26.0, 39.5, 40.2, 49.6, 81.7, 102.4, 110.9, 112.1, 118.6, 118.7, 121.5, 124.2, 129.5, 130.8, 131.1, 136.1, 136.3, 141.6, 147.1, 150.6, 152.6 ; DEPT 135 δ: CH_3, CH pos.: 18.1, 26.0, 39.5, 110.9, 112.0, 112.1, 118.6, 118.7, 128.0, 129.5, 130.8, 131.1, 136.1, 136.3; CH_2 nég.: 40.2; MS-EI: *m/z* (intensité, %) calc. pour [M]: 602.0 and [M+2] 600.03 trouvé 602.0 et 600.0; 521.0 (30) [M-Br]; Anal. calc. pour $C_{27}H_{26}BrIN_2O$: C, 53.93; H, 4.36; N, 4.66 trouvé: C, 53.72; H, 4.18; N, 4.31.

Compound 63

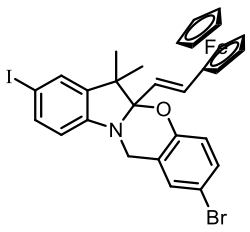

(36mg, 48%). RMN ^{1}H ($CDCl_3$, 400 MHz) δ: 1.17 (s, 3H), 1.48 (s, 3H), 3.96 (s, 5H), 4.23 (s, 2H), 4.34 (s, 2H), 4.44 (ABq, J_{AB} = 17.2 Hz, 2H), 5.84 (d, ^{3}J = 15.9 Hz, 1H), 6.37 (d, ^{3}J = 8.1 Hz, 1H), 6.54 (d, ^{3}J = 15.9 Hz, 1H), 6.71 (d, ^{3}J = 8.5 Hz, 1H), 7.16-7.20 (m, 2H), 7.36-7.39 (m, 2H); RMN ^{13}C ($CDCl_3$, 100 MHz) δ: 18.4, 26.3, 40.7, 49.3, 67.0, 67.4, 69.1, 69.4, 81.2, 81.5, 101.8, 110.8, 112.3, 119.2, 119.9, 121.6, 129.2, 130.8, 131.2, 134.7, 136.1, 141.3, 146.9, 152.5; DEPT 135 δ: CH_3, CH posi.: 18.4, 26.3, 67.0, 67.4, 69.1, 69.4, 77.2, 110.8, 119.2, 119.8, 129.2, 130.8, 131.2, 134.7, 136.1; CH_2 nég. 40.7; MS-EI: *m/z* (intensité, %) calc. pour [M]: 664.9 and [M+2] 666.95 trouvé 665.0 and 667.0; 586.0 (20) [M-Br]; Anal. calc. pour $C_{29}H_{25}BrFeINO$: C, 52.29; H, 3.78; N, 2.10 trouvé: C, 51.93; H, 3.52; N, 1.83.

Compound 64

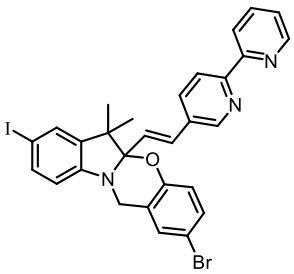

(23 mg, 32%). RMN ^{1}H ($CDCl_3$, 300 MHz) δ: 1.21 (s, 3H), 1.50 (s, 3H), 4.46 (ABq, J_{AB} = 17.1 Hz, 2H), 6.40 (d, ^{3}J = 8.0 Hz, 1H), 6.43 (d, ^{3}J = 16.2 Hz, 1H), 6.73 (d, ^{3}J = 8.5 Hz, 1H), 6.85 (d, ^{3}J = 16.2 Hz, 1H), 7.16-7.21 (m, 2), 7.30-7.33 (m, 1H), 7.36-7.41 (m, 2H); RMN ^{13}C ($CDCl_3$, 100 MHz) δ:18.5, 26.4, 40.7, 50.1, 81.9, 101.6, 111.0, 112.5, 119.0, 120.8, 120.9, 121.2, 123.8, 126.6, 129.4, 131.0, 131.2, 132.5, 134.0, 136.3, 136.9, 141.1, 146.8, 148.2, 142.2, 149.3, 152.2; DEPT 135 δ: CH_3, CH pos.: 18.5, 26.4, 111.0, 119.0, 120.9, 121.2, 123.9, 126.6, 129.4, 131.0, 131.2, 132.5, 134.0, 136.3, 136.9, 148.2, 149.2; CH_2 nég.: 40.7;

Compound 65

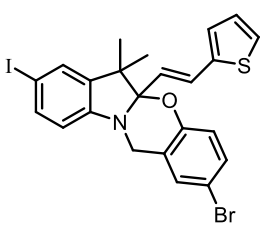

(37 mg, 48 %). RMN ^{1}H (C_6D_6, 300 MHz) δ: 0.87 (s, 3H), 1.29 (s, 3H), 3.84 (ABq, J_{AB} = 17.2 Hz, 2H), 5.87 (d, ^{3}J = 8.3 Hz, 1H), 6.12 (d, ^{3}J = 15.8 Hz, 1H), 6.39 (d, ^{3}J = 8.7 Hz, 1H), 6.53-6.59 (m, 2H), 6.66-6.68 (m, 1H), 6.78 (d, ^{4}J = 2.4 Hz, 1H), 6.91 (dd, ^{3}J = 8.6 Hz, ^{4}J = 2.3 Hz, 1H), 6.92 (d, ^{3}J = 15.8 Hz, 1H), 7.28 (dd, ^{3}J = 8.3 Hz, ^{4}J = 1.8 Hz, 1H), 7.36 (d, ^{4}J = 2.4 Hz, 1H); RMN ^{13}C ($CDCl_3$, 100 MHz) δ: 18.4, 26.3, 40.6, 50.0, 81.7, 101.5, 110.9, 112.3, 119.0, 121.3, 123.2, 125.3, 127.2, 127.6, 129.1, 129.4, 131.0,

131.2, 136.2, 140.8, 141.3, 146.8, 152.2; DEPT δ: CH_3, CH pos.: 18.4, 26.3, 110.9, 119.0, 123.2, 125.3, 127.2, 127.6, 129.1, 129.4, 130.9, 131.2, 136.2; CH_2 nég.: 40.6; MS-EI: *m/z* (intensité, %) calc. pour [M]: 564.9 and [M+2] 562.94 trouvé 565.0 et 563.0; 484.0 (20) [M-Br]; Anal. calc. pour $C_{23}H_{19}BrINOS$: C, 48.96; H, 3.39; N, 2.48 trouvé: C, 48.68; H, 3.12; N, 2.24.

Compound 66

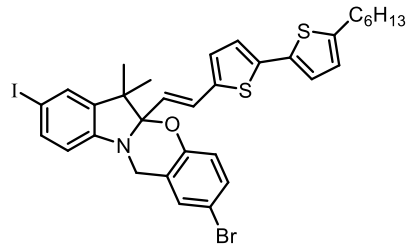

La réaction est effectuée dans le THF (38 mg, 38 %). RMN ^{1}H ($CDCl_3$, 400 MHz) δ: 0.97 (t, ^3J = 6.8 Hz, 3H), 0.99 (s, 3H), 1.14-1.23 (m, 6H), 1.31 (s, 3H), 1.48-1.55 (m, 2H), 2.53 (t, ^3J = 7.6 Hz, 2H), 3.86 (ABq, J_{AB} = 17.4 Hz, 2H), 5.88 (d, ^3J = 8.2 Hz, 1H), 6.07 (d, ^3J = 15.7 Hz, 1H), 6.41 (s, 1H), 6.43-6.44 (m, 1H), 6.47 (d, J = 3.4 Hz, 1H), 6.78 (d, J = 3.6 Hz, 1H), 6.81 (d, ^4J = 2.4 Hz, 1H), 6.87 (d, ^3J = 15.7 Hz, 1H), 6.92 (d, ^4J = 2.4 Hz, 1H), 6.95 (d, J = 3.6 Hz, 1H), 7.29 (dd, ^3J = 8.3 Hz, ^4J = 1.7Hz, 1H), 7.38 (d, J = 1.7 Hz, 1H), RMN ^{13}C (C_6D_6, 100 MHz) δ: 13.9, 18.0, 22.5, 25.9, 28.6, 29.9, 30.0, 31.5, 40.1, 49.9, 82.0, 101.5, 110.9, 112.4, 118.6, 121.3, 123.0, 123.3, 123.9, 125.0, 129.6, 130.9, 131.1, 134.6, 136.4, 138.0, 138.9, 141.2, 145.9, 146.8, 152.2; DEPT 135 δ: CH_3, CH pos.: 13.9, 18.0, 25.9, 110.9, 118.6, 123.0, 123.3, 123.9, 125.0, 128.0, 128.5, 129.0, 129.6, 130.9, 131.1, 136.4; CH_2 nég.: 22.5, 28.6, 30.0, 31.5, 40.1; MS-EI: *m/z* (intensité, %) calc. pour [M]: 731.0 and 729.02 trouvé 731.0 and 729.0; 650 (25) [M-Br]; Anal. calc. pour $C_{33}H_{33}BrINOS_2$: C, 54.25; H, 4.55; N, 1.92 trouvé: C, 54.04; H, 4.31; N, 1.72.

Compound 67

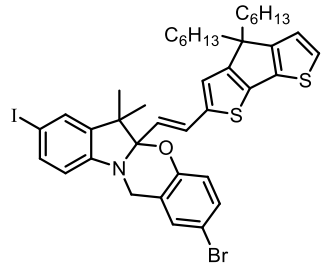

(43 mg, 41 %). RMN ^{1}H ($CDCl_3$, 400 MHz) δ: 0.77-0.84 (m, 6H), 0.90-0.99 (m, 4H), 1.11-1.15 (m, 12H), 1.20 (s, 3H), 1.47 (s, 3H), 1.73-1.79 (m, 4H), 4.44 (ABq, J_{AB} = 16.8 Hz, 2H), 6.03 (d, ^3J = 15.7 Hz, 1H), 6.38 (d, ^3J = 8.2 Hz, 1H), 6.68 (d, ^3J = 8.4 Hz, 1H), 6.79 (s, 1H), 6.86 (d, ^3J = 15.7 Hz, 1H), 6.91 (d, J = 4.9 Hz, 1H), 7.16-7.19 (m, 3H), 7.34-7.38 (m, 2H); RMN ^{13}C ($CDCl_3$, 100 MHz) δ: 14.0, 18.4, 22.6, 24.5, 26.4, 29.7, 31.6, 37.5, 37.6, 40.7, 50.1, 81.7, 101.8, 110.9, 112.2, 119.0, 120.5, 121.4, 121.7, 122.2, 125.6, 129.4, 130.2, 130.9, 131.1, 136.2, 136.7, 140.7, 141.4, 146.8, 152.3, 158.1, 158.8; DEPT 135 δ: CH_3, CH pos: 14.1, 18.4, 26.4, 110.9, 119.0, 120.5, 121.7, 122.2, 125.6, 129.4, 130.2, 130.9, 131.2, 136.2; CH_2 nég. :

22.6, 24.5, 29.7, 31.6, 37.5, 37.6, 40.6; MS-EI: *m/z* (intensité, %) calc. pour [M]: 827.1 et [M+2] 825.12 trouvé 827.1 et 825.1; 746.1 (20) [M-Br]; Anal. calc. pour $C_{40}H_{45}BrINOS_2$: C, 58.11; H, 5.49; N, 1.69 trouvé: C, 58.54; H, 6.04; N, 2.22.

Compound 68

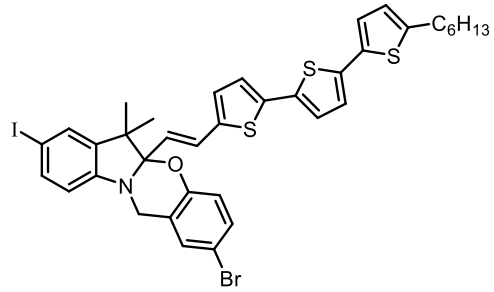

RMN ^{1}H ($CDCl_3$, 300 MHz) δ: 0.88-0.91 (m, 3H), 1.18 (s, 3H), 1.46 (s, 3H), 1.29 (s, 3H), 1.60-1.72 (m, 6H), 2.79 (t, ^3J = 7.6 Hz, 2H), Hz, 3.62 (q, ^3J = 7.3 Hz, 2H), 4.43 (ABq, J_{AB} = 17.2 Hz, 2H), 5.64 (s, 1H), 6.06 (d, ^3J = 15.9 Hz, 1H), 6.37 (d, ^3J = 8.1 Hz, 1H), 6.67-6.69 (m, 2H), 6.82 (d, ^3J = 13.0 Hz, 1H), 6.85 (s, 1H), 6.70-6.99 (m, 2H), 7.03 (d, ^4J = 3.7 Hz, 1H), 7.14-7.16 (m, 1H), 7.18-7.19 (m, 1H), 7.34-7.36 (m, 1H), 7.38-7.39 (m, 1H); RMN ^{13}C ($CDCl_3$, 100 MHz) δ: 8.2, 14.1, 18.4, 22.6, 26.4, 28.8, 29.7, 30.2, 31.6, 32.0, 40.7, 50.1, 63.5, 81.8, 101.5, 110.9, 112.3, 119.0, 121.3, 123.2, 123.6, 124.6, 124.9, 128.4, 129.0, 129.4, 130.9, 131.2, 134.2, 135.0, 136.2, 137.1, 137.4, 139.4, 141.2, 145.9, 146.8, 152.2; (38 mg, 39-42 %). MS-EI: *m/z* (intensité, %) calc. pour [M]: 811.0 trouvé 811.0; 732.0 (30) [M-Br].

Compound 69

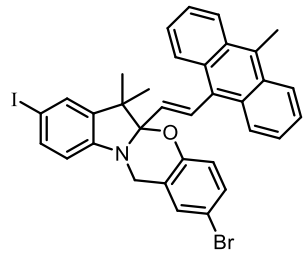

(10 mg, 26 %). RMN ^{1}H (C_6D_6, 400 MHz) δ: 0.92 (s, 3H), 1.43 (s, 3H), 1.77 (s, 3H), 3.81 (ABq, J_{AB} = 17.6 Hz, 2H), 5.82 (d, ^3J = 8.2 Hz, 1H), 6.28 (d, ^3J = 7.7 Hz, 1H), 6.41 (s, 1H), 6.40 (d, ^3J = 24.8 Hz, 1H), 6.88 (d, ^4J = 2.4 Hz, 1H), 6.92 (dd, ^3J = 7.4 Hz, ^4J = 1.1 Hz, 1H), 6.94-7.02 (m, 7H), 7.30 (dd, ^3J = 8.1 Hz, ^4J = 1.7 Hz, 1H), 7.31-7.34 (m, 1H), 7.37 (d, ^4J = 1.7 Hz, 1H); RMN ^{13}C (C_6D_6,100 MHz) δ: 13.2, 18.0, 25.4, 40.1, 49.2, 79.7, 80.5, 101.4, 110.6, 112.7, 119.2, 120.6, 120.8, 121.5, 122.4, 127.2, 129.1, 129.7, 130.3, 130.8, 131.1, 136.4, 140.6, 140.7, 140.8, 140.9, 141.1, 146.8, 152.6; DEPT 135 δ: CH_3, CH pos.: 13.2, 18.0, 25.4, 110.6, 119.2, 120.6, 120.8, 121.5, 127.2, 127.4, 128.0, 129.1, 129.7, 130.3, 130.8, 131.1, 136.4; CH_2 nég.: 40.1; MS-EI: *m/z* (intensité, %) calc. pour [M]: 671.0 et [M+2] 673.03 trouvé 671.0 et 673.0; Anal. calc. pour $C_{34}H_{27}BrINO$: C, 60.73; H, 4.05; N, 2.08 trouvé: C, 60.44; H, 3.77; N, 1.77.

Compound 70

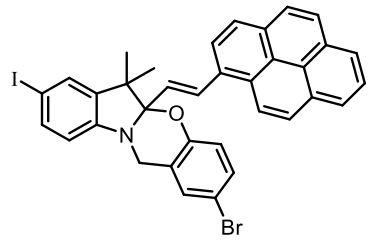

RMN ^{1}H ($CDCl_3$, 300 MHz) δ: 1.32 (s, 3H), 1.61 (s, 3H), 4.55 (ABq, J_{AB} = 17.7 Hz, 2H), 6.44 (d, ^{3}J = 8.2 Hz, 1H), 6.51 (s, 1H), 6.87 (d, ^{3}J = 8.8 Hz, 1H), 7.20 (s, 1H), 7.28-7.29 (m, 1H), 7.41-7.44 (m, 2H), 7.88 (d, ^{3}J = 15.8 Hz, 1H), 7.98-8.10 (m, 5H), 8.14 (s, 2H), 8.17-8.20 (m, 2H), RMN ^{13}C ($CDCl_3$, 100 MHz) δ: 18.6, 26.5, 40.9, 49.9, 81.7, 102.0, 110.9, 112.5, 119.1, 121.6, 122.6, 124.0, 124.8, 124.9, 125.3, 125.5, 126.1, 127.1, 127.3, 127.7, 128.0, 128.4, 129.4, 130.4, 130.8, 131.0, 131.3, 131.4, 133.9, 136.3, 141.3, 147.0, 152.6; DEPT 135 δ: CH_3, CH pos.: 18.6, 26.5, 110.9, 119.1, 122.6, 142.0, 124.9, 125.3, 125.5, 126.1, 127.1, 127.3, 127.7, 128.0, 129.4, 131.0, 131.3, 133.9, 136.3; CH_2 nég.: 40.9; MS-EI: *m/z* (intensité, %) calc. pour [M]: 683.0 et [M+2] 685.03 trouvé 683.0 et 681.0; 602.0 (30) [M-Br]; Anal. calc. pour $C_{35}H_{27}BrINO$: C, 61.42; H, 3.98; N, 2.05 trouvé: C, 61.95; H, 3.79; N, 1.69.

Compound 71

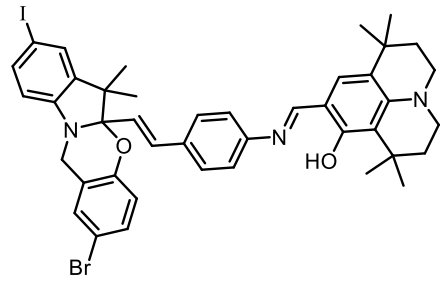

RMN ^{1}H ($CDCl_3$, 300 MHz) δ: 1.27 (s, 12H), 1.50 (s, 6H), 1.71-1.79 (m, 4H), 3.18 (t, ^{2}J = 6 Hz, 2H), 3.27 (t, ^{2}J = 6 Hz, 2H), 4.44 (ABq, J_{AB} = 17.4 Hz, 2H), 6.23 (d, ^{3}J = 16.0 Hz, 1H), 6.39 (d, ^{3}J = 8.1 Hz, 1H), 6.70 (d, ^{3}J = 8.6 Hz, 1H), 6.77 (d, ^{3}J = 16.0 Hz, 1H), 6.97 (s, 1H), 7.13-7.15 (m, 2H), 7.19 (d, ^{3}J = 8.3 Hz, 2H), 7.35-7.39 (m, 4H), 8.38 (s, 1H), 14.07 (s, 1H); RMN ^{13}C ($CDCl_3$, 100 MHz) δ: 14.1, 18.4, 19.8, 22.7, 26.4, 27.2, 30.3, 30.9, 31.8, 31.9, 32.2, 36.3, 39.9, 40.7, 47.0, 47.4, 50.0, 81.7, 101.8, 109.2, 110.9, 112.2, 114.6, 119.0, 121.0, 121.4, 122.7, 127.8, 128.4, 129.3, 129.7, 130.9, 131.2, 132.6, 135.6, 136.2, 141.4, 146.7, 147.0, 149.2, 151.3, 152.4, 160.8, 161.0; DEPT 135 δ: CH_3, CH pos.: 14.1, 18.4, 26.4, 28.4, 30.9, 110.9, 119.0, 121.0, 122.7, 127.8, 128.4, 129.3, 130.9, 131.2, 135.6, 136.2, 161.0 CH_2 nég.:36.3, 39.9, 40.7, 47.0, 47.4.

Compound 74

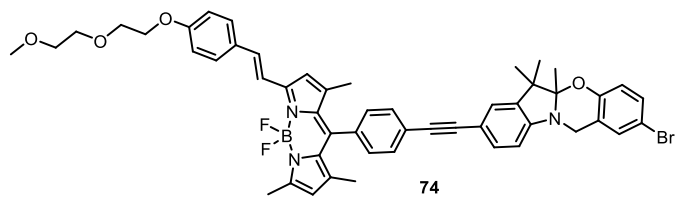

74

Compound **60** (51 mg, 0.115 mmol), BODIPY **73** (64 mg, 0.115 mmol) and **[**$Pd(PPh_3)_2Cl_2$] (8 mg, 10 mol%) were placed in a Schlenk tube and dried under vacuum before addition of *i*-Pr_2NH (1 mL) and THF (5mL). After stirring 5-10 minutes at room temperature, CuI (2 mg, 10 mmol%) was added. The reaction mixture was stirred at room temperature for 3 days. After evaporation of solvents the crude was treated with CH_2Cl_2 and washed with water. The organic layer was dried under anhydrous cotton wood and evaporated under vacuum. The molecule was purified by SiO_2 column chromatography eluting with CH_2Cl_2/AcOEt: 9.5/0.5, v/v (92 mg, 89 %) and green crystals were obtained by diffusion of pentane in CH_2Cl_2. ^{1}H NMR (CD_2Cl_2, 300 MHz) δ: 1.16 (s, 3H), 1.45 (s, 3H), 1.49-1.52 (m, 12H), 2.53 (s, 3H), 3.33 (s, 3H), 3.50-3.53 (m, 2H), 3.79-3.82 (m, 2H), 4.12-4.15 (m, 2H), 4.54 (s, 2H), 6.03 (s, 1H), 6.52-6.62 (m, 3H), 6.92 (d, ^3J = 8.9 Hz, 2H), 7.16 (dd, ^3J = 8.8 Hz, ^4J = 2.4 Hz, 1H), 7.20-730 (m, 5H), 7.47 (d, ^3J = 16.3 Hz, 1H), 7.53 (d, ^3J = 8.8 Hz, 2H), 7.61 (d, ^3J = 8.3 Hz, 2H); ^{13}C NMR (CD_2Cl_2, 100 MHz) δ: 14.4, 14.5, 14.7, 15.7, 18.5, 25.8, 40.0, 47.7, 58.7, 67.6, 69.5, 70.7, 71.9, 86.7, 91.7, 100.8, 108.1, 111.8, 113.6, 114.9, 116.7, 117.4, 119.4, 120.8, 121.1, 124.7, 125.7, 128.5, 128.9, 129.4, 130.9, 131.5, 131.6, 131.9, 132.6, 134.3, 136.1, 138.9, 139.6, 142.6, 142.8, 147.9, 152.1, 153.2, 154.9, 159.8; ^{11}B NMR (CD_2Cl_2, 128 MHz) δ: 0.91 (t, $J_{B\text{-}F}$ = 33.8 Hz); EI-MS: *m/z* (intensity, %) calc. for [M]: 895.3 found: 895.2 (100); 876.1 (20), [M-F]; Anal. calc. for $C_{51}H_{49}BBrF_2N_3O_4$: C, 68.31; H, 5.51; N, 4.69 found: C, 68.17; H, 5.21; N, 4.57.

Compound 75

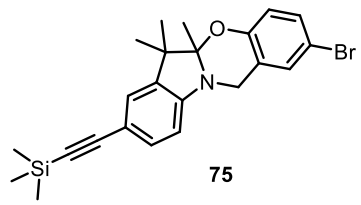

75

[1,3]oxazine **60** (150 mg, 0.319 mmol), $[Pd(PPh_3)_2Cl_2]$ (23 mg, 0.032 mmol) and CuI (6 mg, 0.032 mmol) were placed in an oven-dried and argon-filled Schlenk tube. After addition of *i*-Pr_2NH (0.5 mL) and toluene (5 mL), TMS-acetylene (313 mg, 3.19 mmol) were added than the mixture had been stirred at room temperature for 1.5 h. After evaporation of the solvent, the crude was taken in CH_2Cl_2 and washed with water and brine. The organic phase was dried with Na_2SO_4,

concentrated under vacuum and purified by column chromatography (SiO_2, CH_2Cl_2/petroleum ether: 4/6 v/v). The product was obtained as colorless oil which solidifies under vacuum (135 mg, 96%).^{1}H RMN (400 MHz, $CDCl_3$) δ: 0.22 (s, 9H), 1.14 (s, 3H), 1.48 (s, 3H), 1.50 (s, 3H), 4.44-4.54 (m, 2H), 6.44 (d, ^3J = 8.0 Hz, 1H), 6.59 (d, ^3J = 8.8 Hz, 1H), 7.13-7.23 (m, 4H); ^{13}C RMN (100 MHz, $CDCl_3$) δ: 0.0, 15.8, 18.6, 25.7, 39.1, 47.5, 91.3, 100.4, 106.1, 107.7, 111.8, 113.9, 119.4, 120.3, 125.9, 129.1, 130.8, 131.9, 138.3, 147.5, 125.0; EI-MS: *m/z* (intensity, %) Calc. for [M]: 441.09 and 439.10 resulting from ^{81}Br for ^{79}Br isotopes respectively; Anal. calc. for $C_{23}H_{26}BrNOSi$: C, 62.72; H, 5.95; N, 3.18 found: C, 62.54; H, 5.77; N, 2.95.

Compound 76

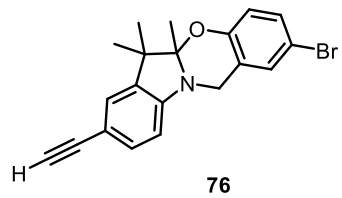

76

A solution of KOH (33 mg, 0.590 mmol) in water (0.25 mL) and methanol (1.0 mL) was added dropwise to a solution of **75** (130 mg, 0.295 mmol) in THF (6 mL). The mixture was stirred at room temperature for 2 h. After evaporation of the solvents the crude was taken with CH_2Cl_2 and washed three times with water. The organic phase was dried with Na_2SO_4, evaporated under vacuum and purified by column chromatography (SiO_2, CH_2Cl_2/petroleum ether: 4/6 v/v). The product was obtained as colorless thin film which solidifies under vacuum (100 mg, 92%). ^{1}H RMN (400 MHz, $CDCl_3$) δ: 1.15 (s, 3H), 1.49 (s, 3H), 1.51 (s, 3H), 2.95 (s, 1H), 4.44-4.57 (m, 2H), 6.46 (d, ^3J = 8.1 Hz, 1H), 6.56 (d, ^3J = 8.8 Hz, 1H), 7.13-7.17 (m, 2H), 7.21-7.26 (m, 3H); ^{13}C RMN (75 MHz, $CDCl_3$) δ: 16.0, 18.8, 25.8, 40.0, 47.7, 74.9, 84.7, 100.5, 107.9, 112.0, 113.0, 119.6, 120.4, 126.1, 129.2, 131.0, 132.2, 138.6, 147.8, 151.1; RMN DEPT 135 (75 MHz, $CDCl_3$) δ (CH_3): 16.0, 18.8, 25.8, 40.0 (CH_2), δ (CH): 107.8, 119.6, 126.1, 129.2, 130.9, 132.2; ES-MS: *m/z* (intensity, %) Calc. for [M]: 367.06, 369.06 found 368.1, 370.1 resulting from ^{79}Br for ^{81}Br isotopes respectively; Anal. calc. for $C_{20}H_{18}BrNO$: C, 65.23; H, 4.93; N, 3.80 found: C, 64.97; H, 4.69; N, 3.66.

Compound 78

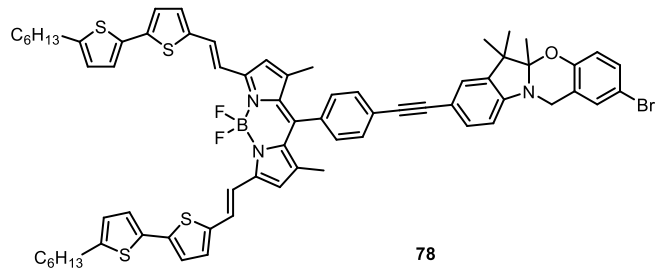

78

Compound **78** (49 mg, 0.134 mmol) and BODIPY dye **77** (100 mg, 0.103 mmol) were placed in an oven-dried and argon-filled Schlenk tube. After addition of toluene (8.0 mL),

[$Pd(PPh_3)_4$], and *i*-Pr_2NH (2.01 mmol, 0.3 mL) the mixture was allowed to react at 75 °C under stirring over-night. Then the solvent was removed and the crude was solubilised in CH_2Cl_2 and washed three times with water. The organic phase was dried with Na_2SO_4, evaporated under vacuum and purified from column chromatography (SiO_2, CH_2Cl_2/petroleum ether: 6/4 v/v). and precipitation with petroleum ether in CH_2Cl_2 solution. The product was yielded as a dark solid which is dark green in solution (88 mg, 71 %). ^{1}H RMN (300 MHz, $CDCl_3$) δ: 0.88-0.93 (m, 6H), 1.19 (s, 3H), 1.30-1.43 (m, 12H), 1.48 (s, 6H), 1.53 (s, 6H), 1.65-1.95 (m, 4H), 2.81 (t, ^3J = 7.5 Hz, 4H), 4.54 (s, 2H), 6.53 (d, ^3J = 8.4 Hz, 1H), 6.58 (d, ^3J = 8.4 Hz, 1H), 6.59 (s, 2H), 6.72 (d, ^3J = 3.6 Hz, 2H), 7.04 (d, ^3J = 3.8 Hz, 2H), 7.10-7.13 (m, 4H), 7.17 (dd, ^3J = 8.7 Hz, ^4J = 2.5 Hz, 1H), 7.23 (d, ^4J = 2.4 Hz, 1H), 7.27-7.32 (m, 6H), 7.46 (d, ^3J = 15.9 Hz, 2H), 7.61 (d, ^3J = 8.1 Hz, 2H); ^{13}C RMN (100 MHz, $CDCl_3$) δ: 14.1, 14.9, 16.0, 18.8, 22.4, 22.6, 25.9, 28.8, 30.3, 31.6, 31.6, 40.1, 47.7, 86.8, 91.9, 100.5, 108.1, 112.0, 113.7, 118.0, 119.6, 120.5, 123.8, 124.2, 124.7, 125.1, 125.7, 128.7, 129.3, 129.5, 131.0, 131.8, 132.0, 133.6, 134.6, 134.7, 136.8, 138.7, 139.8, 140.6, 141.5, 146.4, 147.8, 152.0, 152.1; ^{13}C RMN DEPT 135 (75 MHz, $CDCl_3$) δ (CH_3): 14.1, 15.0, 16.0, 18.8, 25.9 δ (CH_2): 18.8, 28.8, 30.3, 31.6, 40.1 δ (CH): 108.1, 118.0, 119.6, 123.8, 124.2, 125.1, 125.7, 128.7, 129.3, 129.5, 131.0, 131.8, 132. ^{11}B NMR (128 MHz, CDCl3) δ: 1.07 (t, $J_{B\text{-}F}$ = 30.8 Hz); ES-MS *m/z* (intensity, %) Calc. for [M]: 1211.34 (100) found 1212.2, 1210.3 resulting from ^{81}Br for ^{79}Br isotopes respectively, 1130.2 (35) [M-F]; Anal. calc. for $C_{69}H_{67}BBrF_2N_3OS_4$: C, 68.42; H, 5.58; N, 3.47 found: C, 68.24; H, 5.35; N, 3.17.

Compound 79

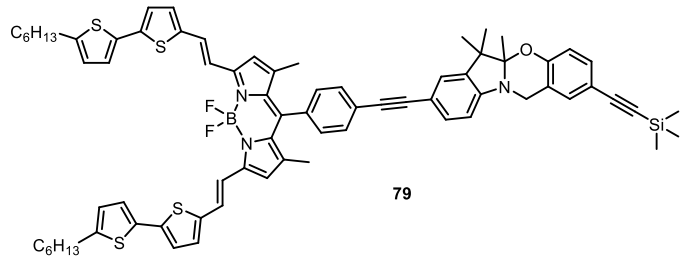

79

Compound **78** (270 mg, 0.223 mmol), [$Pd(dppf)_2Cl_2$] (18 mg, 0.022 mmol) and CuI (4mg, 0.022 mmol) were placed in a Schlenk tube under vacuum for 15-30 minutes and then it was filled with argon before adding the toluene (12 mL), *i*-Pr_2NH (0.5 mL) and TMS-acetylene (328 mg, 3.344 mmol). The mixture was stirred at 95 °C during 12 hours. Than the solvents were evaporated and the crude was solubilised with CH_2Cl_2, washed with water and brine. The organic layer was dried with Na_2SO_4, evaporated and purified from column chromatography (SiO_2, CH_2Cl_2/petroleum ether 6/4 then precipitation of a solution in CH_2Cl_2 with petroleum ether and washing of the solids with pentane). The product was obtained as fine dark powder

which is dark green in solution (229 mg, 85 %). ^{1}H RMN (300 MHz, $CDCl_3$) δ: 0.24 (s, 9H), 0.89-0.93 (m, 6H), 1.18 (s, 3H), 1.28-1.42 (m, 12H), 1.48 (s, 6H), 1.53 (s, 3H), 1.54 (s, 3H), 1.65-1.75 (m, 4H), 2.81 (t, ^{3}J = 7.4 Hz, 4H), 4.52 (s, 2H, C*H*$_2$ oxazine), 6.50 (d, ^{3}J = 8.9 Hz, 1H), 6.56-6.62 (m, 3H), 6.72 (d, ^{3}J = 3.2 Hz, 2H), 7.04 (d, ^{3}J = 3.7 Hz, 2H), 7.10-7.13 (m, 4H), 7.18 (d, ^{3}J = 8.2 Hz, 1H), 7.25-7.32 (m, 7H), 7.46 (d, ^{3}J = 16.1 Hz, 2H vinylic), 7.61 (d, ^{3}J = 8.0 Hz, 2H); ^{13}C RMN (100 MHz, $CDCl_3$) δ:14.1, 14.9, 16.2, 18.9, 22.6, 25.9, 27.1, 28.8, 30.3, 31.6, 40.1, 47.7, 92.0, 100.8, 105.0, 107.5, 108.1, 113.6, 114.7, 117.8, 118.0, 118.5, 123.8, 124.2, 124.7, 125.1, 125.7, 128.7, 129.5, 130.6, 131.8, 131.9, 132.0, 133.6, 134.5, 134.7, 136.8, 138.7, 139.8, 140.6, 141.5, 146.3, 147.9, 152.0, 153.4; RMN DEPT 135 (75 MHz, $CDCl_3$) δ (CH_3):0.07, 14.1, 14.9, 16.2, 18.9, 19.2, 25.9 δ (CH_2): 22.6, 28.8, 30.3, 31.6, 40.1 (*C*H_2 oxazine) δ (CH): 108.2, 117.8, 118.0, 118.2, 123.8, 124.2, 125.1, 125.7, 128.7, 129.5, 130.6, 131.8, 131.9, 131.9; ^{11}B NMR (128 MHz, CDCl3) δ: 1.07 (t, $J_{B\text{-}F}$ = 33.4 Hz); ES-MS: *m/z* (intensity, %) Calc. for [M]: 1227.47 found 1228.2; Anal. calc. for $C_{74}H_{76}BF_2N_3OS_4Si$: C, 72.34; H, 6.24; N, 3.42 found: C, 72.17; H, 5.87; N, 3.09.

Compound 80

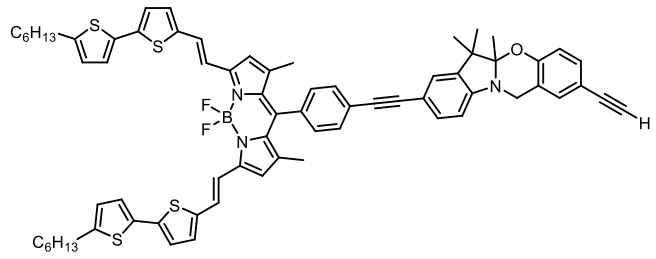

The solution of **79** (208 mg, 0.169 mmol) in CH_2Cl_2 was treated with K_2CO_3 (3.5 g, 25.39 mmol), MeOH (2,0 mL) and water (0.5 mL) and stirred at room temperature for 2-3 days. After filtration of the reaction media, the solution was taken in CH_2Cl_2 (50 mL) and washed several times with water and brine. The organic phase was dried with Na_2SO_4 and evaporated under vacuum before proceeding with the purification of the crude by column chromatography (SiO_2, CH_2Cl_2/petroleum ether 6/4 and further by precipitation). The compound was obtained as dark fine powder which is dark green in solution (85 mg, 43 %). ^{1}H RMN (400 MHz, $CDCl_3$) δ: 0.89-0.93 (m, 6H), 1.19 (s, 3H), 1.33-1.44 (m, 12H), 1.48 (s, 6H), 1.54 (s, 3H), 1.55 (s, 3H), 1.67-1.74 (m, 4H), 2.82 (t, ^{3}J = 7.5 Hz, 4H), 2.98 (s, 1H), 4.54 (s, 2H), 6.53 (d, ^{3}J = 8.5 Hz, 1H), 6.59 (s, 2H), 6.63 (d, ^{3}J = 8.5 Hz, 1H), 6.72 (d, ^{3}J = 3.5 Hz, 2H), 7.04 (d, ^{3}J = 3.9 Hz, 2H), 7.10-7.12 (m, 4H), 7.21 (dd, ^{3}J = 8.5 Hz, ^{4}J = 1.9 Hz, 1H), 7.27-7.32 (m, 7H), 7.46 (d, ^{3}J = 16.0 Hz, 2H), 7.61 (d, ^{3}J = 8.0 Hz, 2H); ^{13}C RMN (100 MHz, $CDCl_3$) δ: 14.1, 14.9, 16.2, 18.9, 22.6, 25.9, 28.8, 30.3, 31.6, 34.1, 40.1, 47.7, 83.5, 86.8, 92.0, 100.8, 108.2, 113.6, 113.7, 117.9, 118.0, 118.6, 123.8, 124.2, 124.7,

125.1, 125.7, 128.7, 129.6, 130.7, 131.8, 131.9, 132.0, 133.6, 134.5, 134.7, 136.8, 138.7, 139.8, 140.6, 141.5, 146.4, 147.9, 152.0, 153.6; ^{11}B NMR (128 MHz, CDCl3) δ: 1.07 (t, J_{B-F} = 33.2 Hz); ES-MS: *m/z* (intensity, %) Calc. for [M]: 1227.47 found 1228.2; Anal. calc. for $C_{71}H_{68}BF_2N_3OS_4$: C, 73.74; H, 5.93; N, 3.63 found: C, 73.54; H, 5.71; N, 3.41.

Compound 81

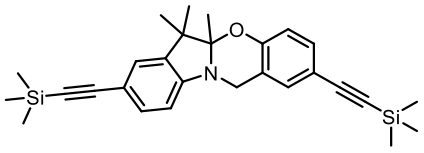

[1,3]oxazine **60** (200 mg, 0.42 mmol), [Pd(dppf)$_2$Cl$_2$] (35 mg, 0.042 mmol) and CuI (8 mg, 0.042 mmol) were placed Schlenk tube. After addition of *i*-Pr$_2$NH (0.6 mL, 4.25 mmol) and toluene (10 mL), TMS-acetylene (626 mg, 6.38 mmol) were added than the mixture had been stirred at room temperature for 12 h at 80 °C. After evaporation of the solvent, the crude was taken in CH_2Cl_2 and washed with water and brine. The organic phase was dried with $MgSO_4$, concentrated under vacuum and purified by column chromatography (SiO_2, CH_2Cl_2/petroleum ether: 3/7 v/v). The product was obtained as colorless oil which solidifies under vacuum (193 mg, 99%).^{1}H RMN (400 MHz, $CDCl_3$) δ: 0.26 (s, 9H), 0.27 (s, 9H), 1.17 (s, 3H), 1.52 (s, 6H), 4.45-4.54 (m, 2H), 6.44 (d, ^3J = 8.5 Hz, 1H), 6.60 (d, ^3J = 8.5 Hz, 1H), 7.19-7.28 (m, 4H); ^{13}C RMN (100 MHz, $CDCl_3$) δ: 0.02, 15.9, 18.6, 25.6, 39.8, 47.5, 91.2, 92.2, 100.6, 104.9, 106.2, 107.7, 113.8, 114.4, 117.6, 118.3, 125.8, 130.4, 131.7, 131.9, 138.2, 147.6, 153.3; ES-MS: *m/z* (intensity, %) Calc. for [M]: 457.23 found 458.1; Anal. calc. for $C_{28}H_{35}NOSi_2$: C, 73.47; H, 7.71; N, 3.02 found: C, 73.18; H, 7.55; N, 2.82.

Compound 82

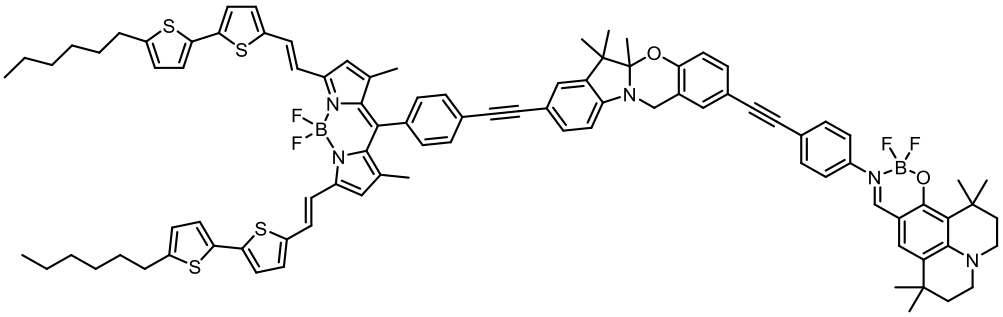

Compound **80** (80 mg, 0.069 mmol) and Boranil **48** (38 mg, 0.069 mmol) were placed in an oven-dried and argon-filled Schlenk tube. The reactants were dried under vacuum for 15-30 minutes before pursuing with the addition of toluene (6 mL), *i*-Pr$_2$NH (1.5 mL) and [Pd(PPh$_3$)$_4$] (8.0 mg, 0.007 mmol) under argon. The reaction media were placed at 60 °C under stirring during 12 hours. After evaporation of the solvent, the crude was directly

purified by column chromatography (SiO_2, CH_2Cl_2/petroleum ether 6/4) and further by precipitation of a CH_2Cl_2 solution with petroleum ether to afford the product as dark thin solids (80 mg, 75 %). ^{1}H RMN (300 MHz, $CDCl_3$) δ: 0.90-0.93 (m, 6H), 1.20 (s, 3H), 1.26 (s, 6H), 1.31-1.43 (m, 12H), 1.47 (s, 6H), 1.53 (s, 6H), 1.55 (s, 3H), 1.56 (s, 3H), 1.65-1.78 (m, 8H), 2.81 (t, ^3J = 7.5 Hz, 4H), 3.28-3.32 (m, 2H), 3.40 (t, ^3J = 6.2 Hz, 2H), 4.57 (s, 2H), 6.54 (d, ^3J = 8.9 Hz, 1H), 6.58 (s, 2H), 6.67 (d, ^3J = 8.7 Hz, 1H), 6.72 (d, ^3J = 3.6 Hz, 2H), 7.0 (s, 1H), 7.04 (d, ^3J = 3.9 Hz, 2H), 7.09-7.12 (m, 4H), 7.2 (d, J = 2.2 Hz, 1H), 7.27-7.33 (m, 7H), 7.43-7.54 (m, 6H), 7.61 (d, ^3J = 8.1 Hz, 2H), 7.93 (s, 1H, C*H*N Boranil); ^{13}C RMN (100 MHz, $CDCl_3$) δ: 14.1, 14.9, 16.2, 18.9, 22.6, 25.9, 28.1, 28.8, 29.8, 30.3, 31.6, 31.7, 32.0, 35.2, 38.9, 40.1, 47.5, 47.8, 47.9, 86.8, 87.6, 90.3, 92.0, 100.8, 107.5, 108.2, 113.6, 114.7, 114.8, 117.9, 118.0, 118.7, 122.2, 122.8, 123.8, 124.2, 124.7, 125.1, 125.6, 125.7, 127.5, 128.7, 128.8, 129.6, 130.2, 131.5, 131.8, 131.9, 132.3, 133.6, 134.5, 134.7, 138.7, 139.8, 140.6, 141.5, 142.9, 146.3, 147.9, 151.5, 152.0, 153.4, 157.0, 158.4; ^{11}B NMR (128 MHz, CDCl3) δ: 0.85-1.40 (m, 2xBF_2); ES-MS: *m/z* (intensity, %) Calc. for [M]: 1550.64 found 1550.5; 1530.5 (35) [M-F]; 1511.4 (15) [M-2F]; Anal. calc. for $C_{94}H_{93}B_2F_4N_5O_2S_4$: C, 72.81; H, 6.05; N, 4.52 found: C, 72.64; H, 5.71; N, 4.17.

Compound 83

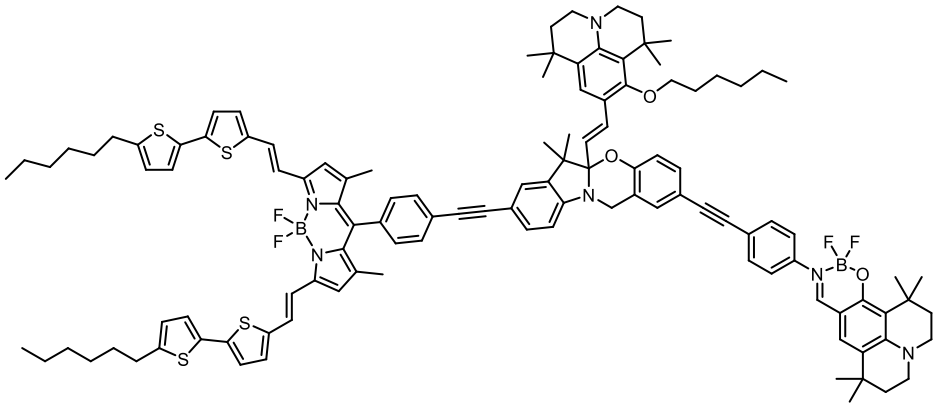

Compound **82** (45mg, 0.029 mmol) and julolidinyl **17** (52 mg, 0.145 mmol) were placed in a Schlenk tube under argon before adding the ethanol (3 mL), 1,2-dichloroethane (4 mL) and trifluoracetic acid (17 mg, 0.145 mmol). The solution was then placed at 90 °C under stirring during 2.5 h. After cooling down to ambient temperature the solvents of the reaction were evaporated and the crude was solubilized in CH_2Cl_2 followed by washing with water several times. The organic phase collected was dried with Na_2SO_4, evaporated under vacuum and the crude obtained was purified from column chromatography (SiO_2, CH_2Cl_2/methanol 0.1 to 1 %). The product obtained after column was precipitated in a CH_2Cl_2 solution with petroleum

ether then washed with pentane to afford it highly pure as a dark powder (20 mg, 36 %). ^{1}H RMN (300 MHz, $CDCl_3$) δ: 0.90-0.93 (m, 9H), 1.26-1.34 (m, 35H), 1.41 (s, 6H), 1.48 (s, 6H), 1.53 (s, 8H), 1.56 (s, 8H), 1.66-1.80 (m, 12H), 2.81 (t, ^{3}J = 7.6 Hz, 4H), 3.03-3.09 (m, 2H), 3.15 (t, ^{3}J = 5.7 Hz, 2H), 3.31 (t, ^{3}J = 5.6 Hz, 2H), 3.40 (t, ^{3}J = 5.9 Hz, 2H), 3.52-3.64 (m, 2H), 4.54 (ABq, J_{AB} = 17.1 Hz, 2H), 6.05 (d, ^{3}J = 16.2 Hz, 1H), 6.58-6.60 (m, 3H), 6.72 (d, ^{3}J = 3.6 Hz, 2H), 6.80 (d, ^{3}J = 9.1Hz, 1H), 6.99 (s, 1H), 7.00 (d, ^{3}J = 16.2 Hz, 1H), 7.04 (d, ^{3}J = 3.7 Hz, 1H), 7.10-7.13 (m, 4H), 7.21-7.25 (m, 2H), 7.28-7.34 (m, 6H), 7.43-7.52 (m, 6H), 7.62 (d, ^{3}J = 8.1 Hz, 2H), 7.93 (s, 1H); ^{13}C RMN (100 MHz, $CDCl_3$) δ: 14.0, 14.1, 14.2, 14.9, 18.6, 22.3, 22.6, 22.8, 25.7, 26.5, 28.1, 28.8, 29.8, 30.0, 30.1, 30.3, 31.2, 31.6, 31.6, 31.7, 32.0, 32.1, 32.3, 32.8, 34.1, 35.2, 36.8, 38.9, 40.4, 40.8, 46.9, 47.7, 47.5, 47.8, 49.8, 53.4, 75.0, 76.7, 86.8, 87.4, 90.5, 92.0, 102.6, 107.5, 108.5, 113.6, 114.6, 114.8, 116.9, 117.4, 118.0, 118.2, 119.7, 122.4, 122.7, 122.8, 123.8, 124.2, 124.8, 125.1, 125.6, 125.7, 126.4, 127.4, 128.7, 129.5, 129.7, 130.2, 131.5, 131.8, 132.0, 132.3, 132.7, 133.6, 134.5, 134.7, 136.9, 139.3, 139.8, 140.6, 141.6, 142.8, 143.4, 146.4, 147.9, 151.5, 152.0, 153.9, 156.0, 157.1, 158.3; ^{11}B NMR (128 MHz, CDCl3) δ: 0.82-1.39 (m, 2xBF_2); HR-MS: *m/z* (intensity, %) Calc. for [M]: 1889.89 found 1890.8979; Anal. calc. for $C_{117}H_{126}B_2F_4N_6O_3S_4$: C, 72.81; H, 6.05; N, 4.52 found: C, 72.64; H, 5.71; N, 4.17.

Compounds 84 to **88** were synthesized according ref.[175].

Compound 89

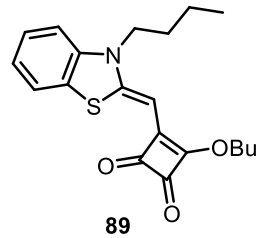

89

In a suspension of 1-butyl-1*H*-indolium **88b** and dibutyl squarate in anhydrous ethanol was added DIPA and the mixture was refluxed during 3 hours. Reaction mixture turns deep yellow after several minutes. The solvent were removed by vacuum distillation and the crude was taken with dichloromethane and washed with water three times. After drying the organic phase with anhydrous Na_2SO_4 and evaporation of the solvent, the product was provided as yellow solids following purification over an aluminium column chromatography (de-activated with 6% water in weight) eluting with CH_2Cl_2/MeOH 0.5% (51% yield). ^{1}H RMN (300 MHz, $CDCl_3$) δ: 0.97-1.03 (m, 6H), 1.43-1.56 (m, 4H), 1.71-1.89 (m, 4H), 3.79 (t, ^{3}J = 7.8 Hz, 2H), 4.79 (t, ^{3}J = 6.7 Hz, 2H), 5.45 (s, 1H), 7.06 (d, ^{3}J = 8.1 Hz, 1H), 7.13-7.18 (m, 1H), 7.30-7.36 (m, 1H), 7.46-7.49 (m, 1H); ^{13}C RMN (100 MHz, $CDCl_3$) δ: 13.8, 18.7, 20.2, 28.8, 32.1, 45.6, 73.5, 78.9, 110.9, 121.9, 123.4, 126.7, 126.9, 141.1, 159.4, 172.7, 185.4, 185.8, 192.9;); ES-MS: *m/z* (intensity, %)

Calc. for [M]: 358.1 found 357.14; Anal. calc. for $C_{20}H_{23}NO_3S$: C, 67.20; H, 6.49; N, 3.92 found: C, 67.04; H, 6.18; N, 3.77.

Compound 92

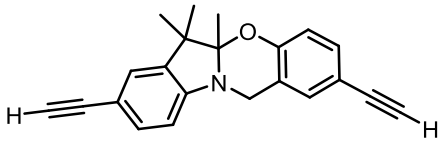

Compound **92** was obtained following the same procedure as compound **76** from compound **81 (**186 mg, 0.41 mmol) and KOH (11 mg, 0.17 mmol) overnight. Desired product **92** wos isolated as yellowish oil solidifying under vacuum (116 mg, 91%). ^{1}H RMN (300 MHz, $CDCl_3$) δ: 1.04 (s, 3H), 1.39 (s, 3H), 1.42 (s, 3H), 2.81 (s, 1H), 2.86 (s, 1H), 4.33-4.46 (m, 2H), 6.35 (d, ^3J = 7.9 Hz, 1H), 6.50 (d, ^3J = 8.4 Hz, 1H), 7.06-7.15 (m, 4H); ^{13}C RMN (100 MHz, $CDCl_3$) δ: 16.16, 18.81, 25.8, 29.7, 40.1, 47.7, 74.9, 75.7, 83.5, 84.7, 100.8, 107.9, 112.9, 113.6, 117.9, 118.5, 126.1, 130.7, 132.0, 132.2, 138.5, 147.9, 153.6; ES-MS: *m/z* (intensity, %) Calc. for [M]: 313.15 found 314.1; Anal. calc. for $C_{22}H_{19}NO$: C, 84.31; H, 6.11; N, 4.47 found: C, 84.11; H, 5.74; N, 4.24.

Compound 93

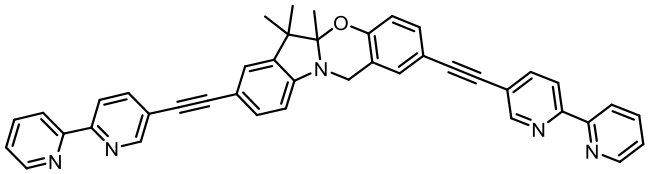

Compound **93** was prepared following the same procedure as compound **81** from compound **92** (100 mg, 0.23 mmol) and 5-bromo-2,2'-bipyridine catalyzed with $[Pd(PPh_3)_4]$. The product was obtained in 35% yield as yellow powder after purification over silica column chromatography eluting with CH_2Cl_2/MeOH 3%. ^{1}H RMN (400 MHz, $CDCl_3$) δ: 1.14 (s, 3H), 1.50 (s, 3H), 1.51 (s, 3H), 4.51 (s, 2H), 6.49 (d, ^3J = 8.8 Hz, 1H), 6.63 (d, ^3J = 8.5 Hz, 1H), 7.21-7.25 (m, 3H), 7.28-7.29 (m, 1H), 7.38-7.42 (m, 1H), 7.59-7.64 (m, 1H), 7.72-7.77 (m, 2H), 7.81-7.85 (m, 2H), 8.31-8.37 (m, 4H), 8.61-8.63 (m, 2H), 8.71-8.73 (m, 2H); ^{13}C RMN (100 MHz, $CDCl_3$) δ: 16.2, 18.9, 25.9, 29.7, 40.1, 47.8, 53.4, 84.6, 85.2, 93.6, 94.8, 100.9, 108.2, 113.5, 114.1, 118.1, 118.7, 120.3, 120.3, 120.6, 121.0, 121.3, 121.3, 123.7, 123.8, 125.8, 128.4, 128.5, 130.4, 131.7, 131.9, 131.9, 132.0, 132.1, 132.2, 136.9, 136.9, 138.7, 139.0, 139.1, 148.0, 149.2, 149.3, 151.4, 151.5, 153.7, 154.2, 154.5, 155.5, 155.6.

Compound 94

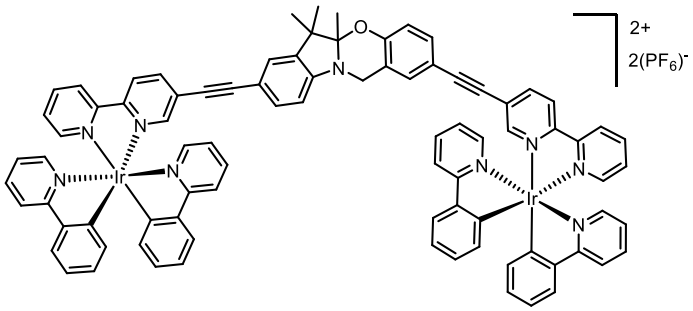

Compound **94** was prepared following the same procedure as compound **51**. ^{1}H RMN (400 MHz, CD_3CN) δ: 1.15 (d, *J* = 2.3 Hz, 3H), 1.50 (d, *J* = 2.6 Hz, 3H), 1.56 (s, 3H), 4.54-4.68 (ABq, 2H), 6.27-6.33 (m, 4H), 6.62-6.66 (m, 2H), 6.92-6.97 (m, 4H), 7.04-7.06 (m, 8H), 7.16-7.19 (m, 2H), 7.21-7.23 (m, 1H), 7.28-7.29 (m, 1H), 7.47-7.52 (m, 2H), 7.61-7.62 (m, 2H), 7.70-7.72 (m, 2H), 7.81-7.88 (m, 8H), 7.95-7.99 (m, 4H), 8.07-8.18 (m, 8H), 8.49-8.53 (m, 4H); ^{13}C RMN (100 MHz, CD_3CN) δ: 15.2, 17.5, 24.7, 39.1, 47.3, 82.2, 82.6, 89.2, 96.4, 98.1, 101.3, 108.3, 111.5, 112.2, 117.0, 117.4, 119.5, 119.6, 119.7, 122.3, 122.4, 123.2, 123.3, 124.0, 124.6, 124.7, 124.8, 125.4, 128.0, 128.1, 130.0, 130.2, 130.7, 131.1, 131.2, 131.5, 132.1, 138.3, 139.0, 140.4, 140.6, 143.7, 143.8, 148.9, 149.0, 149.4, 149.4, 149.7, 149.7, 150.3, 150.4, 151.2, 151.5, 153.6, 154.0, 154.8, 154.9.

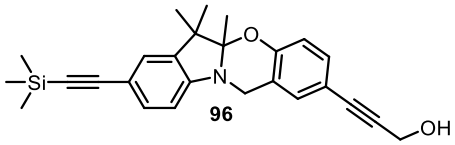

96

Compound 96: ^{1}H RMN (400 MHz, $CDCl_3$) δ: 0.22 (s, 9H), 1.15 (s, 3H), 1.49 (s, 3H), 1.52 (s, 3H), 4.43-4.53 (m, 4H), 6.43 (d, ^{3}J = 8.7 Hz, 1H), 6.59 (d, ^{3}J = 8.4 Hz, 1H), 7.13 (dd, ^{3}J = 8.2 Hz, ^{4}J = 2.3 Hz, 1H), 7.18-7.22 (m, 3H).

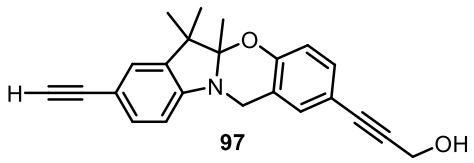

97

Compound 97: ^{1}H RMN (400 MHz, $CDCl_3$) δ: 1.15 (s, 3H), 1.49 (s, 3H), 1.52 (s, 3H), 2.94 (s, 1H), 4.45-4.53 (m, 4H), 6.38 (d, ^{3}J = 8.0 Hz, 1H), 6.60 (d, ^{3}J = 8.3 Hz, 1H), 7.13 (dd, ^{3}J = 8.3 Hz, ^{4}J = 2.1 Hz, 1H), 7.18-7.24 (m, 3H).

Compound 98

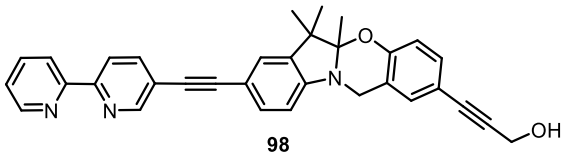

98

Compound **98** was prepared following the general Sonogashira conditions as for **81** from **97** (36 mg, 0.11 mmol) and 5-bromo-2,2'-bipyridine (29 mg, 0.13 mmol). The product was obtained as yellow oil (which solidifies under vacuum) following silica column chromatography (CH_2Cl_2/MeOH 0.5 to 1%), 35 mg, 67%. ^{1}H RMN (400 MHz, $CDCl_3$) δ: 1.18 (s, 3H), 1.53 (s, 3H), 1.54 (s, 3H), 2.94 (s, 1H), 4.47 (s, broad, 2H), 4.52 (s broad, 2H), 6.51 (d, ^3J = 8.7 Hz, 1H), 6.62 (d, ^3J = 8.5 Hz, 1H), 7.14 (dd, ^3J = 8.3 Hz, ^4J = 1.9 Hz, 1H), 7.19 (d, ^4J = 1.9 Hz, 1H), 7.28-7.33 (m, 3H), 7.82 (td, ^3J = 7.8 Hz, ^4J = 1.7 Hz, 1H), 7.88 (dd, ^3J = 8.2 Hz, ^4J = 2.1 Hz, 1H), 8.39 (t, ^3J = 8.1 Hz, 2H), 6.68 (d broad, J = 4.5 Hz, 1H), 8.77 (d, ^4J = 1.8 Hz, 1H); ^{13}C RMN (100 MHz, $CDCl_3$) δ: 16.2, 18.9, 25.9, 40.1, 47.7, 51.6, 84.5, 85.5, 85.9, 94.9, 100.7, 108.1, 113.3, 114.1, 117.9, 118.5, 120.3, 121.0, 121.3, 123.8, 125.7, 130.3, 131.6, 131.9, 137.0, 138.7, 139.0, 148.1, 149.2, 151.4, 153.4, 154.1, 155.6.

Compound 99

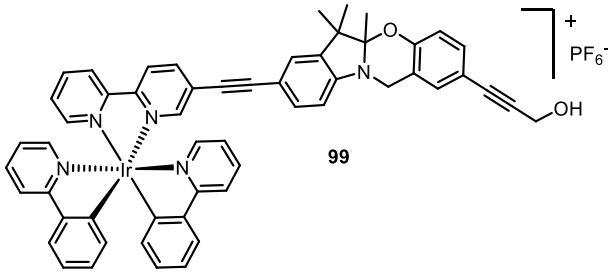

99

Compound **99** was prepared according the same procedure as compound **51** from **98** (35 mg, 0.07 mmol) following anion exchange with an aquaos solution of KPF_6. Purification of the crude from de-activated aluminium column chromtography (CH_2Cl_2/MeOH 0.5 to 1%) provided the complex as orange powder (41 mg, 51 %). ^{1}H RMN (300 MHz, $CDCl_3$) δ: 1.14 (s, 3H), 1.49 (s, 3H), 1.52 (s, 3H), 4.44 (s, broad, 2H), 4.50 (s broad, 2H), 6.27 (t, ^3J = 6.7 Hz, 2H), 6.47 (d, ^3J = 8.4 Hz, 1H), 6.59 (d, ^3J = 8.5 Hz, 1H), 6.90 (td, ^3J = 7.4 Hz, ^4J = 3.5 Hz, 2H), 6.97-7.06 (m, 4H), 7.10-7.19 (m, 4H), 7.35 (t, ^3J = 6.5 Hz, 1H), 7.48 (d, J = 5.5 Hz, 1H), 7.53 (d, J = 5.8 Hz, 1H), 7.76 (d, ^3J = 7.5 Hz, 2H), 7.72-7.77(m, 2H), 7.88-7.92 (m, 4H), 8.03-8.11 (m, 2H) 8.56 (t, ^3J = 8.2 Hz, 2H).

Crystal data and Structure refinements

Identification code		**Compound 25**	**Compound 38**
Empirical formula		C_{42} H_{51} B F_2 I N_3 O	C_{49} H_{56} B F_2 I N_4 O
Formula weight		789.57	892.69
Crystal system		Monoclinic	Triclinic
Space group		P 2_1/c	P -1
Unit cell dimensions	*a* (Å)	14.7692(10)	12.0355(3)
	b (Å)	19.4543(5)	12.7527(4)
	c (Å)	10.8712 (11)	14.7677(10)
	α (°)	90	96.021(7)
	β (°)	96.517(6)	90
	γ (°)	90	96.517(6)
Volume (Å^3)		3900.3(3)	2196.38(17)
Z, Z'		4, 1	4, 1
Calcd density (Mg/m^3)		1.345	1.350
Wavelength (Å)		1.54187	1.54187
Abs. coefficient μ (mm^{-1})		6.807	6.117
F(000)		1632	924
Crystal habit and size (mm)		Dark red cobbledstone 0.325 x 0.280 x 0.110	Dark red plate 0.60 x 0.15 x 0.03
Diffractometer		Rapid II mm007HF – CMF optics	Rapid II mm007HF – CMF optics
Temperature (K)		153(2)	193(2)
θ *range for data collection* (°)		9.07 to 58.93	3.07 to 68.24
Limiting indices		-16 ≤ h ≤ 15, -21 ≤ k ≤ 13, -15 ≤ l ≤ 14	-13 ≤ h ≤ 8, -14 ≤ k ≤ 15, -17 ≤ l ≤ 16
Reflect° collected / unique		18088 / 5383	20810 / 7721
R(int)		0.0825	0.0627
Completeness to θ_{max} *(%)*		96.0 %	95.9 %
Absorption correction			
		Fs_Abscor (CrystalClear-SM)	*Fs_Abscor (CrystalClear-SM)*
Max. and min. transmission		0.47 and 0.25	0.83 and 0.40
Solution method			
Refinement method			
Data / restraints / parameters		5383 / 0 / 459	7721 / 0 / 533
Goodness-of-fit on F^2		1.132	1.025
Final R indices [I>2σ(I)]	R1	0.0494	0.0779
	wR2	0.1108	0.1917
R indices (all data)	R1	0.0658	0.1356
	wR2	0.1439	0.2410
Extinction coefficient		-	0.0013(3)
Largest diff. peak and hole (e. Å3)		0.597 and -1.201	0.967 and -1.030
CCDC deposit number		934638	934637

Identification code		**Compound 74**	**Compound 47**	**Compound 48**
CRYSTAL DATA				
Empirical formula		C_{51} H_{49} B BrF_2 N_3 O_4 0.5(CH_2Cl_2),0.5(CH_2Cl_2)	C_{25} H_{27} B F_2 N_2 O	C_{23} H_{26} B F_2I N_2 O
Formula weight		981.58	420.29	522.17
Crystal system		Monoclinic	Monoclinic	Monoclinic
Space group		P $2_1/c$	P $2_1/n$	P $2_1/c$
Unit cell dimensions	*a*(Å)	19.26(7)	7.4097(1)	17.062(2)
	b(Å)	19.55(9)	16.6008(3)	16.162(3)
	c(Å)	13.28 (4)	17.5139(12)	17.684(3)
	α (°)	90	90	90
	β (°)	90.33(14)	96.835(7)	114.739(3)
	γ (°)	90	90	90
Volume (Å^3)		5000(33)	2139.02(16)	4428.9(12)
Z, Z'		4, 1	4, 1	8, 2
Calcd density (Mg/m^3)		1.304	1.305	1.566
Wavelength (Å)		1.54187	1.54187	0.71073
Abs. coefficient μ (mm^{-1})		2.345	0.739	1.480
F(000)		2032	888	2096
DATA COLLECTION				
Crystal habit and size (mm)		? ? x ? x ?	Red stick 0.60 x 0.15 x 0.06	Orange stick 0.60 x 0.12 x 0.10
Diffractometer		Rapid II mm007HF – CMF optics	Rapid II mm007HF – CMF optics	Enraf-Nonius FR590-Kappaccd
Temperature (K)		193(2)	193(2)	293(2)
θ range for data collection (°)		2.29 to 44.49	3.68 to 65.08	1.313 to 23.87
Limiting indices		-16 ≤ h ≤ 17, -17 ≤ k ≤ 17, -11 ≤ l ≤ 12	-8 ≤ h ≤ 8, -19 ≤ k ≤ 18, -12 ≤ l ≤ 20	-19 ≤ h ≤ 17, -18 ≤ k ≤ 18, -20 ≤ l ≤ 20
Reflect° collected / unique		26011 / 3936	11771 / 3626	23128 / 6841
R(int)		0.209	0.0396	0.0433
Completeness to θ max (%)		100	99.1	99.3
Absorption correction		Semi-empirical from equivalents		
		Fs_Abscor(CrystalClear-SM)	*Fs_Abscor(CrystalClear-SM)*	*Scalepack (HKL 2000)*
Max. and min. transmission		1.00 and 0.44	0.96 and 0. 72	0.86 and 0.71
SOLUTION and REFINEMENT				
Solution method		Direct Methods *(SHELXS-97)*		
Refinement method		Full-matrix least-squares on F^2*(SHELXL-97)*		
Data / restraints / parameters		3936 / 549 / 618	3619 / 66 / 310	6824 / 770 / 802
Goodness-of-fit on F^2		1.411	1.162	1.094
Final R indices [I>2σ(I)]	R1	0.160	0.0509	0.0438
	wR2	0.400	0.1282	0.1067
R indices (all data)	R1	0.256	0.0854	0.0670
	wR2	0.462	0.1786	0.1198
Extinction coefficient		-	0.0035(4)	0.00199 (19)
Largest diff. peak and hole (e. Å3)		0.681 and -0.586	0.217 and -0.280	0.639 and -0.825

Publications

[1] Nano, A.; Gullo, M. P.; Ventura, B.; Armaroli, N.; Barbieri, A.; Ziessel, R. "Panchromatic Luminescence from Julolidine Dyes Exhibiting Excited State Intramolecular Proton Transfer" *Chem. Commun.* **2015**, 3351.

[2] César, V.; Mallardo, V.; Nano, A.; Dahm, G.; Lugan, N.; Lavigne, G, Bellemin-Laponnaz S. "IMes-acac: hybrid combination of diaminocarbene and acetylacetonato sub-units into a new anionic ambidentate NHC ligand" *Chem. Commun.* **2015**, Advance article, DOI: 10.1039/C4CC08641D

[3] Torres-Werlé, M.; Nano, A.; Maisse-François, A.; Bellemin-Laponnaz, S. "Asymmetric benzoylation and Henry reaction using reusable polytopic bis(oxazoline) ligands and copper (II)" *New J. Chem.* **2014**, *38*, 4748-4753.

[4] Nano, A.; Retailleau, P.; Hagon, J. P.; Harriamn, A.; Ziessel, R. "A hybrid bis(amino-styryl) substituted Bodipy dye and its conjugate diacid: synthesis, structure, spectroscopy and quantum chemical calculations*" Phys. Chem. Chem. Phys.* **2014**, *16*, 10187-10198.

[5] Nano, A.; Zissel, R.; Stachelek, P.; Alamiry, M. A. H.; Harriman, A. "Exciplex Emission from a Boron Dipyrromethene (Bodipy) Dye Equipped with a Dicyanovinyl Appandage" *Chem. Phys. Chem*. **2014**, *15*, 177-186.

[6] Nano, A.; Ziessel, R.; Stachelek, P.; Harriman, A. "Charge-Recombination Fluorescence from Push–Pull Electronic Systems Constructed around Amino-Substituted Styryl–BODIPY Dyes" *Chem. Eur. J*. **2013**, *19*, 13528-13537.

[7] Ziessel, R.; Nano, A.; Heyer, E.; Bura, T.; Retailleau, P. "Rational Design of New Thiazolo—Thiazole Dyes as Input Energy Units in Molecular Dyads" *Chem. Eur. J*. **2013**, *19*, 2582-2588.

[8] Nano, A.; Brelot, L.; Rogez, G.; Maisse-François, A.; Bellemin-Laponnaz, S. "Ditopic bis(oxazolines): Synthesis and strucutral studies of zinc(II), copper(II) and nickel(II) complexes" *Inorg. Chim. Acta*, **2011**, 376, 285-289.

Patent

[1] Nano, A.; Ziessel, R.; Jacobe, S. ; Dennler, G. "Intelligent Spacers Based on Asymmetric Photochromic Spiroxazine" Patent (August **2014**), accession number: 1457626.

Communications

[1] 6th ISNSC (International Symposium on Nano & Supramolecular Chemistry) in Bali, Indonesia, 10-14 august 2014.

“New Photochromic Compounds for Controlled Energy Transfer”.

[2] 51th SECO (Semaine d’Etude en Chimie Organique), congres on organic chemistry in Port Leucate, France, 18-24 may 2014.

“Synthesis and Characterization of New Push-Pull Systems Constructed Around Amino-Styryl-Bodipy Dyes”

[3] Journey of Strasbourg’s Chemistry PhD Students, 2013.

“Synthèse et Caractérisation de Nouveaux Systems Push-Pull Construit à Base d’Amino - Styry-Bodipy “

Résumé (in french)

Tout au long de ces années de doctorat, j'ai eu l'opportunité de travailler sur un ensemble de sujets qui portent sur la synthèse organique, la photochimie, la photophysique ainsi que la chimie organométallique. La lumière, émise de façon naturelle ou artificielle est très importante pour la caractérisation et le comportement de nos composés, mais elle est surtout indispensable pour l'ensemble du monde vivant.

La perception de la lumière nous permet de voir tous les objets et les couleurs qui nous entourent. Elle est le seul moyen qui nous permet de connaitre le monde telle qu'il est, ainsi que de pouvoir lire ces lignes en ce moment précis. La lumière interagit avec la rhodopsine, un pigment se trouvant dans les bâtonnets (cellules photoréceptrices) de la rétine de l'œil, en induisant une transformation *photochimique* qui cause par la suite une série de transformations physiologiques informant notre cerveau sur la réception de la lumière. La *photosynthèse* est un autre processus photochimique très important qui se déroule dans les plantes et dans certaines algues (*KingdomProtista*). En présence de la lumière, le dioxyde de carbone est transformé en sucre et simultanément l'énergie accumulée *via* la réaction est stockée grâce à la production de l'adénosine triphosphate (ATP) et du dioxygène. Donc, de manière générale la photochimie est d'une importance majeure pour le développement de la vie sur notre planète mais aussi pour sa protection contre les irradiations électromagnétiques dangereuses venant du soleil. La couche d'ozone qui se trouve au dessus de l'atmosphère nous protège en absorbant des irradiations de longeur d'onde inferieur à 320 nm.[184] L'ozone se dissocie en oxygène qui par la suite est reconverti en ozone *photochimiquement*. Donc la nature est en effet remplie d'exemples à base de systèmes chimiques qui utilisent la lumière comme source d'énergie pour la réalisation des processus dans lesquels ils sont impliqués.

Ainsi le travail de ce doctorat consiste dans le design et la synthèse de systèmes moléculaires optiques qui nous permettent de mieux comprendre des processus importants tel que le transfert photoinduit d'électron ou d'énergie. Pour la caractérisation de nos composés, nous avons employé des techniques expérimentales telles que la Résonance Magnétique Nucléaire (RMN), la spectrométrie de masse et la microanalyse. Les processus photophysiques et photochimiques sont étudiés en utilisant la spectroscopie d'absorption et d'émission et sont

[184]Borrell, P., *Photochemistry - A Primer*, Eds.Edward Arnold, 1973. ebook: https://archive.org.

supportés par des études de voltammètrie cyclique, spectroscopie d'absorption transitoire et DFT (Density Functional Theory). Ce travail consiste essentiellement en quatre importants chapitres.

Une introduction générale dans le domaine de la photophysique et la photochimie en évoquant les concepts importants est donnée dans le premier chapitre afin d'aider le lecteur à mieux comprendre les résultats présentés. Dans le premier chapitre nous décrivant l'interaction de la lumière avec la matière, le processus d'excitation et les divers processus de dé-excitations. Une partie de ce chapitre introduction est consacré a la *julolidine*, une molécule que nous avons utilisé et exploité tout au long des ces travaux pour ses propriétés électroniques très intéressantes. Enfin un projet portant sur le *photochromisme*; un phénomène photochimique très fascinant, a été introduite en Chapitre I et développé plus loin, dans le Chapitre 1V

Nous avons synthétisé et caractérisé de nouveaux colorants organiques à base de BODIPY (Boron DiPYrromethene) qui agissent comme des systèmes push-pull afin de pouvoir étudier et mieux comprendre le phénomène du transfert photoinduit d'électron. Les chromophores push-pull π-conjugués sont des systèmes moléculaires constitués d'une unité électron-donneur (D) et une unité électron-accepteur (A) connectés par un espacer conjugué (D-π-A). Ils possèdent un moment dipolaire (μ) élevé à l'état fondamental et à l'excité et font intervenir un processus de Transfert de Charge Intramoléculaire (TCI) du D vers A sous irradiation. Les résultats obtenus autour des systèmes push-pull font l'objet du deuxième chapitre de la thèse. De manière générale, tel que décrit sur le Schéma 1, l'accepteur est un groupement dicyanovinyl alors que le donneur est un dérivé BODIPY contenant un bras styryl portant un dérivé amine de type julolidine ou triazatruxène.

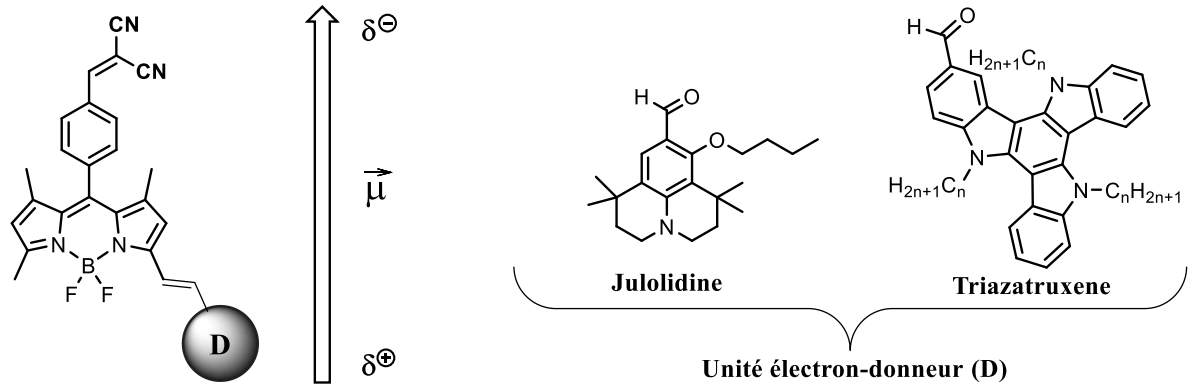

Schéma 1. Représentation générale de nos systèmes push-pull.

Les chromophores push-pull **27**, **30** sont synthétisés en trois étapes à partir du BODIPY **15** (connu aussi sous le nom *BODIPY Knorr*). La condensation du type Knoevenagel entre le BODIPY et l'aldéhyde correspondant (julolidine-aldéhyde ou triazatruxène-aldéhyde) fournit de manière sélective le mono-styryl**25**, **29** malgré la présence en large excès de l'aldéhyde. Par la suite, la réaction de formylation des précurseurs **25**, **29** en présence de monoxyde de carbone et de formiate de sodium, catalysé au Pd(II) conduit à la formation de **26** et **30**respectivement. Enfin la condensation type-Knoevenagel entre le malonitrile et les précurseurs formyles résulte en la formation des chromophores push-pull **27**, **30**.

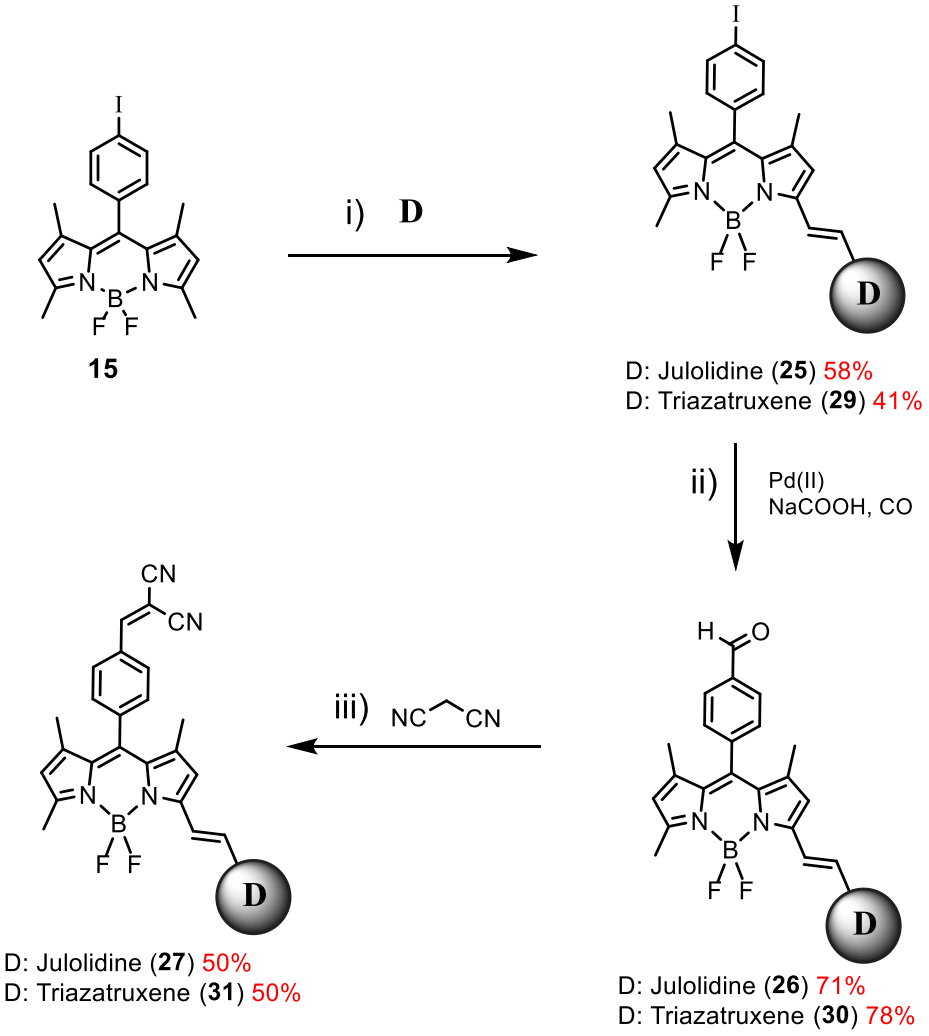

Schéma 2. Schéma de synthèse générale pour les systèmes push-pull obtenus.

Tous les composés ont été caractérisés par RMN (^{1}H, ^{13}C, ^{11}B), spectrométrie de masse, microanalyse et spectroscopie InfraRouge (IR). L'introduction de l'unité dicyanovinyl sur le phényle en position *méso* du cœur indacène du BODIPY supprime l'émission de fluorescence des chromophores **25**, **29** et **26**, **30**. Les molécules push-pull **27**, **31** ayant un system π-conjugué bien étendu présentent un fort caractère de transfert de charge intramoléculaire. Cela est confirmé par les valeurs importantes du moment dipolaire à l'état fondamental (μ_{GS}**27** = 9.3 D, μ_{GS}**31** = 8.0 D) ainsi qu'à l'état excité. Entre autre les constats de radiation diminuent comparant celles des molécules précurseurs (Table 1). Les mono-styryles précurseurs **25**, **29** qui manquent l'unité dicyanovinyl accepteur présentent une forte émission de fluorescence dont le maximum dépend de la nature du solvant. Ilspossèdent des constantes de radiation k_{rad} élevées et des moments dipolaire (μ_{GS}**25** = 2.5 D, μ_{GS}**29** = 3.0 D) faibles à l'état fondamental. Les résultats photophysiques ont été supportés par des calculs de DFT.

Table 1. Photophysical properties collected for **25**, **29**, **27** and **31** in MTHF at room temperature.

	λ_{Abs} (nm)	ε_{Max}/ ($M^{-1}cm^{-1}$)	d_{GS} (D)[a]	λ_{Flu} (nm)	φ_F	τ_F (ns)	k_{Rad} (10^7 s^{-1})[b]	λ_{CR} (eV)[c]
25	631	103 055	2.5	720	0.30	2.8	10.7	0.10
29	607	89 630	3.0	672	0.56	3.5	15.6	0.06
27	638	88 900	9.3	725	0.002	0.13	1.5	0.075
31	619	114 720	8.0	685	0.002	0.26	0.9	0.068

[a]Computed dipole moment for the ground state.[b]$k_{Rad}$was calculated following the equation $k_{Rad} = \varphi_F/\tau_F$. [c]Reorganisation energy accompanying charge-recombination emission extracted from spectral curve fitting.[d]Values found in THF solution of **27** and **31** at rt.

Les travaux effectués sur les chromophores push-pull nous ont permis de constater entre autre les propriétés électroniques très remarquables de l'amine tricyclique julolidine. Les dérivés BODIPY contenant des unités amines ou hydroxyles font partie des molécules cibles pour l'utilisation comme sonde de pH. Ici, le BODIPY est substitué avec deux amines différentes donnant lieu à un distyryl hybride **38**. Le composé est obtenu par condensation Knoevenagel à partir du mono-styryl **25** ou **39** avec l'aldéhyde correspondant. La molécule est jusqu'à présent le premier exemple de dérivé BODIPY contenant deux sites amines différents en position 3,5 du cœur indacène. Elle constitue une nouvelle classe de sonde optique de pH opérant sur une large fenêtre, *i.e.*pH: 2-7. Les études théoriques par la DFT indiquent que le site julolidine est protoné en premier lieu générant l'espèce protonée avec un pKa = 5.75-5.80. Cette protonation a pour conséquence de rendre difficile celle du deuxième site

diméthylphénylamine. Le pKa de l'espèce diprotonée est estimé 2.78-2.70 d'après les expériences de dosages fluorométriques par ajout contrôlé de HCl.

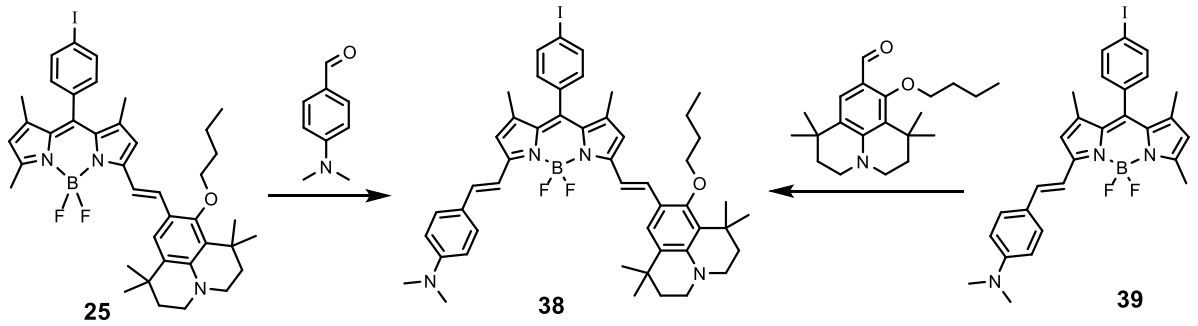

Schéma 3. Synthèse du styryl hybride **38**.

La julolidine est une amine aromatique tertiaire possédant une structure chimique très spéciale où deux chaines N-alkyl subissent une bis-cyclisation autour du cycle aromatique. Par conséquence, cette conformation géométrique de la molécule entraine une parfaite conjugaison du doublet libre de l'azote avec le cycle aromatique et confère ainsi à la molécule une réactivité chimique très inattendue. D'après les recherches bibliographiques, les dérivés de la julolidine sont peu exploités en chimie de coordination. Dans le troisième chapitre nous avons ainsi exploité cette réactivité dans l'élaboration d'une série de ligands dérivés de la julolidine et connue sous le terme *anil* ainsi que leur complexation avec le bore(III) ou des métaux de transitions telles que l'iridium(III) et platine(II).

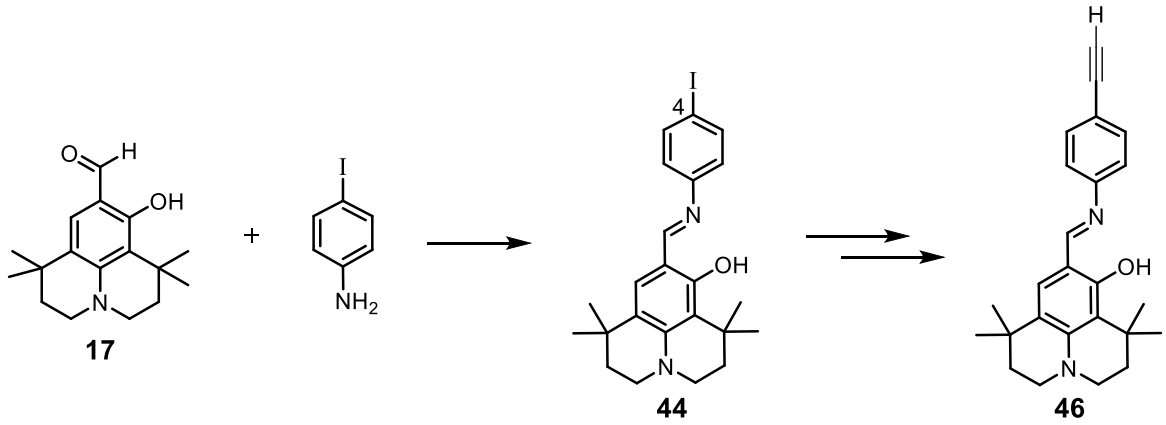

Schéma 4. Synthèse des derivésjulolidine**44** et **46**.

La condensation de julolidine-aldéhyde **17** avec 4-iodoaniline conduit à la formation du dérivé anil **44**possédant un site chélatant du type-N^O. La position iodo de ce dernier est transformée en acétylène terminal en deux étapes. La complexation des ligands type-N^O au BF_2 des molécules **44** et **46** résulte en la formation des boranil **48**, **47** respectivement.

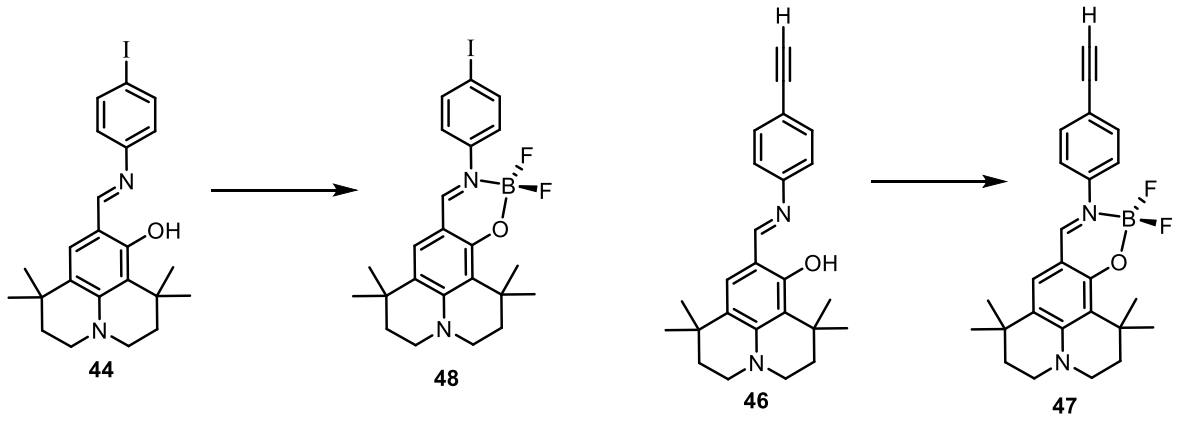

Schéma 5. Structure chimique des ligands anils (**44**, **46**) et leurs complexes boranils (**47**, **48**).

Les études photophysiques des ligands **44** et **46** ont mis en évidence un processus photoinduit de transfert de proton intramoléculaire dans l'état excité, connu plus souvent sous l'anagramme ESIPT (*Excited State Intramolecular Proton Transfer*). Ce processus est à l'origine de la tautomérisation de la forme énol vers la forme cétone des ligands anil en transférant un proton depuis la fonction *ortho*-OH vers l'azote du fragment imine (Schéma 6).

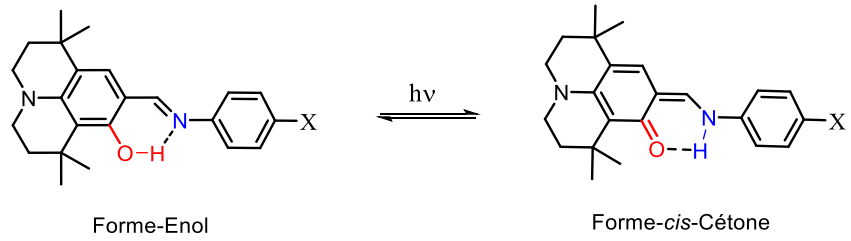

Schéma 6. Les formes tautomères des dérivés anil.

Du fait de cette tautomérisation, les spectres d'émissions des dérivés anils ont révélé une *luminescence panchromatique* due à la double émission provenant de l'espèce énol et cétone (Figure 1). Malgré que les rendements quantiques de fluorescence soient faibles, ces résultats s'avèrent très prometteurs puisque jusqu'à présent l'émission de la lumière blanche est achevée essentiellement en faisant intervenir des systèmes moléculaires (le plus souvent organométalliques) plus complexes. En revanche, la chélation du site N^O au fragment BF_2 supprime le processus ESIPT et augmente de manière importante le rendement quantique de fluorescence des boranils correspondant du fait de la rigidification de la structure de la molécule (Figure 1).

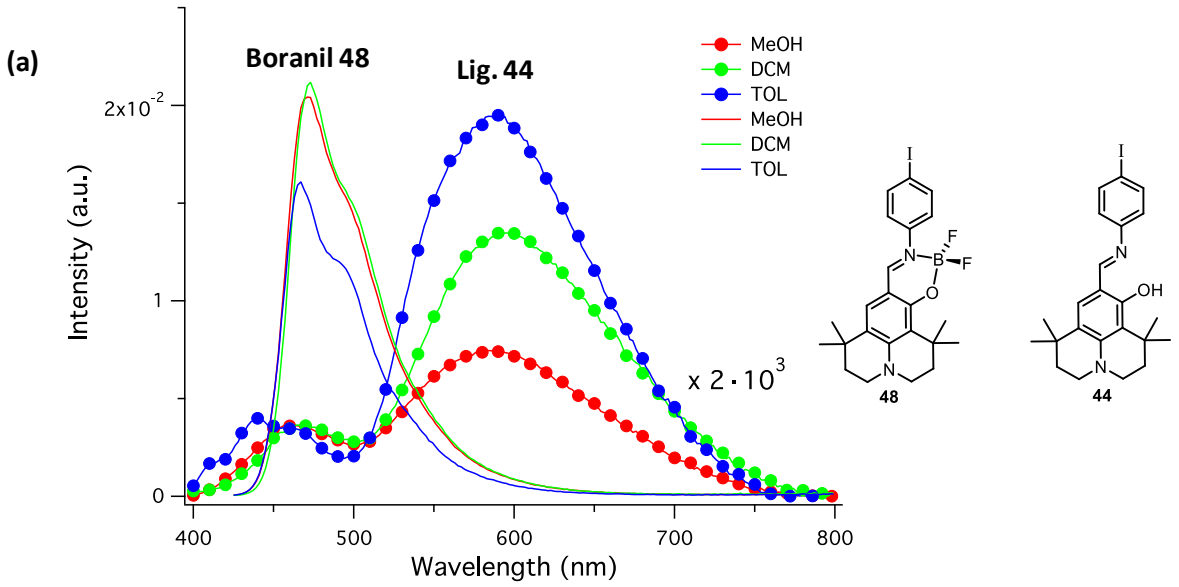

Figure 1. Spectre d'émission du ligand **44** et du boranil **48** dans des solvants différents à température ambiante.

Les ligands dérivés de la julolidine ont été également utilisés pour le design et la synthèse des systèmes multichromophoriques. Ces systèmes sont des entités moléculaires composées de plusieurs unités photo-actives. L'intérêt repose sur le fait que la combinaison de manière appropriée des composantes peut permettre l'activation directe des processus de transfert d'énergie ou d'électrons. Ainsi nous avons synthétisé et caractérisé **52**, **53** et **56** (Schéma 7).

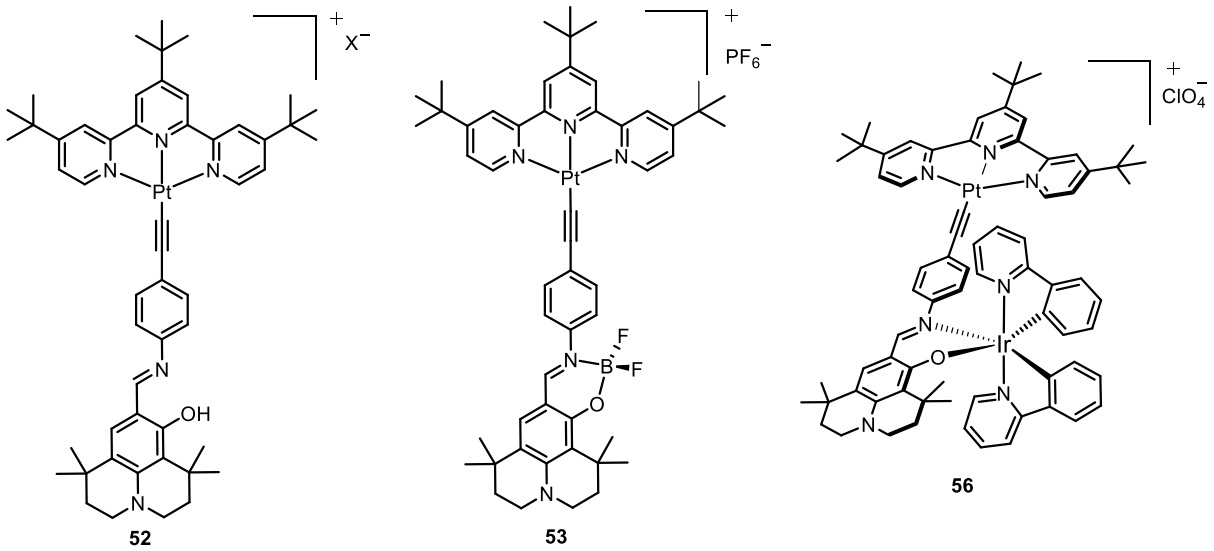

Schéma 7. Les structures chimiques des chromophores **52**, **53**, **56**.

La combinaison du ligand dérivé de la julolidine avec un chromophore de Pt(II) conduit à la formation de la dyade **52** par réaction de couplage catalysé au palladium. Les mesures

photophysiques de cette molécule indiquent que l'excitation électronique par irradiation induit un transfert d'énergie depuis l'unité chromophorique de Pt (^{3}MLCT) vers l'état triplet du ligand julolidine. Ce processus est observé également dans le cas du composé **53** où le site N^O est bloqué par complexation au BF_2. Entre autres, nous avons synthétisé et entièrement caractérisé un complexe hétérométallique original, dinucléaire, basé sur le ligand dérivé de la julolidine. Le complexe ne présente pas de luminescence à température ambiante mais à 77 K,sur une matrice solide, il dispose une large bande d'émission recouvrant entièrement le spectre visible (Figure 2).

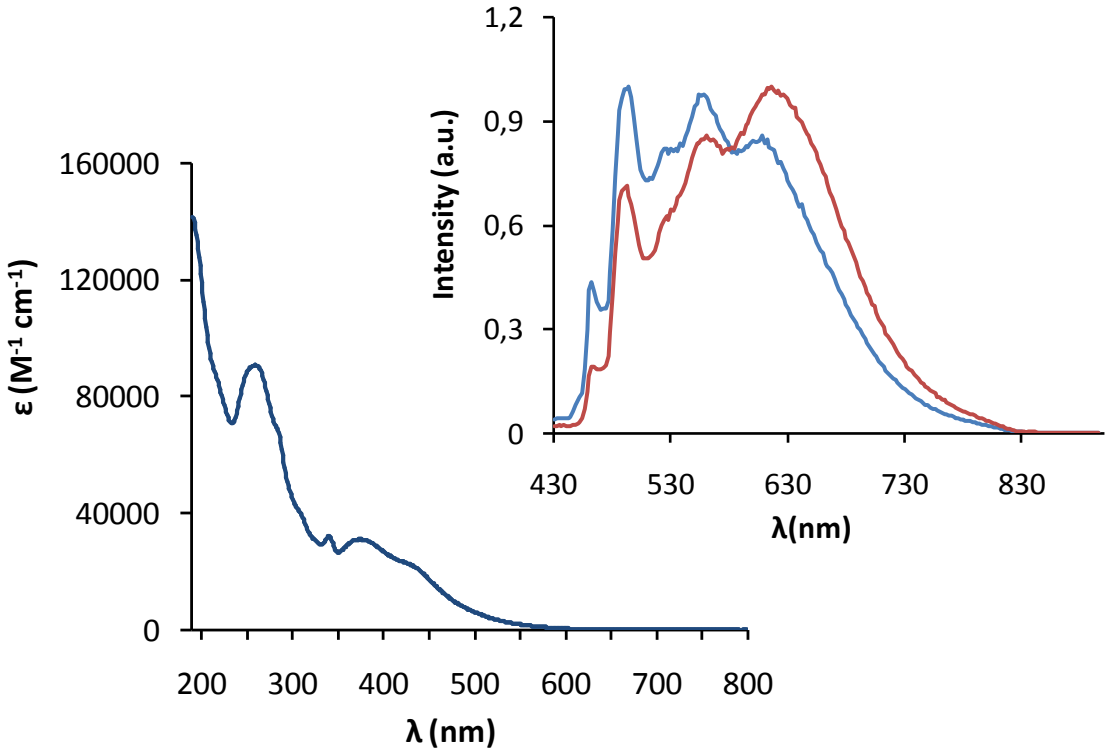

Figure 2. En bas: spectre d'absorption du composé **56** dans une solution d'acétonitrile à température ambiante. En haut: Spectre d'émission de **56** dans une solution mélange CH_2Cl_2:CH_3OH (1:1) à 77K, en bleu (λ_{exc} = 325 nm), en rouge (λ_{exc} = 375 nm).

Durant ces dernières décennies, un intérêt croissant est porté vers les molécules et les assemblages supramoléculaires qui existent sous deux formes thermodynamiquement stables et interconvertibles par des divers stimuli externes. L'intérêt de ce type de molécules réside dans le fait qu'elles peuvent être assimilées à des fonctions logiques telles que le bit (0 et 1) qui est la fonction principale de tous les systèmes digitaux (par exemple les ordinateurs, les téléphones, les appareils photos etc.).

De ce fait, elles peuvent trouver de nombreuses applications dans le domaine de l'électronique moléculaire ainsi que la photonique. Néanmoins, il existe de nombreux exemples dans la nature notamment dans le processus de la photosynthèse ou de la vision.

Ainsi, la transformation d'une espèce A en espèce B sous irradiation électromagnétique avec une longueur d'onde appropriée de façon réversible et accompagnée d'un changement dramatique du spectre d'absorption, est connue sous le nom de *photochromisme* (Figure 3). Ces transformations induisent des changements structuraux et électroniques ayant des conséquences sur les propriétés chimiques et optiques du photochrome ou de l'assemblage porté par l'unité photochrome.

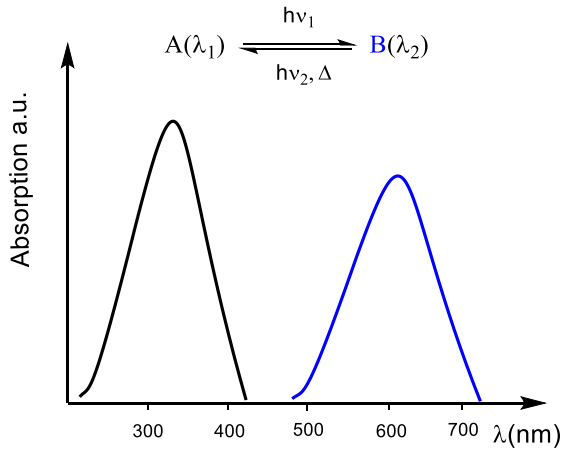

Figure 3. Représentation générale du spectre d'absorption de la transformation photoinduite de l'espèce A vers B.

Les changements optiques peuvent être induits également par voie thermique, le phénomène est appelé *thermochromisme* et lorsque les changements font intervenir un traitement acide, *acidochromisme*. La plupart des réactions photochimiques sont unimoléculaire, il s'agit d'une interconversion entre deux formes isomères, mais elles peuvent aussi être bimoléculaires (généralement des réactions de cycloadditions photoinduits). Dans ces travaux, nous nous sommes essentiellement intéressés par le photochromisme qui fait l'objet du quatrième chapitre. Plus généralement les molécules présentant un photochromisme sont dites photochromes.

Une caractéristique remarquable des molécules photochromes réside dans la possibilité de les assembler avec des fluorophores ou dérivés phosphorescents, composés capables d'émettre de la lumière (fluorescence ou phosphorescence) après excitation, et ainsi de créer des molécules appelées « dyades » ou « triades » dont la luminescence peut être modulée. La lumière peut

être modulée et contrôlée selon le cas où le photochrome est « ouvert » ou « fermé » *vide infra*. Il existe toute une myriade de composés photochromes organiques lesquels sont divisés en différentes familles selon la réaction chimique résponsable de leur photochromisme. Les principales familles sont:

- une isomérisation *cis-trans* (stilbènes, azobenzènes);
- un transfert de protons intramoléculaires (anils);
- une rupture de liaison hétérocyclique (spiroxazine, spiropyrans, 2*H*-chromens);
- une fermeture de cycle (fulgides, diarylethènes).

Notre choix s'est porté sur les dérivés spirohétérocycliques de type spiroxazine dont l'activité photochrome résulte de l'ouverture du cycle oxazine. Plus particulièrement, il s'agit des dérivés [1,3]oxazine reportés pour la première fois par F. M. Raymo *et al.* en 2005.[185] De manière générale, la spiroxazine incolore au départ subit une rupture de la liaison C-O du cycle oxazine sous irradiation ultra violet (Schéma 8). La forme ouverte générée est une forme colorée et caractérisée par des paramètres physico-chimiques différents de celle de la forme fermée.

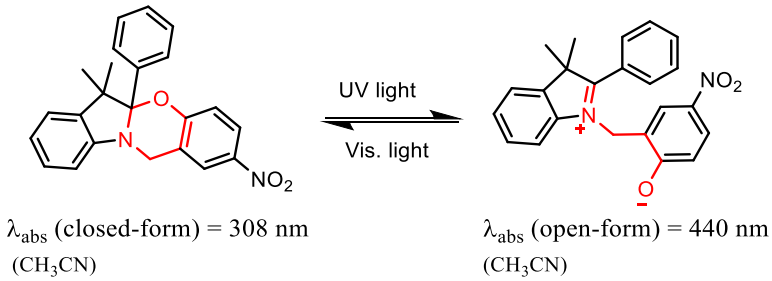

Schèma 8. Le photochromisme d'un dérivé [1,3]oxazine introduite par F. M. Raymo *et al.*

Ainsi nous avons utilisé un dérivé [1,3]oxazine dans le design et la synthèse de triades photocommutables ayant pour but des applications dans les mémoires optiques. La triade obtenue au cours de ces travaux consiste en une unité oxazine liée de façon covalente avec un donneur d'énergie (un BODIPY) et un accepteur d'énergie (le boranil, obtenue lors des travaux antérieurs) dont les paramètres optiques sont représenté dans la Figure 4.

[185] Tomasulo, M.; Sortino, S.; Raymo, F. M. *Org. Lett.* **2005**, *7*, 1109.

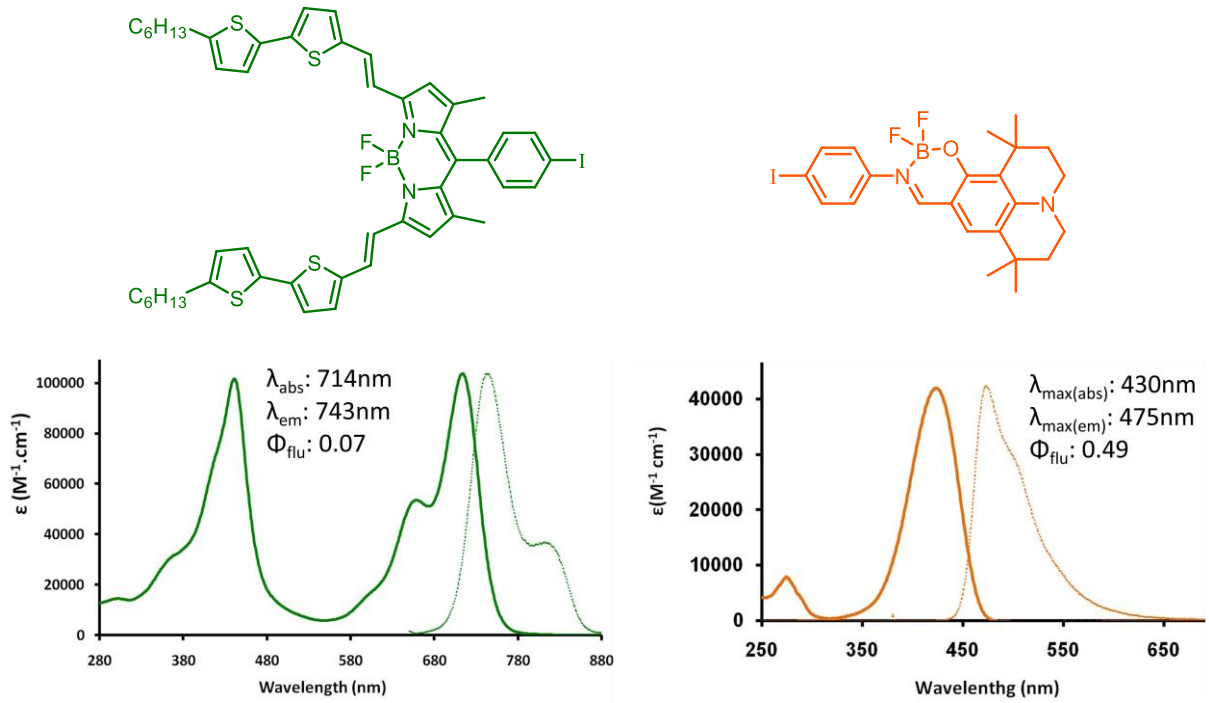

Figure 4. Structure chimique de l'unité donneuse (boranil, orange) et accepteur (BODIPY, vert) d'énergie (haut figure) et leurs spectres d'absorptions et émissions (bas figure).

La méthode de synthèse que nous avons employée pour l'obtention de la molécule commutable consiste en une procédure linéaire, étape par étape, à partir de l'oxazine **60** (Schéma 9). Nous avons synthétisé une spiroxazine de départ comportant un site iodo en position *para* de l'azote du fragment indole et un site bromo en position *para* de l'atome oxygène du fragment phénolate (composé **60**, Schéma 9). Les deux sites ayant différents réactivités chimique, cette fonctionnalisation permet de pouvoir y introduire de façon régiosélective des modules fluorophores différents en utilisant des réactions de couplages-croisés catalysées au palladium. En effet, le composé [1,3]oxazine **60** ne présente pas de propriétés photochromes. Il devient ainsi photochrome après l'ajout d'un module moléculaire π-conjugué et riche en densité électronique sur le groupement méthyle du centre stéréogène. Ainsi, nous avons choisi d'utiliser notre module fétiche, la julolidine, qui permet d'avoir les paramètres optiques convenable pour le photochrome à l'état ouvert.

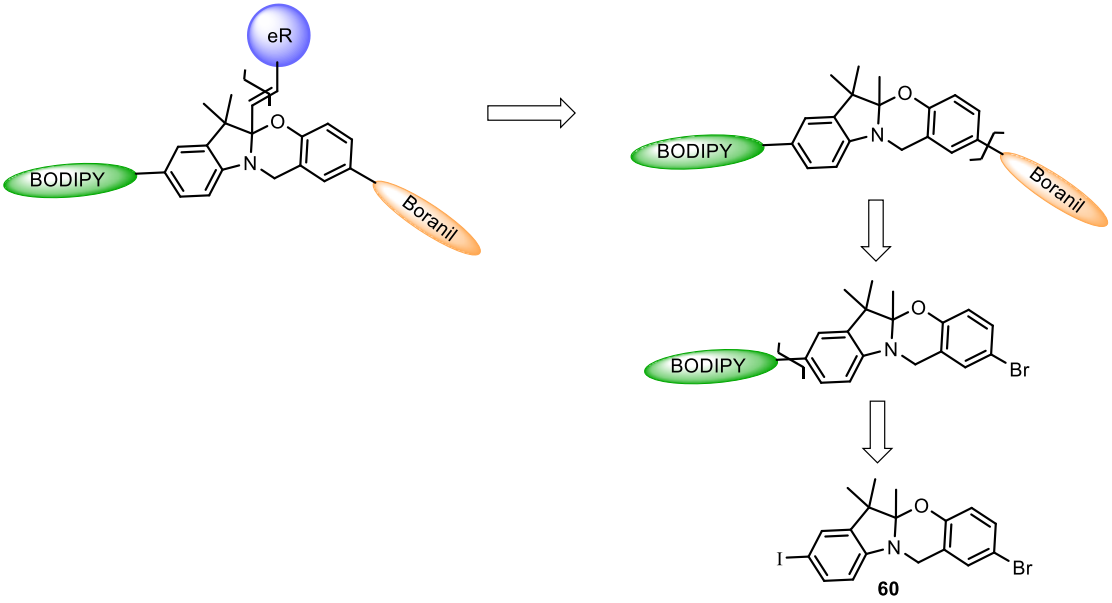

Schéma 9. Schéma rétrosynthétique de la triade désignée.

La stratégie de synthèse du composé **83** consiste dans un premier temps en l'ancrage de l'unité accepteur d'énergie par une réaction de couplage-croisé de Sonogashira catalysée au Pd(0) suivie de l'ancrage du bras boranil également par une réaction de Sonogashira (Schéma 9). L'étape finale est la condensation Konevenagel de la julolidine sur la position stéréogène de l'oxazine.

La triade **83** est obtenue en 9 étapes à partir du composé commercial, le 4-iodophényl hydrazine permettant l'obtention du composé **60**. Le site iodo du **60** est d'abord transformé en acétylène terminal en deux étapes; une réaction de couplage-croisé au $[Pd(PPh_3)_2Cl_2]$ avec le TMS-acétylène et en suite une déprotection au KOH. L'iodo-BODIPY **77** (accepteur d'énergie) est assemblé avec l'oxazine **76** suivant une réaction de couplage-croisé de Sonogashira catalysée au $[Pd(PPh_3)_4]$. Par la suite, le site bromo du **76** est transformé en acétylène terminal en employant des conditions réactionnelles plus ardues dues à la faible réactivité de ce site. La réaction de Sonogashira entre le composé **80** et l'iodo boranil **48** catalysée au $[Pd(PPh_3)_4]$ conduit à la formation de la pré-triade **82** avec un bon rendement réactionel. La condensation Knoevenagel entre l'aldehyde-julolidine et la pré-triade **82** en milieu acide résulte en la formation du composé **83** avec un rendement correct (36 %) tenue compte de la longue procédure de synthèse (Schéma 11).

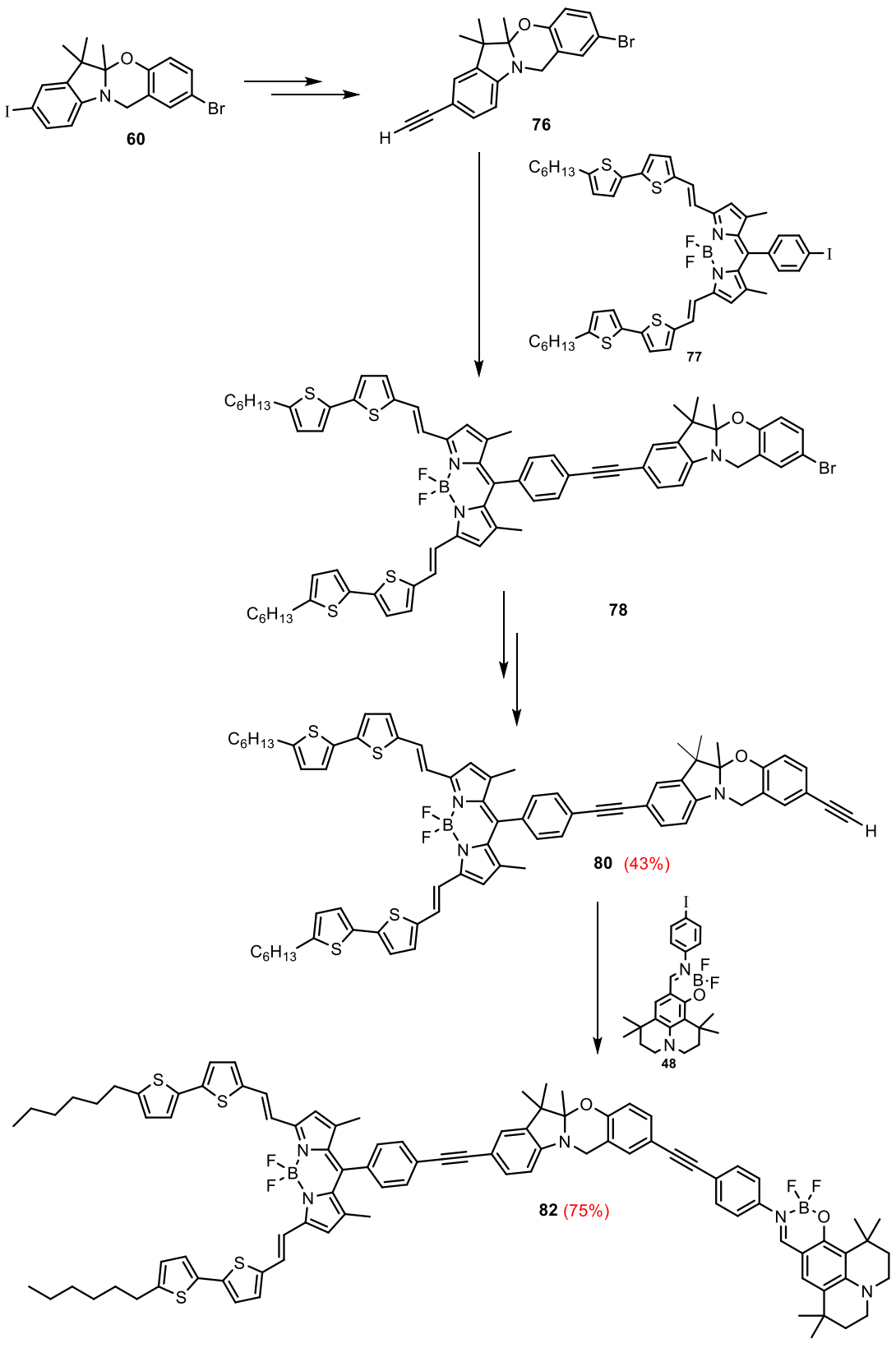

Schéma 10. Schéma de synthèse de la triade **83**.

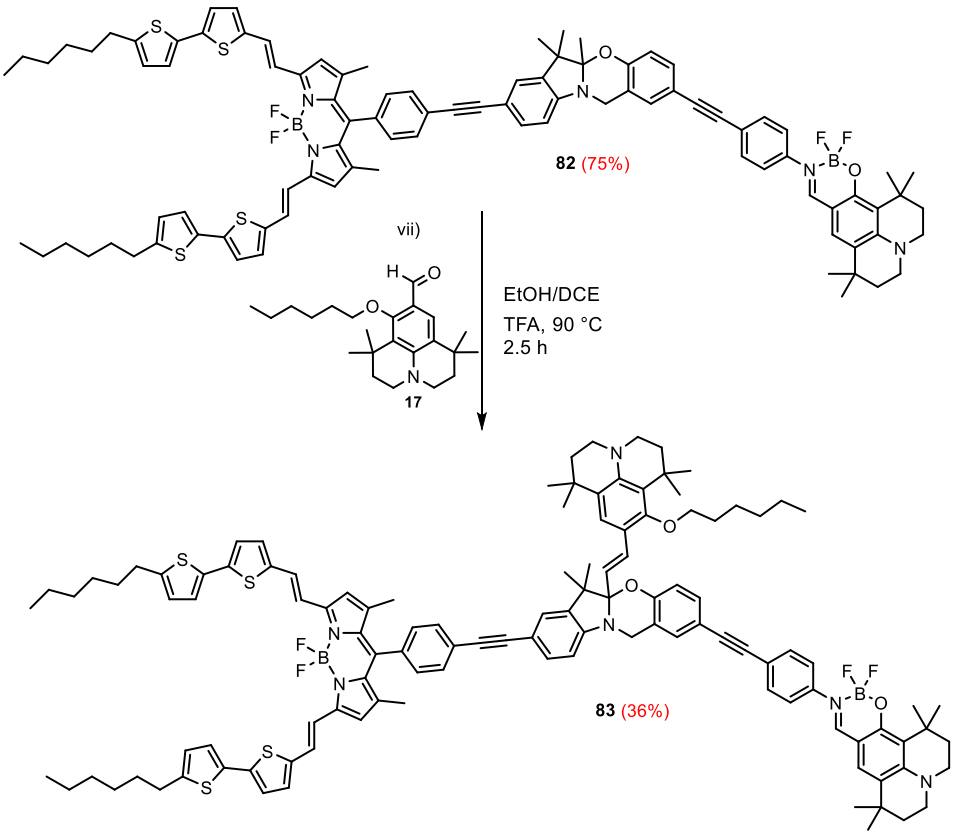

Schéma 11. Étape finale de la synthèse de la triade **83**.

La structure chimique de la triade **83** est confirmée par des études de RMN de ^{1}H, ^{13}C, ^{11}B ainsi que la spectrométrie de masse et la microanalyse.

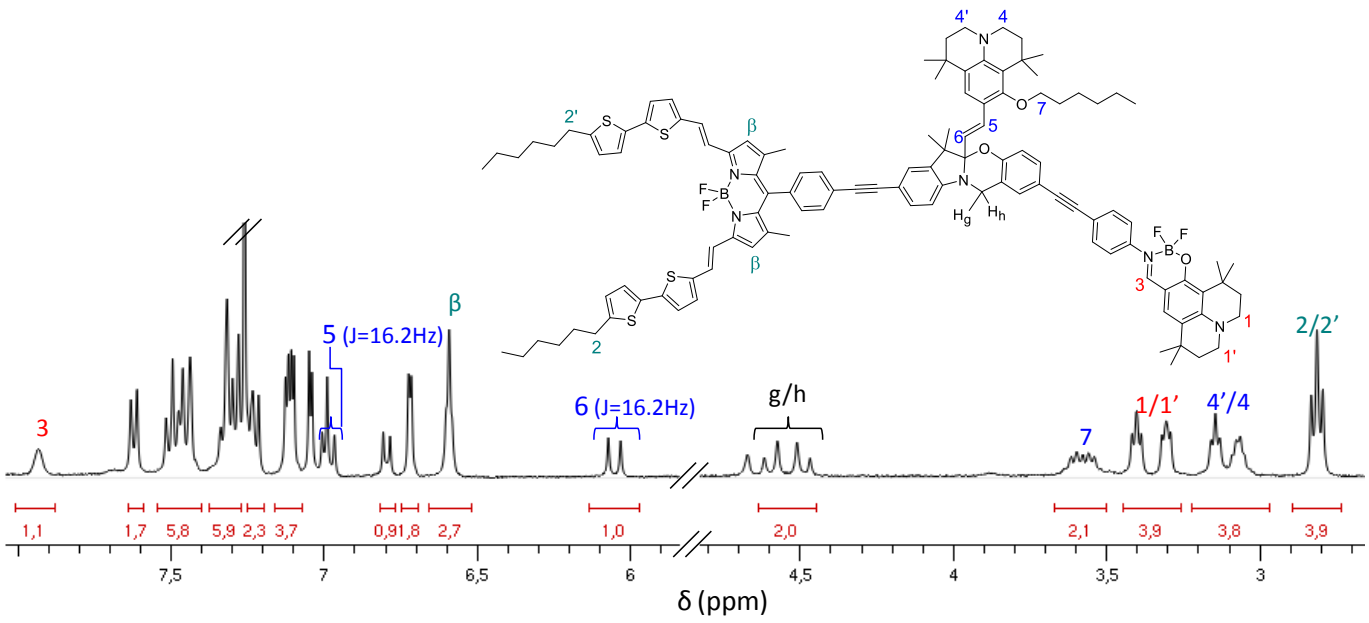

Figure 5. Le spectre RMN ^{1}H du **83** dans $CDCl_3$ à température ambiante, représenté partiellement pour clarté.

Les études photophysiques préliminaires réalisées en collaboration avec le Prof. Sortino de l'Université de Catania, ont mise en évidence un processus de transfert électronique d'énergie très efficace depuis le donneur d'énergie (le boranil) vers l'accepteur d'énergie (le BODIPY) lorsque le photochrome se trouve dans la forme fermée. En conséquence, l'émission de fluorescence depuis le BODIPY après excitation du donneur d'énergie est observée. En revanche, l'ouverture par traitement acide de la triade bloque le transfert d'énergie vers le donneur en l'orientant vers l'unité photochrome. Ceci induit l'extinction d'émission de fluorescence depuis le BODIPY. Ces résultats ont confirmé le caractère commutable de l'émission de luminescence de la triade finale **83** en contrôlant l'ouverture/fermeture du photochrome. Des études afin d'induire une ouverture optique de l'unité photochromes sont au moment d'écrire ce manuscrit de thèse, en cours.

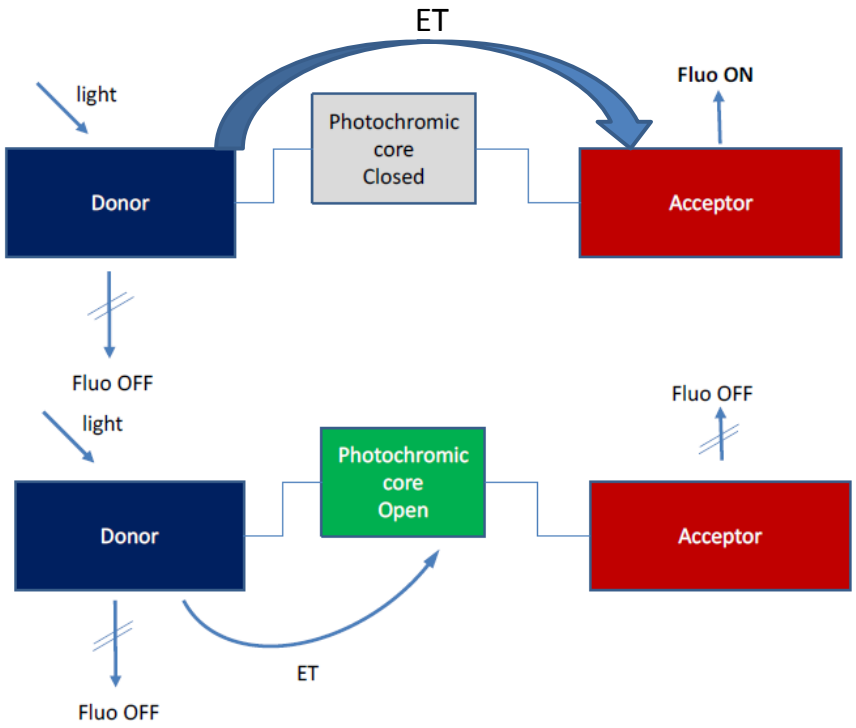

Figure 5. Représentation schématique du mécanisme de transfert d'énergie dans la triade **83**.

A côté de la triade **83** nous avons désigné et initié la synthése d'un autre composé analogue, le **84**, dont l'accepteur d'énergie est un dérivé squarine (Figure 6). Ce dernière a été choisie notamment en raison de ces proprités photophysiques très optimales; une seule bande d'absorption, rendement quantique de fluorescence élevè (λ_{abs} = 682 nm; ε_{max} = 295 000 M^{-1} cm^{-1}; φ_F = 0.85).

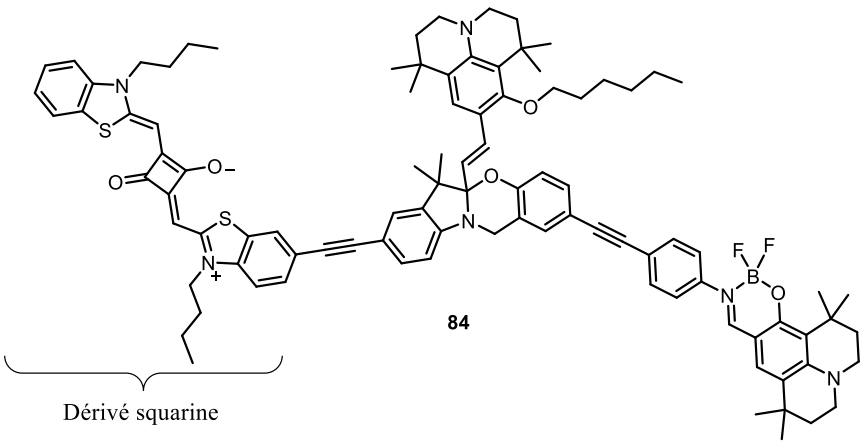

Figure 6. Strucutre chimique de la triade **84** désignée dont la synthèse est un projet en cours.

Depuis une quinzaine d'années, les photochromes organiques sont aussi combinés avec des complexes organométalliques. Les travaux de Prof. J.-M. Lehn figurent parmis les premiers exemples dans la littérature dans ce domaine.[186] Les systèmes photochromiques hybrides c'est-à-dire un centre photochrome organique combiné à des entités métalliques, sont étudiés entre autre afin d'obtenir des matériaux avec des capacités de lecture non-destructives, un parametre très important pour les dispositifs de stockage des donnés optiques. Les diaryléthènes sont régulièrement investiguées due à leurs propriétés remarquables de stabilité thermique et la résistance à la fatigue.

Inspirés par les travaux reportés dans la littérature nous avons désigné des systèmes photochromiques basé sur la [1,3]oxazine (Figure 6). Autour de ce module nous avons souhaité incorporer un chromophore dérivé d'Ir(III) et un chromophore d'Os(II) afin de délancher un processus de transfert d'énergie depuis l'unité chromophorique d'iridium vers l'unité d'osmium de façon controlable par l'ouverture/fermeture du photochrome.

[186] Fernandez-Acebes, A.; Lehn, J.-M. *Chem. Eur. J.* **1999**, *5*, 3285.

Entre autre nous avons souhaité mettre en evidence l'ouverture optique du cœur photochromique oxazine à partir d'un état triplet. La synthèse complète du système désigné n'a pas pu être achevée et en conséquence des mesures optiques n'ont pas pu être réalisées, mais ces travaux s'inscrivent dans les perspectives de cette thèse.

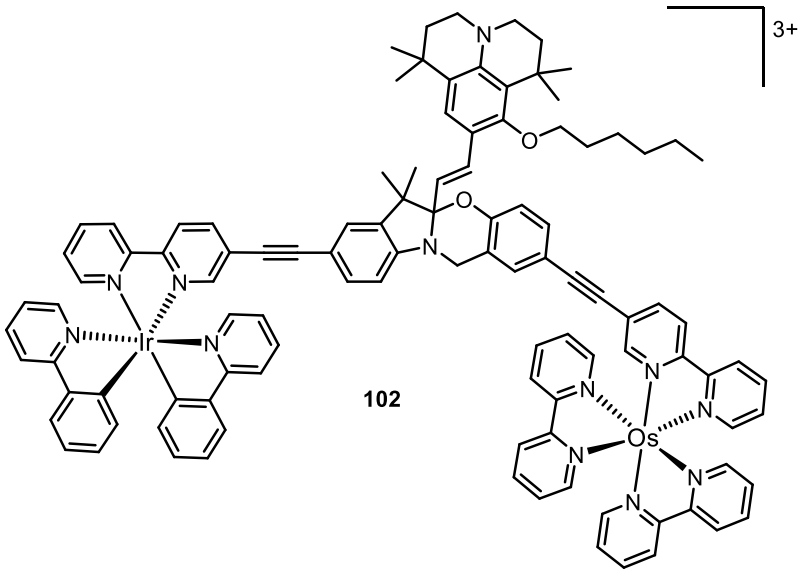

102

Figure 6. Structure chimique du système photochrome hybride désigné.

Adela NANO

Towards optical memories: switchcable optical systems for electron and energy transfer processes

Résumé

Le travail de cette thèse de doctorat est axé sur le design, la synthèse et la caractérisation de systèmes moléculaires organiques et organométalliques luminescents dans le but de déclencher des processus de transfert photoinduit d'électron (PeT) ou d'énergie (EET) pour des applications dans les dispositifs optiques ou électroniques. Nous nous sommes d'abord intéressés aux molécules de type push-pull car elles s'avèrent être des modèles intéressants pour l'étude du PeT. Nos systèmes sont construits autour de BODIPY qui sert d'espaceur entre le donneur d'électron (julolidine ou triazatruxène) et l'accepteur d'électron (une unité dicyanovinyl). Les études en électrochimie et spectroscopie ont montrés un caractère à transfert de charge très prononcé. Entre autre nous avons synthétisé et étudié une série de ligands de type N^O (type base de Schiff) dérivés de la julolidine, une amine cyclique avec des propriétés électroniques très inattendues. Ces ligands, subissent des processus de transfert photoinduit de proton à l'état excité (ESIPT) et leurs spectres d'émission présentent une luminescence panchromatique. La compléxation des ligands N^O au BF_2 supprime l'ESIPT et augment les rendements quantiques de fluorescence. Les ligands derivés de la julolidine sont combinés avec d'autres unités chromophoriques *i.e.* Ir(III), Pt(II) afin de construire des systèmes multichromophoriques et stimuler des processus de EET entre les composants. Lors de ces travaux de thèse nous nous somme particulièrement intéressés aux systèmes moléculaires photocommutables dont l'unité centrale est un photochrome, le [1,3]oxazine. L'oxazine est combiné à un module moléculaire qui sert de donneur d'énergie et un module accepteur d'énergie choisie de façon optimale afin d'induire un transfert électronique d'énergie de manière contrôlé.

Mots clés: transfert d'énergie, push-pull, BODIPY, ESIPT, photochrome, photocommutable

Abstract

The present doctoral thesis work deals with the design, synthesis and characterization of organic and organometallic luminescent molecular frameworks for triggering Photoinduced electron Transfer (PeT) and Electronic Energy Transfer (EET) processes for applications in optical and electronic devices. First, we turned toward the organic push-pull chromophores because they are useful model systems for studying the mechanism of PeT process. We synthesized new push-pull systems bearing a dicyanovinyl fragment as the electron-acceptor and a strong electron-donor such as julolidine and triazatruxene covalently linked through a BODIPY dye bridge. Electrochemical and photophysical studies showed a pronounced charge transfer character within the push-pull systems. Furthermore, we synthesized and studied a series of chelating N^O-type ligands (Schiff base-type), based on the strong electron-donating julolidine motif, displaying ESIPT process. Their luminescence profiles exhibited panchromatic luminescence band covering the whole spectrum. Complexation of N^O-site with boron difluoride suppressed the ESPIT process and highly increased the fluorescence quantum yield. The N^O-chelating ligands were combined with Pt(II) chromophore, B(III) and Ir(III) such as to obtain multichromophoric frameworks. According to the photophysical studies, EET processes were observed within the multichromophoric systems. We successfully obtained a new florescent switching triad constructed around a photochromic core, [1,3]oxazine, which bears an energy-donor and an energy-acceptor module such as to directly control the EET process.

Keywords: energy-transfer, push-pull, BODIPY, ESPIT, photochrome, fluorescent-switching